UNIVERSITY OF SOUTHERN QUEENSLAND

Mechanical treatment of microorganisms using ultrasound, shock and shear technology

A dissertation submitted by

Talal F Yusaf

For the Award of
Doctor of Philosophy
2011

Abstract

Microorganism disruption using ultrasound treatment is the focus of this thesis. There has been aboard spectrum of theoretical and experimental work on microorganisms disruption methods undertaken in the past. However, there is a lack of fundamental understanding on the actual reason of microorganism disruption using ultrasound. The reported literature in the microorganisms and cell disruption research field indicates that shock wave and shear effects occur together in typical ultrasound processing systems and may both contribute to microorganism disruption. However the question of whether the real cause of disruption is shock and/or shear remains unanswered.

To address this issue, two independent mechanical devices – a shock apparatus and a shear apparatus were developed for this study. An ultrasound apparatus operated in a batch configuration was also used for microorganism disruption.

The ultrasound work includes a detailed experimental characterisation of processing conditions associated with the ultrasound treatment. The heat transfer through the ultrasound chamber and the suspension mixing during the ultrasound treatment was evaluated using theoretical and experimental approaches. It was found that one second was sufficient to have complete suspension mixing in the ultrasound chamber and 13.5% of the total ultrasound energy was lost to the surroundings as heat. *Saccharomyces cerevisiae* was selected as a sample microorganism in this study, and a log reduction of 4 was achieved when ultrasound treatment was used.

To determine how the yeast cell wall disrupts using a shock treatment, a finite element model was developed and the simulation results showed that von Mises stress generated due to dynamic external pressure loading was concentrated at the bottom part of the cell wall of the yeast. A vertical gas gun was commissioned to apply a dynamic load on a water-filled tube. To understand the relationship between the dynamic stress and the microorganism behaviour when subjected to external pressure, a plastic bag full of yeast suspension was placed at the bottom of the tube.

The result showed that the yeast disruption rate using the shock wave treatment was relatively modest when an external shock loading pressure of around 115 MPa was used.

In the case of shear stress treatment, analysis of the intense turbulent flow region of the apparatus combined with the experimental results demonstrated that when the energy dissipation rate in the turbulence region is high and the eddies are smaller than the size of the cell, the likehood of yeast disruption is high. The microorganism mechanical properties combined with the calculated energy dissipation rate were used to simulate the yeast disruption efficiency using shear stress. The results showed that a maximum yeast log reduction of 4 was achieved with the shear apparatus in the absence of pressure rise.

The specific energy required for yeast disruption in these three mechanical methods was evaluated and a comparison was made with two relevant conventional methods: homogenizer and Ultra High Temperature (UHT) treatments.

It was found that the specific energy required to achieve a log reduction of 2.5 was 108 MJ/kg in the case of shear and around 0.905 MJ/kg in the case of ultrasound. In the case of shock treatment, the maximum log reduction achieved was 0.57 which required 0.00477 MJ/kg. Therefore, on the assumption that log reduction is proportional to the specific treatment energy, for a 1 log reduction, 0.008 MJ/kg is required for the shock treatment, 0.46 MJ/kg is required for the ultrasound treatment, and around 48 MJ/kg is required for the shear treatment. These results show that shock wave treatment requires less specific energy to achieve the same yeast log reduction as the shear or ultrasound treatment. This implies that the cause of microorganism disruption using ultrasound is shock wave energy.

Additional work in the finite element simulation and shock treatment apparatus is recommended to extend this study to different microorganisms and cells.

CERTIFICATION OF DISSERTATION

I certify that the ideas, experimental work, results, analyses, software and conclusions in this dissertation are entirely my own effort, except where otherwise acknowledged. I also certify that the work is original and has not been previously submitted for any award, except where otherwise acknowledged.

Talal F. Yusaf 15.5.2011

Signature of Candidate Date Date

ENDORSEMENT

15.5.2011

Signature of Principal Supervisor Date

15.5.2011

Signature of Associate Supervisor Date

ACKNOWLEDGEMENT

I would like to express my sincere thanks and appreciation to my supervisor Professor David Buttsworth, for his guidance, and providing me with excellent experience to pursue my PhD work and my appreciation to him for his insightful remarks, valuable comments and ideas. A great number of colleagues deserve thanks for their valuable guidance and assistance. First, the assistance of my Dean Professor Frank Bullen, my associate supervisor Associate Professor Nigel Hancock, second, my great thanks go to my beloved brothers Dr Belal Yousif and Ziad Awad for providing a constant source of encouragement and support, my wife Dr Nazik Itaiwi, my mother, and my kids whom used always to encourage me in critical times when I face a problem in my study. Experiments performed by the research team (David Buttsworth, Talal Yusaf, Rod Speering and Tanya Shepherd), using the research equipment commissioned by the author of this thesis, have contributed data to this work and is referenced when appropriate. Special thank goes to DRDC (Dairy Australia) for funding this project.

Table of Contents

List of Tables

List of Figures

CHAPTER I

Introduction

1.1 Overview

Experimental studies of microorganism inactivation using mechanical treatments have been performed since the 1950s and it is clear that mechanical methods such as ultrasonic treatment, shock wave treatment, and shear stress treatment can damage or destroy certain microorganism. Ultrasonic treatments for example have been used in food processing applications such as milk sterilization and homogenisation. However, commercial implementation of ultrasonic treatments, in milk sterilization, has not yet occurred for a number of reasons. Certainly, the advantages of mechanical treatments from economic and energy perspectives are not yet clear. The three main mechanical methods for microorganism disruption that are addressed in this thesis are:

1. High power ultrasound,
2. High hydrostatic pressure and shock waves, and
3. Shear treatments.

Research into the use of mechanical means for microorganism disruption has been conducted on different microorganism and some results have been reported (Balachandran et al., 2006). But there is a lack of technical information about the real cause of microorganism disruption, this gap of information needs to be addressed. This thesis addresses this need by developing and implementing new mathematical models for ultrasonic, shock wave and shear treatments. Experimental work was also conducted, and results were compiled and analysed to provide a substantial explanation on the cause of disruption resulting from these three methods.

1.2 Background and hypothesis

Ultra heat treatment (UHT) is widely used to destroy microorganism in milk; however UHT significantly reduces the nutritional value of the milk and can lead to a burnt flavour (Sahoo et al., 2002). In order to maintain milk quality, ultrasonic treatments have been proposed, as these methods do not directly heat the milk to the temperature involved in UHT treatment.

There is no specific theory to explain the real cause of disruption of microorganism due to ultrasound. When an ultrasonic wave passes through a liquid, bubbles or (cavities) can produce cavitations. Schebra et al. (1991) claims that the collapse of these cavitations causes local shock waves with accompanying high temperatures and pressures that could be responsible for a microorganism's disruption. Akbari et al. (2007) showed that the amplitude of the ultrasound wave influences the intensity of cavitation and the higher the amplitude, the higher the intensity of cavitations.

When small gas bubbles oscillate during the compression and rarefaction phases of the sound waves as in stable cavitation, strong eddies are developed in the surrounding area of the bubbles which ultimately dissipate into the liquid. This effect, which is known as micro streaming, causes large localised forces to shear 'rub' the membrane surfaces of surrounding organisms and cause physical damage. Doulah (1975) and Doulah et al. (1977) claim that yeast cell disintegration in ultrasonic cavitation occurs by shear stresses developed by viscous dissipative eddies arising from shock waves.

Both strong shock wave and shearing flow effect are generated by high power ultrasound but the dominant effect on microbial disruption has not yet been resolved (Smith et al., 2000a). It is unclear how ultrasonication destroys microorganism. However, research suggest that cavitation is one way with other possibilities being shear forces, localized heating and free radical formation (Hughes and Nyborg, 1962). Micro jets, acceleration, resonance effects and collisions between the microorganism are also other possibilities that have been suggested as mechanisms of destruction (Loske et al., 1998). It is hypothesized that shear forces and shock

waves operate together in typical high power ultrasonic processing system to contribute to microorganism disruption.

1.3 Ultrasonic treatment

The killing potential of ultrasound was discovered when sonar was used in anti-submarine warfare, it was noticed that the source waves were killing fish. This instigated research into ultrasound as a method of destroying or inactivating cells. In the 1960s research was concentrated in understanding the mechanism of ultrasound interaction with microbial cells (Hughes and Nyborg, 1962). By 1975, it had been shown that brief exposure to ultrasound caused the thinning of the cell membrane due to the separation of the cytoplasm membrane from the wall cell (Alliger, 1978). During the 1980s research continued to look at the effect of ultrasound in combination with other treatments such as heat (Ordonez et al., 1987; Garcia et al., 1989; Wringley and Liorca., 1992).

The progress of investigations on the effect of ultrasound on microorganism was parallel to that of the technology of instrumentation (Balachandran et al., 2006). The first ultrasonic apparatus comprised piezoelectric generators of quartz submerged in oil that generated ultrasonic waves of a very high frequency but low intensity (10 W/cm^2, approximately). When applied with sufficient intensity, ultrasound has the potential to destroy bacteria although the bactericidal effects of the ultrasonic treatment vary with organism, the duration of the treatment and the intensity of the ultrasound (Scherba et al., 1991).

The work in this thesis involves delivering ultrasonic energy into a yeast suspension in a batch configuration for certain interval of time. The ultrasonic work includes evaluating the heat transfer in the suspension, and assessing the Residence Time Distribution (RTD) using image process techniques and comparing experimental results with the reported literature. RTD was considered to ensure treatment uniformity of all microorganism.

1.4 Pressure disruption of microorganism

The use of shock waves to destroy microorganism is considered one of the developed methods. The form of shock waves used in inactivation of microbes is shock waves in aqueous ambient such as water.

Although many studies have been conducted in the past decades, the real cause of the microorganism death using shock wave processing is yet to be identified. A fundamental study is necessary to understand the effect of the dynamic and static stress due to the pressure loading on the cell wall rupture. A thorough investigation and fundamental mathematical simulation is needed to understand the relationship between the dynamic load and the cell wall rupturing.

The effect of dynamic stress on cell wall behaviour (rupturing) due to shock waves has not yet been addressed by others. For a good understanding of the influence of the dynamic stress on cell wall rupture, a Finite Element (FE) model was developed using the commercial software ABAQUS. This model will help to deduce the cell wall stress for given values of external pressure.

1.5 Shear stress for microorganism disruption

Microstreaming in ultrasonic processing causes large localized forces to shear the cell membrane surfaces resulting in physical damage to the cells (Doula, 1977). In addition to this microstreaming effect, which is normally associated with stable cavitation, an additional shear effect will result from the transient cavitation processes as the viscosity ultimately dissipates a large fraction of the absorbed ultrasonic energy. These shear forces do not necessarily break the cell into fragments but can cause damage to the cell wall. The microorganism can therefore become more fragile and susceptible to subsequent heat treatment.

This thesis aims to explain microorganism disruption due to shear flow effects. A model for microorganism disruption in turbulent flow and an experimental study are combined in an effort to give a better understanding of the real cause of microorganism disruption in shear flow. Most of the scientific papers did not discuss

the effect of the combination of shear force and eddies generated due to the turbulence flow. A mathematical model has been developed to couple both eddies and shear stress.

1.6 Summary of thesis structure

The thesis is broken down into seven chapters.

- **Chapter 1** and **chapter 2** introduce the thesis and explain some non-conventional methods for microorganism disruption.

- **Chapter 3** investigates the use of ultrasonic techniques for microorganism disruption. The first part focuses on theoretical aspects of ultrasonic disruption. The second part of this chapter details the experimental work as well as discussing and analysing the results. This chapter will cover the following items

    1. A literature review combined with theoretical considerations to provide a fundamental understanding of the cause of a microorganism's disruption using ultrasound. *Saccharomyces cerevisiae* was used as representative microorganism, because of its well established mechanical properties.
    2. The experimental work which includes a detailed of explanation of the ultrasonic experimental apparatus, the yeast preparation and counting, and the test procedure. Two basic experimental ultrasonic configurations are introduced in this chapter:
        i. Energy assessment configuration. It is essential to evaluate the net ultrasonic power dissipated into the suspension. A 30 mL suspension was exposed to approximately 238 kW/m^2 of ultrasonic power intensity at 20 kHz. The net heat transfer from high power ultrasonic device to the suspension was evaluated. Measurements of the convective heat transfer at the surface of the processing cell were obtained through a transient heat transfer experiment.
        ii. Mixing assessment configuration. A batch configuration was evaluated to ensure that all microorganism spend sufficient time

under the high power ultrasonic device, and ultimately secure the microorganism disruption. Evaluating the RTD helps understanding and improving the mixing process to obtain homogeneous milk.

3. The last part of this chapter will discuss and analyse the experimental results. The effectiveness of yeast destruction was found to be reasonably acceptable; however the treatment time was an important factor that was considered in this experimental work.

- **Chapter 4** involves a detailed fundamental theoretical study of cell wall rupture using external hydrostatic pressure. This chapter includes a description of the shock wave apparatus that was used in this study. This chapter consists of four main elements:
    1. Analysis to help explain the response of microbe static behaviour when it subjected to external pressure loads.
    2. Numerical Simulation using FE software ABAQUS to help understand the microorganism dynamic and static behaviour when it subjected to external pressure.
    3. Experimental work using a shock wave apparatus to apply external pressure loads to a suspension of *S. cerevisiae*. This involves the impact of a high-speed piston on a volume of liquid. The shock wave generated could disrupt the microorganism in the absence of the any thermal stress or/and shear force.
    4. The results from the experiments will then analysed and verified the context of the simulation from point 1 and 2.

- **Chapter 5** focuses on the shear stress, and details both theoretical and experimental works. The shear experimental apparatus was designed and constructed to make sure that microorganism disruption occurred due to shear stress in the absence of pressure elevation and thermal stress. This chapter aims to:

    a) provide a fundamental engineering understanding of the relationship between the shear stress generated on the cell wall of the microbe due to the laminar and turbulent flow and the mechanical properties of the cell,

b) describe the use of a shear rotary device that generates sufficient shear forces that will disrupt microorganism in the absence of the significant temperature and pressure effects. Various energy levels of shear treatment were tested and disruption results were used for prediction of microorganism disruption, and
c) discuss and analyse the results obtained from the model and the experimental work.

- In **chapter 6**, the specific energy required for yeast disruption using ultrasound, shock and shear treatments was estimated. The specific energy results were compared with homogenizer and UHT.

- **Chapter** 7 of this thesis is conclusion and suggestion for further work.

CHAPTER II

Alternative Methods for Microorganism Disruption

This chapter reviews various techniques for microorganism disruption. Methods of treatment to destroy microorganism can be categorized as thermal treatment method and non-thermal treatment methods. Non-thermal treatments are the alternative methods considered in this chapter. The alternative methods, where heat is not the cause of the death of the microorganism, include mechanical treatment, electrical treatment, and ultraviolent treatment, bead milling treatment, shear stress treatment and high hydrostatic pressure treatment. Homogenization techniques may, as a side effect, also induce microorganism disruption.

2.0 Thermal methods

Thermal methods can be regarded as the traditional approach for microorganism disruption. Temperatures in the range 160 ^{o}C to 280 ^{o}C are commonly used. Thermal methods are commonly used in the food industry and dairy product industry. The exposure time to kill microorganism varied from 2.5 to 30 minutes depending on the nature of the bacteria (Tan, 1999). Pasteurisation is one of the most important steps in processing milk. However, these processes may alter the nutritional quality and milk flavour, rendering it a less desirable product. UHT is one form of sterilisation which is widely used to destroy the microorganism in milk (Prakash et al., 2010). Thermal process treatments can also be used to kill the complex microorganism in wastewater by exposure to 300 ^{o}C for 1.75 minutes (Tan, 2004).

2.1 Mechanical methods

Mechanical methods aim to disrupt microorganism without adding substances or changing the internal structure of the suspension containing the microorganism. For optimization of mechanical methods a good understanding of the mechanical properties of the cell wall and the cytoplasm are required, so that the likely mechanical loads and disruption probability can be identified.

The mechanical methods for microorganism disruption that are discussed in this thesis are ultrasonic, shock wave, and shear treatments. Mechanical methods are recommended to treat bacteria that required high energy (power) for disruption, because this method can generate sufficient energy and shear to rupture those microorganisms.

2.1.1 Ultrasonic methods

When ultrasound is applied with sufficient intensity and time, it has the potential to cause the death of microorganism (Scherba et al., 1991). As stated earlier, the destructive potential of ultrasound was discovered when sonar was investigated and used for anti-submarine warfare. Scherba et al. (1991) reported that the source waves were killing fishes (Hughes and Nyborg, 1962), eventually, leading to research in ultrasound as a method of destroying or inactivating cells (Akbari et al., 2007).

In the 1960s, research concentrated on understanding the mechanism of ultrasound interaction with microbial cells (Hughes and Nyborg, 1962). By 1975, it had been shown that brief exposure to ultrasound caused thinning of cell walls. This led to separation of the membrane from the cell (Alliger, 1978). Ultrasonic waves passing through a liquid consist of alternate rarefaction and compression waves. If these waves have sufficiently high amplitude, bubbles or cavities are produced and this phenomenon is known as cavitation (Sherba et al., 1991). Theoretical analyses to describe the relationship between the generation of cavitation and ultrasound strength are discussed in chapter 3.

2.1.1.1 High power Ultrasound for sterilization

High power ultrasound can generate localized high pressure and temperature when cavitation bubbles collapse. The high pressures generated are thought to be responsible for cell disruption (Scherba at el., 1991). The high temperatures formed in cavitation bubble collapse also have some effect on the suspension treatment process. Other researchers contend that the combination of pressure and temperature generated by high power ultrasound contribute to the death of the microorganism (Balachandran et al., 2006).

During the 1980s, researches continued to study the effect of ultrasound in combination with other treatments for use in the food industry (Ordonez et al., 1984; Garcia et al., 1989; Wringley and Liorca, 1992). Furthermore, the effects of low frequency ultrasound combined with increased temperature on the disruption of microorganism in milk suspended in water has been investigated (Ciccolini et al., 1997). The tests were conducted at different treatment temperatures of 45 °C, 50 °C and 55 °C and ultrasonic powers of 50 W, 100 W and 180 W.

Koda et al. (2009) used an ultrasound power of 12.8 W and frequency of 20 kHz to treat 50 cm^3 of water contaminated with along reduction *S.Mutans* for 15 mins and reported a percentage reduction of about 97% or

$$\log \frac{N}{N_\circ} = -1.5 ,$$

where N/N_o is the surviving ratio of the microorganism.

The results of Koda et al. (2009) indicate that ultrasonic waves do not completely destroy the cells, but damage some of them by increasing the cells sensitivity to heat. The optimum ultrasonic power for a maximum deactivating effect was found to be around 100 W. The following section will cover the combination of ultrasonication with other techniques related to temperature, pressure and pH.

2.1.1.2 Combination of Ultrasound with temperature

Microorganism become more sensitive to heat treatment if they have undergone an ultrasonic treatment (Ordonez *et al.*, 1984; Garcia *et al.*, 1989). The combination of heat treatment with ultrasonic treatment is called "thermo-sonication" (Earnshaw et al., 1995). As mentioned in Chapter 1, Ordonez et al. (1987) studied the thermo-sonication, on the survival of a strain of *Staphylococcus aureus* in a phosphate buffer. Garcia et al. (1989) found that thermo-sonication (5 W/mL) on *Bacillus subtilis* was not significantly effective in killing the spores in water at temperatures close to boiling point (100 ^{o}C). The low effectiveness was attributed to the decrease in the violence of bubble collapse due to the higher vapour pressure acting like a cushion (Garcia et al., 1989; Alliger, 1975).

From the literature, it can be concluded that bacterial cells generally become more sensitive to heat treatment after being subjected to ultrasound treatment. Sequential or simultaneously applied ultrasonic and heat treatments result in the destruction of bacteria at much lower temperatures than would be required for heat treatment alone. Earnshaw et al. (1995) demonstrated that the elimination of bacteria can be improved by subjecting them to a combination of ultrasonic and heat treatment compared with bacteria that are subjected to ultrasonic treatment only. The conclusions Raso et al. (1994) were consistent with those of Earnshaw et al. (1995). Garcia et al. (1989) reported a reduction of 43% in the heat resistance of *Bacillus subtilise* (*B. subtilise*) when it was subjected to ultrasonication in hot water at temperature from 70^{o}C to 95^{o}C.

2.1.1.3 Combination of Ultrasonic with temperature and pressure

When the temperature of a liquid exceeds the boiling point, a loss in the cavitation effect takes place due to the high vapour pressure (Garcia et al., 1989). In order to overcome this problem, pressure is often applied to thermo-sonication. This kind of combination treatment is known as Mano-Thermo-Sonication (MTS). In the MTS

technique, cavitations can be generated by ultrasound despite the high temperature of the liquid (Earnshaw et al., 1995).

2.1.1.4 Other possible combinations involving Ultrasound

Apart from thermo-sonication and MTS treatment, there are other combinations that have proven to be effective against microorganism.

Combination with pH *control*

Microorganisms have been observed to vary in their response to ultrasonic treatment when subjected to treatment at different pH (Kinsloe et al., 1954). It was found that a lower pH value reduces the resistance of microorganism during ultrasonic treatments (Kinsloe et al., 1954), which lead to a better destruction result.

Combination with chemical control

Lillard (1993) demonstrated that the effectiveness of ultrasound treatment can be enhanced by the use of a chemical such as chlorine. In this research, the focus is on mechanical methods; therefore, other reported possible combinations related to chemical control is not explained further.

2.1.2 Shock wave treatment

A shock wave can be generated by methods such as shock tubes or electrical discharge shock wave generators (Yu et al., 2009). It has been reported that a static pressure of about 100 MPa is required to destroy bacteria (Loske et al., 1998), a pressure at which the proteins structure would not be changed. However, the destruction of microorganism at static pressure cannot be attributed due to evaluate static pressure is a very different process to shock treatments and ultrasound treatments which are fundamentally dynamic processes.

Oshima et al. (1997) used a shock tube to generate a transient positive pressure of about 0.1 MPa with pulse duration of approximately 900 μs. However *Escherichia*

coli (*E. coli*) was found to be difficult to destroy. Tamagawa and Akamastsu (1997) used the same diaphragm-less shock tube as Oshima et al. (1997) for their experiment on recombinant cells of *Escherichia coli*. The pressure pulses generated with their device had a duration of about 20 μs and an amplitude of up to 14 MPa. They noticed that cell rupture occurred after 100 shock waves at 14 MPa. This suggests that using higher pressures will lead to a higher level of damage to the microorganism, for repeated shock wave loads.

The research of Kerfoot et al. (1992) aimed to isolate the effects of shock waves on of *Pseudomonas aerugmiosa*, *Streptococcus faecalis*, *Streptococcus aureus* and *Escherichia coli* as well as to determine whether bactericidal activity exists. For this purpose, an electrohydraulic lithotripter of 20 kV was used together with a shock wave rate of 100 shocks per minute (Garcia et al., 1989). The result of the study was discouraging as no bactericidal activity was noticed.

Loske et al. (1998) studied the effects of an experimental electrohydraulic shock wave generator on an *Escherichia coli* suspension. The frequency of the device used was 0.4 kHz with a capacitance of 80 nF and voltage of 20 kV. The duration of the experiment was 24 minutes while the pressure pulse amplitude and pulse duration were 44 MPa and 4 μs respectively. The cells were suspended in tap water, which had a conductivity of about 960 μs and a temperature of 27 ^{o}C. The treatment resulted in a log reduction 0.9 (from 10^6 to 10^5 CFU/mL). Lado et al. (2002) found that to inactivate the entire cell population, 6 D or about 143 minutes would be required. The results of this study differ from those of Kerfoot et al. (1992) who used the same 20 kV electrohydraulic lithotripter.

Loske et al. (1998) concluded that the effectiveness of shock wave microbial inactivation depends on the maximum pressure amplitude (peak compression and rarefaction), the rise time, duration of the pulse and the repetition rate. The authors also noted that the importance of the cell container and the environment around the cell tube would influence the transmission of shock waves to the cells.

2.1.3 Shear treatments

Several mechanical devices using shear stress for the disruption of microorganism have been investigated, including bead mills, presses, ultrasonication, microfluidization and homogenization (Geciova et al., 2002). The primary cause of the disruption in these devices appeared to be a shearing effect, though in the case of ultrasonication shock waves will also present.

When small gas bubbles oscillate during the compression and rarefaction phases of the sound wave, strong eddies are developed in the area surrounding the bubbles which ultimately spread into the liquid. This effect, which is known as microstreaming, leads to significant localized shear forces that rub the membrane surfaces causing membrane disruption (Doula, 1977).

A high pressure homogenizer is one of the devices used in the milk industry that utilises mechanical shear force to break-up particles to smaller sizes. This device works by pushing the contaminated suspension through a small orifice at very high pressure. The suspension is circulated through a closed system where microorganisms are subjected to repeated shear stresses. A wet milling device is another mechanical means of sterilization that operates in a similar way to the homogenizer. The treatment involves mixing the suspension with small glass beads. The device consists of a cylindrical chamber, a driver to rotate the chamber, and an impellor to mix the suspension and the beads (Melih and Murray, 1998).

2.2 Non-Mechanical methods

2.2.1 Pulse electrical field (PEF)

Pulsed electric fields (PEF), oscillating magnetic fields (OMF) and light pulses (LP) are attractive and popular methods used in the food industry and research laboratories for sterilization purposes (Guyot et al., 2006). These methods offer good alternatives to conventional thermal processes where nutritive aspects and costs are a concern. These methods avoid the use of chemical preservatives that may cause a

change in the nutritional value of the food. To adopt this technology in a larger scale, a good understanding of the electrochemistry is required (Yu et al., 2009; Mosqueda et al., 2008).

The PEF method is strongly affected by the required electric power and the time to apply the power. PEF used to kill *S.cerevisiae* (Guyot et al., 2006) in a medium of water and glycerol and the power applied was low-intensity electric fields and with long-duration pulses (Guyot et al., 2006). The destruction was attributed to the direct effect of the electromechanical phenomena and the indirect effect of the membrane polarization phenomena. Hence, it was suggested that the technique used high intensity electric field with short duration pulses (Guyot et al., 2006).

The application of using electrical fields in biological cells medium such as contaminated suspension can cause build up of electrical charges at the membrane of the cell as reported by Schoenbach et al. (1997). Membrane disruption takes place when the critical value of the cellular system the exceeds the induced membrane potential of approximately 1 V, e.g. corresponds to an external electric field of about 10 kV/cm for *E. coli* (Castro et al., 1993). Many PFE theories have been suggested to explain microbial disruption. The common studies focused on electrical breakdown and electroporation or disruption of cell membranes (Zimermmann 1986; Castro et al., 1993; Vega-Mercado et al., 1996).

Dunn et al. (1987) studied with homogenized milk contaminated with *Salmonella Dublin* (*S. Dublin)*, and then treated using 36.7 kV/cm and 40 pulses for 25 mins. It was found that there was no *S. Dublin* after the PEF treatment. The concentration of the bacteria in the milk was 10^7 CFU/mL in the untreated milk, while the treated milk presented about 4×10^2 CFU/mL, i.e. a log reduction 5. Furthermore, Dunn (1996) showed that there are no changes on milk flavour, chemical and/or physical quality related to subsequent cheese making. A log reduction 3 was achieved when *E. coli* was used.

2.2.2 Non-Thermal plasma

Plasma is a neutral ionized gas; it includes photons, electrons, positive and negative ions, free radicals and excited and non-excited molecules (Moreau et al., 2008). Plasma can be either thermal or non-thermal depending on the conditions of its creation. Non-thermal plasma is created with low pressure and low power, such as the plasma which is generated by an electric discharge with low pressure gas (Moreau et al., 2008). Factors that affect the activity of plasma in terms of destroying microorganism are: the electric charge that causes the interaction between the microorganism and the plasma, the diffusion constant of the microorganism and the acidity (pH) of the medium. The general mechanism of this method is that the surface of the cell wall absorbs components from the plasma to form volatile components that are then removed from the cell causing its destruction (Lerouge et al., 2000).

2.2.3 Ultraviolet (UV) method

Ultraviolet light is an electromagnetic radiation that occurs for example in sunlight and can also be emitted by electric arcs. Ultraviolet light is used to kill microorganism, but when used alone is not as effective as the other methods that have mentioned previously (Ward et al., 2000). Since ultraviolet light is propagated by electrical fields, the parameters which affect its effectiveness are the level of electric power and the time. Other factors that impact on this method of sterilisation include the medium which contains the microorganism and the type of microorganism which will be treated by the ultraviolet light. The unique element of this method is that ultraviolet light could attack the *DNA* as well as the cell wall of the microorganism. Ultraviolet light combined with laser light has been used to inactivate *B. Cereus* (Armstrong et al., 2006). Laser application alone was not enough to disrupt the microorganism effectively and ultraviolet light was effective for exposure duration of more than six minutes (Ward et al., 2000). While a combined treatment of laser and ultraviolet light can be an optimum method to kill bacteria such as *B. Cereus.* According to these cited references, the combination of

UV with other methods can produce better microorganism disruption. The UV method requires high security equipment and this makes it expensive.

2.2.5 Chemical treatment methods

Some chemical methods rely on the addition of chemical substances to weaken the structure of the microorganism. Some examples are identified below

a. *Biofilm removal caused by chemical treatments:* biofilm is an aggregate of microorganism in which cells are stuck to each other and to a surface (Chen, 2000).

b. *Using supercritical carbon dioxide and hydrogen peroxide to kill Bacillus anthracis: Bacillus anthracis* is a Gram-positive spore-forming, rod-shaped bacterium with a width of 1-1.2µm and a length of 3-5µm. These bacteria can be found in the blood of sheep suffering from anthrax, which is a fatal disease (Geciova et al., 2007). An example of chemical treatment is *Inhalation spores of B. anthraces'* can be chemically killed by a mixture of supercritical carbon dioxide ($SCCO_2$) and hydrogen peroxide (H_2O_2). The percentage of peroxide is 30% and the purity of carbon dioxide is 99.8%. This method uses medium temperature and high pressure to effectively kill *B. anthracis* (Geciova et al., 2007).

c. *Chemical Process*: another way to chemically treat the bacteria is via a chemical processes such as hydrogenations and oxidations. An example of this method is the *oxidative killing of microorganism by neutrophils. Neutrophils* are the most abundant type of white blood cells in mammals and form an essential part of the immune system (Roos et al., 2003). This method has wide applications in medicine.

2.2.5 Other methods

There are several other methods of treating microorganism which are beyond the scope of this study. They include physical, enzymatic, ionizing and osmotic methods.

Physical methods are commonly used for cells with weak membranes and require breaking the cell wall without rupturing its cytoplasm, which is similar to the mechanical methods. *Enzymatic methods* involve attacking the enzyme of the cell without destroying the integrity of the cell. *Ionizing radiation* is another method which is designed to produce safe healthy food, while maintaining the nutrition values and sensory qualities (Beatrice et al., 2002). *Osmotic shock or osmotic stress* is a method where a sudden change in the solute concentration around a cell leads to a fast change in the water movement across the membrane (Flores and Galston, 1982).

2.3 Conclusion

Much research has been conducted in the past decades in an effort to replace conventional thermal methods of microbe treatment with alternative technologies. The alternative methods suggested involve chemical, mechanical, or electrical treatment. Research studies have demonstrated that non-conventional methods such as mechanical treatment can be improved by either pre-treatment or combined treatments. A combination of ultrasound with heat or/and pressure has proven to be a good solution for certain bacteria and spores. Whilst a large number of techniques result in membrane or cell wall damage, very few methods adequately meet the demands of industry in terms of energy efficiency, environmental issues, and cost effectiveness. According to Smith et al. (2000a), physical methods are generally inefficient, and not used in industry, while chemical methods alone cause a reduction in protein, and they depends significantly on the physiological state of the microorganism. Adding chemicals to a product often leads to undesirable contamination.

The mechanical methods adopted in this work have many advantages for hard microorganism at low operating cost and higher efficiencies. Three mechanical methods to replace thermal treatment are proposed in this thesis. These methods are ultrasound. Hydrostatic High Pressure (HHP), and shear stress and will be discussed in chapters 3, 4 and 5 respectively.

CHAPTER III

Ultrasound Disruption of Microorganisms

3.0 Introduction

Ultrasound is a known means to disrupt biological structures. In spite of the significant academic work that has been done on high power ultrasonic treatment, no practical system for milk processing (for example) has been developed because of variable experimental results, lack of theory and insufficient reporting on experimental work.

Ultrasonic treatments of microorganism are sensitive to a wide range of parameters that have been thoroughly reported in the literature. Hence, apparently conflicting results are sometimes reported and replication of previously reported treatments is often difficult (Kinsloe et al., 1954; Alliger, 1978; Sala et al., 1995). Furthermore, prohibitively high power levels have sometimes been necessary to inactivate certain bacteria. Hence, the advantage of ultrasonic treatments from economic and energy perspectives is not yet clear.

The work in this chapter is provided in six parts

1. Introduction to cavitation theories in ultrasound and the cavitation influence on microorganism disruption,
2. heat transfer through the ultrasound chamber wall,
3. suspension mixing using image processing techniques,
4. yeast preparation and viable process of counting the colony forming units per millilitre,

5. ultrasound apparatus based on the results obtained from heat transfer modelling evaluation and
6. ultrasound experimental results and discussion, this part consists of three main elements; collecting results and discussion, analysing the results and conclusion.

3.1 Cavitation induced by ultrasound

3.1.1 Cavitation

Cavitation refers to the process of bubble growth that occurs when the pressure inside a liquid system, at any point, is reduced to a critical value known as the cavitation threshold. The cavitation threshold is the pressure at which cavitation starts and it depends on a number of factors that will be discussed in the following sections. The cavitation threshold is directly proportional to the hydrostatic pressure applied to the liquid. The bubbles oscillate according to the amplitude of the pressure waves generated which determines whether the cavitation produced is either stable or transient.

3.1.2 Stable and transient cavitation

When a suspension is subjected to ultrasound, two types of cavitation can develop depending on the frequency, amplitude and the power of the device, stable cavitation and transient cavitation.

Stable cavitation refers to small bubbles oscillating during the compression and rarefaction cycles produced during ultrasound. In stable cavitation, the average bubble size changes only after many thousands of the oscillating cycles. This type of cavitation is less violent than transient cavitation and occurs with high frequency, low amplitude sound waves.

In contrast to stable cavitation, transient cavitation occurs when the bubble size changes much more rapidly (within a few oscillatory cycles). The bubbles then

collapse with different intensities. On collapsing, the high energy burst momentarily produces high pressure up to 100 MPa and high temperature up to 5000 K in the surrounding region. Stable cavitation can change to transient cavitation during the oscillating cycles. An important difference between both types of cavitation is that stable cavitation bubbles do not implode while the transient cavitation bubbles do. The main mechanism in which cavitation acts in the destruction of microorganism appears to be the implosion of the bubbles which creates either high energy shock or shear stress which can disrupt cell walls. Due to the lower energy dissipation of stable cavitation, transient cavitation is preferred for optimum cell destruction.

3.1.3 Temperature rise due to ultrasound

When ultrasonic sound waves pass through a medium, thermal effects can occur. However, it has been found that the thermal impact is insignificant in terms of producing a temperature rise in biological systems, when using an ultrasonic frequency of 26 kHz at various intensity levels (Scherba et al., 1991). According to the research conducted by Scherba at al. (1991), the maximum rate of temperature rise due to ultrasound is too small to inflict significant harm on the biological systems of the microorganism. Therefore, ultrasonically induced thermal effects are not responsible for altering biological systems of microorganism under the exposure conditions. Sanz et al. (1985) successfully used an ultrasound device that can generate a power of 120 W at 20 kHz.

3.1.4 Power input

In general, the level of cell damage is higher when the power is higher. It is known the velocity and pressure of any particle is increased when power is increased (Chamber and Gaines 1932). In addition, Chamber and Gaines (1932) stated that if the power provided by the oscillator is high enough, cavitation will occur even in the absence of gas. They also pointed out that cavitation does not occur throughout the entire cell sample (i.e. it is confined to restricted regions), and only occurs in the region adjacent to the free ends of the ultrasound probe.

3.1.5 Energy transfer effects ultrasound

The collapsing bubbles in the transient cavitation of the ultrasound field transfer ultrasonic energy into hydrodynamic energy due to the release of elastic waves (Doulah and Hammond, 1975; Doulah et al., 1977). Collapsing bubbles disintegrate into eddies which in turn break up further to form a new set of eddies. The process of breaking up will continue until eddies become small enough to be dissipated by the viscosity of the medium.

3.1.6 Exposure time and cell density

Consideration of the exposure time and the density of the cell sample indicated that the fraction of undamaged cells decreased as the exposure time to ultrasound irradiation was increased. However, the effectiveness of the ultrasound in the destruction of the cells decreased as the density of the cell sample was increased (Ciccolin et al., 1997). These effects were more prominent for large volumes of the sample.

3.1.7 Effect of species of microorganism

Different species of microorganism exhibit different resistances to ultrasound. Large sized microorganisms are generally more sensitive to ultrasound as the area directly in contact with ultrasound is larger. *Coccal forms* are more resistant than rod-shaped bacteria (Jacobs and Thorney, 1954; Alliger, 1978). *Spore gram-positive* micro-organisms are more resistant than *gram negative*, and *aerobic* (requiring oxygen) are more resistant than *anaerobic* bacteria (Ahmed and Russel, 1975).

3.1.8 Factors influencing cavitation intensity

There are a number of factors influencing cavitation intensity (Earnshaw et al., 1995).

Liquid temperatures is an important factor as many liquid properties affecting cavitation intensity are related to temperature. A change in temperature also results in changes to the viscosity of the liquid medium, the solubility of gas in the liquid, the diffusion rate of the dissolved gasses in the liquid and the liquid vapour pressure. The viscosity of the liquid must be minimized to gain maximum cavitation effect as a more viscous liquid environment makes the ultrasound strength easily disrupted and could hamper the formation of cavitation bubbles and thus the implosion of the cavities. In order to minimize viscosity, the temperature has to be increased. At high temperatures, the vapour pressure is increased and the tensile strength of the liquid is decreased. However, the intensity or the violence of the bubble collapse or implosion is cushioned by this vapour pressure. Due to this, at temperature close to the boiling point of the liquid (100 °C for water at atmospheric pressure), the violence of the bubble collapse decreases as the liquid starts to boil at the cavitation sites.

The second factor is the frequency of the ultrasound. The frequency of the ultrasound is an important factor as it determines the maximum bubble size before implosion. In general, cavitation intensity is inversely related to the ultrasound frequency. For low frequencies, the cavitation bubbles are bigger in size and thus produce higher energy when they collapse (greater intensity of implosion). For high frequency ultrasound (approximately 1 MHz), however, the cavitation bubbles are difficult to produce and at frequencies greater that 2.5 MHz there would be no cavitation bubble formation. The energy liberated during cavity implosion depends on the ratio of the maximum bubble size to the initial radius of the bubble. The maximum or resonance radius of a gas (air) bubble in water at atmospheric pressure, given as a, for frequencies of less than 10^6 cycles per second, is given by the relationship $a = 3.0/f$ where a is in millimetres and the frequency is in kilocycles per second (Hughes and Teshima, 1962). Bubbles whose sizes are less than the resonance size attract each other and coalesce until they grow to the resonance size. After the resonance size is reached, the bubbles then vibrate or oscillate according to the pressure waves generated. If the pressure wave is high enough, the bubbles grow at a very fast rate. When the energy supplied by the ultrasound is not enough for the bubbles to retain their vapour phase, the bubbles experience sudden condensation back to their liquid phase. These condensed bubbles then impact each other violently creating shock waves with

accompanying very high-localized temperature and pressure. This is the basis of transient cavitation. If the pressure levels are lower, the evolution of the bubble diameter is weak and occurs over a long period of time. This results in slow growth of the bubbles and is the basis for stable cavitation.

Amplitude of the ultrasound. The amplitude of the ultrasound determines the intensity of cavitation. The higher the amplitude of the sound waves, the higher the intensity of cavitation. When there is no ultrasound, the liquid molecules remain very close to each other due to liquid tensile strength. However, when ultrasound is used, the rarefactions and compression cycles will be generated within the liquid molecules. When the negative pressure generated in the expansion cycle is low enough to overcome the tensile strength thus fracturing the liquid, small bubbles are formed which are the nuclei of cavitation. This happens for high amplitude of ultrasound. Tensile strength in pure liquids is very high and for example, the tensile strength of the pure water is about 10^5 kPa and difficult to overcome (Beer et al., 2005).

Viscosity of the liquid environment. If the viscosity of the liquid environment were high, cavitation would decrease as the penetration of the ultrasound through the liquid medium would be less. A low frequency, high power (high intensity) ultrasound would be a better choice than a high frequency ultrasound wave (in which the wave is more easily dispersed) to achieve penetration in a liquid with high viscosity. Alternatively the liquid could be heated to decrease its viscosity.

3.2 Heat transfer in the ultrasonic processing cell

An initial experiment was conducted to evaluate the net heat dissipated in a small volume of water subjected to 117 W at 20 kHz.

3.2.1 Introduction

The aim of this work was to assess the overall heat loss through the walls of container when ultrasonic power was applied. This was achieved by measuring the

convection heat transfer at the surface of the processing cell. It was anticipated that quantification of the heat transfer associated with ultrasonic processing would enable future experimental results on microorganism disruption to be reported with greater clarity. These results would also contribute to an accurate assessment of the economic viability of any future proposed ultrasonic treatment processes.

3.2.2 Experimental apparatus

The ultrasonic treatment apparatus consisted of a commercial ultrasonic processor (Dr. Hielscher GmbH, type: UIP500) attached to a 316 stainless steel processing cell as illustrated in Fig. 3.1. The cell for these heat transfer experiments was operated in a batch configuration with a perspex base which did not have a flow port.

The ultrasonic processor provided approximately 117 W of power (at 20 kHz) to a sample of approximately 4 mL of water in the processing cell. Three thermocouples (type K) were located at various points around the processing cell as illustrated in Fig. 3.1. The most important thermocouples are the water temperature thermocouple (giving the value, T_w) and the thermocouple located at the perspex surface in contact with the water (giving the value, T_{sp}). The thermocouple located on the lower surface of the perspex (giving the value, T_l) was used to indicate the time at which the heat transfer within the perspex departed from the assumed semi-infinite process. Signals from the thermocouples were amplified using an integrated circuit with cold junction compensation (Analogue Devices, AD595) and the temperature signals (voltages) were recorded at 20 Samples/s using an A/D card and Lab-View software.

In this study there was a need for adequate cooling arrangements to reduce the temperature of the liquid, so that microorganism would be inactivated by ultrasound without thermal influences. As a large portion of the energy provided by the ultrasound oscillator ultimately dissipates as heat, it was necessary to prevent any undue increase in the temperature of the irradiated material.

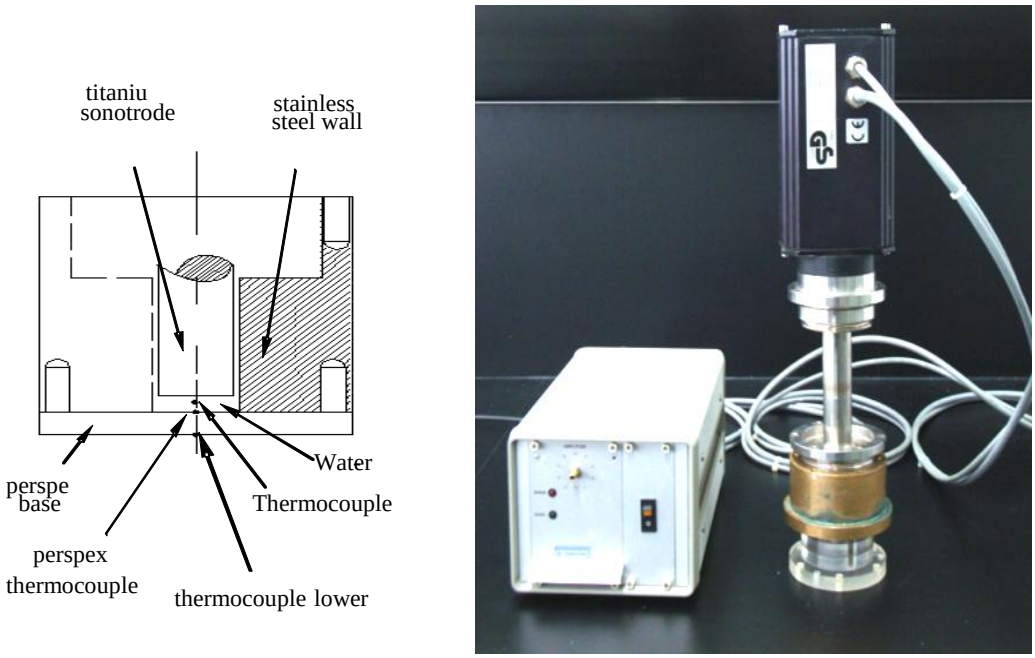

Fig. 3.1 Illustration of the ultrasonic processing cell for heat transfer experiments.

3.2.2 Experimental results

Measurements from the three thermocouples over a period of 5 min (300 s) are presented in Fig. 3.2. Time 0 in Fig. 3.2 corresponds to the point at which the ultrasonic processor was switched on. The temperature differences relative to the initial (pre-run) level are presented in Fig. 3.2. It is these differences in temperature that are necessary in the transient heat flux analysis. The initial temperatures indicated by each thermocouple were: T_w=15°C, T_{ps}= 17°C, and T_l= 18°C.

Two relatively large disturbances appeared on the signal from the water temperature thermocouple – the first at about 15 s and the second at around 140 s on the time scale in Fig. 3.2. The second of these disturbances has been removed from the signal presented in Fig. 3.2, and hence the data appears smooth in this region. These disturbances were attributed to thermocouple sensitivity from the ultrasonic treatment (causing microscopic cavitation bubbles). This disturbance did not affect the results of this test because only average water temperatures were required.

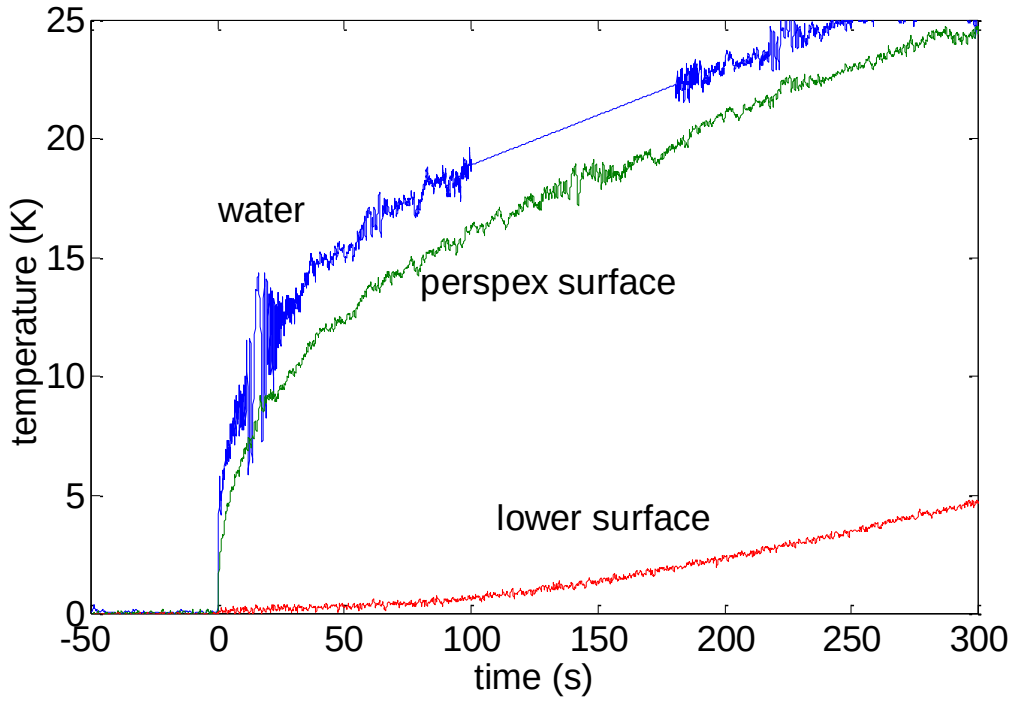

Fig. 3.2 Temperature measurements from thermocouples in the heat transfer experiment of water, upper and lower prespex surface.

3.2.3 Heat transfer analysis

3.2.3.1 Perspex surface

Provided the substrate into which heat is transferred can be regarded as semi-infinite, the surface heat flux can be identified from measurements of surface temperature (Carslaw and Jaeger, 1959). In the case of a flat surface without any lateral conduction effects, Schultz and Jones (1973) demonstrate that the appropriate expression is:

$$q = \frac{\sqrt{\rho c k}}{\sqrt{\pi}} \int_0^t \frac{dT_s}{d\tau} \frac{1}{\sqrt{(t-\tau)}} d\tau, \qquad 3.1$$

A numerical implementation of equation 3.1 has been used to identify the heat flux (q) to the surface of the perspex from the T_s results (in Fig. 3.3) for a certain period of time (τ). Approximate values for the perspex thermal properties of density,

specific heat and conductivity ρ, *c*, and *k* are presented in Table 3.1. Assuming the calculated value of heat flux applies across the entire perspex surface exposed to the water (an area of 531 mm^2), the heat transfer to the perspex surface can be obtained as illustrated in Fig. 3.3.

Table 3.1 Properties of materials used in the processing cell construction.

Material	ρ	c	k	α
	(kg/m^3)	(J/kgK)	(W/mK)	(10^{-6} m^2/s)
Perspex	1200	1450	0.2	0.11
Stainless steel	8300	470	13	3.3
Titanium	4500	520	22	9.4

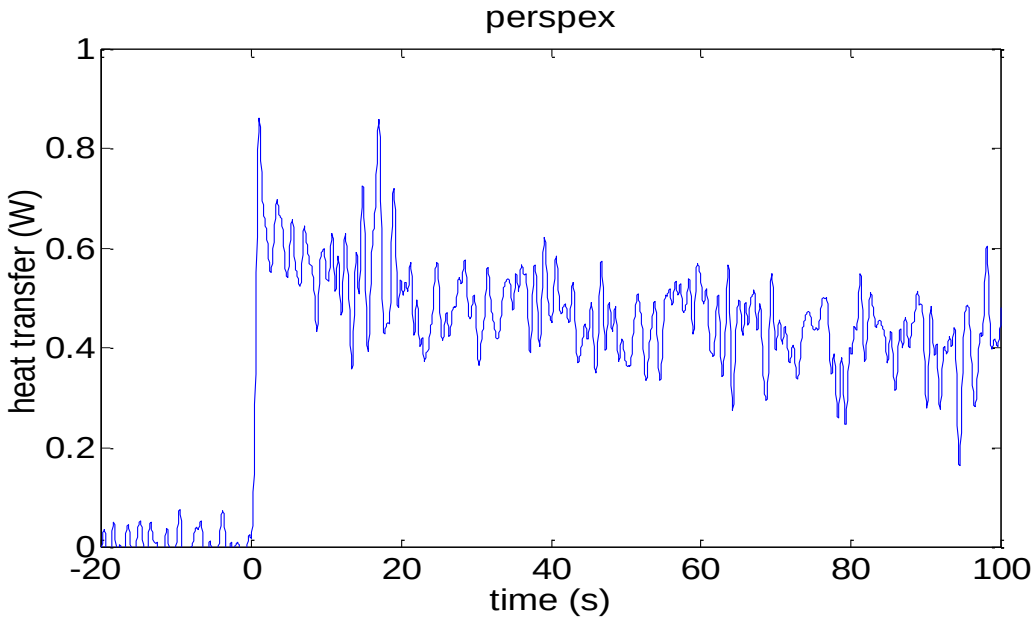

Fig. 3.3 Heat transfer to the Perspex in the heat transfer experiments.

From Fig. 3.2 a measurable increase in temperature at the lower surface of the perspex is apparent approximately 1 min after heating begins. This is to be expected since the thickness of the perspex was x = 12.7 mm and the thermal diffusivity of perspex (Table 3.1) was $\alpha = 0.11\times10^{-6}$ m^2/s, so that the heat penetration time (Schultz and Jones, 1973) is

$$t = \frac{x^2}{16\alpha} = 92 \text{ s.} \qquad 3.2$$

Thus, approximately semi-infinite conditions persist for about 100 s after the start of heating (the time at which the ultrasonic processor was switched on). Provided the induced flow and thermal transport conditions within the processing cell remain constant during the experiment, the surface heat flux should be proportional to the difference in temperature between the water and the surface,

$$q = h(T_w - T_s), \qquad 3.3$$

where h is convective heat transfer coefficient. Equation 3.3 was used in conjunction with the water and perspex surface temperature measurements and the perspex heat flux results from equation 3.3to estimate the heat transfer coefficient. Results from this analysis are presented in Fig. 3.4. Convective heat transfer coefficient data prior to the start of the ultrasonic processor is not meaningful and has not been included in Fig. 3.4. Likewise the data from around 15 s is contaminated by the large disturbance on the water thermocouple at this time and hence is also not included in Fig. 3.4.

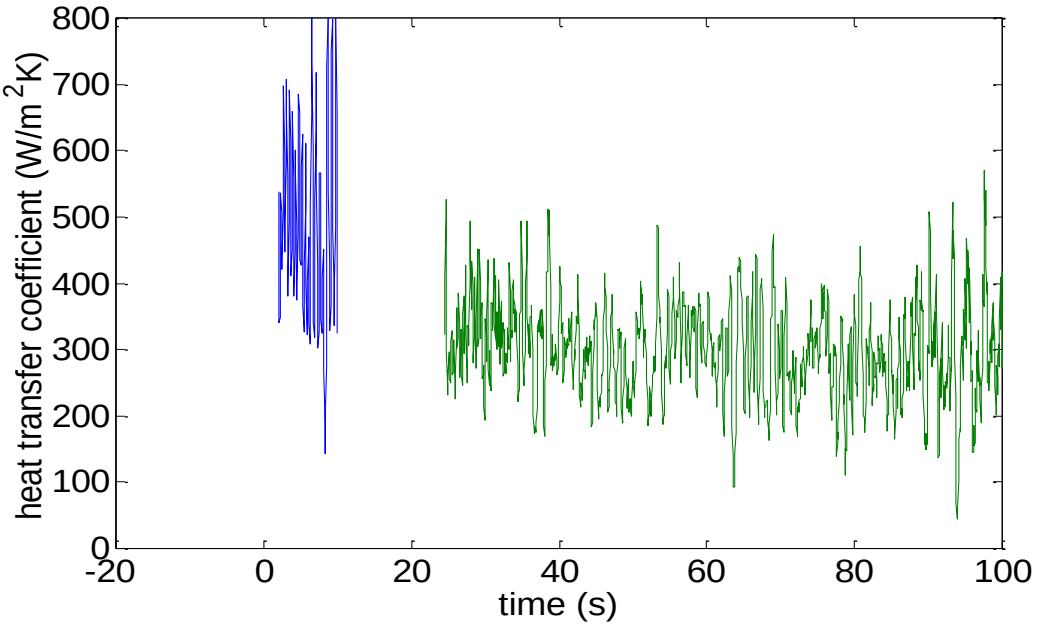

Fig. 3.4 Heat transfer coefficient at the Perspex surface from the heat transfer experiment.

From Fig. 3.4, it can be observed that the apparent heat transfer coefficient is not exactly constant, but steadily decreases from a value of approximately 500 W/m^{2}K at the start of heating to about 300 W/m^{2}K at a time 100 s after the start of heating. In this experiment, the water temperature changed by around 18°C in the first 100 s. The associated changes in viscosity and thermal conductivity would be around 30% and 5% respectively. Thus some variation in the heat transfer coefficient would be expected. Another effect that may contribute to the apparent variation in heat transfer coefficient is the fact that the ultrasonic processor may actually require a few minutes to reach a steady operating condition. Another factor that may contribute to the apparent variation in heat transfer coefficient with time is lateral conduction. Such effects have been assumed to be negligible. However, lateral conduction is likely to be present since there will be a heat flux-induced temperature difference between the perspex and the stainless steel.

3.2.3.2 Stainless steel surface

In the case of the vertical stainless steel wall which is a concave cylindrical surface, a convenient (approximate) expression for the relationship between the heat flux and the measured surface temperature is (Buttsworth and Jones, 1997)

$$q = \frac{\sqrt{\rho c k}}{\sqrt{\pi}} \int_0^t \frac{dT_s}{d\tau} \frac{1}{\sqrt{(t-\tau)}} d\tau + \frac{k}{2R}(T_s - T_i), \qquad 3.4$$

the Laplace transformation of equation 3.4 is,

$$\overline{q} = \sqrt{\rho c k}\,\sqrt{s}\,\overline{T_s} + \frac{k}{2R}\overline{T_s}, \qquad 3.5$$

where the over line denotes the Laplace transformation. Assuming the convective heat transfer coefficient is constant, the Laplace transformation of equation 3.5 is,

$$\overline{q} = h(\overline{T_w} - \overline{T_s}). \qquad 3.6$$

Subtracting equation 3.6 from equation 3.5 gives an expression for the surface temperature:

$$\overline{T_s} = G(s)\overline{T_w}, \qquad 3.7$$

with the transfer function between the water temperature and the surface temperature given by

$$G(s) = \frac{h}{\sqrt{\rho c k}} \frac{1}{\sqrt{s} + a}, \qquad 3.8$$

where,

$$a = \frac{k + 2Rh}{2R\sqrt{\rho c k}}. \qquad 3.9$$

The inverse Laplace transformation of equation 3.8 is

$$g(t) = \frac{h}{\sqrt{\rho\, c k}} \left(\frac{1}{\sqrt{\pi\, t}} - a e^{a^2 t} \operatorname{erfc}(a\sqrt{t}) \right). \qquad 3.10$$

The surface temperature history can therefore be obtained from equation 3.7 using the convolution integral,

$$T_s = \int_0^t g(\tau) T_w(t - \tau) d\tau. \qquad 3.11$$

No thermocouple was located on the stainless steel surface. However, the surface temperature history can be estimated using equation 3.11 if the heat transfer coefficient on the stainless steel is assumed to be constant and equal to the heat transfer coefficient measured at the perspex surface. This assumption is reasonable and acceptable as shown in Fig. 3.4. The constant value adopted for the convective heat transfer coefficient was h = 500 W/m^{2}K. The derived surface temperature history for the stainless steel is presented in Fig. 3.5.

Having estimated the stainless steel surface temperature history (Fig. 3.5), the surface heat flux can be calculated using equation 3.1. Heat transfer to the stainless steel as determined with this method is presented in Fig. 3.6. As was the case with the perspex results in Fig. 3.3, the heat flux results (expressed in W/m^2) have been

scaled by the relevant surface area (1633 mm^2 in this case) for presentation in Fig. 3.6.

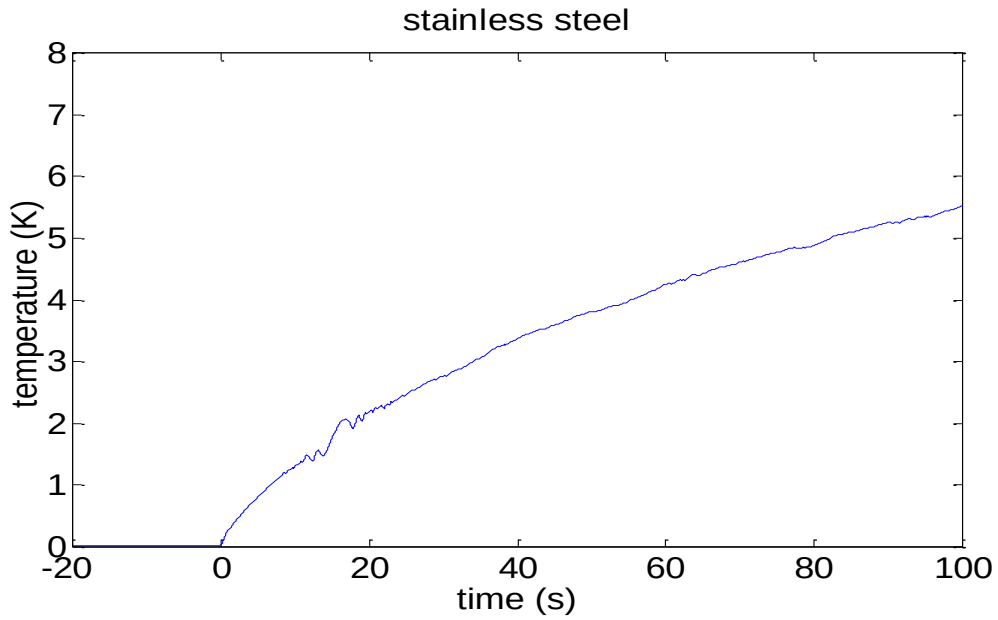

Fig. 3.5 Assumed surface temperature of the stainless steel in the heat transfer experiments.

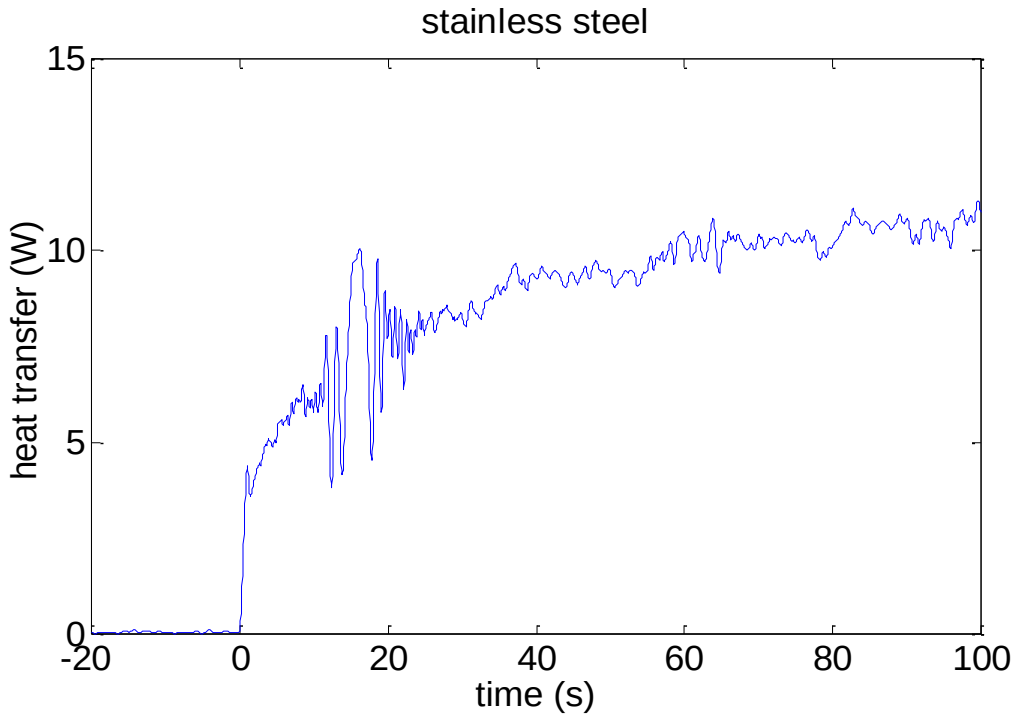

Fig. 3.6 Heat transfer to the stainless steel deduce from the heat transfer experiment.

Limitations of the above analysis include the approximate nature of equation 3.3 which produces results within 1% of the actual solution for heating times such that $\frac{\alpha t}{R^2} \approx 0.1$, according to Buttsworth and Jones (1997).

3.2.3.3 Titanium surface

Heat transfer to the titanium surface (the sonotrode tip) can be estimated using the analysis outlined in the previous section. Slight adjustments to the analysis in 3.3.3.2 needs to be made to accommodate the fact that the titanium is a flat surface ($R \to \infty$) with significantly different thermal properties to the stainless steel (see Table 3.1). When this is done, the resulting heat transfer across an area of 380 mm^2 (the area of the sonotrode) is obtained as presented in Fig. 3.7.

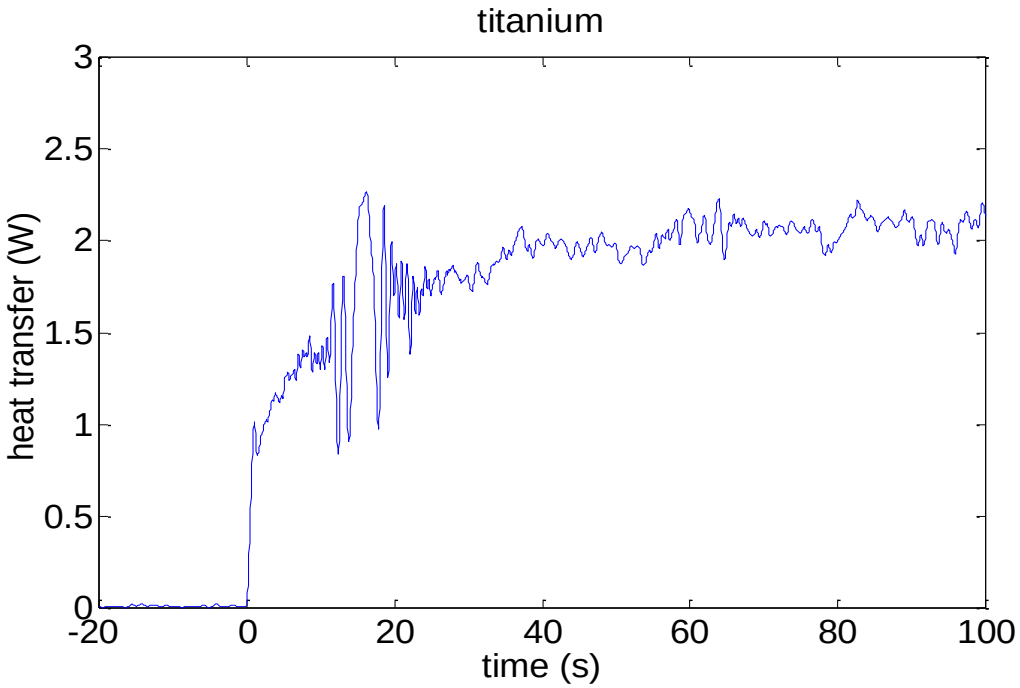

Fig. 3.7 Heat transfer to the titanium deduced from the heat transfer experiment.

3.2.5 Discussion and conclusion

Due to the transient nature of the present experiments, the heat transfer to the surfaces of the processing cell varies with time. To obtain some indication of relative

magnitudes, the time 100 s after the start of the ultrasonic processor is considered. At this point, the heat transfer to the perspex, stainless steel, and titanium surfaces is approximately 0.4, 11, and 2.1 W respectively. Thus the combined heat transfer from the water is 13.5 W of the applied ultrasonic power.

A transient one dimensional heat conduction modelling has been applied to evaluate the heat transfer to the surfaces of an ultrasonic processing cell. The processing cell was filled with water and instrumented with thermocouples. Ultrasonic power at 20 kHz and approximately 85 W was applied for a few minutes and temperature histories were recorded. Estimates for the current configuration suggested that less than 15.9 % of the applied ultrasonic power was removed from the processing volume in the form of heat. Such heat transfer can have a significant impact on efficiency calculations for the ultrasonic processor based on calorimetric experiments in this and related configurations. The 15.9 % lost was considered in the subsequent experimental work of this chapter where the net ultrasound power dissipated in the suspension was evaluated. One of the limitations of the present data and analysis is that the heat transfer coefficient appears to vary with time, however the variation was not very significant and the impact on the final heat transfer result was marginal. The modelling deficiencies such as the semi-infinite one dimensional heat conduction assumption, may also contribute to the apparent variation with time.

3.3 Mixing characterization within the ultrasonic processing cell

3.3.1 Introduction

To adequately assess the potential of high power ultrasound in the present application, it is necessary to have some knowledge of the uniformity of the treatment. To achieve uniform ultrasound treatment for yeast in the suspension, a theoretical and experimental mixing investigation was conducted in this work. Evaluating the mixing time is a very important factor to confirm that the yeast cells in the suspension are subjected to uniform ultrasound energy.

The flow field established within a high power ultrasound processor has a critical influence on the uniformity of treatment. The intensity of the acoustic field varies with position relative to the ultrasound source (Pugin, 1987) and strong acoustic streaming (Lighthill, 1978) can be established within the processing volume which convects the fluid into or out of the high intensity treatment regions.

For uniform treatment in a batch reactor arrangement, the characteristic mixing time within the vessel should be small, relative to the treatment time. Cadwell and Fogler (1971) measured the rate of CO_2 absorption by glycerol in a batch reactor with and without ultrasonic agitation. They related the enhanced absorption with ultrasound to a surface renewal effect associated with the vortex structures they observed in batch configurations with 20 kHz and 800 kHz agitation. Vichare et al. (2001) analysed conductivity measurements in a sonochemical batch reactor to yield mixing time results for different geometric configurations.

For continuous flow systems, the treatment uniformity (or lack thereof) can be characterized using a RTD (e.g., see Levenspiel et al., 1999). There are many standard techniques for the measurement of RTDs which usually involve introducing a trace element (such as a saline solution or a dye) at the entrance to the processing device and measuring the concentration of the tracer just downstream of the vessel (Levenspiel et al., 1999; Missen et al., 1999; Fogler, 1999). Measurements of the RTD in ultrasonic processing configurations have been performed using such tracer methods (Gondrexon et al., 1998; Monnier et al., 2000).

In the work of Gondrexon et al. (1998), a NaCl tracer pulse was injected into the inlet stream entering their ultrasonic cell. The RTD was identified by monitoring the conductivity within the outlet pipe. Over the tested range of ultrasonic powers and reactor flow rates, the reactor behaved as a continuous stirred-tank reactor (CSTR). Similarly Monnier et al. (2000) characterised macromixing in their continuous flow ultrasonic reactor by injecting KCl in the inlet and monitoring conductivity in the outlet for different ultrasonic powers and flow rates. In contrast to the arrangement of Gondrexon et al. (1998), the configuration of Monnier et al. (2000) had a characteristic performance between that of a plug flow reactor and a CSTR. For

continuous flow arrangements, there are established methods for estimating an effective turbulent diffusivity or as a non-dimensional parameter, the vessel dispersion number, based on an appropriate dispersion model and the measured RTD (Levenspiel et al., 1999; Missen et al., 1999; Fogler, 1999).

However, the introduction of the injection and detection hardware into the system can add a substantial volume which distorts the Residence Time Distribution (RTD) (Monnier et al., 2000). Ideally, the actual input to the system should be measured or at least quantified in some manner so that deviations from the ideal impulse or step inputs can be accommodated if necessary through appropriate analysis of the tracer concentration histories (Levenspiel, 1999). However, even if such measurements are made, the mixing that takes place as the flow enters and leaves the processor can make a significant contribution to the apparent RTD (Fogler, 1999). That is, if significant mixing takes place either side of the important reaction or treatment zone, then it will be difficult to identify the actual mixing that takes place within the treatment zone.

The technique introduced in this work avoids the difficulties in determining the true RTD by (i) considering the case of an ultrasonic batch reactor arrangement, and (ii) visualizing the mixing process within the high power treatment zone itself. The mixing results are interpreted with the aid of a one dimensional diffusion analysis to yield effective values of turbulent diffusivity. If a geometrically similar continuous flow configuration is adopted, the effective turbulent diffusivity should remain unchanged at each power level provided the through put of material contributes minimal mixing energy.

3.3.2 Apparatus, methods, and calibration

3.3.2.1 Ultrasonic processor and mixing experiments

The ultrasonic processor used was a commercial device with a 22 mm diameter probe tip (sonotrode, BS20d22 titanium), operating at a frequency of 20 kHz. The general arrangement of the apparatus used in the experiments is illustrated in Fig.

3.8. Mixing experiments were conducted using a 50 mL Pyrex beaker (internal diameter of approximately 36.5 mm) filled with 30 mL of water and the probe tip immersed to a depth of 7 mm. The water was tap water with no special treatment. The relative position of probe tip within the beaker of water is shown in Fig. 3.8. The probe tip is actually uniform in diameter; the apparent increase in the probe diameter in the submerged regions in Fig. 3.9 is due to refraction. The probe tip is approximately 22 mm from the bottom of the beaker.

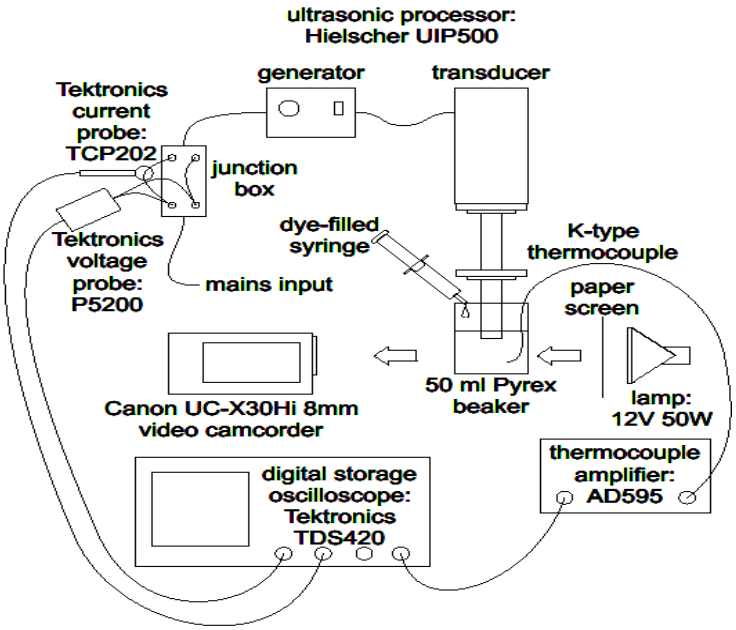

Fig. 3.8 Experimental apparatus used in the mixing experiment.

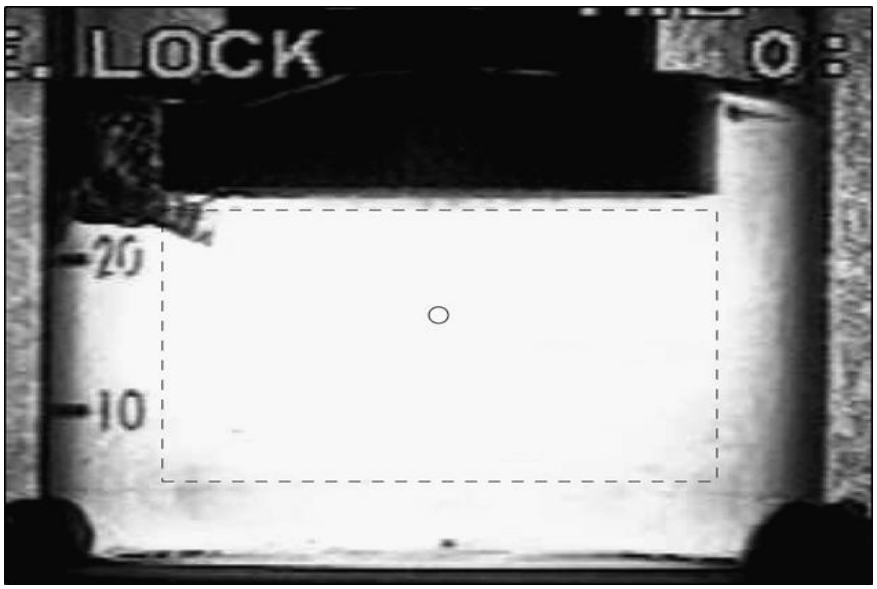

Fig. 3.9 Image of the probe tip and beaker used in mixing experiments.

With the water stationary in the beaker and the system at a uniform initial temperature of approximately 20 ^{o}C, the ultrasonic processor was switched on. After approximately 5 s, a drop of blue food colouring (volume around 0.01mL) was injected into the water and proceeded to mix under the agitation of the ultrasonic processor. The mixing process was imaged using a Canon UC-X30Hi 8 mm video camcorder and recorded directly onto VHS tape. Mixing sequences were digitised from the VHS recordings using Pinnacle hard/software and a sequence of around 40 images was saved in jpeg format.

The beaker was back-lit with a 12 V 50 W halogen bulb with DC excitation. The light from the bulb was made somewhat diffuse by placing paper towel between the bulb and the beaker. This relatively high intensity lighting allowed the exposure on the video camera to be manually set to the minimum possible: 1/10,000th of a second. The framing rate remained at the standard 1/25th of a second, but the development of mixing was clearly captured because of the short expose time for each frame. The camera iris was also set manually to avoid the camera automatically adjusting the exposure during the experiments.

Five different amplitude level settings on the ultrasonic generator were tested: 20, 40 60, 80, and 100%. These values correspond to the markings on the dial of the ultrasonic generator, and these values are not related in a linear manner to the electrical power drawn by the generator or the thermal energy dissipated in mixing volume.

3.3.2.2 Input electrical power

The electrical power delivered to the ultrasonic generator from the AC mains (240V, 50Hz) was identified by recording the voltage and current signals on a Tektronics digital storage oscilloscope (TDS420A) as illustrated in Fig. 3.8. The voltage and current data was recorded at a rate of 10 kSamples/s giving around 200 samples per AC cycle. Data was transferred to a PC for analysis.

The instantaneous electrical power delivered to the generator varied through the AC cycle, so results derived from this equation were averaged over the period of each AC cycle. Results from this analysis for three of the five power level settings are shown in Fig. 3.10 for the first few seconds of operation after switch-on.

The electrical power delivered to the generator approaches a steady-state condition after about 1 s of operation. The results in Fig. 3.10 established that the droplet addition should take place after at least one second of processor operation to ensure steady input of electrical power. Results in Fig. 3.10 are also relevant to the analysis of the thermocouple signal, the first second of operation should be avoided in the calorimetric analysis due to the unknown power delivery by the sonotrode during the start-up transients.Fig. 3.11 shows the variation in electrical power input to the ultrasonic generator with the dial settings. Although the minimum dial setting on the generator was around 26%, it is certainly not 26% of the maximum electrical power input under these conditions. The vertical bars associated with each data point in Fig. 3.11 correspond to a variation of ±2% which is representative of the measured variability associated with manually setting the control dial.

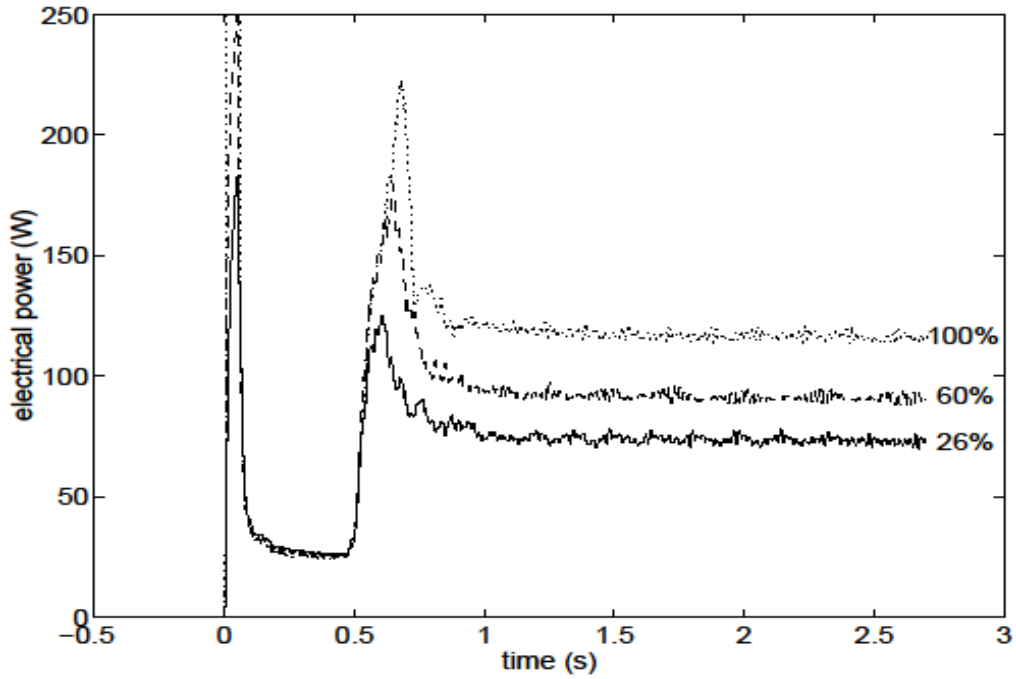

Fig. 3.10 Variation of input electrical power during start-up of the ultrasonic processor in the mixing experiments.

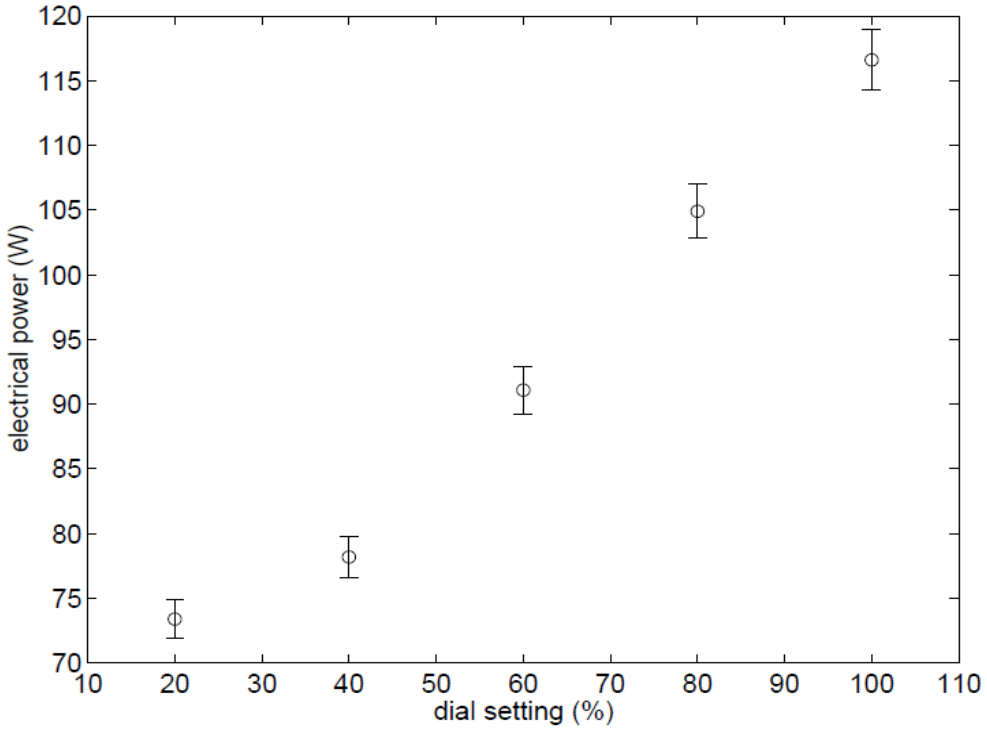

Fig. 3.11 Steady state input electrical power for the five dial settings up of the ultrasonic processor in the mixing experiments.

3.3.2.3 Thermal dissipation

To confirm the amount net energy dissipated into the suspension, and confirm the results obtained from the heat transfer work (section 3.2), an additional energy experiment was conducted.

To establish the rate of thermal energy dissipation in the water, separate experiments were performed in which a bare wire K-type thermocouple (wire diameter approximately 0.2 mm) was inserted approximately 5 mm from base of the Pyrex beaker, near the centre. The thermocouple signal was amplified using an AD595 chip with the 'cold junction' being formed on the printed circuit board. The voltage signal from the amplifier was recorded using the TDS420A digital storage scope as illustrated in Fig. 3.8.

The thermocouple and amplifier circuit was calibrated using a water bath and a mercury-in-glass thermometer as the reference from approximately 20 ^{o}C to 50 ^{o}C.

Even using this calibration, the absolute temperatures from the thermocouple and amplifier are probably still not accurate to better than 1 ^{o}C. However, absolute values of temperature are not required; only temperature changes are of interest for the calorimetric analysis. Thus, for the temperature changes of a few ^{o}C that are observed in the experiments, it is estimated that the measured temperature changes are accurate to within 5%.

Calorimetric experiments were performed at the five power level settings (26, 40, 60, 80 and 100%) and experiments were repeated using different volumes of water (20, 30, 40, and 50 mL) in the Pyrex beaker. A few seconds after processor switch-on, the measured variation of water temperature with time was approximately linear. However, there was some tailing-off of the temperature rise which was noticeable after about 30 s, presumably due to heat loss from the water to the beaker and probe.

The thermal energy that is dissipated by the water can be estimated using the following equation

$$P_{thermal} = mc\frac{dT}{dt} \qquad 3.12$$

where m is the mass of the water in the beaker, c is the specific heat capacity of the water (taken as 4200 J/kgK for this analysis), and dT/dt is the rate of temperature change identified from a linear regression to the data between 5 and 20 s after processor switch-on. The thermal dissipation estimated in this manner for each power level is presented in Fig. 3.12. The horizontal bars associated with each data point represent the ±2% variability in the manual setting of the generator, and the vertical bars represent the variation in the results for the four different water volumes that were tested. There was no consistent variation in the results across the four water volumes that were used in these experiments. The thermal dissipation indicated in Fig. 3.12 will underestimate the actual thermal dissipation of ultrasonic energy because of heat losses to the beaker and the probe tip.

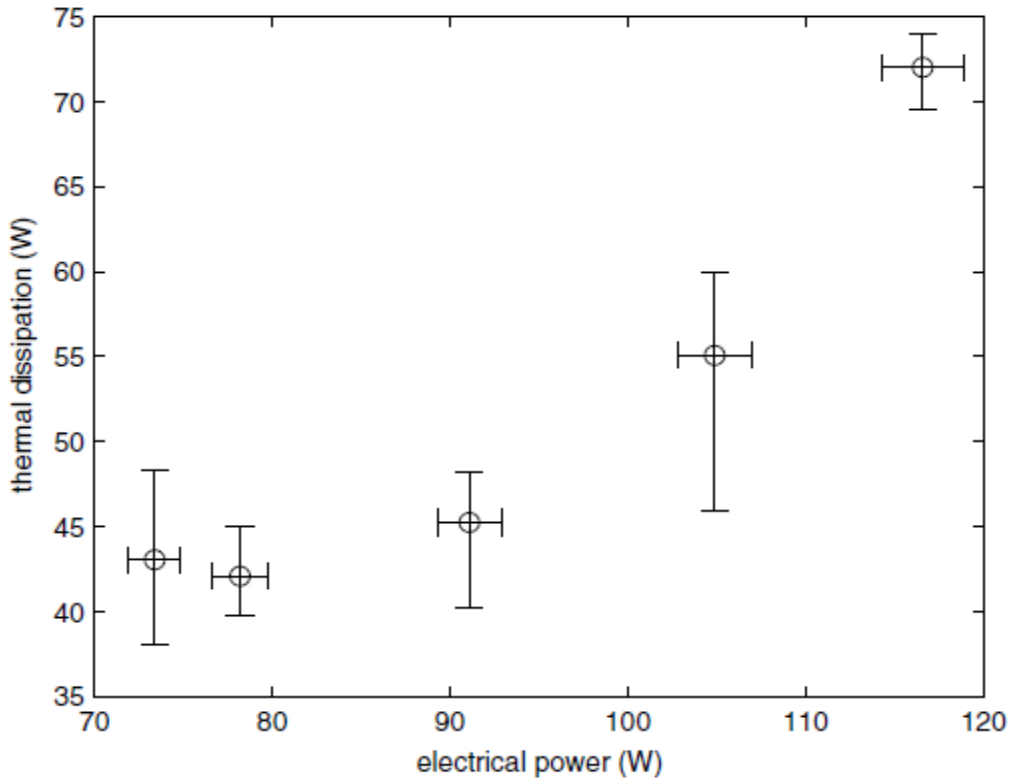

Fig. 3.12. Rate of thermal energy dissipation for the five levels of input electrical power on the ultrasonic process in the mixing experiments.

3.3.2.4 Image calibration

The saturation component of the video images was used in the analysis of the mixing process. Fig. 3.13 presents a typical calibration of the saturation component with the dye concentration in normalised scales. The different lines in this figure correspond to different locations within the image for the same variation in dye concentration. The normalisation is such that a concentration of 0.0 indicates no dye, and 1.0 corresponds to the fully-mixed dye concentration. A saturation of 0.0 corresponds to the level when no dye is present and a value of 1.0 corresponds to the fully-mixed dye value. A concentration of 0.9 was used to define the mixing time in the subsequent analysis and this corresponds to a normalised saturation of approximately 0.97, Fig. 3.13.

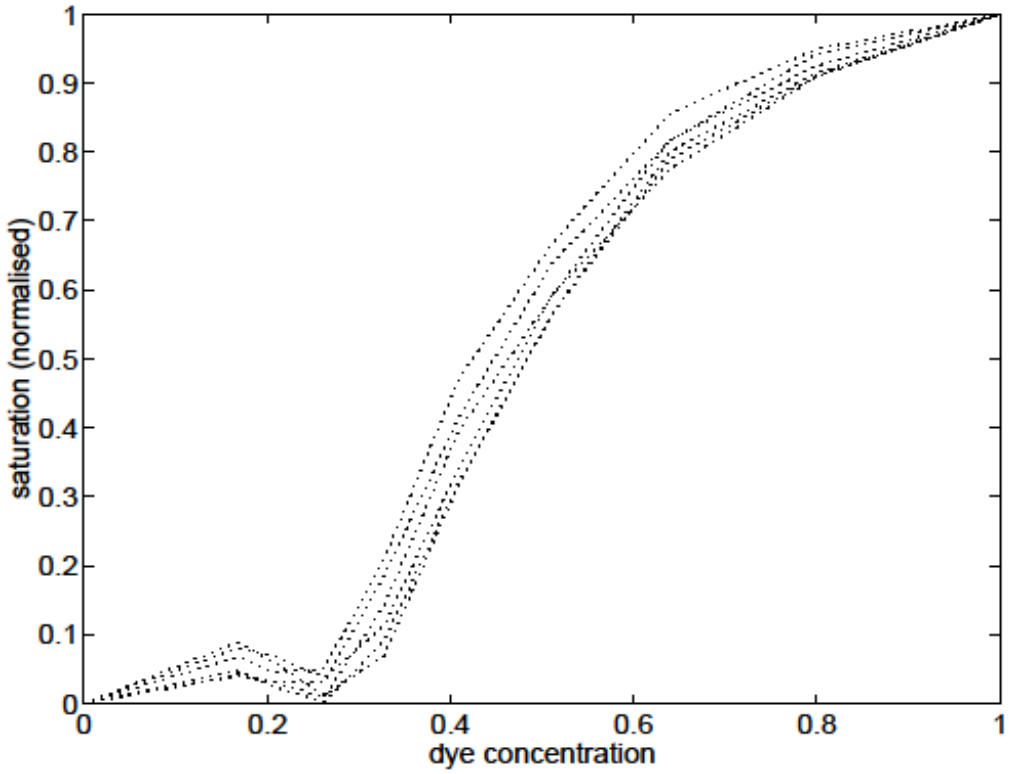

Fig. 3.13 Normalised saturation component of the video image as a function of dye concentration for different positions within the image in the mixing experiment.

3.3.2.5 RTD experiments

To demonstrate that results from the mixing experiments in the batch reactor arrangement can be used to deduce a residence time distribution (RTD) in a similar continuous flow configuration, an additional experiment was performed. The arrangement for this experiment consisted of a processing geometry similar to that of the Pyrex beaker with the addition of inlet and outlet pipes as illustrated in Fig. 3.14.

The flow rate through the system was 4.7 mL/s and the inlet and pipe diameters were 2 mm. The diameter of the processing volume was 37.5 mm and the volume of water in the processing volume was 31 mL. The vertical distance from the centre of the inlet pipe to bottom of the processing volume was 28.5 mm.

A droplet of saline solution was added at the top surface of the water, in a manner similar to that of the dye mixing experiments, and the injection timing was detected with a pair of electrodes positioned between the saline dropper outlet and the surface

of the water. The recirculating arrangement was adopted as a convenient way to ensure the water level in the treatment volume remained constant. The volume of the pipe work and pump was designed so that saline tracer did not enter through the inlet to the processing volume on the times scales of interest in the determination of the RTD of the ultrasonic processing arrangement. Ice bath cooling of the recirculating water resulted in a steady state operating temperature slightly below room temperature.

Detection of the saline arrival in the outlet pipe was achieved using a pair of electrodes as illustrated in Fig. 3.14 and the voltage (V_{out}) was recorded on the Tektronics TDS420A oscilloscope at a sample rate of 1.0 kSample/s. The electrodes in the outlet pipe were gold plated with a diameter of 1.4 mm and were separated axially by 3.5 mm between centres. The outlet pipe diameter at the location of the electrodes was 3mm. Calibrations of the detection system indicated that V_{out} varied with saline concentration in a linear manner (estimated maximum error of 5%) for the present experiment. A thermocouple was positioned in the processing volume near the outlet pipe and both the experiment and the linearity calibration were performed when the system reached the steady state operating temperature of 16.1 ^{o}C.

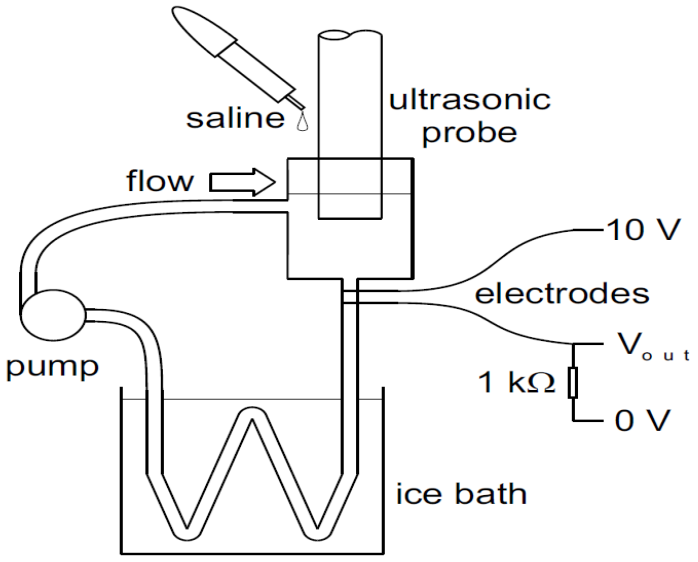

Fig. 3.14 Illustration of arrangement used for characterising RTD in the mixing experiments.

3.3.3 Mixing results and analysis

Fig. 3.15 presents a sequence of images showing the initial stages of dye mixing for the 26% setting and the dye injected from the top left as represented in Fig. 3.8. For each power setting, two experiments were performed: one with injection at the top left, the other with injection at the top right. The sequence in Fig. 3.15 illustrates the acoustic streaming commonly observed in ultrasonic experiments. The frame in which the droplet first appears is taken as corresponding with the time of zero seconds.

To identify the mixing time, a specific window within the image was identified as illustrated by the broken line in Fig. 3.9. The rays within this broken line on the image have passed through approximately 50% of the total liquid volume. Note that refraction effects give the illusion that the rectangular prism represented by the broken line encapsulates more than 50% of the liquid volume. The central circle in Fig. 3.9 identifies the location of the ray passing through approximately the centre of the total volume of the liquid.

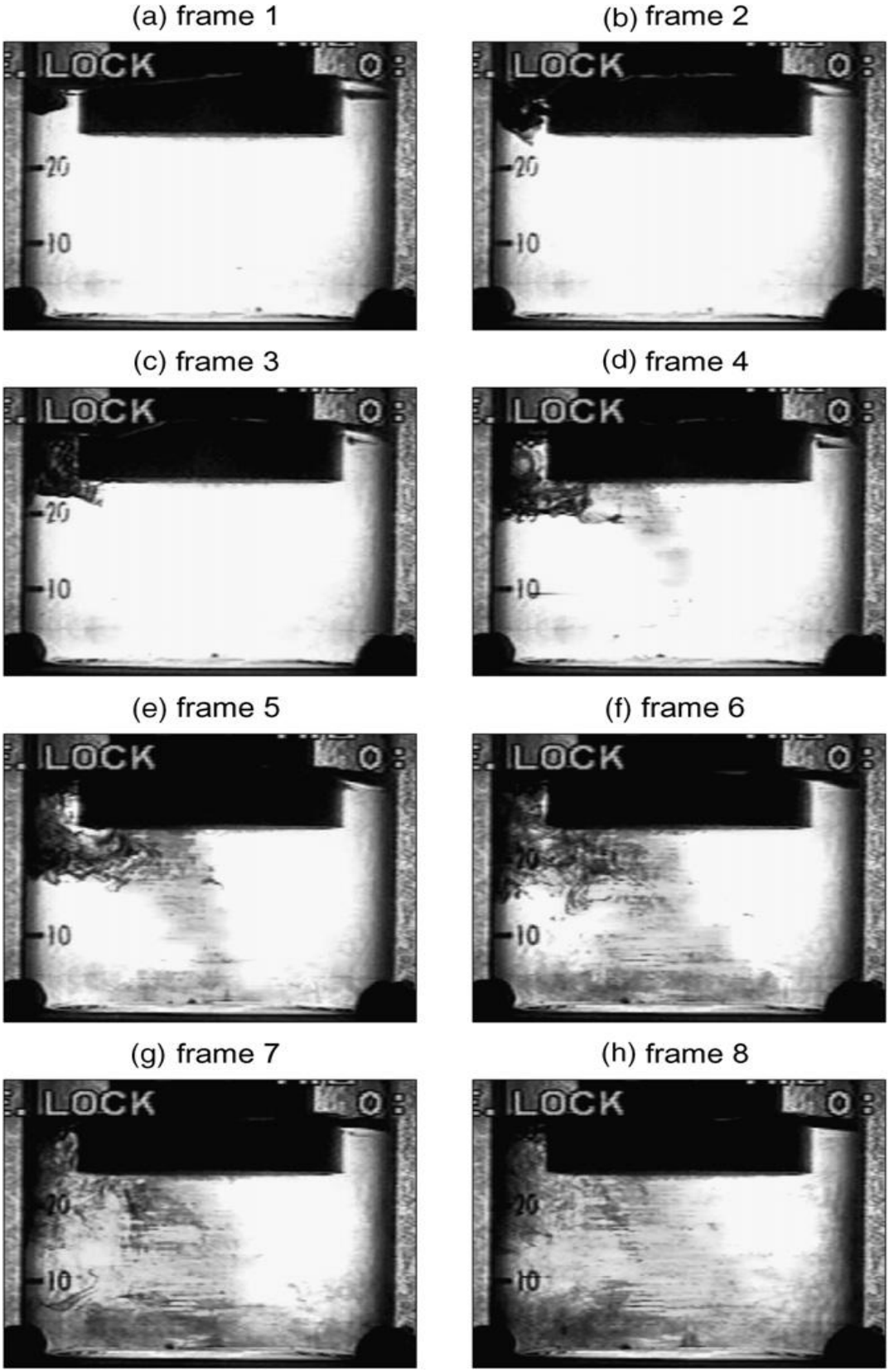

Fig. 3.15 A sequence of video frames showing the development of mixing for the 26% setting with dye injection on the left. Frame 1 which corresponds to a time of 0 s, shows the die droplet having just entered the water.

The saturation component at each pixel of each digitized image was normalised using frames taken prior to the droplet addition and images taken after complete mixing was achieved (when there was no further change in the saturation component of each pixel with time). The normalised saturation of each pixel generally varied between 0.0 (corresponding to no dye) and 1.0 (corresponding to the final or fully mixed dye concentration). However, for pixels close to the injection point, transient values larger than 1.0 were registered soon after injection due to the presence of high dye concentrations at these locations and times. Fig. 3.16 presents the variation in normalised saturation averaged over the window identified in Fig. 3.9 for the two droplet injection locations and the 26% power setting. The open symbols in this figure indicate the time at which the normalised saturation reaches a value of 0.97, which, according to the calibration should correspond to an average concentration of approximately 0.90.

Times to reach an average concentration of 0.90 within the 50% volume window were identified for the other power levels in the same way and Fig. 3.17 presents these results. The vertical bars in Fig. 3.17 give the time limits identified from the two different experiments (droplet injection at the top left and top right), and the horizontal bars represent the uncertainty in setting the power level. As expected, the higher power levels produce more rapid mixing. Within the range of powers investigated, and given the uncertainties in the experimental data, the linear regression (the broken line in Fig. 3.17) provides a reasonable representation of the data.

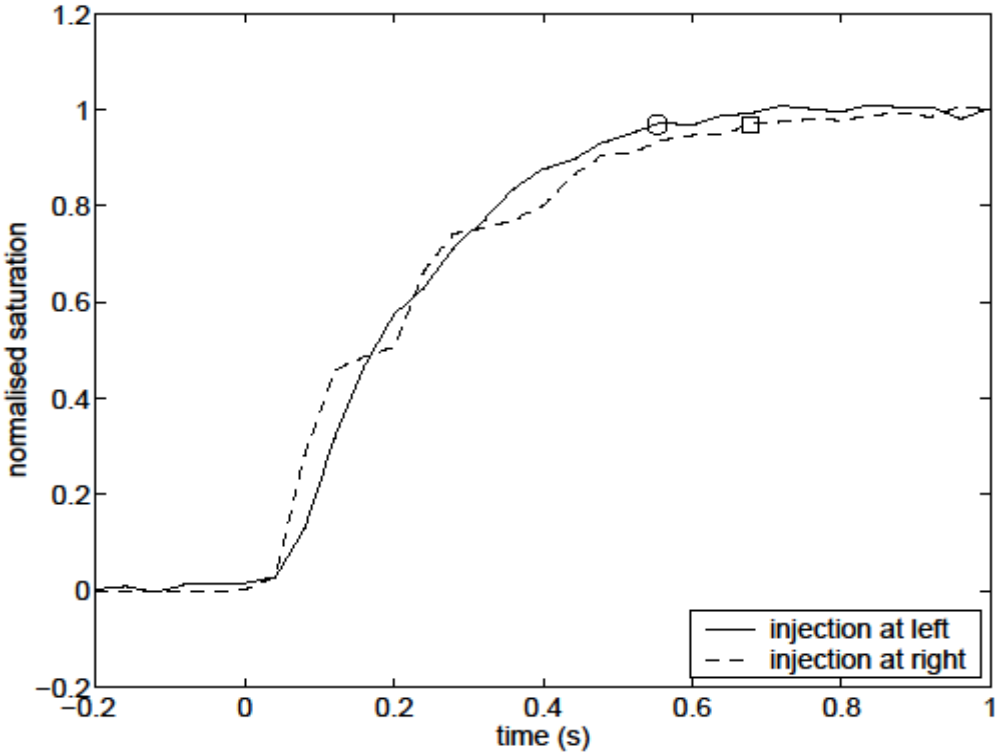

Fig. 3.16 Variation of saturation as a function of time for the 26% setting for the two different injection positions. The open symbols indicate the time at which the normalised saturation reaches 0.97.

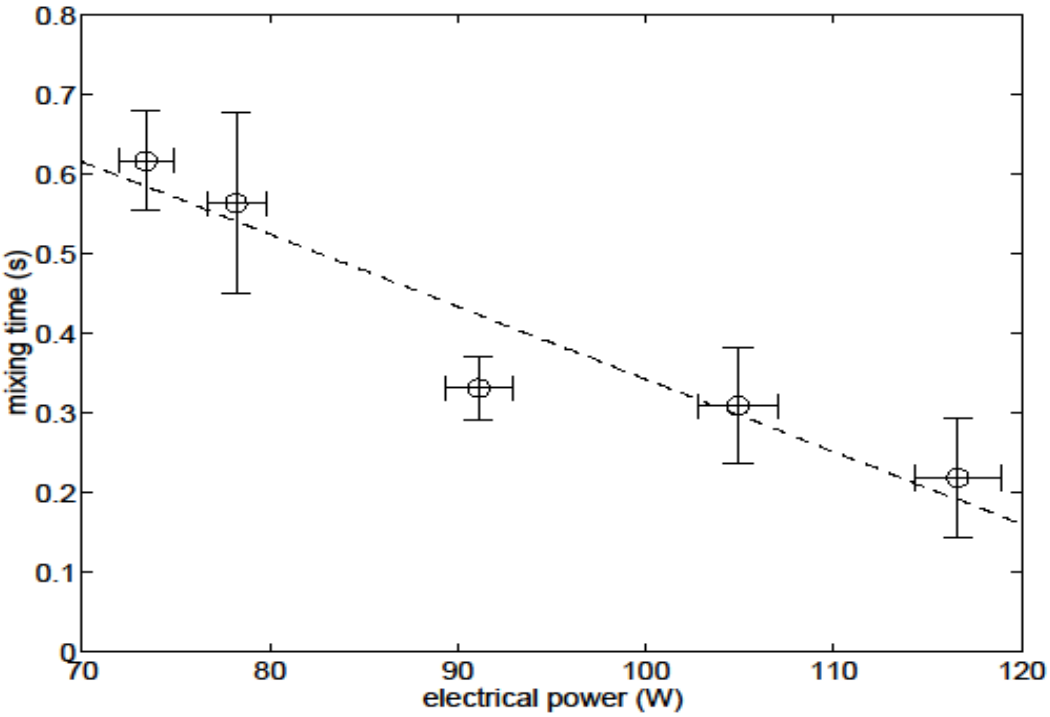

Fig. 3.17 Time to reach a 90% concentration in the 50% volume region (the mixing time) for the five levels of input electrical power. The broken line represents the linear regression for the data.

3.3.4 One dimensional diffusion analysis

The results presented in Fig. 3.17 are sufficient for the characterization of mixing in this particular ultrasonic batch reactor. Considering the one-dimensional diffusion equation of 3.13 for the dye concentration C,

$$\frac{\partial C}{\partial t} = D\frac{\partial^2 C}{\partial^2 x^2} \qquad 3.13$$

Where *x* is the distance, t is the time, and D diffusivity. The appropriate boundary conditions for this equation are,

$$\frac{\partial C}{\partial t} = 0, \qquad 3.14$$

when $x = 0$ (the location nearest the dye injection location), and $x = l$ (the furthermost point from the injection location within the volume). That is, the dye cannot enter or leave the volume during the mixing process ($t > 0$). If the initial distribution of dye concentration is,

$$C = f(x) \qquad 3.15$$

at the time the droplet enters the water ($t = 0$), then the solution of equation 3.13 is (Carslaw and Jaeger, 1959),

$$C(x,t) = \frac{1}{l}T\int_0^l f(x')dx' + \frac{2}{l}\sum_{n=1}^{\infty} e^{-Dn^2\pi^2 t/l^2}\cos\frac{n\pi x}{l}\int_0^l f(\acute{x})\cos\frac{n\pi \acute{x}}{l}d\acute{x} \qquad 3.16$$

Equation 3.16 is presented graphically in Fig. 3.18 for different positions within the limits of the volume. The concentration in Fig. 3.18 is non-dimensional and the normalisation was the same as that adopted in the experiments; the time is likewise a non-dimensional parameter Dt/l^2. The time at which the non-dimensional concentration reaches the value of 0.9 is clearly a strong function of position. For

example, at a location x/l = 0.25, the concentration reaches 0.9 at $Dt/l^2 = 0.00802$ and then overshoots the steady state value, while at x/l = 0.75 (further from the point of injection), the concentration does not reach 0.9 until $Dt/l^2 = 0.268$ (beyond the range shown in Fig. 3.18). It is worth noting that Fig. 3.18 indicates the concentration history averaged over the central 50% of the volume reaches a concentration of 0.9 at Dt/l2 = 0.644 (as indicated by the open symbol) and this is slightly ahead of concentration history at precisely the centre of the volume (compare the solid line with the nearby broken line in Fig. 3.18).

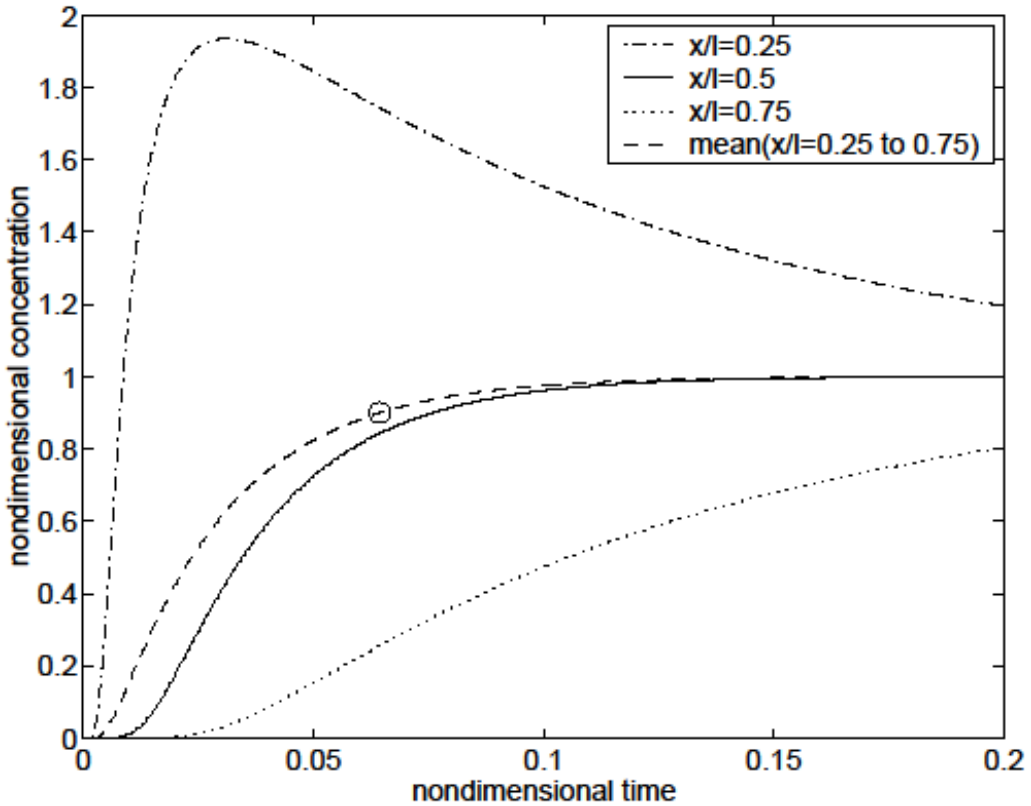

Fig 3.18 One-dimensional diffusion model results. The open symbol indicates the time at which the normalised concentration reaches 0.90 for the centred 50% volume case.

Taking l = 45 mm which is the largest distance across the volume, the effective diffusivity can be identified from $D = 0.644l^2/t$, where t is the mixing time to reach a concentration of 0.9 in the identified volume. The results of this analysis are presented in Fig. 3.19. The vertical and horizontal bars correspond directly with those in Fig. 3.17. Again, within the range of powers investigated, and given the

uncertainties in the experimental data, the linear regression (the broken line in Fig. 3.19) provides a good representation of the data.

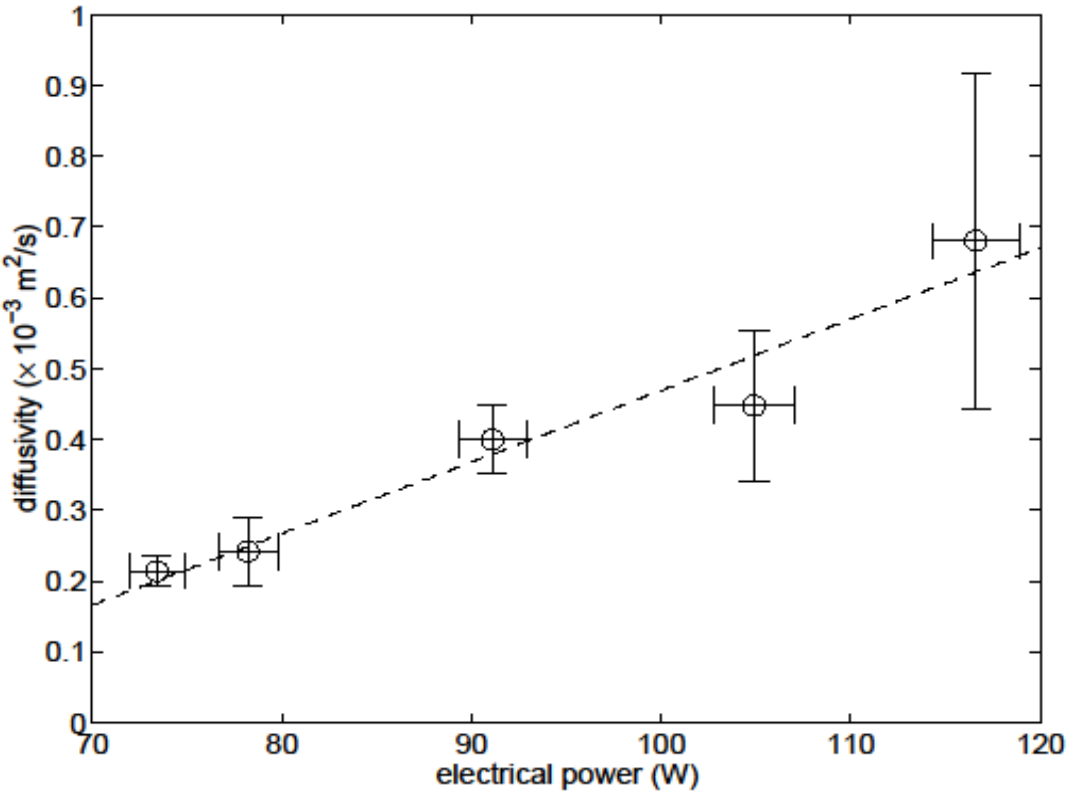

Fig 3.19 Diffusivity over the range of input electrical powers based on the mixing time data and the one-dimensional diffusion analysis. The broken line represents the linear regression for the data.

If these results were applied to a geometrically similar continuous processing arrangement with the inflow delivered to the cell via a relatively small diameter pipe, then an appropriate dispersion model for estimating the RTD might be either the closed-closed or closed-open model (Missen et al., 1999) depending on the flow outlet arrangement. For example, in the arrangement used in Monnier et al. (2000), where the flow enters the cell via a relatively small diameter (3 mm) pipe positioned below the probe tip and passes out of the high intensity region along the probe shank, the appropriate dispersion model is perhaps the closed-open one. The effective diffusivity identified above could be applied directly in such a dispersion model provided the fluid through put does not substantially alter the cell mixing characteristics. Certainly the RTDs measured by Monnier et al. (2000) display the requisite elements of such dispersion models. However as mentioned previously, such RTDs may not be a true reflection of the mixing in the high intensity ultrasound

region beneath the probe tip because of distortions that arise due to additional mixing in the injection and detection cells.

3.3.5 RTD results

An experiment was performed to validate the claim that the diffusivity identified in the batch mixing arrangement can be used in estimating the RTD of a geometrically similar continuous processing arrangement. The adopted arrangement was described in section 3.3.2.5, and the ultrasonic generator was operated at the lowest power setting. The results from this experiment are presented in Fig. 3.20. Care was taken to ensure that the introduction of the injection and detection systems would have minimal impact on the mixing characteristics of interest. The origin of the time axis in Fig. 3.20 corresponds to the time at which the saline drop entered the water as identified from the injection timing electrodes.

The boundary conditions for this processing arrangement are best approximated as closed-closed since there was minimal mixing across the inlet and outlet. In the case of closed-closed boundary conditions, analytical solutions for the governing equation are not available, although graphical representations for certain values of D/uL are presented in many texts (eg, Levenspiel, 1999; Fogler, 1999), where D is the diameter, u is the velocity, and L is the length.

The diffusivity for the lowest power setting identified from the mixing experiments and the one dimensional analysis was approximately 0.22×10^{-3} m^2/s (Fig. 3.19). For the flow rate of 4.7 mL/s and a volume diameter of 37.5 mm, the average flow speed in the vertical direction was u = 4.27 mm/s. The vertical distance from the inlet to the outlet pipe was L = 28.5 mm. Therefore, based on the previously presented mixing results and the current operating conditions the vessel dispersion number for this case is estimated as D/uL = 1.8. The comparison between the experimental RTD result and the theoretical simulation using the dispersion equation and closed-closed boundary conditions (Fogler, 1999) is shown in Fig. 3.20. For the experimental results, the non-dimensional time t/t_m is the actual sampling time t divided by the

mean residence time t_m = 6.7 s. (The mean residence time was identified from the volume, 31.5 mL divided by the flow rate, 4.7 mL/s).

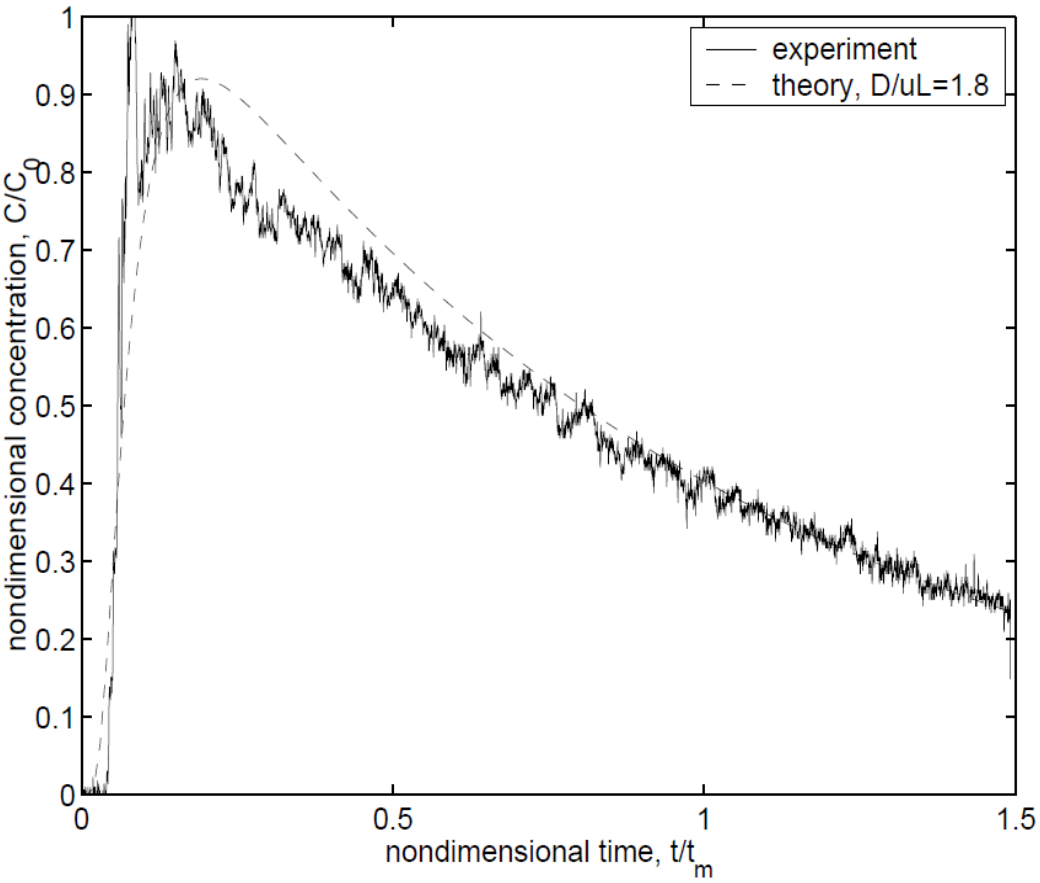

Fig. 3.20 Variation of non-dimensional concentration (C/C_0) with non-dimensional time (t/tm) from the RTD experiment and comparison with theoretical curve for D/uL = 1.8 and closed–closed boundary conditions.

The non-dimensional concentration C/C_o is the instantaneous concentration C divided by the tracer concentration that would appear at the outlet immediately after injection if the mixing were instantaneous and complete following the droplet entry to the water C_o. The experimental result has been scaled in the vertical direction to match the theoretical results at the non-dimensional time t/t_m = 1. Such scaling was necessary because, although a calibration was performed on the concentration detection system, there was not sufficient precision in dispensing the saline droplet volume to use the available calibration to accurately determine the C_o.

The equality of the experimental and simulated results in the vicinity of t/t_m = 1 is forced by the adopted scaling, Fig. 3.20. However, the value of the maximum in each

result (around C/C_o = 0.9 when the noise is smoothed out in the case of the experiment) and its timing (around t/t_m = 0.1) indicates a good level of correlation between the experiment and the simulation. There were some slight geometrical differences between the batch and continuous flow arrangement, principally in the vessel diameter and its volume. However, the differences are very minor and the results in Fig. 3.20 demonstrate that it is appropriate to estimate the RTD for a continuous flow system from a geometrically similar batch arrangement when necessary.

3.3.6 Summary of mixing in ultrasonic processing

A new technique for the identification of mixing characteristics associated with high power ultrasonic treatment at 20 kHz has been detailed. The mixing rate within the batch arrangement (30 mL) is a function of the applied ultrasonic power, but the macroscopic mixing is substantially complete within one second for absorbed ultrasonic power levels greater than 40 W (thermal dissipation).

A method to deduce the effective diffusivity from the mixing time measurements in the batch reactor has been demonstrated. The effective diffusivity increased with ultrasonic power and ranged from about 0.2×10^{-3} m^2/s to 0.7×10^{-3} m^2/s for input electrical power levels from about 70 to 120 W. Such values of diffusivity may be applied directly in a dispersion model for the RTD in the high intensity region in continuous flow cell arrangements provided the in/out flow does not substantially augment the mixing adjacent to the probe tip. Therefore, coupling the effective turbulent diffusivity identified in a batch reactor with a suitable dispersion model for the reactor provides an alternative approach to the deduction of RTD when determining the actual RTD in the high intensity zone of steady flow sonochemical reactors is problematic.

In continuous flow processing arrangements where the processing region of interest extends only a few mm beneath the probe tip, or when the processing volume is quite small, the direct visualisation method developed here may find application. However, the characteristic mixing times in such configurations at comparable power levels

will be shorter than those observed in this work. Thus, higher video framing rates would be required in such applications.

The outcome results of this model demonstrated a new method to identify mixing characteristics associated with the present work of ultrasound treatment. The mixing time was a very important factor to confirm that the microorganisms in the suspension are subjected to uniform ultrasound energy. Thus mixing was identified. It was found that the mixing rate in the present batch apparatus can be completed in one second for an ultrasound power of greater than 40 W. (thermal dissipation).

3.4 Microbial disruption in an ultrasonic processing cell

3.4.1 Introduction

The use of ultrasound techniques in microbial disruption is not commercially used in the food and dairy product industries. An experimental apparatus was developed to evaluate the microorganism disruption using ultrasound. In this section yeast log reduction will be evaluated for different ultrasound power.

The work aims to also establish comparison data for other treatments such as UHT, shear stress and shock wave (Chapter 6 of the thesis will cover this comparison study).

3.4.2 Apparatus

This section describes the application of a commercial ultrasonic device UIP 500 (previously described) to destroy microorganisms. Fig. 3.21 shows the ultrasound apparatus used in the current work. The ultrasound machine consists of a generator, transducer and sonotrode. As indicated in the manufacturer's instruction manual, the generator provides electrical oscillations of 400 W to power an ultrasonic device with a frequency of 20 kHz which is transferred to the transducer. The transducer converts electrical oscillations into mechanical vibration and is an interface between the generator and the sonotrode. The sonotrode carries the vibrations from the

transducer to the suspension. In these experiments, the sonotrode was immersed in a suspension of commercial yeast, *S. cerevisiae*. The ultrasound device generates heat which is dissipated into the suspension and the heat can affect the quality and the accuracy of the experiments. Results obtained from heat transfer section of this chapter were considered to evaluate the correct net power dissipated into the suspension. A means of a temperature control was also included in the present configuration so that there would be no thermal effect on the microorganism disruption. As a result, an ice bath configuration was added to the original design to maintain the suspension temperature sufficiently low to avoid thermal disruption of microorganism. An image of the machine showing the adopted ice bath in the ultrasound machine is displayed in Fig. 3.21. A set of thermocouples were used to monitor the temperature of the yeast suspension, wall and air temperature. Once the suspension temperature reached 45 ^{o}C the apparatus was shut down to allow the setup to cool down.

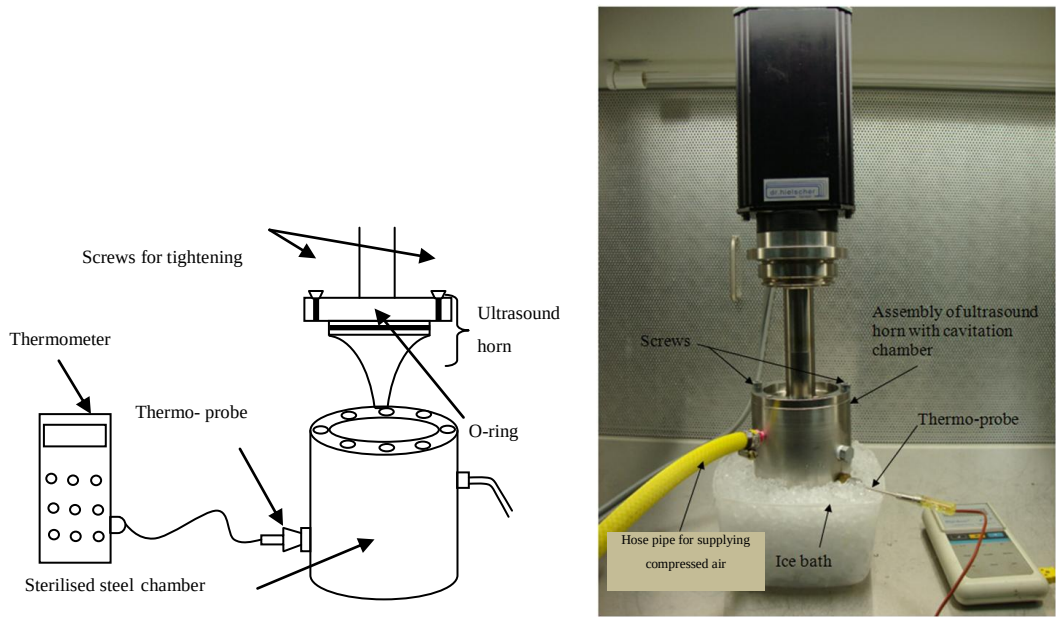

a) b)

Fig. 3.21 a) Schematic diagram illustrates the assembling of the setup b) image of the chamber immersed in an ice bath.

3.4.3 Yeast preparation and test procedure

Yeast was grown and tested at the laboratories of University of Southern Queensland. *S. cerevisiae* was chosen as they are easy to grow, have well established mechanical properties, are large enough for counting, readily available and are not expensive.

3.4.3.1 Yeast preparation:

Stock yeast, Luria Bertani Broth (LB) Broth, 4% glucose solution and 0.9% saline solution, are required to grow *S. cerevisiae*. A shaking incubator and centrifuge were used to mix the solution, following the steps below

1. Mix the stock yeast solution with LB Broth and 4% glucose solution to make a nutrient solution.
2. Place the nutrient solution in a shaking incubator at 37 ^{o}C for approximately 20 hours.
3. Centrifuge the solution at 6000 g for approximately 10 minutes.
4. Resuspend in 0.9% saline solution.

Freshly prepared yeast solutions were required for experiments in this chapter as well as chapter 4 and 5.

3.4.3.2 Procedure for preparing the samples

A yeast suspension was prepared with a concentration of approximately 10^5 CFU/mL. Yeast suspensions were used in ultrasonic, shock wave test and shear stress tests. With each test, an untreated sample was also reserved for comparison purposes. This provided an accurate means of comparing different test with different test conditions.

Agar was used as a food for yeast, preparation of agar plates using a dilution series was prepared in a very accurate method. The average final value for the agar plate

count is obtained by taking the averaging counting of CFU/mL. It was noticed that there was no significant variation in the three individual counts, the average value gives a result that is accurate enough to identify if cells were destroyed.

3.4.4 Viable count

In this work, the number of microorganisms before and after each treatment (ultrasound, shock wave treatments and shear stress) had to be evaluated. This was done to determine whether or not the specified treatment had been effective in microorganism disruption. The number of colony form units per millilitre (CFU/mL) was determined using a viable count procedure in standard sterile laboratory conditions as follows:

1. Prepare a dilution series by placing 900 mL of distilled water in each test tube and labelling them from 1 to 10.
2. Use a pipette to place 100 µl of microorganism solution into one of the test tubes and mix the solution. The 100 µl of the solution in tube 1 was pipetted into tube 2. Repeat the process until the final tube is reached.
3. Divide a nutrient agar plate into equal segments. Drop onto the agar 3 drops each containing 10 µl from each dilution, one segment per dilution.
4. Place the Petri dishes in the incubator for approximately 24 hours at 37 ^{o}C.
5. Incubate and observe each segment of the Petri dish and then select the segment containing a countable number of colonies, then count the number of colonies in each drop and calculate the average.

To find the final result, the average and the inverse of the dilution are multiplied and further multiplied by 100 to obtain the results in colony forming units per millilitre. For example, if the average was 9.1 colonies; dilution was 1/100, the result would be $9.1 \times 100 \times 100 = 9.1 \times 10^4$ CFU/mL.

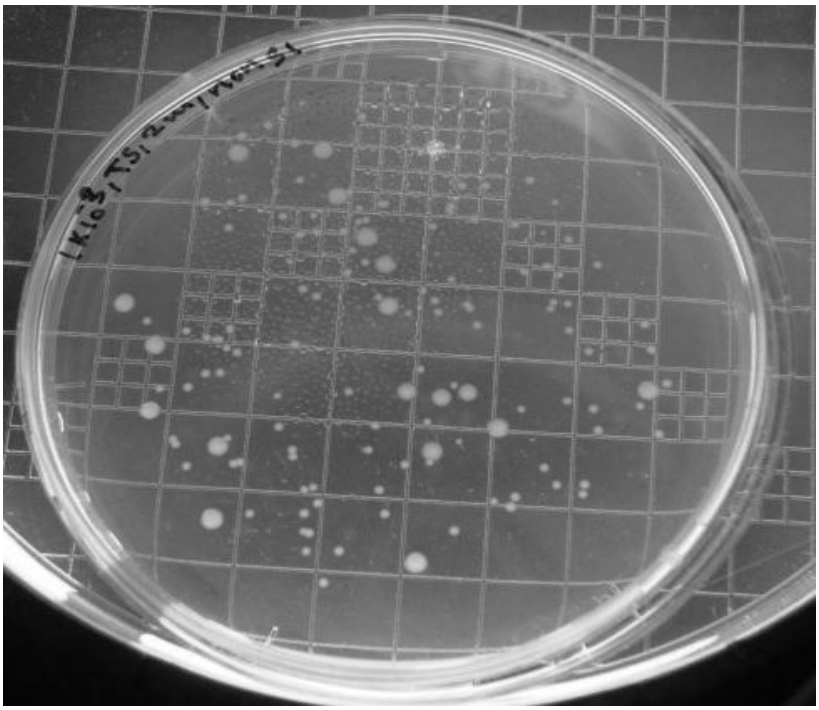

Fig. 3.22 Petrie dish with yeast growth.

3.4.5 Experiment preparation

The procedure of conducting the ultrasound experiments started with sterilising the equipment, carrying out the ultrasound treatment and taking treated samples to evaluate yeast counting. The treated sample was then refrigerated and transferred to the biological laboratory for analysis. An appropriate environment for the experiment was established and the ultrasound treatment completed as follows

1. A 50 mL beaker, the ultrasonic sonotrode, thermocouples and flask were washed in methylated spirits and flushed with compressed air. A 30 mL of yeast suspension was transferred from the conical flask to the beaker and an ice bath was prepared.
2. The thermocouples were connected and the ultrasound transducer placed into position to ensure that the beaker was not in contact with the sonotrode before the ultrasound was activated.
3. When the ultrasound was turned on, temperature of the yeast suspension, air temperature and beaker temperature were monitored and recorded. If the

temperature of the yeast suspension approached 45 ^{o}C the system was shut down.

4. The yeast sample was transferred to a sterile test tube and stored in a refrigerator. Culturing and counting process will take place. Further testing was undertaken if needed.
5. A viable count determined the number of CFU/mL before and after the treatment.

This procedure was also followed for the shock wave and shear and tests. The outcomes from these experiments are reported in chapters 4 and 5. As power dissipated into the yeast suspension could cause the temperature to rise, the ultrasound treatment was carefully monitored and treatment times regulated to keep the temperature below 45 ^{o}C to ensure that thermal effects did not impact on the test results.

3.4.6 Ultrasound experimental work

A series of ultrasound experimental test (Fig. 3.23) were performed. The results presented in this chapter will be compared with the traditional method of treatment such as homogenization and UHT as well as the two other methods that were adopted in this thesis, shock and shear.

An electrical experimental test was conducted to evaluate the net electrical energy converted into mechanical energy as the amplitude changes. Three different electrical power settings of 74 W, 104 W and 117 W, which is equivalent to a dial amplitude of 20, 70 and 100 respectively, were used in the experimental work. The net magnitude of energy dissipated into the suspension was evaluated based on the results obtained from section 3.3.

3.4.7 Experimental results

An initial test was conducted at an amplitude of 20 (power of 74 W) over different treatment times ranging between 0 (no treatment) to 300 s. Due to several factors

related to the experimental conditions such as suspension temperature and the way yeasts were counted, this test had to be repeated three times to ensure the reliability of the results. The initial concentration of the suspension prior the treatment was 6.3×10^4 CFU/mL, 1.53×10^6 CFU/mL, and 2.17×10^7 CFU/mL. Another test was conducted by the research team members, using the research equipment commissioned by the author of this thesis, for a period of 30 s at an ultrasound power of 74 W, the suspension temperature was closely monitored and recorded over time. The results of this test indicated that a yeast log reduction of 0.25 was achieved at treatment time of 30 s as shown in Fig. 3.23, while maximum suspension temperature was around 45 ^{o}C. The treatment time was then increased to be 60 s at same ultrasound power, and the yeast log reduction was calculated and found to be 0.8, some improvement was achieved. The treatment time was then gradually increased up to 240 s. The yeast reduction results was recorded and presented in Fig. 3.23. It was found that maximum yeast log reduction 2.5 was achieved when treatment time was 240 s and the suspension temperature was 55 ^{o}C. The results confirmed that the ultrasound apparatus was able to achieve a yeast log reduction of 2.5 at 240 s at 74 W, 20 kHz, and suspension temperature of between 45 ^{o}C to 55 ^{o}C. Due to the high suspension temperature, further experiments with higher amplitude and lower suspension temperature (below 35 ^{o}C) were required.

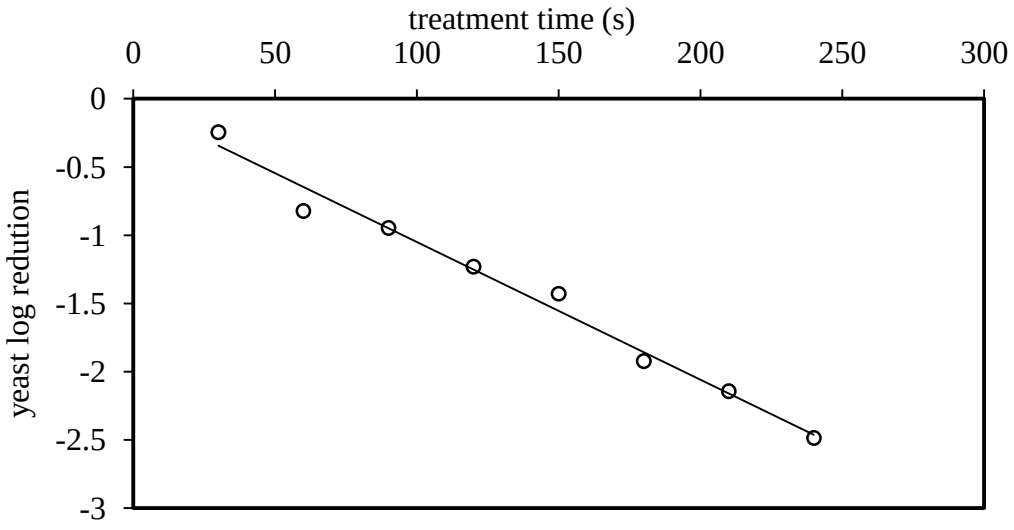

Fig. 3.23 The effect of treatment time on yeast log reduction at amplitude of 20 (74 W), at suspension temperature of between 45 ^{o}C and 55 ^{o}C. The raw data was obtained by Speering (2004) using the research equipment commissioned by the author of this thesis in the initial stage of the candidature.

Further tests were conducted using different amplitude and treatment time while suspension temperature was carefully monitored and controlled below 30 ^{o}C. In this test, the ultrasound chamber was submerged in an ice bath to ensure that yeast disruption occurred in the absence of thermal effect. Three amplitudes of 20, 70 and 100 were used in this test, and these amplitudes correspond to ultrasound power of 74 W, 104 W and 117 W respectively, the treatment time ranging between 240 s and 900 s. Table 3.2 illustrates the yeast log reduction results for different treatment time and different amplitudes. As shown in Table 3.2, higher yeast log reduction occurred at higher treatment time. The yeast log reduction of 4 was achieved when the treatment time was around 365 s at ultrasound power of 117 W (amplitude = 100). The yeast log reduction of 2.5 was achieved at treatment time of 292 s and an ultrasound power of 117 W.

Table 3.2 Summary of the yeast log reduction results using different amplitude, ultrasound power and treatment time, suspension temperature was controlled to around 30 ^{o}C.

Amplitude	Power	Log reduction 2.5	Log reduction 4
	(W)	Treatment time (s)	Treatment time (s)
20	74	540	900
70	104	360	600
100	117	292	365

3.5 Conclusion

Cavitation and Ultrasound

The literature review presented in this chapter indicates that when an ultrasonic wave propagates through a suspension, bubbles or cavities can be produced, the collapse of these cavitations cause local shock waves which may be responsible for microorganism disruption (Schebra et al., 1991). However shear effects and turbulent mixing may contribute to disruption so the actual mechanism responsible for a microbe's disruption in low frequency, high power ultrasonic processing systems has not yet been clearly identified. The theoretical and the

experimental work reported in this chapter provide the foundation for further investigation into the disruption process.

Energy transfer in ultrasonic processing

1. The heat losses associated with the ultrasound components: steel chamber, perspex base, and sonitrode (titanium) were experimentally evaluated using a transient one dimensional heat conduction model. The result of this model indicated that heat losses through the perspex, stainless steel, and titanium surfaces are approximately 0.4, 11, and 2.1 W respectively. The combined heat lost through solid surface was approximately 13.5 W of the total input applied ultrasonic power which was 117 W. Heat transfer will have a significant impact on efficiency calculations for the ultrasonic processor based on calorimetric experiments in this and related configurations. Although subsequent disruption experiment were performed in an ice bath, the heat transfer must be determined to make sure that the cell wall temperature and the yeast suspension temperature will be maintained below 45 ^{o}C to avoid yeast disruption due to thermal stress.
2. Experiments were conducted to evaluate the actual electrical energy and that was converted into useful ultrasound energy available for microorganism disruption. The maximum electrical power input was found to be 117 W and 74 W was the minimum power, while the maximum thermal energy dissipation rate was approximately 73 W and the minimum thermal energy was approximately 42 W.

Mixing quality in ultrasound processing

1. A new technique for the identification of mixing characteristics associated with high power ultrasonic treatment at different power was successfully implemented and evaluated. It was found that for a batch arrangement of 30 mL, homogeneity was achieved in approximately one second.

2. The mathematical method to deduce the effective diffusivity from the mixing time measurements in this ultrasound apparatus has been verified. Combining the effective turbulent diffusivity identified in a batch reactor with a suitable dispersion model for the reactor can provide an alternative approach to the deduction of RTD when determining the actual RTD in the high intensity zone of steady flow sonochemical reactors is problematic.

Microorganism disruption in ultrasound processing:

1. The results generated from the experimental ultrasonic work indicated that ultrasonic treatment is capable of destroying yeast over different treatment times and amplitudes.
2. Three different power inputs with different time exposures were investigated to determine the *S. cerevisiae* disruption when it subjected to ultrasound. The results showed that the concentration of yeast cells in the suspension decayed exponentially with time of exposure and that by increasing the power input, the rate at which the cells are destroyed is similarly increased.
3. Yeast log reduction result demonstrated that the experimental outcome were acceptable and consistence. For example, to achieve yeast log reduction of 2.5 at a treatment time of 292 s and 365 s, an ultrasound power of 117 W is needed.

CHAPTER IV

Pressure Disruption of Microorganisms

4.0 Introduction

Although a significant amount of experimental data on the pressure disruption of microorganism does exist, a large variability in results is also apparent. Furthermore, the dominant mechanisms for disruption have not yet been identified with any certainty. Hence, there remain large uncertainties regarding suitable optimisation strategies for pressure processing techniques.

As a step towards understanding the physical response of the microorganism to quasi-static pressure and shock treatments two models that may offer some assistance have been developed. In the first model, the deformation of cell walls is treated using thick walled spherical shell analysis, and the cell contents are treated as an isotropic material characterised using a single value of bulk modulus. Using this approach, the cell wall stress for given values of external pressures can be deduced. From the cell wall stress, failure can be inferred with the aid of a suitable failure theory. Von Mises theory of failure is adopted in this work and the properties of *S. cerevisia* are used as a representative of the microorganism.

The second model presented in this chapter is a Finite Element (FE) analysis developed using ABAQUS to aid the understanding of the dynamic behaviour of a microorganism when it is subjected to external pressure. The remaining part of this chapter then discusses the application of a shock tube apparatus to generate shock loading on a yeast suspension. The experimental results obtained with the current apparatus are discussed and analysed within the context of the pressure and shock

loading models. Results from other studies are also discussed and compared with the present work.

4.1 Quasi static pressure disruption – an introduction

In order to maintain food quality in the sterilised product, non-thermal processing alternatives such as high power ultrasound, pulsed electrical field (PEF), high pressure carbon dioxide (HPCD), and high hydrostatic pressure (HHP) treatments have been proposed as possible alternative. These methods do not aim to increase the temperature of the foods during processing, though some temperature increase may occur as a consequence of the treatment. Although these alternative techniques may offer solutions for maintaining food quality, disincentives to their implementation include the capital cost of the new processing equipment, re-skilling of staff, food product safety concerns, and other technical problems (Devlieghere et al., 2004; Estrada-Giron et al., 2005). For example, in the case of HHP and HPCD treatments, it appears that certain vegetative bacteria are resistant to the pressure treatments, and furthermore, batch processing is most easily implemented but this does not suit many operations.

In the case of HHP treatment, food is subjected to pressures ranging between 300 MPa and 600 MPa (Splimbergo et al., 2002). The HHP process involves a pressure rise from 1 bar to the high pressure (300 MPa – 600 MPa), then the pressure is held for some time (varying from 2 minutes to 20 minutes, depending on the bacteria), and the last stage is to decompress the food back to 1 bar. In a recent HHP study, the explosion of the bubbles due to the cavitation generated in the suspension is believed to be the main cause of the microorganism rupture (Gonzalez et al., 2009). Lin et al. (1994) and Nakamura et al. (1994) reported that the decompression rate can be the most significant parameter enhancing the disruption of the cell wall.

In the case of HPCD treatment, food is subjected to pressures ranging between 10 MPa and 20 MPa (Splimbergo et al., 2002). The process consists of a pressurization followed by CO_2 penetration into the cell and finally sudden pressure releas, usually to atmospheric pressure. The rapid gas expansion within the cell is believed to rupture the cell like “a popped balloon” (Spilimbergo et al., 2002). The CO_2 has a

strong ability to penetrate through the cell wall, making it fragile. The accumulated amount of CO_2 helps to disorder the structure of the cell wall and increase its permeability, and therefore lower pressures and decompression can be used to rupture the cell. The solubility of the CO_2 is not strongly dependent on the increase of the pressures above 10 MPa (Spilimbergo et al., 2002). A higher pressure and rapid decompression are important to enhance the process of the membrane (cell wall) disruption (Lin et al., 1994; Hong and Pyun, 1999). Zhang et al. (2004) confirmed that the biological activity of both *S. cerevisiae* and *Spores of Absidia coerulea* are influenced by the decompression rate (7.5 MPa at 30 ^{o}C and 30-90 minutes). However, tests by Enomoto et al. (1997) on *S. cerevisiae* showed that rapid decompression did not always enhance the disruption because rupture happens at the stage of pressurizing. The Enomoto et al. (1997) result conflicts with the outcome of Spilmbergo et al. (2002). According to Arreola et al. (1991) and Hong et al. (1997), decompression had no significant effect on the quality of bacteria disruption in their experiments. Others reported the death of the cell is due to the temperature drop associated with the decompression process using CO_2 (Debs-Louka et al., 1999).

4.2 An introduction to shock disruption

The stress developed within the cell wall can be estimated by modelling the microorganism as a spherical shell. Depending on the type of the microorganisms, a cylindrical model may be a better approximation in some cases. The approach for a cylindrical geometry is identical to that presented here, but the results are different.

The cell wall is the outer layer of the cell which covers the cell membrane and the cell cytoplasm. The cell membrane is also known as the plasma membrane. It is the cell wall that experiences stress due to external loading. In many research analyses (especially mathematical models) membrane materials are treated as they thought they are cytoplasm materials (Hartmann et al., 2006; Schlegel, 1992).

The cell wall can be found in bacteria, yeast, algae and plant cells, while it is absent in animal cells one of the difference between the animal cell and the yeast cell is that the yeast cell is surrounded by a cell wall to protect the membrane and the cytoplasm, while the animal cell has no cell wall.

In the present work, the cell wall is assumed to be composed of a homogeneous, linear elastic material. The material within the membrane is considered to be entirely cytoplasm and is likewise treated as a homogeneous, linear elastic material. The stress distribution on a yeast cell wall in a spherical shell under hydrostatic pressure uniform load is investigated. Perrier-Cornet et al. (1999) and Hartmann et al. (2006) used the same approach in evaluating the mechanical properties of the cell when it was subjected to a uniform external pressure loading. A similar mathematical approach developed by Hartmann et al. (2006) was adopted in the present work. The von Mises stress and strain results were then compared with the Hartmann et al. (2006) mathematical model and with their experimental results. The von Mises stress and strain results in the present work and Hartmann et al. (2006) were found to be comparable.

This analysis proceeds by: (1) considering the internal pressure that develops within the cytoplasm as a consequence of the mechanical deformation of the cell wall; (2) combining the internal pressure-shell deformation relationship with the spherical shell equations to determine the ratio of internal to external pressure; and (3) considering the von Mises stress equations which can then be used to evaluate the stress state of the shell, the cell wall of the microorganism.

4.2.1 Cytoplasm deformation

If an isotropic material element is under the stresses σ_x, σ_y, and σ_z, the change of its volume per unit volume (e) can be written as (Beer et al., 2005)

$$e = \frac{\Delta V}{V} = \frac{1-2\nu}{E}(\sigma_x + \sigma_y + \sigma_z), \qquad 4.1$$

where

ΔV = the change of the volume

V = initial volume

ν = Poisson's ratio for the material

E = modulus of elasticity of the material

σ_x, σ_y and σ_z = normal stress components along x, y and z axes respectively.

The cytoplasm is assumed to be an isotropic fluid and hence each stress component σ_x, σ_y and σ_z in equation 4.1 is identical and equal to the internal hydrostatic pressure P_i which develops as a result of the deformation of the wall. This internal pressure is related to the volume change of the internal material and its bulk modulus according to equation 4.2

$$P_i = B(\frac{\Delta V}{V}) = B(1-\frac{a_2^3}{a_1^3}), \quad 4.2$$

where the bulk modulus or the modulus of compression B of the internal material (the cytoplasm) is

$$B = \frac{E}{3(1-2\nu)}, \quad 4.3$$

and a_1 = internal radius before the loading,

a_2 = internal radius after the loading.

4.2.2 Cell wall deformation and stress

The thick wall spherical shell theory provides an analytical approach that can be used to evaluate the tangential and normal stress within a spherical shell subjected to an external and/or internal pressure. Although in the constitutive law, the relationship between the stresses-strain in a yeast cell wall is not well defined as reported by Stenson et al. (2010), several studies (Smith et al., 2000a; Hartmann et al., 2006) demonstrated that a linear elastic material model is an appropriate approach that can be used when evaluating the mechanical properties of yeast cells. Thus, in the present work, the relationship between the stress and strain of the yeast cell wall is considered to be linear. Hartmann et al. (2006) used linear isotropic elastic material model in their study to understand the yeast disruption when the cell is subjected to a uniform external pressure. This approach matches with the assumptions of the present work, in which it is assumed that the yeast cell remains spherical during a compression process.

A thin walled shell theory approach is more appropriate when the ratio of the cell thickness to its diameter is less than 0.05. In this case, the tangential stress and hoop stress would be constant across the wall thickness (Beer et al., 2005). In the case of a thin walled shell theory, the radial stress can be neglected. For *S. cervesia* the thickness of the cell wall to its diameter ratio ranged between 0.03 and 0.05 (Smith et al., 2000a; Hartmann et al., 2006; Stenson et al., 2010), therefore, a thick or a thin walled shell theory can be adopted. Hartmann et al. (2006) and Schlegel (1992) adopted a thick-walled theory in their works. The advantages of using thick walled spherical theory is that the radial stress through the cell wall would be calculated across the thickness of the cell wall as reported by Hartmann et al. (2006). In the present work, a thick walled spherical shell theory is adopted, and therefore, the tangential and the radial stresses are to be considered in the mathematical calculations.

Hartmann et al. (2006) in their linear spherical shell model showed that the external pressure transmitted through the shell to the cytoplasm decreased marginally. It was also reported that the pressure drop through the cell wall varied with the material properties of the cell wall, the cytoplasm and the thickness of the cell wall (Hartmann et al., 2006). Therefore, in the present work, it becomes important to study the effect of the wall thickness on the yeast disruption.

Consider a spherical shell with an internal diameter of *a* and an external diameter of *b*, Fig. 4.1. The internal pressure P_i arises due to the elasticity of the cell wall and the external pressure P_e. The two stress components that are generated along an element of the shell can be described using the two equilibrium equations (Timoshenko and Goodier, 1982), which are

$$\sigma_r = \frac{P_e b^3 (r^3 - a^3)}{r^3 (a^3 - b^3)} + \frac{P_i a^3 (b^3 - r^3)}{r^3 (a^3 - b^3)}, \tag{4.4}$$

and

$$\sigma_t = \frac{P_e b^3 (2r^3 + a^3)}{2r^3 (a^3 - b^3)} - \frac{P_i a^3 (2b^3 + r^3)}{2r^3 (a^3 - b^3)}, \tag{4.5}$$

where

a = internal radius, and

b = external radius.

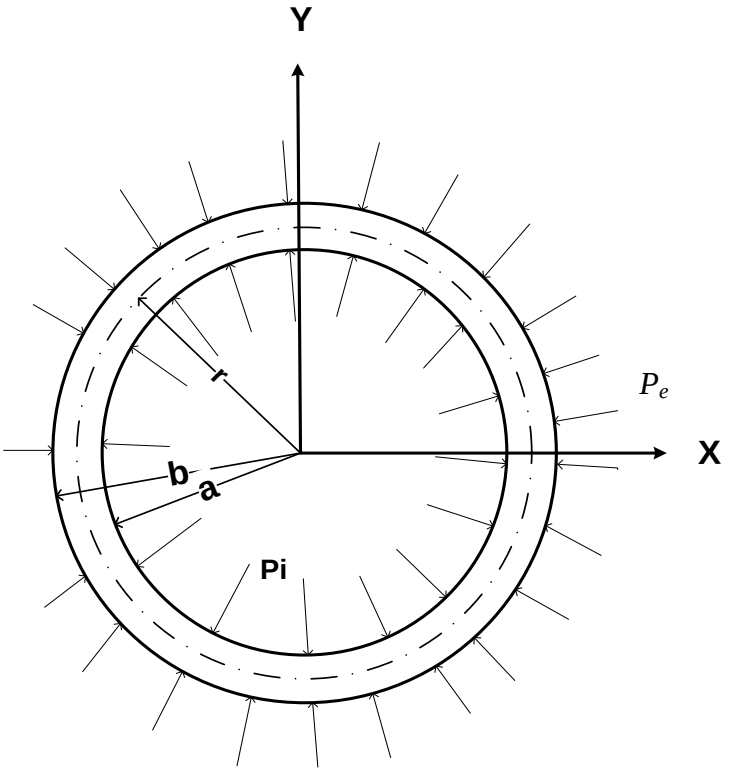

Fig. 4.1 Spherical shell configuration

If we consider the internal surface of the shell, and thus substitute $r = a$ in equation 4.4 and 4.5, the tangential and radial stresses at the internal surface of the spherical shell are

$$\sigma_r = \frac{P_i(b^3 - a^3)}{(a^3 - b^3)} = -P_i, \tag{4.6}$$

and

$$\sigma_t = \frac{3P_e b^3}{2(a^3 - b^3)} - \frac{P_i(2b^3 + a^3)}{2(a^3 - b^3)}. \tag{4.7}$$

The strain in the tangential direction (ε_t) generated at the internal surface of the wall due to the external pressure is (Beer et al., 2005)

$$\varepsilon_t = \frac{\sigma_t}{E}(1 - \nu) - \nu\frac{\sigma_r}{E}. \tag{4.8}$$

Now the tangential strain at the internal surface can be written as:

$$\varepsilon_t = \frac{a_2 - a_1}{a_1} = \frac{a_2}{a_1} - 1, \quad 4.9$$

and therefore,

$$\frac{a_2}{a_1} = \varepsilon_t + 1. \quad 4.10$$

Equation 4.2 includes the ratio

$$(\frac{a_2}{a_1})^3 = (\varepsilon_t + 1)^3 = \varepsilon_t{}^3 + 3\varepsilon_t{}^2 + 3\varepsilon_t + 1. \quad 4.11$$

Since only small tangential strains are considered ($\varepsilon << 1$), we can write

$$(\frac{a_2}{a_1})^3 = 3\varepsilon_t + 1, \quad 4.12$$

with a maximum error O($\varepsilon_t{}^2$). Substituting equation 4.12 in equation 4.2 yields

$$\varepsilon_t = \frac{-P_i}{3B}. \quad 4.13$$

The internal to external pressure ratio can be obtained by substituting σ_r and σ_t of equation 4.6 and 4.7 in equation 4.8, and also replacing the strain in equation 4.8 with equation 4.13.

$$\frac{P_i}{P_e} = \frac{1}{\frac{1}{3}\frac{(1+\nu)}{(1-\nu)} + \frac{1}{3}\frac{(1-3\nu)}{(1-\nu)}(\frac{a}{b})^3 + \frac{2}{3}\frac{E}{B}\frac{1}{(1-\nu)}(1-(\frac{a}{b})^3)}. \quad 4.14$$

In the present work, it is assumed that the strain value is very small, and thus the terms $\varepsilon_t^3 + 3\varepsilon_t^2$ in equation 4.11 can be ignored (approximating zero). This approximation is acceptable in the analytical work as recommended by Hartmann et al. (2006). For example, the tensile stress and the modulus of elasticity of a commercial yeast is 25 MPa and 150 MPa respectively as reported by Kleinig (1997), the calculated strain is then 0.16. In this case, the calculated $\varepsilon_t^3 + 3\varepsilon_t^2$ is 0.08, which is a very small value comparing with the product of $3\varepsilon + 1$, which is 1.32. Thus, $\varepsilon_t^3 + 3\varepsilon_t^2$ term can be ignored in equation 4.11.

4.2.2.1 Cell permeability

Permeability is not a core part of the study reported here. It is however important to demonstrate that permeability in yeast cell is not a major issue. Feng and Yang (1973) and Lardner and Pujara (1980) assumed the yeast cell to be a spherical cell filled with an incompressible liquid. The incompressible liquid volume was assumed to be constant, this implied im-permeability of the cell wall material. This approach was confirmed by Perrier-Cornet et al. (1999). Stenson et al. (2010) used a micromanipulation compression rate to study the mechanical properties of cells and assumed that the water transfer from the cell wall during the compression to be negligible. Fleet (1991) reported the yeast cell wall to be a non-permeable substrate (Kleinig, 1997). Thus in the present work, it has been assumed that the initial compression of the cells is pure compression with no major mass transfer, which means the cell is non-permeable. The internal to an external pressure ratio will then be close to one.

Osmotic pressure is the hydrostatic pressure contributed to prevent the water flow across the membrane due to concentration difference of the solution on either side. A single microorganism such as yeast maintains a higher internal pressure than that of the surrounding medium. This pressure is counteracted by the cell wall and referred to a cell turgor pressure. It was reported that in the case of yeast, the effect of the static pressure on the cell wall properties is insignificant (Hartmann et al., 2006).

Levin et al. (1978) assumed that the turgor pressure of yeast cell wall was 1.33 MPa, the yeast wall thickness 90 nm, and cell diameter $5\mu m$. Using these data, the expected tensile stress in the cell wall is 20 MPa using the following relationship (Kleinig, 1997) in equation 4.15.

$$\sigma = \frac{Pr}{2t} \qquad 4.15$$

Kleinig (1997) assumed that the shape of the yeast is spherical, and his calculation showed that the tensile cell wall pressure is 25 MPa. It would be expected that the yeast cell can withstand a pressure of around 20 to 25 MPa as suggested by this simple calculation and the recommendation of Kleinig (1997).

The cell wall is able to stretch during the growth phase, and to also respond to any external changes in the cell's osmotic environment (Levin et al., 1978). Ludwig (1997) and Hartmann et al. (2004) confirmed that the effect of high hydrostatic pressure is more significant on slender bacteria rather than these with a spherical shape. Hartmann et al. (2004) assumed that mechanical state of yeast cell does not change during the holding pressure. Thus, in the present work, it can be assumed that the hydrostatic pressure will have no significant effect on the osmotic pressure. A saline was used to prepare the inoculums and to balance the osmotic pressure of the cell with the medium.

4.2.3 Stress normalized by external pressure

The tangential stress at the internal surface of the cell wall, normalized with the external pressure, can be obtained by substituting the internal to external pressure ratio represented in equation 4.14 in equation 4.7 giving

$$\frac{\sigma_t}{P_e} = \frac{3}{2}\frac{1}{(\frac{a}{b})^3 - 1} - \frac{P_i}{P_e}. \qquad 4.16$$

4.2.4 Von Mises stress

In general, the von Mises stress σ_v and strain ε_v can be evaluated using the stress components along *x*, *y* and *z* axes (Beer et al., 2005)

$$\sigma_v = \sqrt{\frac{(\sigma_x - \sigma_y)^2}{2} + \frac{(\sigma_y - \sigma_z)^2}{2} + \frac{(\sigma_z - \sigma_x)^2}{2} + 3(\tau_{xz}^2 + \tau_{xy}^2 + \tau_{yz}^2)}, \qquad 4.17$$

$$\varepsilon_v = \frac{2}{3}\sqrt{\frac{(\varepsilon_x - \varepsilon_y)^2}{2} + \frac{(\varepsilon_y - \varepsilon_z)^2}{2} + \frac{(\varepsilon_z - \varepsilon_x)^2}{2} + \frac{3}{4}(\gamma_{xz}^2 + \gamma_{xy}^2 + \gamma_{yz}^2)} \qquad 4.18$$

where

τ_{xz} = shear stress along *x*-*z* axes

τ_{xy} = shear stress along *y*-*x* axes

τ_{yz} = shear stress along *y*-*z* axis

ε_x = strain along *x* axes

ε_y = strain along y axes

ε_z = strain along *z* axes

γ_{xz} = strain due to shear on *xz*

γ_{xy} = strain due to shear on *xy*

γ_{yz} = strain due to shear on yz.

In the case of a uniformly loaded 2D spherical configuration, the tangential stress is the same in all directions, this yields

$$\tau_{xx} = \tau_{zx} = \tau_{yz} = 0, \qquad 4.19$$

and at allocation where the z axes is aligned with the radial direction,

$\sigma_x = \sigma_y = \sigma_t, \sigma_r = \sigma_z$, and thus, the von Mises stress σ_v is

$$\sigma_v = \left|\sigma_t - \sigma_r\right|, \qquad 4.20$$

which is a general result for uniformly loaded spherical shell.

4.3 Physical properties of microorganism cells

Several methods have been used to evaluate the mechanical properties of microorganisms' cell walls. Most of these methods are based on the measurement of the cell wall deformation due to applied loading. A widely used technique consists of squeezing the microorganism between two parallel plates and measuring simultaneously the distance between the two plates and the compression force. These techniques are often used to evaluate only the bursting force (Zhang et al., 1992; Rachik, 2006). Atomic Force Microscopy (AFM) is a widely used nano-indentation technique for the measurement of the cell elastic properties. Force versus indentation curves are usually analysed with the aid of mathematical or numerical models to provide quantitative information on sample elasticity (Touhami et al., 2003).

In order to apply the shell analysis of the previous section to the identification of mechanical disruption of microorganism due to pressure effects, representative values for the physical properties of microorganism are required. In this section, some techniques for identification of certain physical properties of microorganism

are reviewed and representative values for the relevant physical properties of *S. cerevisiae* identified from the literature. Table 4.1 presents the dimensions and the mechanical properties of yeast adopted in the present work. The following subsection discusses the origin of the values presented in Table 4.1.

Table 4.1 *S. cervisiae* geometric and mechanical properties adopted in this work.

Dimensions	*S. cervisiae dimension and material properties*
Radius	2.5-2.7 μm
Thickness	0.135 μm
Thickness / Radius	approximately 0.05
Modulus of elasticity	
Cell wall	112 MPa
Cytoplasm	6.2 MPa
Density	
Cell wall	3500 kg/m^3
Cytoplasm	1100 kg/m^3
Bulk modulus	
Cytoplasm	2.2 GPa
Poisson's ratio	
Cell wall	0.4
Cytoplasm	0.4995
Cell wall Strength	
von Mises stress	70 MPa
von Mises strain	0.85

4.3.1 Dimensions

According to Smith et al. (2000a), yeast cell diameters can range from approximately 3 μm to 6 μm, depending on the growth phase. The diameter of the cell is likely to be around 5 μm. The cell wall thickness to the cell radius ratio was assumed to be around 5% following Smith et al. (2000a). Another work reported that a commercial yeast radius is between 2.5 – 2.8 μm, and the thickness to the radius ratio is around 0.037 (Smith et al., 2000c).

4.3.2 Modulus of elasticity – cell wall

Svaldo (2006) investigated the mechanical properties of *S. cerevisiae* by performing AFM measurements. A quantitative evaluation of the cell wall elasticity was obtained through the Hertz-Sneddon model which showed that coated cells (with hard protein layers) are characterized by a Young's modulus higher than the value of the uncoated cells and similar to the value observed on the bud scar region of uncoated cells. The Young's modulus of the cell itself was reported to be 1.79 (±0.08) MPa for encapsulated cells, 1.12 (±0.02) MPa for uncoated cells without bud scar and 2.0 (±0.2) MPa for uncoated cells with bud scar. Svaldo (2006) used a combined AFM imaging and nano-indentation measurement for bud scar and its mother of *S. cerevisiae,* and observed a higher rigidity of the bud scar compared to the mother cell. For uncoated mother cells, the Young's modulus value was 0.6 (±0.4) MPa while the value was 6.1 (± 2.4) MPa for the bud scar. From the Young's modulus values, it was noticed that the bud scar is about 10 times stiffer than the mother cell surface, a finding which was consistent with the presence of chitin in the bud scar as reported by DeMarini (1997). These values, which are in the range of MPa, are in agreement with values reported in literature for bacterial cell such as *E. coli* of Yao (1999), but they are about hundred times smaller than the value of 150 MPa reported for yeast by Smith et al., (2000b, and c) and Hartman et al. (2006).

It appears these widely different values may be attributed to different growth phases and whether the measurement was conducted on the cell as a whole or the wall of the cell (Smith et al., 2000b). Middelberg (1992) determined that the Young's modulus of the wall of a single *S. cerevisiae* cell was about 100 MPa and showed that yeast cells strengthen as they enter the stationary phase by increasing the wall thickness without altering the average elastic properties of the cell wall material. Smith et al. (2000a), reported the Young's modulus of the commercially available yeast cells' wall to be 112 MPa (±3 MPa) during the exponential growth phase and 107 MPa (±2.8 MPa) during the stationary phase. Smith et al. (2000c) reported that the Young's modulus of a commercial yeast cell with a wall thickness of 90 nm and radius of 2.7 µm was approximately 127 MPa (±4 MPa) during the stationary phase. Hartman et al. (2006) tested different types of microorganisms and the yeast cell wall

modulus of elasticity was reported to be 150 MPa. From the relevant literature, it can be concluded that that average modulus of elasticity of the yeast cell wall is in the range of 100 MPa to 150 MPa.

4.3.3 Poisson's ratio

Fry (1995) indicated that the relationship between the mechanical properties of the plant cell walls and the structure of the wall is not fully understood. The contribution of other wall components and their interaction with cellulose is not clear (Cosgrove, 2000). Wang et al. (2004) reported that there is no reliable method of measuring the material properties of walls of single cells. There is a difference between the cellular Poisson's ratio and the actual value for the cell wall. In this research, the cell wall Poisson's ratio is of interest.

According to Guillaume et al. (2002), the cellular Poisson's ratio, i.e., the value of Poisson's ratio obtained by treating the cell as a single unit, remains unknown. However experiments by Maniotis et al. (1997) reported that the animal cell Poisson's ratio is around 0.25 (±0.05). In experimental work by Savldo (2006), the Poisson's ratio of the biological cell was assumed to be 0.5. Touhami et al. (2003) agreed with Svaldo (2006) and assumed that the Poisson's ratio can reasonably be treated as 0.5 since biological cells are composed of soft material like water. Lardner and Pujara (1980) treated the tomato cell as incompressible, with a Poisson's ratio of less than 0.5.

Wang et al. (2004) conducted experimental and simulation work on the actual cell wall Poisson's ratio. Wang et al. (2004) considered the cell wall material to be incompressible with an equivalent Poisson's ratio of less than 0.5, but claimed there is no sufficient and/or reliable method to measure the Poisson's ratio of the tomato cell wall. Wang et al. (2004) tested a tomato cell wall under compression between two plates and performed simulations for different Poisson's ratios in the range from 0.3 to 0.5. The results were not particularly sensitive to the value of Poisson' ratio and therefore Wang et al. (2004) used a Poisson's ratio of 0.4 for all subsequent modelling.

In the simulations by Guillaume et al. (2002), when a cell stretch was applied, the Poisson's ratio of the cell was varied from 0.2 to 0.5, while other parameters were kept constant. Guillaume et al. (2002) reported that strains varied by 15% over the range of Poisson's ratio values. However, in the models of hydrostatic pressure or fluid shear, Poisson's ratio was treated as an important factor and it reduced the maximal, median, and average maximal strains by 93% when Poisson's ratio was varied from 0.2 to 0.5 Guillaume et al. (2002). Therefore, Poisson's ratio was of importance in hydrostatic compression or fluid shear experiments, which applies predominantly compressive stresses. Hartmann et al. (2006) used different Poisson's ratios for different cell wall in the range between 0.3 and 0.499. In the case of yeast, Hartmann et al. (2006) assumed the Poisson's ratio of the cell to be 0.499. From the cited papers, it was found that the most common yeast cell wall Poisson's ratio value used was 0.4, and that will be adopted in this work.

4.3.4 Bulk modulus

Hartmann et al. (2006) suggested that cytoplasm has a viscosity of 1.5 Pa.s and a bulk modulus of elasticity of 2.29 GPa. Hartmann et al. (2006) ignored the viscous properties in their analyses as they were considered to be very small and to have no significant impact on the stress. Smith et al. (2000c) reported that the cytoplasm is assumed to hold similar properties to water (as biological cells are composed of largely liquid material) and hence a Young's modulus of 6.2 MPa was assumed. Assuming the cytoplasm has a Poisson's ratio value of 0.4995 and E of 6.2 MPa, thus the bulk modulus elasticity (B) of the cytoplasm is calculated as 2.2 GPa using the equation

$$B = \frac{E}{3(1 - 2\mathrm{v})}\,, \tag{4.21}$$

where

B = Bulk modulus of elasticity

E = Modulus of elasticity

v = Poisson's ratio.

As reported by Hartmann et al. (2006), the physical properties of the cytoplasm are very close to pure water, and this assumption is valid because of the high percentage of water in the cytoplasm. The *B* value of pure water is approximately 2.2 GPa, and value of 2.2 GPa was adopted in this work based on equation 4.21.

4.3.5 Cell wall and cytoplasm density

Cell wall and cytoplasm density are required for the dynamic analysis of section 4.6 so a simple calculation was employed to estimate the cell wall density based on the cell density and the cytoplasm density. In the case of commercial yeast quoted by Kleinig (1997), the cell density was 1330 kg/m^3, and the wall thickness to radius ratio was 5%. If the cytoplasm density is assumed to be slightly higher than water, say 1050 kg/m^3, this will lead to a cell wall density of 3500 kg/m^3 as shown via the following equations.

$$M_{cell} = M_{cyt} + M_{mem,} \quad 4.22$$

$$\rho_{mem} = \rho_{cell} (V_{cell}/V_{mem}) - \rho_{cyt(}V_{cyt}/V_{mem}), \quad 4.23$$

where,

ρ_{cell} = cell density,

ρ_{cyt} = cytoplasm density,

ρ_{cw} = cell wall density,

V_{cell} = cell volume,

V_{cyt} = cytoplasm volume,

V_{cw} = cell wall volume,

M_{cell} = mass of the cell,

M_{cyt} = mass of the cytoplasm, and

M_{cw} = mass of the cell wall.

4.3.6 Cell wall strength

The von Mises stress and strain methods were developed to help predict the yielding of metals in which are stresses are present in all three directions. The von Mises approach provides a simple way of reducing the combination of the stresses in three directions into a single failure criterion. Von Mises stress theory is a possible failure

criterion that is commonly used to evaluate the yeast cell wall rupture (Smith et al., 2000b; Hartmann et al., 2006; and Stenson et al., 2010). Stenson et al. (2010) reported that von Mises stress is often used to determine the yielding point of ductile material (such as cell wall) – the point at which is begins to deform plastically. Stenson et al. (2010) reported that the corresponding stress and strain failure of yeast cell were 102 MPa and 0.55. However these figures do not match with the reported von Mises stress and strain suggested by Smith et al. (2000b). This was because Smith et al. (2000b) assumed the stretch cell ratio was constant as explained by Stenson et al. (2010).

In line with the work of Smith et al. (2000b) determined that the von Mises stress and strain. The von Mises strain to rupture of the cell wall was 82% (±1.4) for the exponential phase, 80% (±1.6) for stationary phase and 75% (±8) for the commercial yeast (Smith et al., 2000b). The stresses produced in a thin wall rigid sphere filled with liquid has been evaluated by Kleinig and Middelberg (1998) using micromanipulation techniques, but no further progress in understanding and characterizing the mechanical properties of the yeast cell wall was obtained.

Following Smith et al. (2000b), Hartmann et al. (2006), Stenson et al. (2010) and Kleinig (1997), the von Mises stress and strain required to rupture the cell wall of the yeast will be taken as 70 MPa and 0.85 respectively.

Another failure criterion is the strain energy per unit volume (Stenson et al., 2010). The energy required to break the cell wall should be greater than surface energy of the cell wall which depends on the mechanical properties of the cell wall. Stenson et al. (2010) reported that a strain energy of 30 MJ/m^3 is required to break the yeast cell wall.

4.4 Result and discussion of quasi-static analysis

4.4.1 Comparison with Hartman et al. (2006) analysis

The internal pressure generated in the cytoplasm, the radial stress and the tangential stress generated in the cell wall were calculated using a thick wall spherical shell theory. The results were then compared with the Hartmann et al. (2006) model using yeast material properties given in Table 4.1. Table 4.2 shows very good agreement between the internal to external pressure ratio results provided by the Hartmann et al. (2006) model and the presented quasi-static analysis. As illustrated in Table 4.2, the difference percentage between the two results is very small.

Table 4.2 Comparison of P_i/P_e results between Hartmann et al. (2006) and the present static analytical model.

a/b	P_i/P_e Hartmann et al. (2006)	P_i/P_e Present model	Difference
0.90	0.9997	0.9990	0.0007%
0.93	0.9998	0.9993	0.0005%
0.96	0.9999	0.9996	0.0003%
0.99	0.9999	0.9999	0.0000%

4.4.2 Assessment of σ_t/σ_r

The ratio of tangential to radial stress generated at the inner surface of the cell wall can be calculated directly using three dimensional stress-strain equations (Beer et al., 2005)

$$\sigma_x = \frac{E[(1-\nu)\epsilon_x + \nu(\epsilon_y + \epsilon_z)]}{(1+\nu)(1-2\nu)}, \tag{4.24}$$

$$\sigma_y = \frac{E[(1-\nu)\epsilon_y + \nu(\epsilon_z + \epsilon_x)]}{(1+\nu)(1-2\nu)}, \tag{4.25}$$

$$\sigma_z = \frac{E[(1-\nu)\epsilon_z + \nu(\epsilon_x + \epsilon_y)]}{(1+\nu)(1-2\nu)}, \quad 4.26$$

Considering a point on the spherical cell wall which crosses the y-axis,

$\sigma_r = \sigma_y$, and $\sigma_t = \sigma_x = \sigma_z$, and $\varepsilon_x = \varepsilon_z$.

The ratio of the tangential stress and radial stress can therefore be achieved by dividing equation 4.25 by equation 4.26, and using $\epsilon_x = \epsilon_z$, this yields:

$$\frac{\sigma_t}{\sigma_r} = \frac{\nu}{1-\nu}, \quad 4.27$$

Equation 4.27 indicates that σ_t/σ_r varies with the cell wall Poisson's ratio only. For example, when the cell wall is assumed to have $\nu = 0.5$, σ_t is expected to be equal to σ_r (according to equation 4.27). For this case, equation 4.6 and 4.7 were solved to find the tangential to radial stress ratio using B = 2.2 GPa, E = 6.2 MPa, ν = 0.4995 for different *a/b* ratio and it was found that the tangential stress is equal to radial stress as shown in Fig.4.2. As shown in Fig. 4.2, von Mises stress calculated from equation 4.20 is equal to zero for the case ν = 0.4995, and this matches with the results obtained from equation 4.27, where the tangential stress must equal to the radial stress in this case.

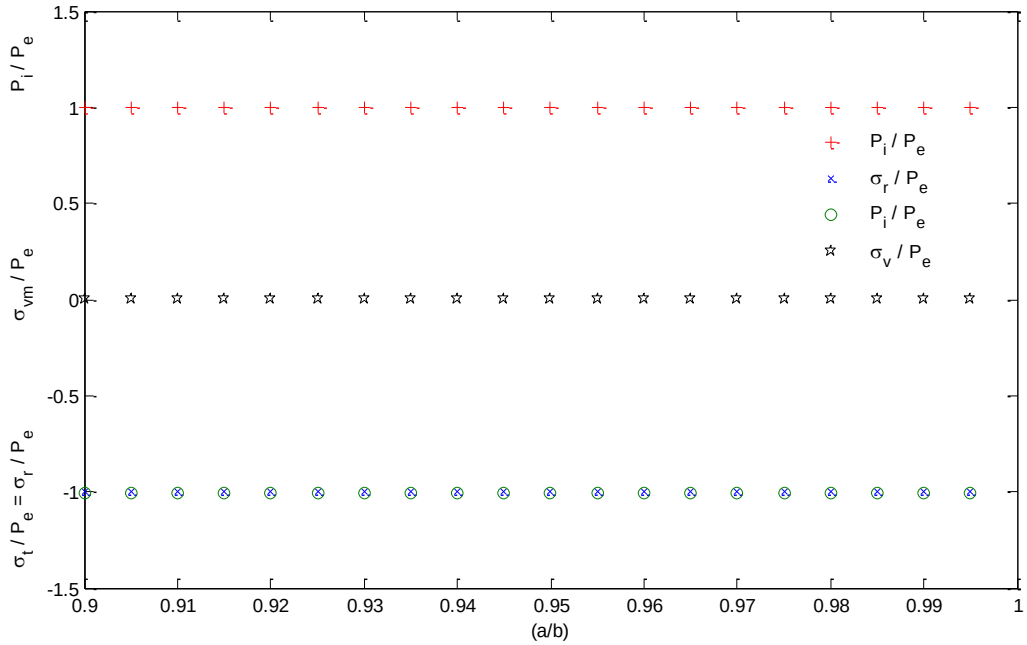

Fig.4.2 The normalized internal pressure, tangential stress, radial stress, and von Mises stress for different radius ratios and E = 6.2 MPa, B = 2.2 GPa, ν = 0.4995.

4.4.3 Normalized internal pressure (P_i/P_e)

The effect of Poisson's ratio (ν), modulus of elasticity (E) and bulk modulus (B) on the internal to external pressure ratio (P_i/P_e) for different internal to external radius ratios (a/b) was investigated. Fig. 4.3 represents the relationship between a/b and P_i/P_e for different Poisson's ratios (ν). Fig. 4.3 shows that P_i/P_e is approaching one when the thickness of the shell wall decreases for the ν values of 0.35, 0.4, 0.45 and 0.4995. The E of the cell wall is 112 MPa and the B of the cytoplasm is 2.2 GPa for this calculation (as given in Table 4.1) giving the value of E/B = 0.05.

As shown in Fig. 4.3, when ν increases, the P_i/P_e values decrease. For example P_i/P_e = 0.98 for a/b = 0.9 and ν = 0.4995, while the P_i/P_e = 1.07 when ν = 0.35 for a/b = 0.9. Over the range of a/b values considered in Fig. 4.3, the P_i/P_e values vary between 0.98 and 1 when ν = 0.4995, however P_i/P_e varies between about 1.08 and 1 for ν = 0.35. This result closely follows the results obtained from Hartmann et al. (2006). In the case of *S. cervasia* considered in this work, where ν = 0.4, B = 2.2 GPa, and E is 112 MPa or E/B = 0.05, the P_i/P_e ratio is about 1.024 when a/b is 0.95 as shown in Fig. 4.3.

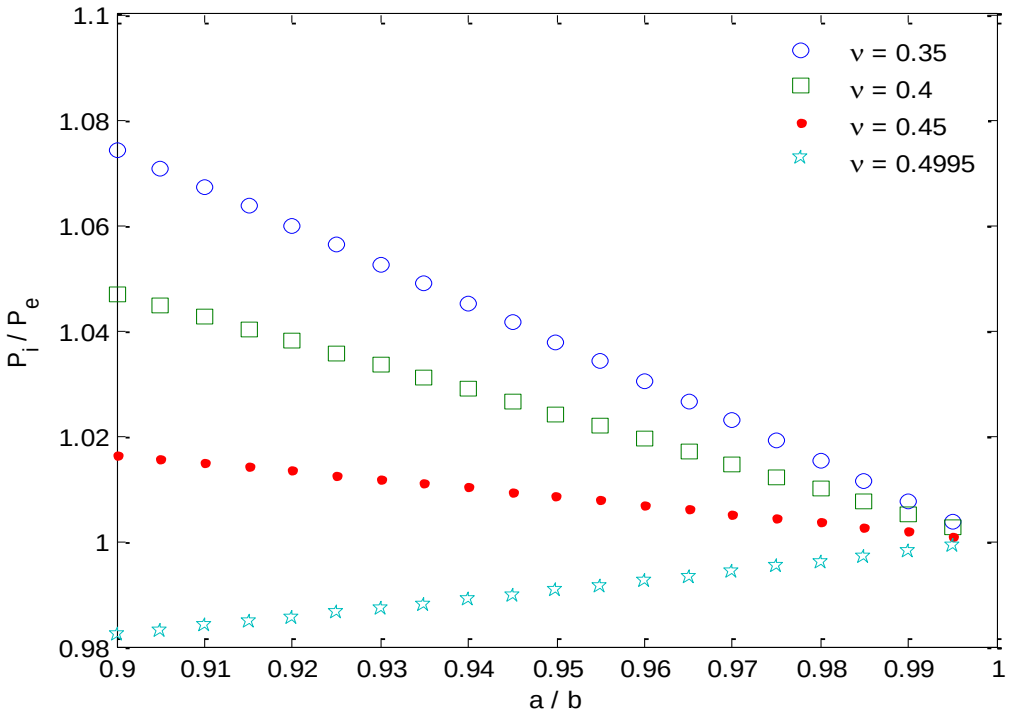

Fig. 4.3 The effect of ν values on P_i/P_e as a function of a/b when E/B = 0.05.

Fig. 4.4 shows that the P_i/P_e ratio increases when the E/B values decrease. The results presented in Fig. 4.4 shows that P_i/P_e is approaching unity when a/b is approaching one for E/B values of 0.002, 0.05 and 0.11. The E/B values of 0.002, 0.05 and 0.11 were selected because a similar range of these values has been reported in the literature (Smith et al., 2000c; Hartmann et al., 2006 and Wang et al., 2004). In the case of the *S. cervisiae* (Table 4.1) the P_i/P_e value is approximately 1.024 when a/b = 0.95, ν = 0.4, and E/B = 0.05 as shown in Fig. 4.4.

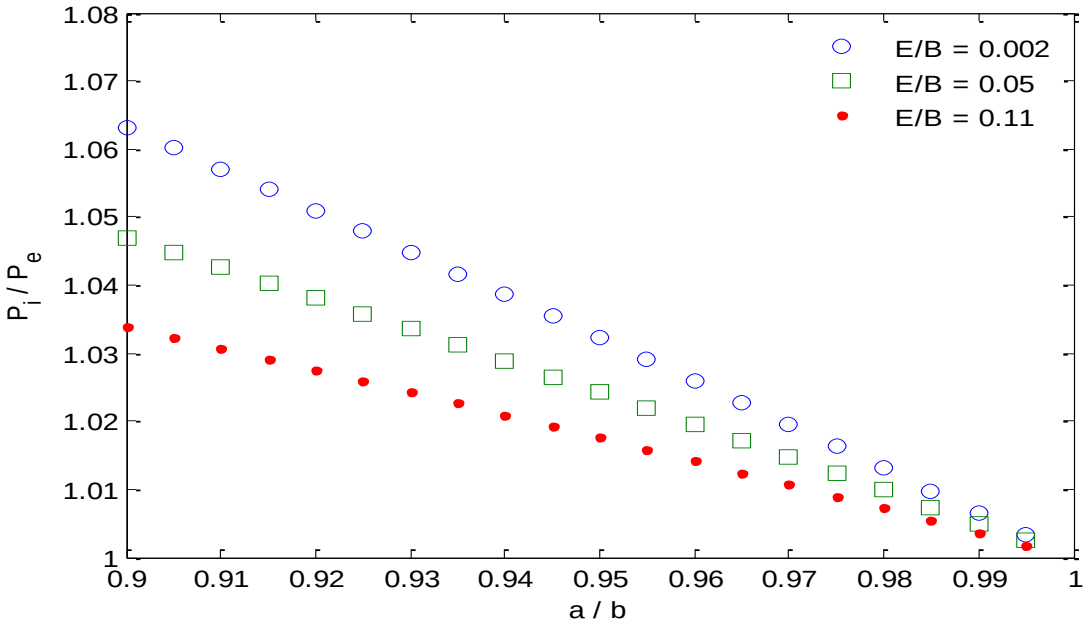

Fig.4.4 The relationship between the *a/b* ratio and P_i/P_e for different *E/B* values and cell wall Poisson's ratio of 0.4.

4.4.4 Tangential and radial stress

The effect of Poisson's ratio and the *E/B* ratio on the normalized tangential and radial stress at the inner surface of the cell wall for different *a/b* ratios are studied in this section. Fig. 4.5 shows the relationship between the *a/b* ratio and σ_t/P_e and σ_r/P_e for ν values of 0.35, 0.4, 0.45 and 0.4995 and *E/B* of 0.05. Results presented in Fig. 4.5 illustrate the following:

1. When the spherical shell becomes thinner (i.e. *a/b* values approaching 1), σ_t/P_e increases for ν values of 0.35, 0.4, 0.45, but not in the case when ν = 0.4995 (as the cell wall material becomes water-like). When ν = 0.4995, σ_t/P_e decreases slightly for *a/b* approaching one, Fig.4.5 (a). The radial stress follows the same trend as the tangential stress when ν = 0.4995, while the radial stress increases when *a/b* increase for cell wall ν values between 0.4 and 0.35, Fig.4.5 (b).
2. Some researchers believe that ν has a significant influence on the stress generated in the cell wall while others believe differently (Touhami et al. 2003; Svaldo 2006; Smith et al., 2000a; Wang et al., 2004). Touhami et al. (2003) in their experimental work agreed with the result reported by Svaldo (2006) that Poisson's ratio has an insignificant effect on the tangential stress

developed on the cell wall when a static load is applied. The present results indicated that the Poisson's ratio has a minor effect on the tangential stress developed at the cell wall when $\nu = 0.4995$, but it has a significant effect on this stress when ν is 0.35 or 0.4, which is probably a better approximation in the case of yeast.

3. As discussed in section 4.3.3, Wang et al. (2004) tested a tomato cell wall under compression (experimentally and numerically) between two plates for different Poisson's ratio in the ranged from 0.3 to 0.5. The result showed that there was no great difference in the external force required to rupture the cell at a given deformation for a change of Poisson's ratio. Therefore Wang et al. (2004) used a Poisson's ratio of 0.4 for all subsequent modelling. On the other hand, in the model of hydrostatic pressure reported by Guillaume et al. (2002) showed that the Poisson's ratio played an important factor in the stress-strain calculation and the change of the Poisson's ratio from 0.2 to 0.5 reduced the average maximal strains by 93%. The difference between these two results could be due to the different test configurations. In the present study, the configuration is closer to Guillaume et al. (2002). The analytical results of the present work, Fig. 4.5, demonstrates that Poisson's ratio is an important factor in the calculation of stress and strain, thus the effects of ν needs to be carefully evaluated.
4. Analytical results presented in Fig. 4.5, show that the change of *a/b* ratio has an important influence on the tangential and radial stress developed on the cell wall for different Poisson's ratio. In the case of *S. cervisiae*, the results of the normalized tangential stress for different *a/b* ratio is presented in Fig. 4.5a. The results show that when *a/b* is 0.95 (corresponding to yeast) the normalized tangential stress is approximately -0.775, negative sign show the direction), when $E/B = 0.05$ and $\nu = 0.4$.
5. Fig.4 .5b shows the relationship between *a/b* ratio and radial stress for different Poisson's ratio. The results of this curve are identical to the curves for P_i/P_e, which is the expected result as indicated in equation 4.6. In the case of yeast, the results show that when *a/b* is 0.95 (yeast) the normalized radial stress is expected to be approximately 1.024, when $E/B = 0.05$ and $\nu = 0.4$.

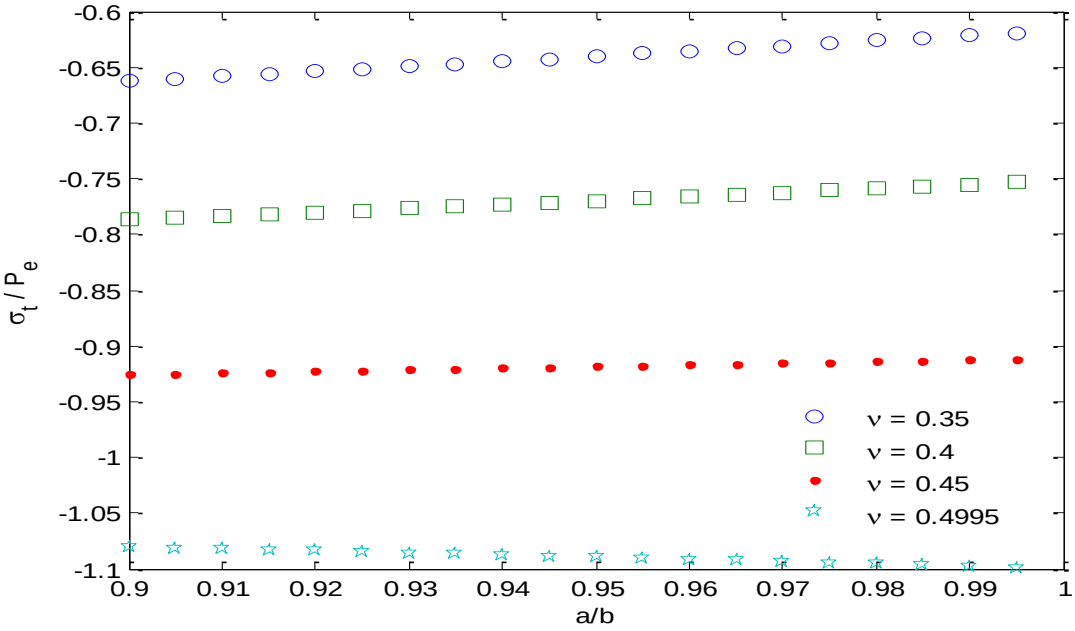

a) Normalized tangential stress

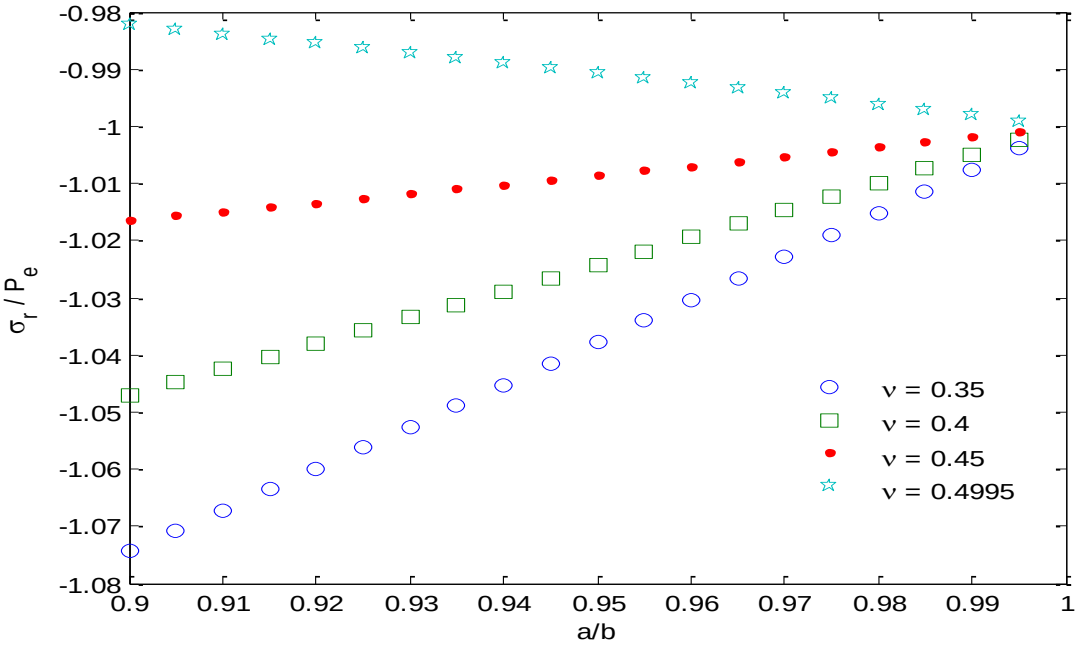

b) Normalized radial stress

Fig. 4.5 The relationship between the internal to external radius ratio and a) the normalized tangential stress and b) the normalized radial stress for different Poisson's ratios and E/B = 0.05.

Fig. 4.6 describes the effect of the a/b ratio on σ_t/P_e for different E/B values of 0.002, 0.05 and 0.11. This figure shows that the increase of a/b leads to an increase in σ_t/P_e

stress for *E/B* values of 0.002, 0.05 and 0.11. As for yeast cells with *B* = 2.2 GPa, *E* = 112 MPa and ν = 0.4, and *a/b* = 0.95, the value of σ_t/P_e is 0.775.

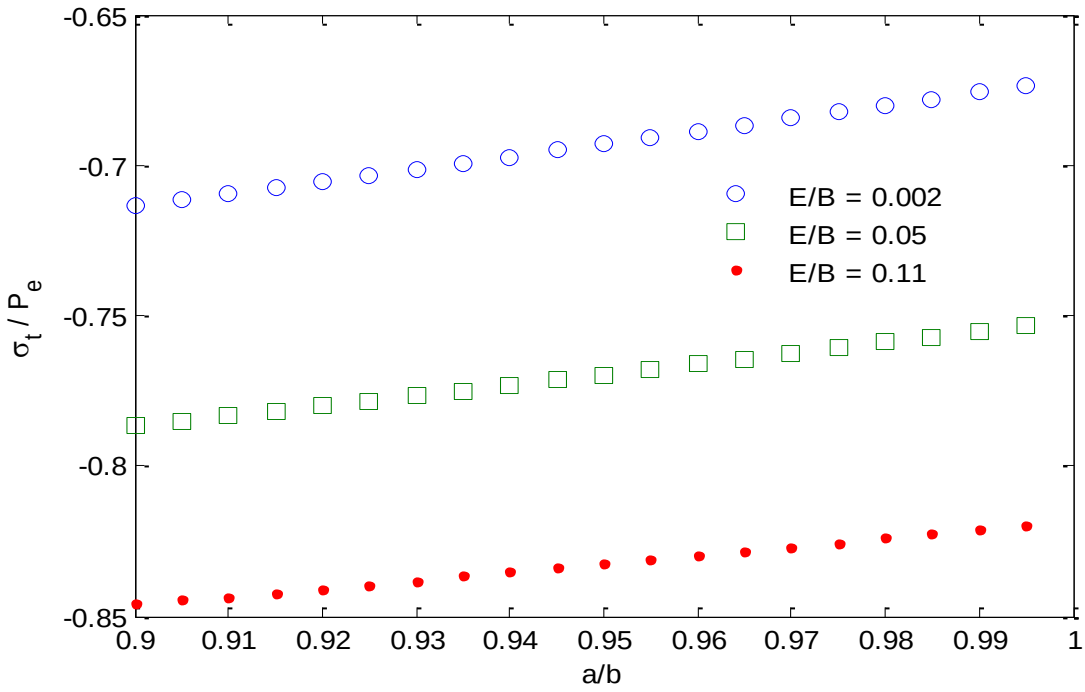

Fig. 4.6 The relationship between the *a/b* ratio and the normalized tangential stress and different *E/B* ratios for ν = 0.4.

4.4.5 Von Mises stress

The relationship between the *a/b* ratio and the normalized von Mises stress (σ_v/P_e) for different ν values is presented in Fig. 4.7. As discussed in section 4.3, previous researchers have assumed that the cell wall material fails at a critical von Mises stress and von Mises strain, the values of which can be determined experimentally (Smith et al., 2000b; Hartmann et al., 2006; Stenson et al., 2010). In the present study, σ_v/P_e was evaluated for different *a/b* ratios. The von Mises stresses represent a simple way of representing the combination of the stress in three dimensions as a single stress. The Poisson's ratio values in this study were varied from 0.35 to 0.4995 as reported section 4.3.3.

As can be seen in Fig. 4.7, when ν = 0.35, σ_v/P_e reaches a value of 0.42 at *a/b* = 0.9, while σ_v/P_e reaches a value of 0.09 and 0.13 when ν = 0.4995 and 0.45 respectively. These are rational results, since σ_v/P_e is the difference between the normalized

tangential and radial stress (Fig. 4.5). Fig .4.7 also shows that the increase of *a/b* ratio will have only a small influence on σ_v/P_e for high Poisson's ratios such as 0.4995 and 0.45, this figure shows a very minor change of σ_v/P_e when *a/b* changes. In the case of *S. cervisiae*, where it is assumed that ν = 0.4, *E/B* = 0.05 and *a/b* ratio 0.95, the σ_v/P_e value is around 0.255.

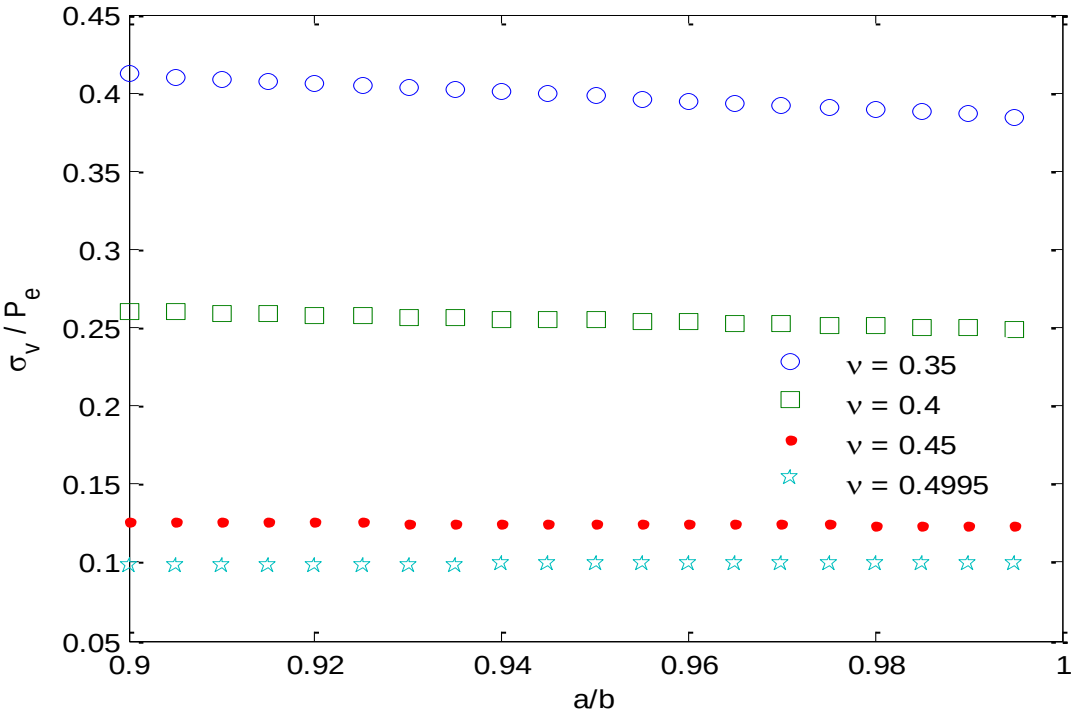

Fig. 4.7 The relationship between the internal to external radius ratio and von Mises stress for different Poisson's ratios, and *E/B* = 0.05.

The relationship between the σ_v/P_e and *a/b* for *E/B* values of 0.002, 0.05 and 0.11 is presented in Fig. 4.8, which shows that the σ_v/P_e values decrease when the cell wall becomes thinner (*a/b* values increase).

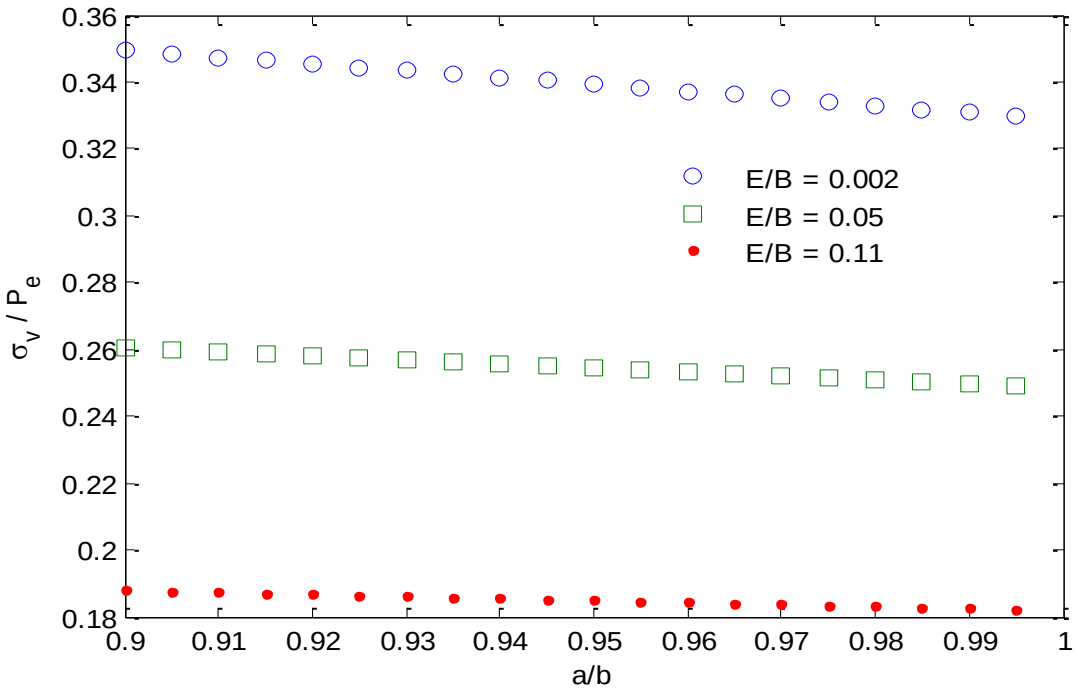

Fig. 4.8 The relationship between the internal to external radius ratio and von Mises stress for different *E/B* ratios, and ν = 0.4.

4.4.6 Conclusion

This parametric study has shown the following.

1. The internal to external pressure ratio and radial stress developed in the cell wall of the yeast increases when the cell wall Poisson ratio's and *E/B* decreases. In the case of yeast where it is assumed *v* = 0.4, *a/b* = 0.95 and *E/B* = 0.05, the extended to internal pressure ratio was found to be 1.025.
2. The tangential stress developed on the cell wall was found to be increased when Poisson's ratio and *E/B* decreased. In the case of yeast, the normalised tangential stress was found to be -0.775.
3. The normalized von Mises stress was found to be increased when the cell wall Poisson's ratio the *E/B* value decreased. The normalized von Mises stress was found to be around 0.255 in the case of yeast.

The analytical results obtained from this model will be used in the discussion of the numerical simulations and of the experimental work.

4.5 An introduction to the FE simulations

A numerical model was developed using the commercial *FE* software package (ABAQUS 2010) to study the dynamic behaviour of a microorganism modelled as a spherical shell and with dimensions and physical properties close to *S. cerevisiae*. The microorganism model will be suddenly subjected to external uniform pressure loadings.

An existing USQ gas gun has been used with different pistons to generate shock wave pressures in the range of 100 MPa to 400 MPa. The ABAQUS model was developed to help understand the extent of cell wall rupturing achieved using this facility. The effect of shock loading on the microorganism's cell wall was investigated numerically using von Mises stress theory of failure as it has been used extensively by others in related application (Smith et al., 2000b; Wang et al., 2204; Hartmann et al., 2006; and Lee et al., 2000). A single cell of yeast was used in this simulation and was assumed to be isotropic, incompressible with the material properties presented in Table 4.1. The governing equations and other mathematical equations can be found in the ABAQUS manual help.

Tamagawa and Akamatsu (1997) used a free piston shock tube with the ability to generate a pressure wave of between 10 and 40 MPa. The experiment was used to determine the threshold of maximum pressure, rise time, and energy for damage to various living tissue such as red blood cells and cancer cells. In their work, Tamagawa and Akamatsu (1997) used an optical device to determine the degree of the cell damage using a deformation approach. The cell diameter reported in Tamagawa and Akamatsu (1997) was larger than the yeast, being in the range of 10 micrometer. Tamagawa and Akamatsu (1997) reported that the effect of the concentration of cell, on the cell disruption, was very significant. This effect was also related to the distance between the cells, Young’s modulus of the cell wall, cell diameters (Tamagawa and Akamatsu, 1997).

A shock work was conducted by Lee et al. (2000) using two stage shock treatment. The results showed that transdermal delivery increased with increasing the peak pressure (Lee et al., 2000). Lee at al. (2000) claimed that the shock tube extends the

envelope of the parameters available for the study of biological effects of the shock wave. Hosokawa (1997) reported that using a shock tube to generate pressure waves of 4 MPa for treatment of non adherent cells, including normal and transformed thymus cells and leukaemia cells, destroyed cells proportionally with pulse pressure. Tougher cells such as fibroblast cells and melanoma cells required higher pressure up to 6.5 MPa.

Kerfoot (1990) demonstrated that there was no significant killing of four species of bacteria tested using 4000 repeated high energy shock waves in the range of 5 MPa. Kerfoot (1990) raised many questions to be answered: for example, do high energy shock waves kill bacteria? If so, is there a large enough kill to be clinically significant? Are high pressure shock waves bactericidal to all, some or none of the different strain of bacteria, and finally are different types of a shock wave more effective bactericidal agents? According to Morgan (1988), high energy shock waves generate a physical effect including free radical production, development of high pressures and acoustic cavitation.

The above cited papers investigated the damage and disruption quality using shock waves. The applications of disruption using shock waves were mostly concentrated on the soft and fragile cell such as blood cell and cancer as well as live animal cells. The present work investigates the effect of dynamics pressure rise on the yeast cell wall rupturing. The analytical calculation presented in section 4.4 aimed to analyse the stress developed in the cell wall due to external static loads. The remainder of this chapter will focus on dynamic (shock) effects on the cell wall rupturing while using the quasi-static results as a point of reference.

The material properties presented in Table 4.1 are used in comparing the results of this FE simulation with the analytical solution presented in section 4.3. The analytical and numerical results for P_i/P_e, σ_v/P_e, and σ_t/P_e are expected to be comparable especially when the FE model is solved for static loading. Another aim of this section is to evaluate the effect of the stress amplification due to the pressure wave reflection between the cell wall and the cytoplasm of the microorganism.

4.6 FE model structure and validation

Model geometry

Fig. 4.9 illustrates the model geometry for the spherical (axi-symmetric) microorganism configuration adopted for this simulation. The model consists of a long water tube containing a single yeast cell sitting on the centre line of the tube. A detail description of the shock tube apparatus is presented in section 4.10. The model consists of three parts: cell wall, cytoplasm, and water. Since the size of the yeast is very small compared to the water tube (in the range of micrometer), the cell wall thickness to radius ratio was maintained. The interface between the materials was treated as "hard contact, surface to surface explicit" with no damping and no separation. These were used to simulate the impact transient process and pressure transfusion through the water to the cell wall and cytoplasm of the cell. The friction and the viscosity were not considered in this simulation.

Mesh construction

As recommended by the ABAQUS manual, a 11543 quadratic triangular element explicit type named CAX6M was used for part 1 (water) and part 3 (cytoplasm), and 2000 linear triangular element explicit type CAX3 was used to build part 2 (cell wall). The total number of nodes that was used to build the geometry of this model was 24680 (see Figure 4.9). Validation and error estimation of the model was conducted (Appendix A and B) to ensure that numerical errors were sufficiently small while maintaining a sufficient simulation time. As shown in the results presented in Appendix C the mesh density used in these simulations was based on convergence of the results.

Configuration assembly

The geometry was developed using the pre-processing ABAQUS software. The surface located at the top of the tube was subjected to a uniform external loading pressure; the pressure was maintained for few microseconds to make sure that the pressure wave travelled through to the bottom of the tube. The cell wall and the

cytoplasm of the cell (part 2 and part 3 respectively) and the water (part 1) were assembled as one unit. The cytoplasm and cell wall were connected as a tied surface with no separation. The validation results and the choice of the mesh arrangement are discussed in Appendix C.

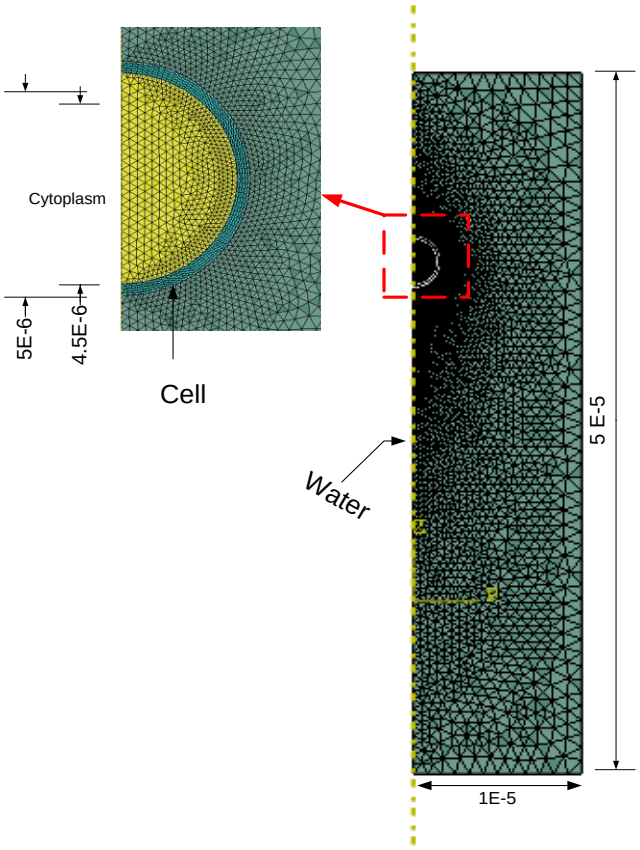

Fig.4.9 Model structure – spherical shell configuration (dimensions are measured in unit of length; the cell wall thickness to radius ratio is constant).

Material properties

The cell wall material properties were selected according to the literature review data presented in section 4.2 and summarized in Table 4.1.

Boundary conditions

The boundary conditions applied to the geometry were:

1. BC-left: this is an axis of symmetry.
2. BC-right: there is no horizontal movement, U1 = 0, since the water is assumed to be rigidly constrained in the lateral direction.
3. BC-bottom: no movement in any direction will occur U2 = 0, and the lateral constraint is imposed by the axis of symmetry and the BC – right.

Pressure wave propagation

The model structure presented in Fig. 4.9 was used in this simulation. The pressure wave was propagated through the water, hit the cell wall, and penetrated through the cytoplasm. A tabulation of uniform pressure values applied on the top surface of the tube with initial pressure of 1 MPa, is presented in Table 4.3. The pressure was applied when the simulation time increased from zero to 10^{-7} ms; was and held for 0.75 ms, until the pressure wave reached the bottom of the water tube (detail results are presented in Appendix C.

Table 4.3 Amplitude of external pressure applied to the top surface of the model with step time of simulation

Time (ms)	Amplitude pressure (MPa)
0	0
10^{-7}	1
0.75	1

The maximum time step size that should be used in the simulation can be estimated from the stability limit. The time step size should remain smaller than the smallest transit time of a dilatational wave across any of the elements in the mesh $\Delta t_{limit} = \frac{L_{min}}{C_d}$, where L_{min} is the smallest element dimension in the mesh and C_d is the dilatational wave speed. Thus the element size and the time step size must be considered simultaneously to avoid numerical stability problems. The simulation time step size refers to the period over which equations are integrated in order to

produce a new solution which is then used to update the mesh properties ready for the next time step. To avoid numerical errors related to time stepping, Δt_{limit} must be greater than the time step size. In the present work, the size of the elements were adjusted to ensure the time step size will stay smaller than Δt_{limit}. The pressure history of a node located in the water is presented in Fig.4.10 for an applied pressure load of 1 MPa on the top surface of the tube.

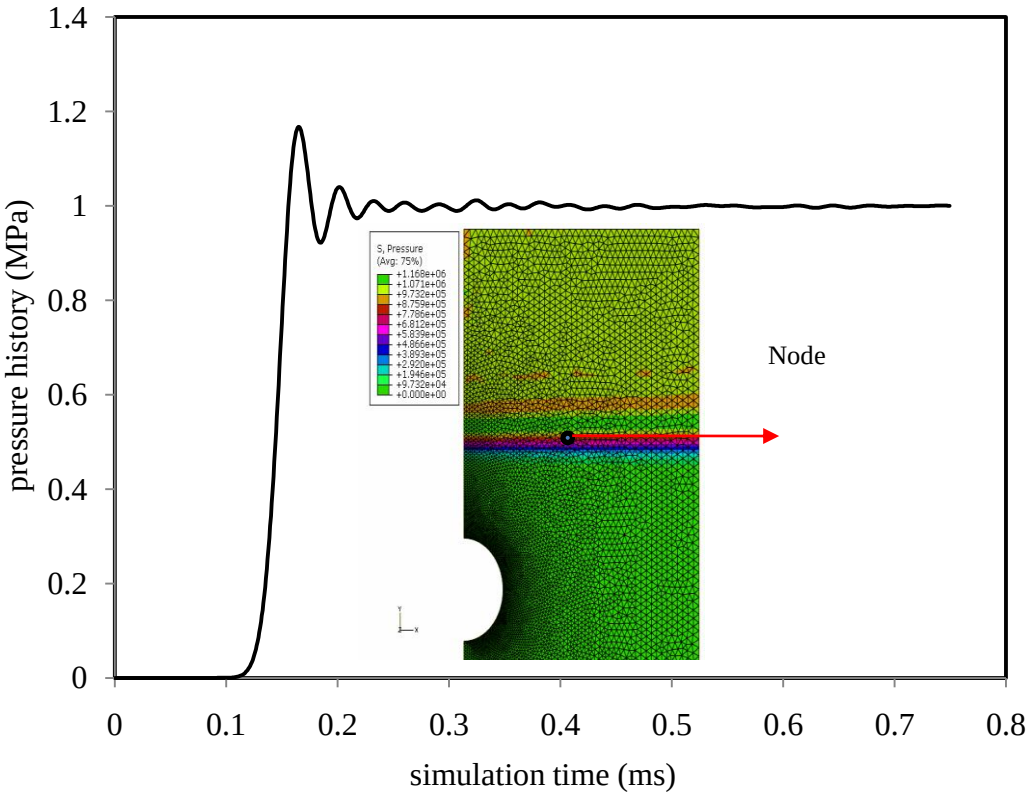

Fig. 4.10 Sample of pressure history from a node located in the water.

4.7 Statics results from FE simulation

The model arrangement presented in Fig. 4.9 and discussed in section 4.5 was also solved using a static general step, the results were then compared with the analytical results in section 4.2 to provide a further demonstration of the validity of the numerical model. Von Mises stress was used to assess the likelihood of yeast disruption in this simulation.

4.7.1 Pressure ratio P_i/P_e

A preliminary static simulation was first performed with uniform material properties applied throughout the entire domain. A 100 MPa external static pressure was applied on the top of rectangular geometry given in Fig. 4.9 using water-like material properties of density, modulus of elasticity and Poisson's ratio of 1000 kg/m^3, 6.2 MPa and 0.4995 respectively. To validate the numerical results, the stress as generated along the *x*, *y* and *z* axes were calculated using equation 4.27. The numerical result showed that for P_y = 100 MPa, the horizontal and vertical stress is σ_x = 99.999 MPa and σ_y = 100 MPa, while the von Mises stress is close to zero. These results match those obtained from the analytical calculation using equation 4.20 and 4.27.

Next, a Poisson's ratio of 0.4 was used in this static simulation. The simulated σ_x was 66.667 MPa and σ_y was 100 MPa, while the von Mises stress was approximately 28 MPa, which is the difference between the horizontal and vertical stress. These numerical results showed a very good agreement with the analytical calculation presented in section 4.4, where the von Mises stress was around 26 MPa.

After achieving these results, the properties of the cell wall, cytoplasm and water presented in Table 4.1 were used in the simulation. The initial results obtained from this model were assessed and compared with the results obtained from section 4.4 using water-like material and found to be very comparable. Table 4.4 presents a comparison of the numerical and analytical results.

Table 4.4 Analytical and FE results for the case of static loading with water-like material properties to compare the analytical and simulation results.

Normalized Stress or Pressure	Analytical method	FE method	Difference (%)
σ_t/P_e	1.003	1.004	0.2
σ_r/P_e	0.998	0.996	0.2
σ_v/P_e	0.009	0.008	0.1
P_i/P_e	0.998	0.996	0.2

Hartmann et al. (2006) claim that P_i/P_e is equal to one when the cytoplasm B is 4 GPa, and E and ν of the cell wall are 150 MPa and 0.499 respectively. These material properties were used in the analytical model and the result of P_i/P_e was found to be 1.002 which is in a good agreement with the Hartmann et al. (2006) results. The assumption made by Hartmann et al. (2006) that cell wall ν equals 0.499 means the tangential stress essentially is equal to the radial stress for any particular point located in the cell wall and thus σ_v is predicted to be very small approaching zero (equation 4.2). Using the von Mises theory of failure, a microorganism with a cell wall ν = 0.5 will not rupture because σ_v is very insignificant (close to zero). However, most of the yeast cell wall Poisson's ratio values reported in the recent literature are in the range of 0.3 to 0.4. In other cases such as animal cells and blood cells, the cell wall ν is close the Poisson's ratio of the cell (close to 0.4995), but it is not the case for yeast, because the yeast cell wall is not a fluid-like material but a fibre material as reported by Kleinig (1997).

A good agreement was found between the FE results of this work and Hartmann et al. (2006) results as presented in Table 4.5. Hartmann et al. (2006) studied three different cytoplasm - cell wall configurations (cases 1, 2 and 3, as shown in the first column of Table 4.5. These configurations were used in the FE model and were solved to yield values of P_i/P_e. For example, in case 1, the P_i/P_e values of the two works (Hartmann et al., 2006 and the present work) were very close (1 and 1.002) and the difference was 0.02%. In general, results presented in Table 4.5 show a very good agreement between the presented FE model results and the Hartmann et al. (2006) results. The last case presented in Table 4.5 (case 4) shows the P_i/P_o stress using mechanical properties identified in Table 4.1. The results of this comparison

show good agreement, Table 4.5, case 4, where the difference between two results was 0.485%.

Table 4.5 Comparison between Hartmann et al. (2006) results and our simulation.

case	a/b	B_{cyt} (GPa)	E_{mem} (GPa)	$\nu\nu_{mem}$	Hartmann et al. (2006) model (A)	P_i/P_o From FE model (B)	Difference (%) $\left\|\frac{(A-B)\times 100\%}{A}\right\|$
1	0.96	4	0.150	0.4995	1	1.002	0.02%
2	0.99	4	210	0.3	0.672	0.674	0.3%
3	0.99	4	70	0.3	0.866	0.863	0.346%
4*	0.95	2.2	0.112	0.4	1.029	1.024	0.485%

* Yeast properties presented in Table 4.1 were used in this case.

4.7.2 Von Mises stress σ_v and strain ε_v

Using the properties of Table 4.1 and static loading, the normalized σ_v/P_e value was evaluated using the FE model. For 100 MPa external static pressure, σ_v would be approximately 28 MPa. This value varies with the location of the node through the thickness of the cell wall. The FE simulation results show that σ_v developed in cytoplasm of the cell is relatively insignificant in comparison to the cell wall, since it remains in a hydrostatic stress state. Alexander et al. (2000) evaluated σ_v as failure theory from the experimental data (when ε_v and E is given) using equation 4.28:

$$\sigma_v = \frac{2}{3} E \varepsilon_v, \qquad 4.28$$

which is valid for a spherical geometry.

For σ_v = 28 MPa and E of cell wall = 112 MPa, from equation 4.28, ε_v = 0.38. According to Smith et al. (2000b), rupture in the yeast cell wall can only happen if the ε_v value is above 85%, or at least between 75% and 100%. Therefore, no failure is expected to occur when a 100 MPa external static pressure is used. Thus, the external pressure had to be increased. Since both analytical and FE models are assumed to be linear elastic, it is expected that σ_v/P_e and ε_v/P_e are constants. The

calculated FE results demonstrated that the σ_v/P_e and ε_v/P_e are constants of 0.28 and 0.0038 MPa^{-1} respectively. The external static pressure required to generate a stain of 0.85 in the cell wall can be identified by scaling the above results and will be 226 MPa.

Experimental results from Perrier-Cornet et al. (1995) showed that a volumetric shrinkage of 25% occurred in *S. cervesia* when a 250 MPa external pressure was applied. Perrier-Cornet et al. (1995) claim that the mass transfer between the cell and the medium led to a change in the cell wall properties and finally caused cell wall rupturing. However, comparing their treatment pressure of 250 MPa with the present static analysis suggests that the cell wall could have ruptured directly through a mechanical process, rather than via a transfer process.

Hartmann et al. (2006) reported that when a pressure load of 400 MPa is applied on a yeast cell, the wall of the cell will rupture at a maximum σ_v stress of 70 MPa and maximum effective ε_v of about 0.8. As indicated in section 4.7.1, if the cell wall has similar properties to water, it would be very difficult to develop a σ_v of 70 MPa unless ν values are reduced. Thus, the Hartmann et al. (2006) assumption of using the cell wall properties of $\nu = 0.5$ is likely to be inaccurate. To simulate Smith et al. (2000b) conditions where von Mises failure stress was around 100 MPa, the applied external pressure for failure would have to be around 357 MPa.

4. 8 Dynamic results from FE simulation

4.8.1 Uniform properties throughout domain

The initial testing of the dynamic simulation was conducted using water properties for cytoplasm and cell material properties. The initial dynamic simulation results show that the pressure wave can smoothly travel through the water, cytoplasm and cell wall zones with no disruption or reflection in this case since the material properties of the cytoplasm and the cell wall were treated as the same as the surrounding water. The results of this numerical simulation are presented in Fig. 4.11, which demonstrated that the radial stresses at any point in the geometry are equal (see Fig. 4.11). Fig. 4.11 displays five sections along the geometry with a

different simulation time. The results shows that the pressure wave required about 0.025 ms to reach the upper part of cell wall, and that the wave leaves the cell wall at about 0.28 ms. These results were obtained when water material properties are used throughout the domain, and detail of this simulation can be found in Appendix B.

Results from three nodes located in the water, cell wall and cytoplasm were selected from this simulation, and are presented in Fig. 4.12. These results show that the radial stress is essentially the same regardless the location of the nodes. These results (especially the cell wall results) will be used for comparison with other simulations where three different materials are used for the water, cytoplasm, and cell wall.

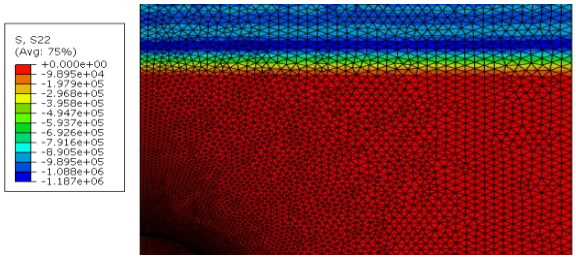

Simulation Time = 0.025 ms

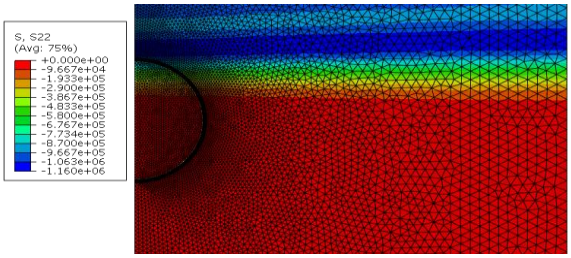

Simulation Time = 0.19 ms

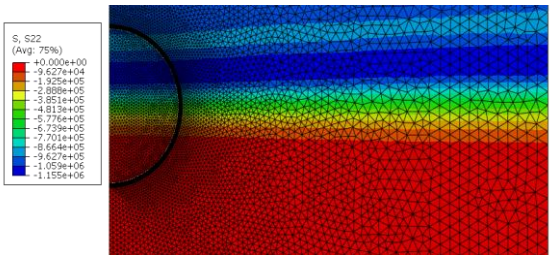

Simulation Time = 0.22 ms

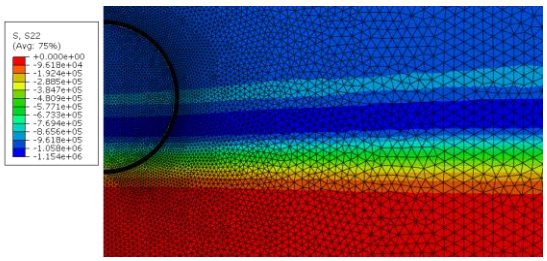

Simulation Time = 0.24 ms

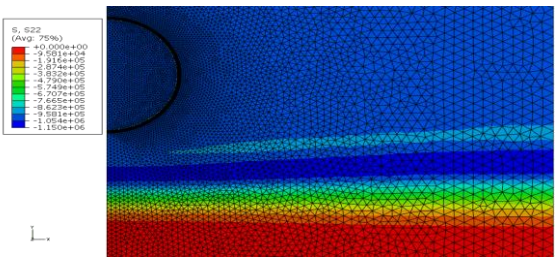

Simulation Time = 0.28 ms

Fig. 4.11 Images of the radial stress wave propagation through the water, cell wall and the cytoplasm using material properties of E = 112 MPa, ν = 0.4995 and density 1000 kg/m^3 throughout the entire domain (part 1, 2 and 3).

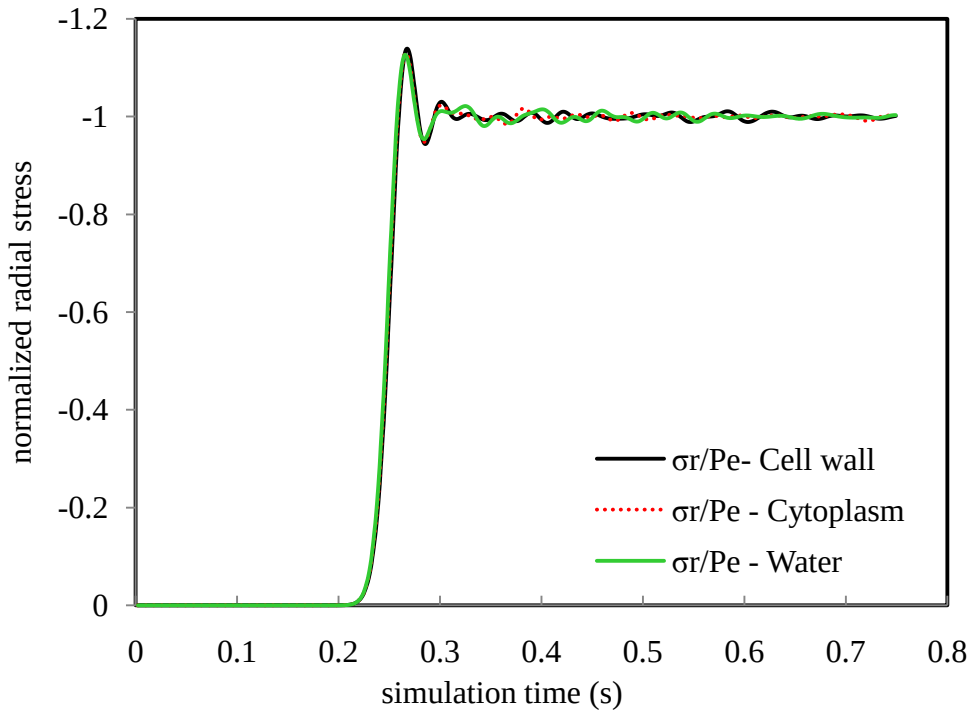

Fig. 4.12 Normalized radial stress against simulation time for three elements in the geometry located in part 1, 2 and 3 for a simulation where the water, cell wall, and cytoplasm have properties of ρ = 1000 kg/m^3, E = 6.2 MPa and ν = 0.4995.

4.8.2 Cell wall - stress and strain

In this simulation the material properties of water, cell wall and cytoplasm presented in Table 4.1 were used. The effect of the external pressure loadings on the cell wall was evaluated using σ_v and ε_v theories of failure. A 1 MPa dynamic uniform pressure was applied at the top surface of the water tube shown in Fig. 4.9. Four nodes in four different locations of the cell wall were selected to examine the maximum σ_v generated on the cell wall. These four nodes were located on the inner diameter of the cell wall in four different locations. The simulated σ_v result and the node locations are graphically presented in Fig. 4.13.

The result shows that the maximum value of σ_v/P_e occurred at node number 4 (green solid curve in Fig. 4.13). Node 4 is located at the bottom (inner diameter) of the cell wall. Another set of nodes (4, 5, 6 and 7) were selected to identify the maximum σ_v/P_e value through the thickness of the cell wall, see Fig. 4.14. The results presented in Fig. 4.14 confirmed that the maximum σ_v/P_e occurred in the node number 4 which

is located at the inner diameter of the cell wall. Thus, node 4 was selected to be the focus for this study.

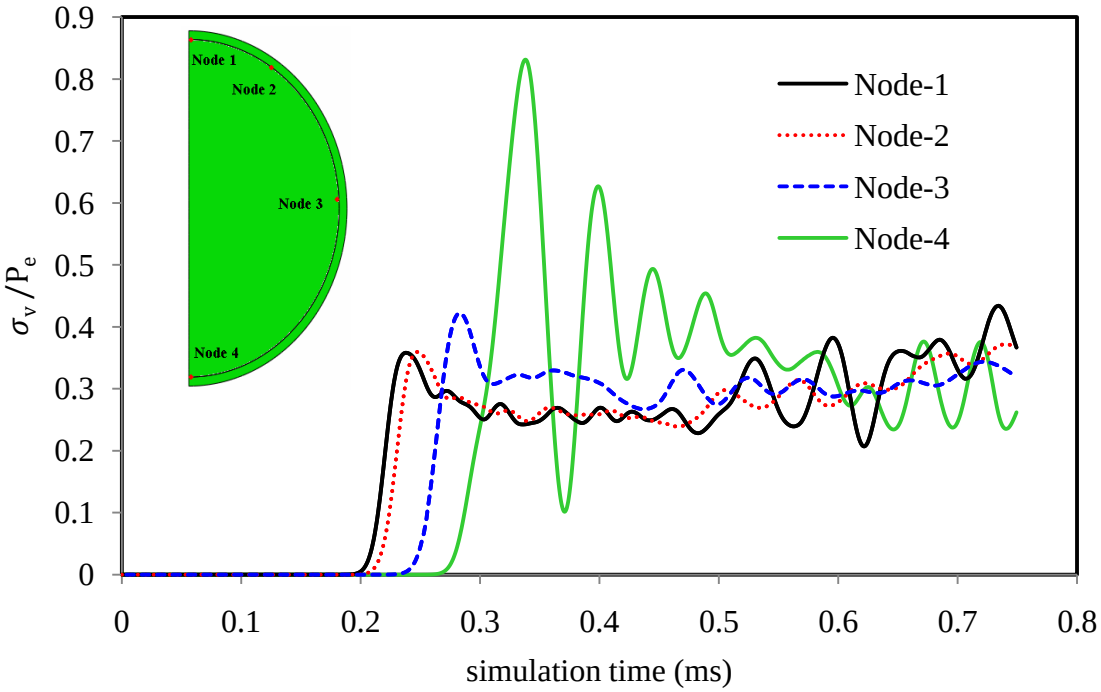

Fig. 4.13. Normalized von Mises stress generated on four different nodes in different locations along the inner circumference of the cell wall.

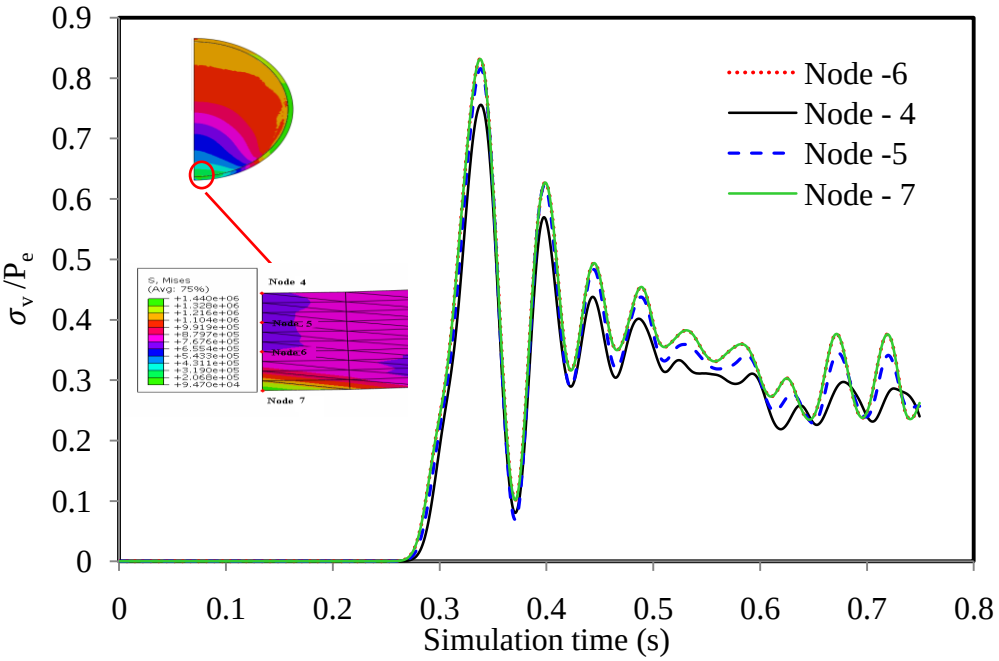

Fig. 4.14. Normalized von Mises stress generated on four nodes through the cell wall thickness at the lowest point on the circumference of the cell wall.

The stress generated at node number 4 of the cell wall shows that the maximum σ_v/P_e is approximately 0.85, while the average σ_v/P_e generated in the cell wall over the time period from 0.3 ms to 0.4 ms was approximately 0.45. As discussed in the previous section, the static σ_v/P_e value was calculated and found to be 0.28. This result shows that the maximum dynamic von Mises stress is approximately three times greater than the static von Mises values generated in the same cell wall using the same mechanical properties given in Table 4.1. The stress rise at a simulation time of about 0.3 ms (presented in Fig. 4.13, and Fig. 4.14) was due to the combined effect of transmission through the cytoplasm and water, and the pressure wave reflection between the cytoplasm and the lower part of the cell wall (node 4).

To illustrate the event, a zoom-in image of the node 4 zone (at simulation time of 0.3 ms) was selected and presented in Fig. 4.15. The water wave arrives before the cytoplasm wave, and thus a wave reflection is expected to occur due to the wave speed differences. As shown in Fig. 4.16, the total simulation time of 0.32 ms was found to be sufficient to allow the wave to travel through the water, cytoplasm and cell wall.

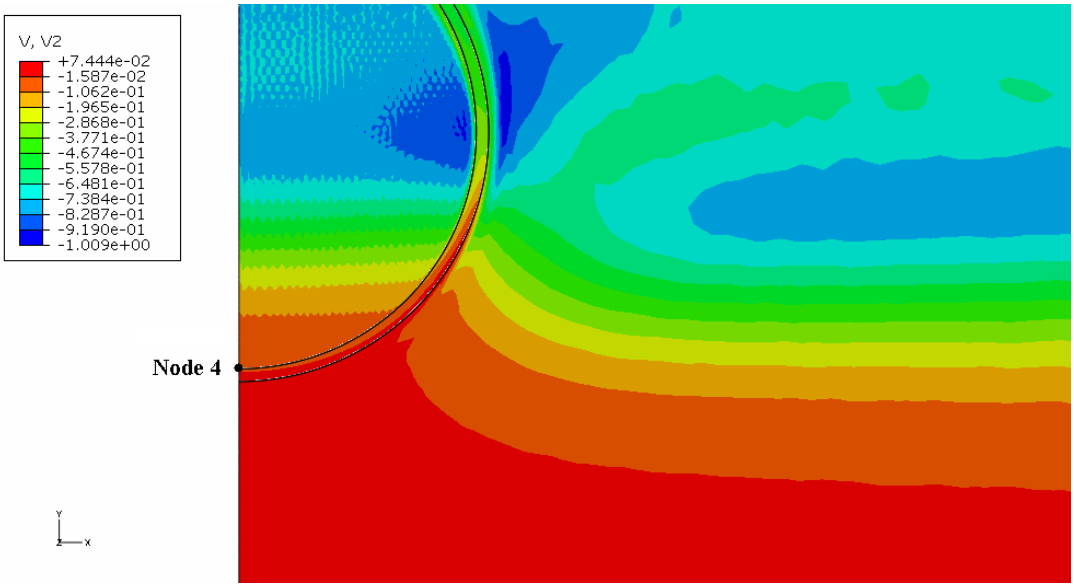

Fig. 4.15 Wave speed through the water, cell wall and the cytoplasm using material properties presented in Table 4.1 throughout the entire domain (part 1, 2 and 3).

Fig. 4.16 shows the pressure wave travelling through the cell at different simulation times (pressure map). Fig.4.16 (a) shows that the pressure wave passes through the cell wall toward the cytoplasm, with the pressure value reaching about 0.5 MPa at

0.21 ms. At the time of 0.22 ms, the pressure wave reached 1.17 MPa as shown in Fig 4.16(b). The maximum pressure of 1.6 MPa was achieved in this simulation as shown in Fig.4.16 (d) for a simulation time of 0.32 ms. Reasons for selecting the pressure instead of von Mises stress for the map is because the von Mises stress in the cytoplasm is approaching zero (in the case of cytoplasm). The corresponding von Mises stress at the simulation time of 0.32 ms (Fig.4.17 (d)) was around 0.85 MPa. The reasons of von Mises stress rise will be discussed in the next subsection.

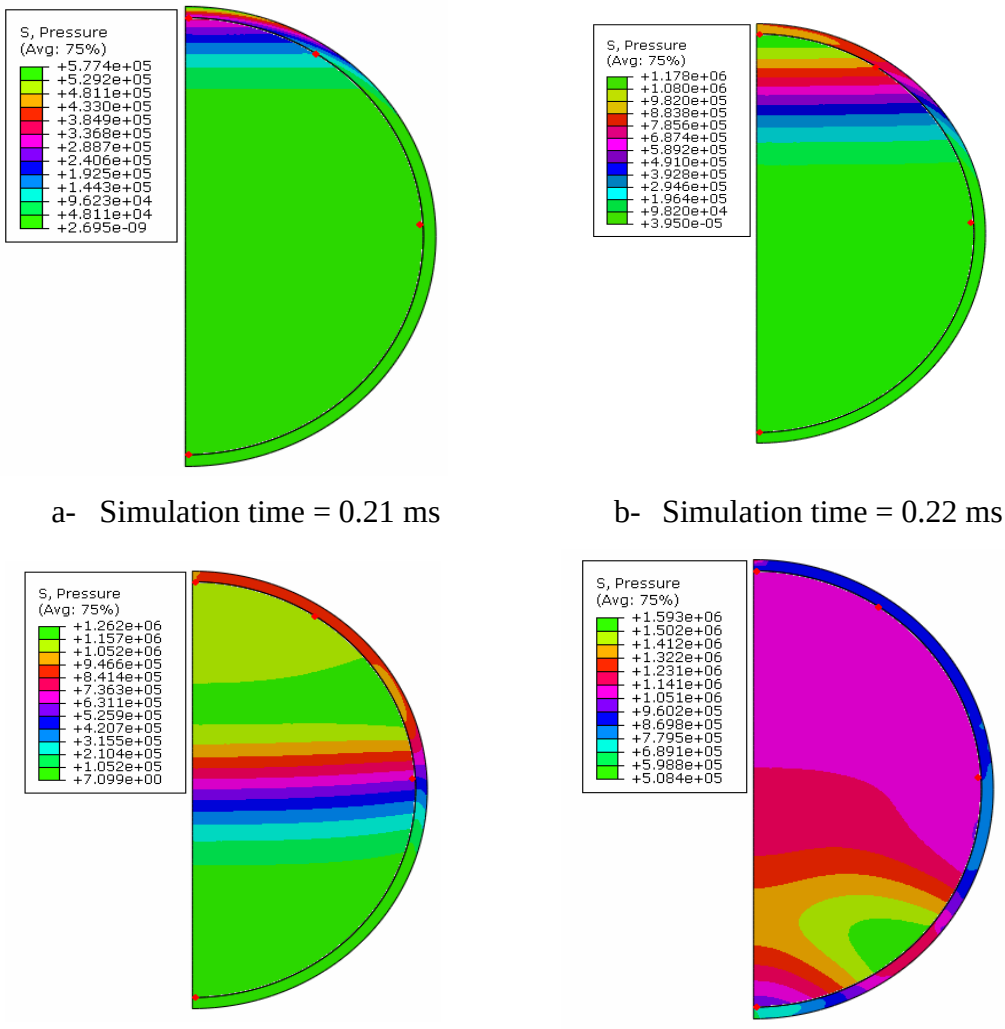

a- Simulation time = 0.21 ms

b- Simulation time = 0.22 ms

c- Simulation time = 0.26 ms

d- Simulation time = 0.32 ms

Fig. 4.16 Maps of pressure wave travelling through the cell at different simulation times of a- 0.21 ms, b- 0.22 ms, c- 0.26 ms and d- 0.32 ms.

4.8.3 Cell wall stress due to external pressure loading

Lardner and Pujara (1980) and Smith et al. (2000a and b) state that the cell failure is expected to occur in the cell wall, however there was no information on the exact location on the cell wall where the failure occurred. The simulation result indicates the likely failure location is the point on the inner surface of the cell wall furthest from the oncoming shock wave.

As previously demonstrated, σ_v/P_e generated on node 4 (the node on the inner surface of the cell wall further from the oncoming shock wave) is the part of maximum von Mises stress. The σ_v/P_e, σ_r/P_e, and σ_v/P_e stresses generated in node 4 are presented in Fig. 4.17. The maximum σ_v/P_e is the difference between the maximum radial stress and the maximum tangential stress (2.26 – 1.41 = 0.85) and occurs at a simulation time of about 0.33 ms as indicated in Fig. 4.17.

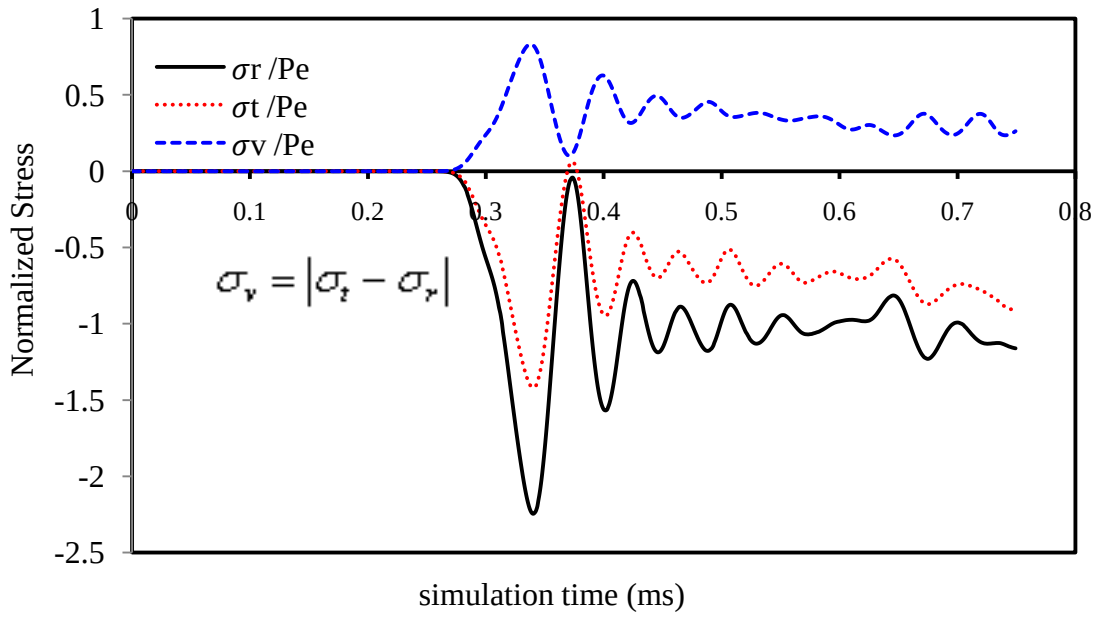

Fig. 4.17 Normalized von Mises stress and the tangential and radial stresses at node 4 using cell wall mechanical properties presented in Table 4.1.

Fig. 4.18 and Fig. 4.19 display the normal stress wave in the water, cytoplasm, and cell wall for different simulation times. As shown in Fig. 4.18, the wave travels smoothly through the water, where the radial stress along y axis is 1.0 MPa for simulation times less than 0.19 ms. Once the pressure wave reached the cell wall at a

simulation time of about 0.19 ms, the first element of the pressure waves started to reflect from the cell due to the material properties associated with the yeast cell. From Figs. 4.18 and 4.19, the maximum radial stress occurs when the wave reached the bottom of the cell wall, at the simulation time of 0.32 ms.

Four different external pressure loadings were applied to the water tube surface to confirm the linear relationship between the von Mises stress and applied external dynamic pressure. The four different pressure values that were used in this simulation were 100 MPa, 200 MPa, 400 MPa and 800 MPa. Node number 4 was again assessed in this work; σ_v/P_e stress at the node 4 was evaluated and the data is presented in Table 4.6. The relationship was found to be linear as stated in the validation section of this chapter. As it can be seen from Table 4.6, the normalized von Mises (σ_v/P_e) and strain ε_v/P_e was found to be constant of 0.85 and 1.14 MPa^{-1} respectively.

Table 4.6 Values for σ_v/P_e and ε_v/P_e for different external dynamic pressure.

P_e (MPa)	σ_v (MPa)	σ_v/P_e	ε_v	ε_v/P_e (MPa^{-1})
100	85	0.85	1.14	0.0114
200	170	0.85	2.27	0.0114
400	340	0.85	4.55	0.0114
800	680	0.85	9.1	0.0114

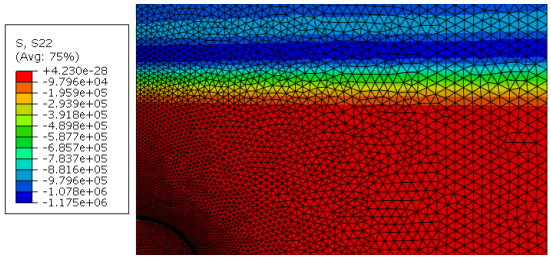

a- Simulation Time = 0.13 ms

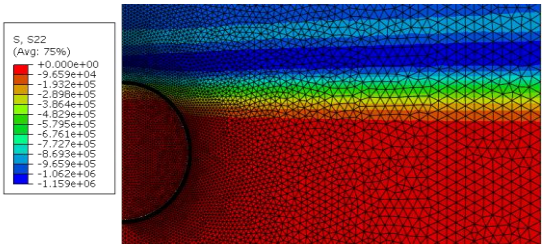

b- Simulation Time = 0.19 ms

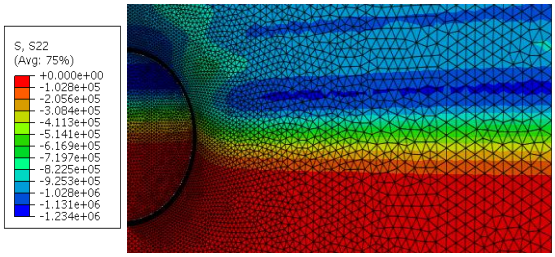

c- Simulation Time = 0.24 ms

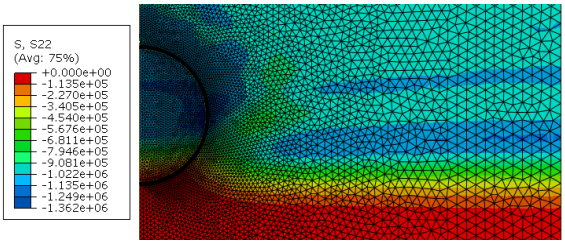

d- Simulation Time = 0.28 ms

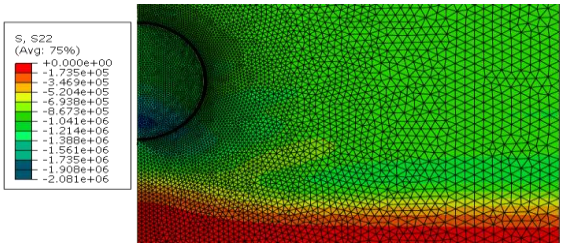

e- Simulation Time = 0.32 ms

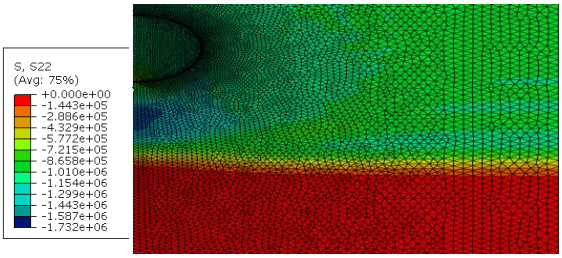

f- Simulation Time = 0.36 ms

Fig. 4.18 Illustration of radial stress wave travelling along R axis through the water (E = 6.2 MPa, ν = 0.4995 and ρ = 1000 kg/m^3), cell wall (E= 112 MPa, ν = 0.4 and ρ = 3500 kg/m^3) and the cytoplasm (E = 6.2 MPa, ν = 0.4995 and ρ = 1100 kg/m^3) for the domain in the vicinity of the yeast cell.

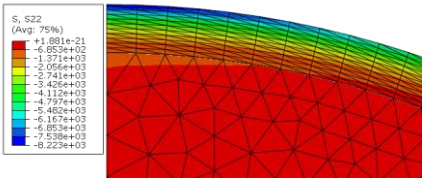

a- Simulation Time = 0.19 ms

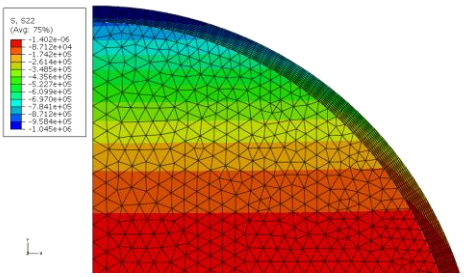

b- Simulation Time = 0.22 ms

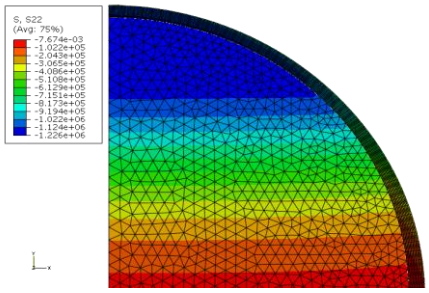

c- Simulation Time = 0.24 ms

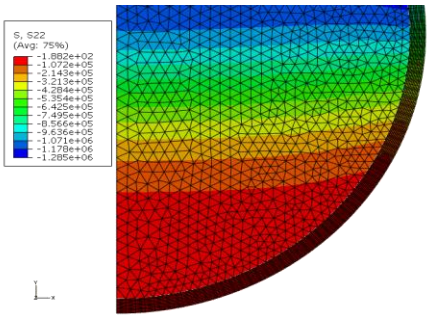

d- Simulation Time = 0.27 ms

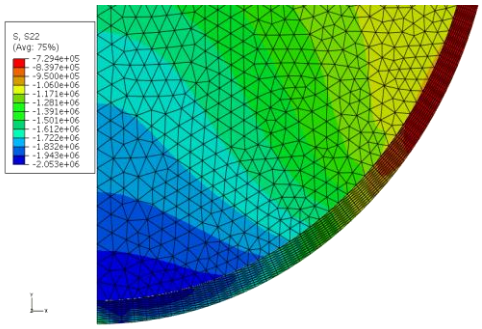

e- Simulation Time = 0.33 ms

Fig. 4.19 Illustration of radial stress wave along R axis travelling through the water (E = 6.2 MPa, ν = 0.4995 and ρ = 1000 kg/m^3) the cell wall (E= 112 MPa, ν = 0.4 and ρ = 3500 kg/m^3) and the cytoplasm (E = 6.2 MPa, ν = 0.4995 and ρ = 1100 kg/m^3) for the yeast cell only.

Smith et al. (2000b) indicated that the cell wall rupture of a single yeast cell occurred when the strain of the cell wall was around 82% (±1.4) for the exponential growth phase, and 80% (±1.6) for the stationary growth phase (Smith et al., 2000b). From the simulated strain results shown in Fig. 4.20, it can be seen that the maximum strain of approximately 0.99% can be achieved at an external pressure of 1 MPa. The simulated von Mises strain to external pressure ratio obtained from the previous section was around 0.0114 MPa^{-1}, which is located within the reported strain range that is capable of rupturing the cell wall. Thus cell wall rupture is expected to occur at σ_v/P_e of 0.85 at 100 MPa.

From this simulation, it was demonstrated that σ_v and ε_v presented in this work are theoretically sufficient to disrupt a yeast cell when external dynamic pressure greater than 100 MPa, since the reported disruption range was greater than the required σ_v and ε_v of cell wall disruption.

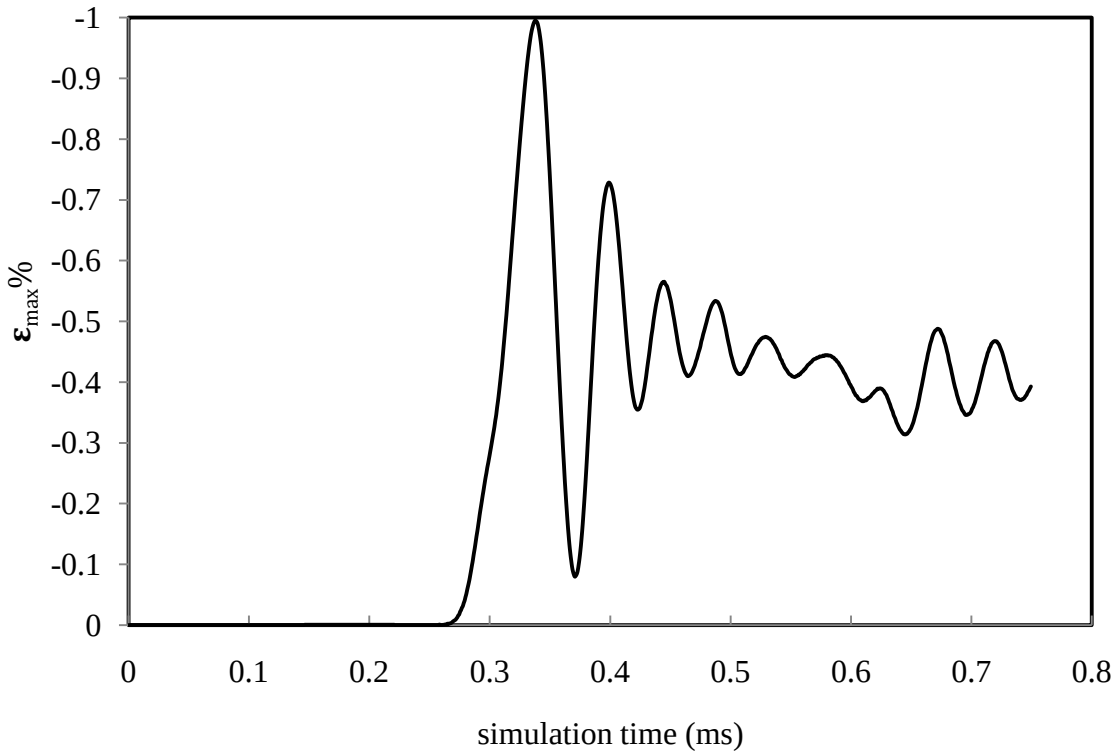

Fig. 4.20 ε_{max} at node 4 located at the cell wall using E = 112 MPa, ν = 0.4 and ρ = 3500 kg/m^3 at normalized pressure of 1.

4.8.4 Dynamic focusing of pressure waves

From the results presented in section 4.6.5, it was found that maximum σ_v/P_e occurred in node 4 as shown in Fig. 4.13 and 4.14. The pressure rise in this node occurs due to the reflection of the pressure wave at the bottom part of the cell wall. When the front part of the pressure wave (Fig.4.19 (d) – red and orange colour) reaches node 4, the pressure wave will reflect while the remaining part of the wave (Fig. 4.19 (e), green and blue) continues to travel towards node 4. The effective accumulation of the incident wave and the reflected wave in the vicinity of node 4 leads to an increase in the stress in the lower part of the cell wall, and this point therefore experiences the maximum stress. Fig. 4.13 show that the maximum σ_v/P_e of node 1 located at the top of the cell wall is approximately 0.3, while the maximum σ_v/P_e of node 4 is 0.85, which is three times greater than the maximum σ_v/P_e of node 1. This static and dynamic simulations show that the von Mises stress developed in node 4, using a dynamic model, is three time greater than von Mises stress using a static model at the same node.

To understand and analyse the cause of σ_v/P_e rise in node 4 of the cell wall, the sound speed in the cytoplasm was evaluated. The sound speed of the wave can be calculated using equation 4.29

$$C = \sqrt{\frac{B}{\rho}} \qquad 4.29$$

The bulk compressibility (B) can be calculated using equation 4.38

$$B = \frac{E}{(1 - 2\nu)} \qquad 4.30$$

From equation 4.29 and 4.30, the following observation can be made

1. The pressure wave speed in a fluid increases when B increases.
2. Since B is directly proportional with E, thus the wave speed is expected to increase when E increases as shown in equation 4.29 and 4.30.
3. When ν decreases, the B will increase (for a fixed E), and this leads to increase the speed of the wave as shown in equation 4.30.

The above three observations showed that wave speed changes with respect to the mechanical properties of cytoplasm, cell wall and water. Another reason for the stress rise in the dynamic mode could be due to the acoustic waves travelling through different areas. When the wave travels from a wide area such as water to a very narrow area such as a cytoplasm, the acoustic wave will increase, and thus pressure will increase.

4.9 Sensitivity to uncertainty in physical properties

The transmission and reflection of the shock wave are influenced by the cell wall and cytoplasm mechanical properties. This introduces significant complexity as the literature cites a range of mechanical properties. Given the uncertainties in the physical properties of the cell wall and cytoplasm, simulations were performed to evaluate the effect of possible variations in these properties on yeast cell rupturing under shock loading.

4.9.1 Cytoplasm Poisson's ratio

Cytoplasm Poisson's ratio (ν) is an important factor as it will influence the σ_v/P_e generated on the cell wall. The effect of ν on the σ_v/P_e stress generated on the cell wall was investigated using three different cytoplasm ν values of 0.4995, 0.4 and 0.3. The relationship between the speed of the pressure wave travelling through the cytoplasm and the Poisson's ratio of the cytoplasm (equation 4.30) shows that the increase in ν will increase the speed of the wave. Thus using a low ν value will provide sufficient time for the pressure wave to travel through the cytoplasm, impact the bottom of the cell wall and reflect back to be combined with the pressure wave travelled downward and finally increase the stress on the bottom of the cell wall. Fig. 4.21 shows that the σ_v/P_e increases from 0.85 when ν = 0.4995, to approximately 8.5 when ν = 0.3. In the case of ν = 0.3, the speed of the sound in the cytoplasm was approximately 330 m/s, and this low speed will give sufficient time for the wave to travel down and impact the cell wall and reflect back causing pressure rise.

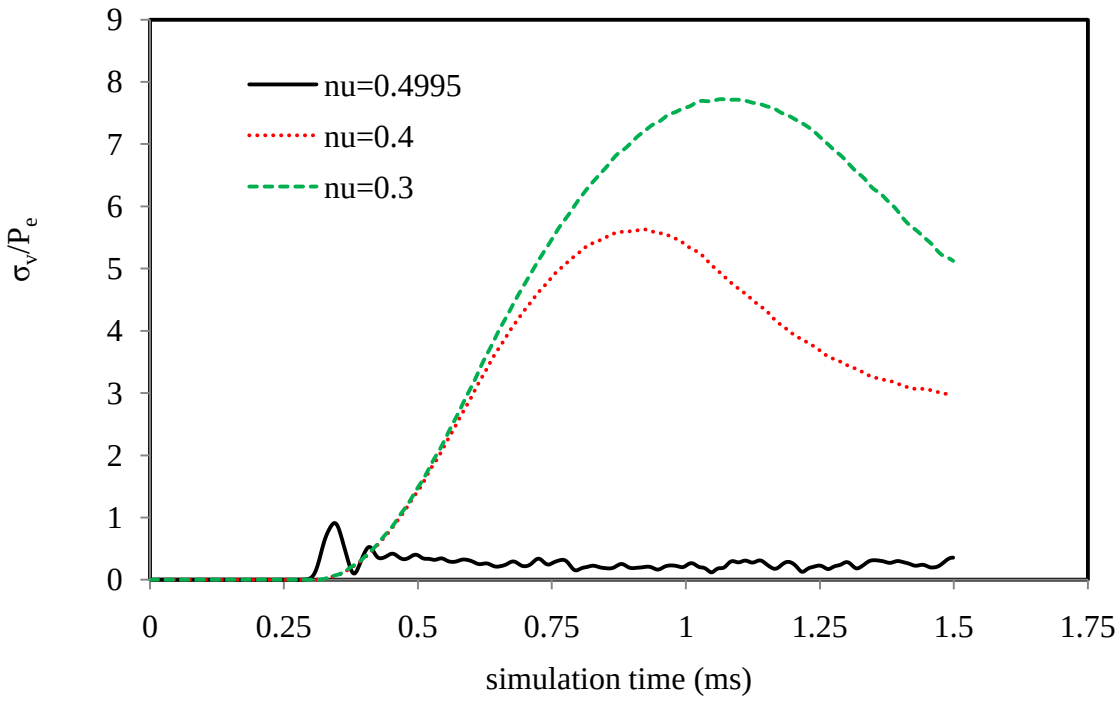

Fig. 4.21 The effect of cytoplasm Poisson's ratio on σ_v/P_e, using material properties presented in Table 4.1.

4.9.2 Elasticity of the cytoplasm

The effect of the *E* of the cytoplasm on σ_v/P_e is investigated in this section, while Poisson's ratio and density are remained unchanged. The results show that when *E* values increase from 6.2 MPa to 10 MPa and 30 MPa, the σ_v/P_e value decreases by approximately 10% and 20% respectively, see Fig. 4.22.

The relationship between the speed of the sound and the *E* of the cytoplasm shows that an increase in *E* will increase the speed of the wave. The time required for the wave to reach node 4 will be small. This means there will not be a sufficient time for the wave to hit the bottom of the cell and multiply the pressure, as discussed in section 4.8.

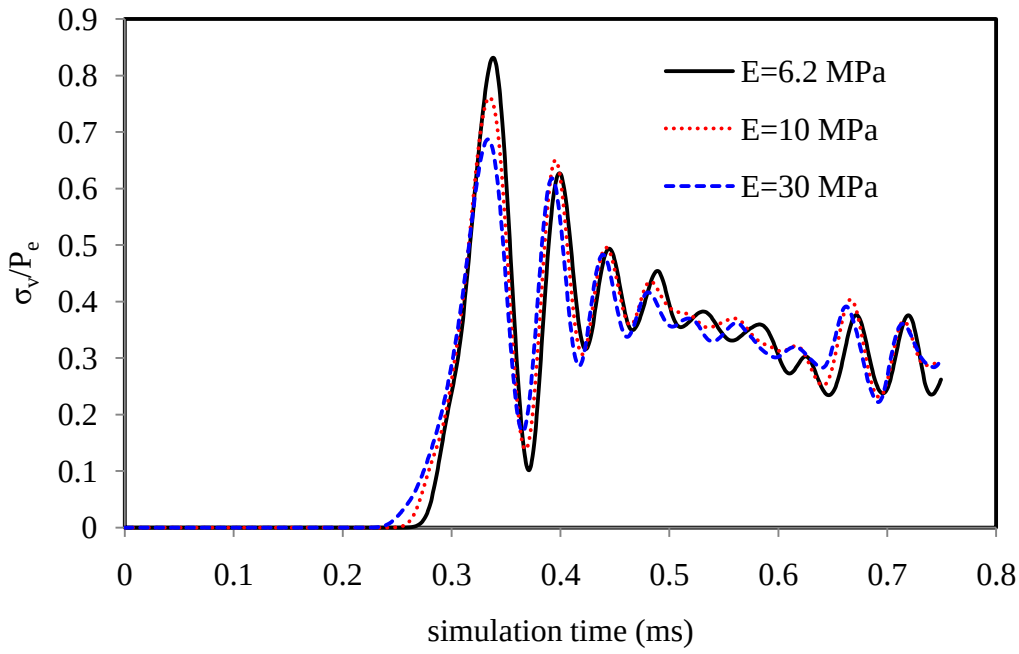

Fig. 4.22 The effect of cytoplasm *E* values on σ_v/P_e using material properties presented in Table 4.1.

4.9.3 Cytoplasm density

The density of cytoplasm was one of the factors influencing the magnitude of the σ_v/P_e values when the external pressure loading was applied. It was found that the maximum σ_v/P_e generated on the cell wall due to the pressure wave reflection at the bottom of the cell wall, node 4, was increased from 0.85 to 0.89, when the cytoplasm density increased from 1100 kg/m^3 to 2500 kg/m^3 as shown in Fig.4.23. The simulated results shows also that increasing the density of the cytoplasm from 1100 kg/m^3 to 1500 kg/m^3 will increase the σ_v/P_e by approximately 1.5%, which is insignificant. As indicated in the previous section, the increase of σ_v/P_e on the cell wall was due to the pressure wave reflection that occurred at the bottom of the cell wall. Considering equation 4.29, the speed of the sound in the cytoplasm decreases when the cytoplasm density increases. Therefore the pressure wave reflection will be increased as there will be sufficient time for the wave to travel, impact the bottom of the cell wall and reflect back to combine with the pressure wave. This process leads to an increase in stress at node 4.

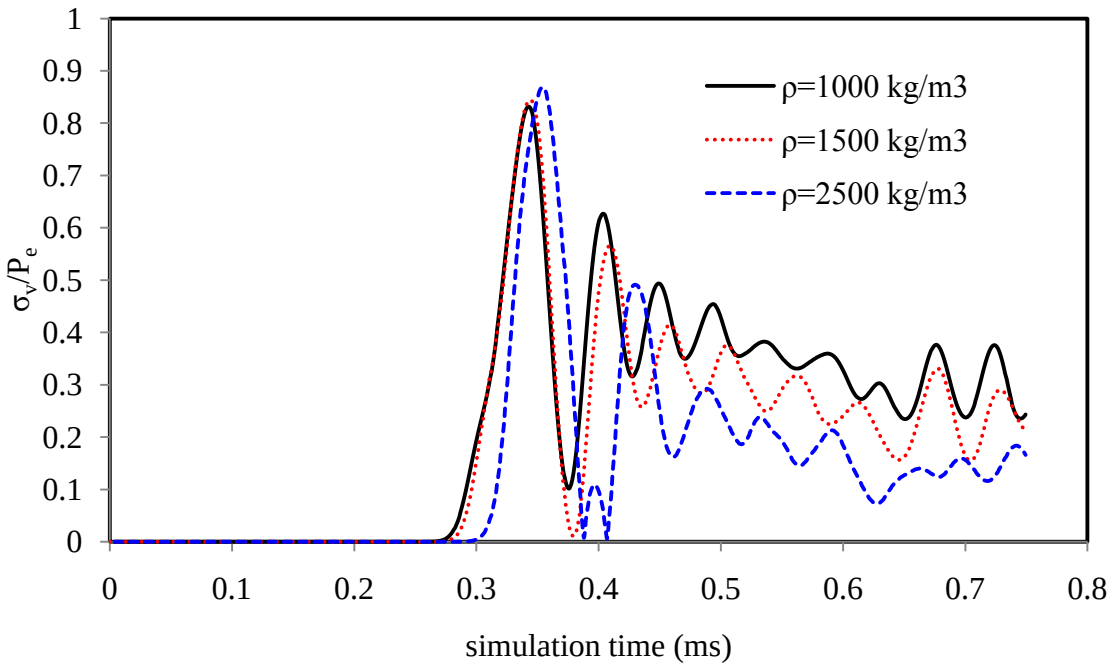

Fig.4.23 The effect of cytoplasm density on σ_v/P_e using material properties presented in Table 4.1.

4.9.4 Cell wall Poisson's ratio

The relationship between the cell wall ν values and σ_v/P_e was investigated for the different cell wall Poisson's ratios that were reported in the literature in section 4.2 (0.35 to 0.4995). The results presented in Fig. 4.24 show that σ_v/P_e increases when ν decreases. Another simulation was conducted using a ν value of 0.4995. The result shows that possibility of rupturing the cell wall with ν close to a fluid value (ν = 0.5) is very unlikely since σ_v/P_e and ε_v will be very small (Table 4.7).

Table 4.7 shows that σ_v/P_e and ε_v decrease when Poisson's ratio increases. As given in Table 4.7, σ_v/P_e = 2.1 and ε_v = 2.8 when ν = 0.2. The ε_v value decreased to be 0.99 and σ_v/P_e = 0.85 when ν = 0.4. This means the possibility of having cell wall rupture is high when the ν value is low. The last row of Table 4.7 shows that the von Mises stress and strain are close to zero when Poisson's ratio is 0.4995. These results agree with the analytical and FE static simulations.

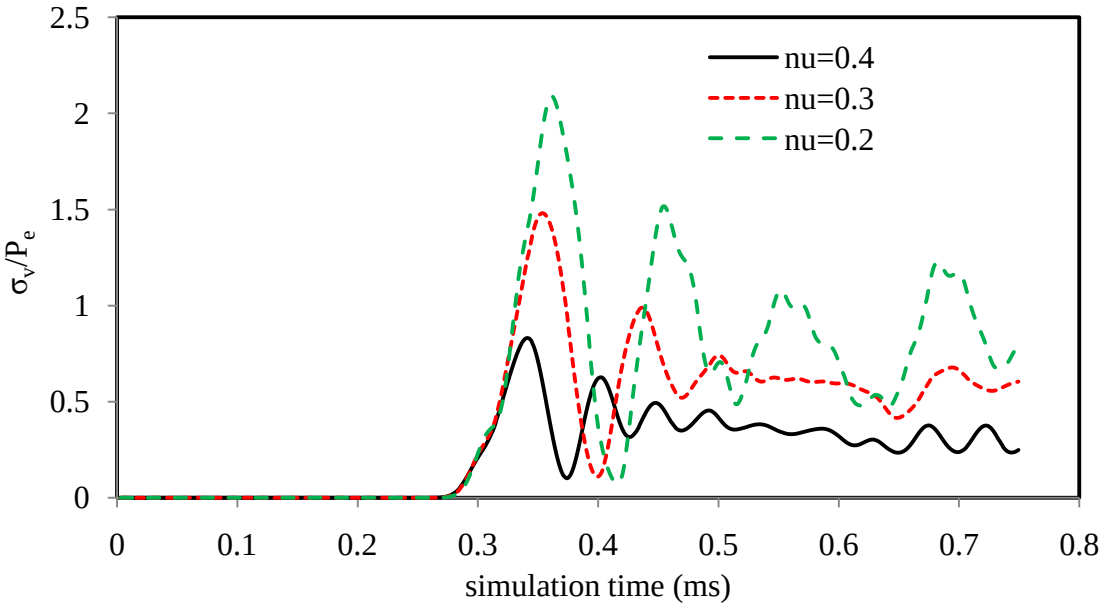

Fig.4.24 The effect of Poisson's ratio on σ_v/P_e using material properties presented in Table 4.1.

Table 4.7 Simulated σ_v and ε_v results for different cell wall ν values.

ν	σ_v/P_e	ε_v
0.2	2.1	2.8
0.3	1.5	1.99
0.4	0.85	0.99
0.4995	0.00198	0.0026

4.9.5 Cell wall elasticity

The effect of the E of the cell wall on σ_v/P_e and ε_v was also investigated. The simulation results show that the change of the cell wall E values has a significant influence on the σ_v/P_e value. A cell wall E of a commercial yeast of 112 MPa was initially used in this simulation (Smith et al., 2000a). It was found that the corresponding σ_v/P_e was 0.85 when the cell wall E = 112 MPa and ν = 0.4 as shown in Table 4.8. When the E value increases to 220 MPa, 440 MPa, and 880 MPa, the σ_v/P_e was noticed to be marginally increased to be 0.91, 0.92 and 0.94 respectively and ε_v decreased to be 0.620, 0.31 and 0.16 respectively.

Table 4.8 Simulated σ_v and ε_v results for different cell wall *E* values.

E (MPa)	σ_v / P_e	ε_v
112	0.85	1.139
220	0.91	0.620
440	0.92	0.310
880	0.94	0.160

4.9.6 Cell wall density

Simulations were conducted using same basic material properties, except the cell wall density was changed. Since the most commonly reported cell wall density values are in the range of 1000 kg/m^3 to 3500 kg/m^3, a set of density values of 1000, 1100, 2500, and 3500 kg/m^3 was selected for these simulations. The simulated results for σ_v/P_e are presented in Table 4.9. As shown in Table 4.9, the change of the cell wall density has a very modest impact on σ_v/P_e values. Thus, the change of the cell wall density will have less impact on the cell wall rupturing.

Table 4.9 σ_v / P_e and ε_v simulated dynamics results for different cell wall density values.

Density (kg/m^3)	σ_v / P_e	ε_v
1000	0.81	1.085
1100	0.815	1.09
2500	0.84	1.125
3500	0.85	1.139

4.9.7 Summary of the FE simulation results

The results from the FE simulations presented in this chapter can be summarized as follows:

1. The FE static model was compared with the analytical calculation and other reported simulation results. Very good agreement between the two models as well as the reported results were achieved (Hartmann et al., 2006; Smith et al., 2000a).

2. Von Mises stress was adopted as a theory of failure based on the data reported in the literature review. The σ_v/P_e generated on the cell wall was evaluated, and stress focussing due to a dynamic effect was found to occur at the inner surface of the cell wall at the location furthest from the oncoming shock wave (node number 4 in Fig. 4.15).
3. The maximum dynamic value of σ_v/P_e in node 4 was found to be three times greater than the static σ_v/P_e value. The stress increase was analysed and the reason for this rise was found to be due to the pressure wave focusing and reflection when it reached the bottom part of the cell wall. It appeared likely that the region of the cell wall further from the oncoming shock is the location where cell wall rupture will occur.
4. A parametric study was performed to evaluate the effect of the yeast cell mechanical properties on the cell disruption using von Mises theory of failure. The simulation results showed that, σ_v/P_e increases when:
    a) the E and ν values of the cytoplasm decrease and,
    b) the E and ν values of the cell wall decrease.

The parametric study also showed that the cell wall and cytoplasm density have less effect on the von Mises stress.

4.10 Shock disruption experiments

4.10.1 Experimental apparatus

The results obtained from the FE model can provide valuable information about when and where the rupture may occur in the yeast cell wall. Simulation results generally have less value without some experimental verification so experimentation was conducted. Fig. 4.25 shows a schematic illustration of the vertical gas gun tunnel at USQ

The experimental shock wave apparatus used in this work was designed to provide different external pressure loading of between 100 MPa and 300 MPa on yeast suspension. The pressure wave propagates through the water tube with a speed of sound of around 1450 m/s. The shock wave will then hit the bottom of the water tube

and reflect back to join the wave, a sample of the shock test is shown in Fig. 4.26. This range of pressure was selected based on the FE analysis which indicated cell wall rupture (based on von Mises theory of failure) would occur for such loading.

A vertical gas gun was commissioned in the hydraulics laboratory of USQ. With reference to Fig. 4.25, the experimental apparatus consists of the following components :

1. An air reservoir tank at the top of the apparatus. The air reservoir was connected to a compressor which can generate pressures of 4 MPa.

2. A 3.1 m long and 25.5 mm bore tube (barrel), this tube is connected to the bottom of the tube. Four light sources attached to the tube and these light sources were used to capture electrical signals to evaluate the speeds of the pistons.

3. Three pistons made of Brass and Aluminium with different lengths. These pistons were launched with high speeds so they can generate different external pressure on the surface of a water tube. The pressure values ranging between 100 MPa – 400 MPa.

4. A water filled tube with a diameter of 25.5 mm was placed at the barrel exit; the water pressure values were recorded at a point located half way along the tube. A connector tube was used to allow the piston to travel from the reservoir to the water tube.

5. A plastic bag full of yeast suspension was placed in the tube.

It is important to note here that the time required for the pressure rise within the cell wall is very small in comparison to the yeast cell response time associated with the hydraulic conductivity, Smith et al. (2000c). Smith et al. (2000c) reported that the yeast cell wall hydraulic conductivity is between 0.1 to 1 $\mu m. MPa^{-1}. s^{-1}$. For yeast hydraulic conductivities between 0.1 and 1, the calculated cell respond time is between 0.25 to 2.5 s (where the yeast cell diameter is 5 µm and pressure load is 100 MPa). In contrast, the treatment time of the shock is calculated to be around 1×10^{-9} s, thus the treatment time is relatively small. This result is consistent with others. For

example, Stenson et al. (2010) reported that the time required to allow sufficient water loss through the cell was very small, and was ignored even their non-shock loading work.

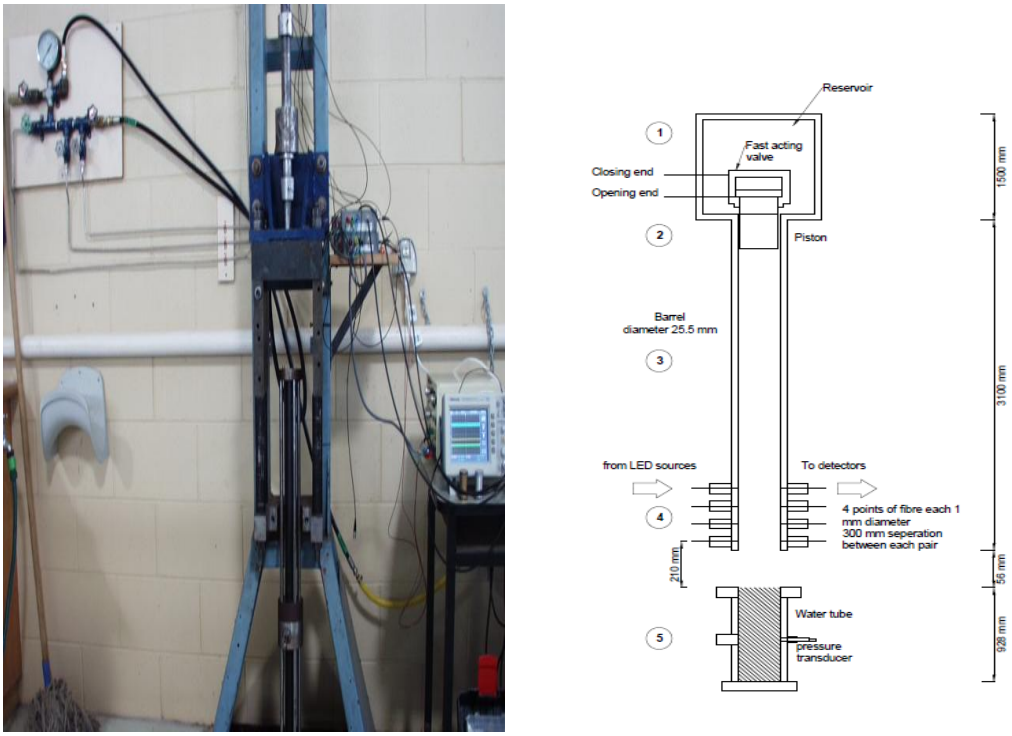

Fig.4.25 Image and schematic illustration of the vertical gas gun at USQ.

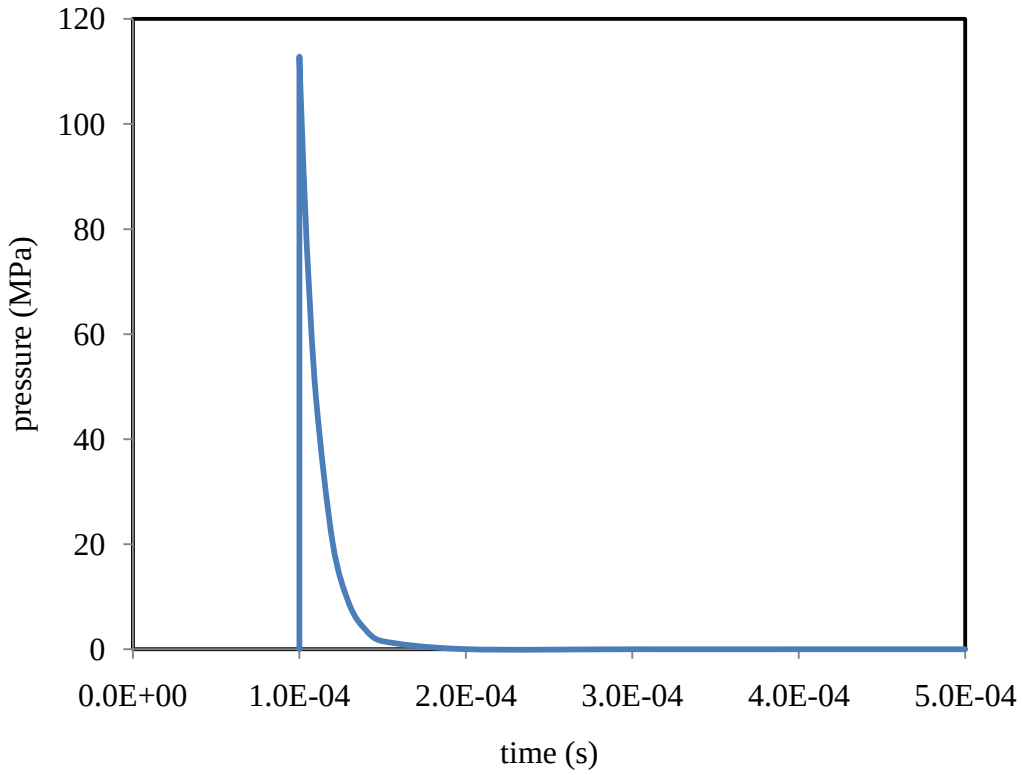

Fig. 4.26 The pressure wave propagation through the water tube against time.

4.10.2 Methodology

As detailed earlier, *S. cerevisiae*, commonly known as yeast, was used because it is easy to grow, readily available and inexpensive. The procedure for yeast preparation and counting was described in sections 3.5.2.

A 15 mm long plastic bag made of LDPE was used to house the yeast suspension. A 0.5 ml volume of the yeast suspension was pipetted into the plastic bag and then sealed using a bagging machine. The sample was then stored in the refrigerator at 4°C until the tests were performed to make sure the yeast cell remain live.

The bag thickness initially used was 35 µm, but these bags tended to rupture during the shock exposure, so a stronger plastic bag of 45µm thickness LDPE was used in the tests to avoid any failure on the bag. The plastic bag was held in place at the bottom of the water tube using sticky tape. Sample of the suspension was shocked treated; the number of CFU per millimetre of yeast was counted and compared with

initial CFU/mL before the shock treatment. This was done by means of a viable count.

For each test, two small plastic bags full of a yeast suspension were stuck to the bottom of the water tube as shown in Fig.4.20. The sample cradle is then connected to the water tube and bolted prior the tube being filled with water. The connector tube was then bolted to the water tube and placed under the gas gun apparatus. The tube was lifted and bolted to the gun tube apparatus.

After connecting the water tube to the barrel, the piston was fired at 0.6 MPa pressure. Four optical sources and detectors had to be connected to the barrel. A 1 mm diameter fibre optic cable was used to capture the pressure signals. A PCB pressure transducer (model number 109C12, serial number 5095, with a sensitivity of 10.19 mV/MPa) was used to capture the pressure signal. Two Bourdon-tube pressure gauges were used to measure the reservoir pressure immediately prior to opening the fast acting valve. The signals were then recorded using optical detectors, pressure transducer and digital storage oscilloscopes (Tektronix TDS210 and 2014). The signals were then transferred from the oscilloscopes to a computer via the serial communications port and subsequently analysed.

4.11 Experimental results

Experimental shock treatment was performed by the author of this thesis and Shepherd (2004). From the above experimental results, four tests results were selected for this study (114 MPa, 114.5 MPa, 115.7 MPa, and 116.6 MPa) and are presented in Table 4.10. The corresponding piston velocities of these pressures are between 79 m/s and 81 m/s. As shown in Table 4.10, the average shock pressure used was about 115 MPa, while the log yeast reduction varied between 0.23 to 0.57 MPa. The results presented in Table 4.10 shows that maximum yeast reduction of 0.57 can be achieved when pressure average of 115 MPa is applied. The average yeast log reduction was found to be around 0.25 and this value will be used in chapter 6 for comparative study. Overall, the results of yeast disruption did not achieve the expected level and the underpinning reasons are discussed.

Table 4.10 The log reduction and for different shock tests using different shock pressure and yeast suspension concentration (Shepherd, 2004).

Test	Shock pressure (MPa)	Piston velocity (m/s)	Before treatment (CFU/mL)	After treatment (CFU/mL)	$\lvert \log reduction \rvert$
Control	-	-	2.5×10^5	2.5×10^5	0
Test 1	114	79.2	1.46×10^5	1.16×10^5	0.13
Test 2	114.5	79.5	1.3×10^7	0.9×10^7	0.25
Test 3	115.7	80.3	6.3×10^5	5.6×10^5	0.5
Test 4	116.6	81	5.3×10^5	3.0×10^5	0.57

4.12 Reasons for modest yeast disruption results

The experiments yielded less disruption than anticipated due to a number of reasons.

1. The yeast suspension was subjected to the external pressure for only a very short time (one pressure pulse) in comparison to similar work reported in the literature. For example, Perrier-Conet et al. (1995) required ten minutes of exposure to reduce the cell volume by 15-20% using shock treatment of 250 MPa pressure on *Saccharomycopsis fibuligera* cells. Splimbergo et al. (2002) reported treatment times from 2 minutes to 20 minutes, by repeating the shock treatment, depending on the bacteria. In the present study, the treatment time was very short and there was no recurrence treatment. If the yeast suspension had been subjected to an increased number of shock waves, the like-hood of microorganism disruption is expected to be higher. However, in this case, the microorganism disruption could then be due to fatigue stress.

2. Smith et al. (2000b), Lee et al. (2004) and Hartmann et al. (2006) conducted their experimental works on a single yeast cell, while in the present experiments the yeast aggregation (colony) forming units in one millilitre was in the range of 1×10^5 CFU/mL (Table 4.10). Comparing results with Smith et al. (2000b), Lee et al. (2004) and Hartmann et al. (2006) is not very accurate.

3. Another possible reason (related to point 2) for modest yeast disruption using shock treatment is that before any sort of treatment, cells may have grouped and made aggregation (colony) forming units. When such as sample is treated, the pressure load may be just sufficient to break up the groups of aggregation (colony) forming units without reducing the viability of the component cells. Therefore, when both the control and test samples are counted, some of the viable test appears to have more colony forming units than the control sample. Better estimates of some other techniques such as Coulter Counter can be used in the future to evaluate the size of cell distribution.

4. When shock treated, some of the samples did not have a uniform dispersion of aggregation (colony) forming units. It is assumed that the shock intensity is greatest at the centre of the water tube. It was expected that the number of aggregation (colony) forming units were well distributed in the bag; however this may not be the case. Thus the entire samples would not be subject to the full intensity of the shock wave.

4.13 Effect of sample bag on microorganism disruption

Another possible reason for the modest level of yeast disruption in the experimental results was due to the energy lost in the plastic bag containing the yeast suspension. The bag is able to absorb or reflect some of the pressure waves, thus reducing the energy available for treatment of the yeast.

A FE element model using ABAQUS was developed to investigate and analyse the effect of the plastic bag material on the process of yeast cells rupturing in the plastic bag. An explicit dynamic step was used with same mesh quality and density that was used in the simulation described in section 4.4. The procedure of verification and validation of spherical model was adopted and repeated to validate this model where the plastic bag shape assumed to be cylindrical.

A small plastic bag made of low density polyethylene LDPE was used in this simulation. This bag was simulated using the geometric model presented in Fig. 4.27. According to Willett (1994), the Poisson's ratio and the density of the LDPE is 0.43 and 1300 kg/m^3 respectively. The modulus of elasticity of the LDPE was reported by Mfoumou et al. (2006) in the range of 80 to 127 MPa for LDPE. A value of 127 MPa was selected for this work. A uniform pressure load of 100 MPa was applied on the surface of the tube and the pressure load was held constant until the pressure wave reached the bottom of the tube, having passed through passed the bag. The bag was positioned in the middle of the water tube.

The effect of the plastic bag material on the pressure propagation through the bag was simulated. As discussed earlier, the experimental results demonstrated that there was only a small amount of yeast disruption when the shock wave technique was used. In this section, the external pressure magnitude value was simulated with and without the plastic bag. Fig. 4.27 shows that the pressure value was reduced by approximately 35% when the plastic bag was used. The two curves in Fig. 4.28 represents two nodes located inside the bag and outside the bag. This means, the net magnitude of the pressure transmitted into the bag for yeast disruption was approximately 65% of the applied external pressure. Therefore, the calculation must be adjusted to incorporate the 35% losses, and thus the yeast cell disruption was not achieved when only 100 MPa pressure was applied. This is a good explanation of why very little microorganism disruption was observed experimentally.

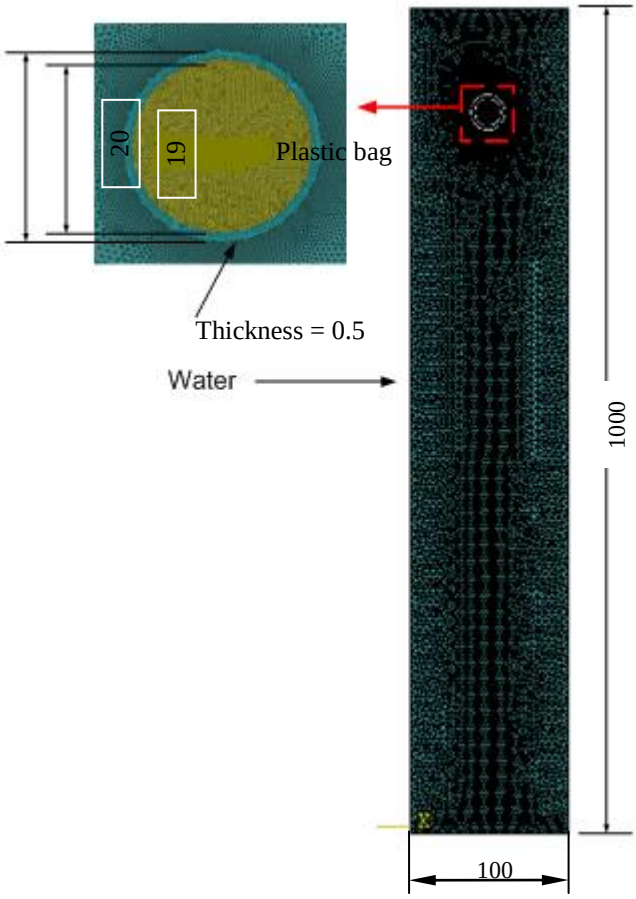

Fig. 4.27 Plastic bag full of yeast cell in a water tube (measurement in mm)

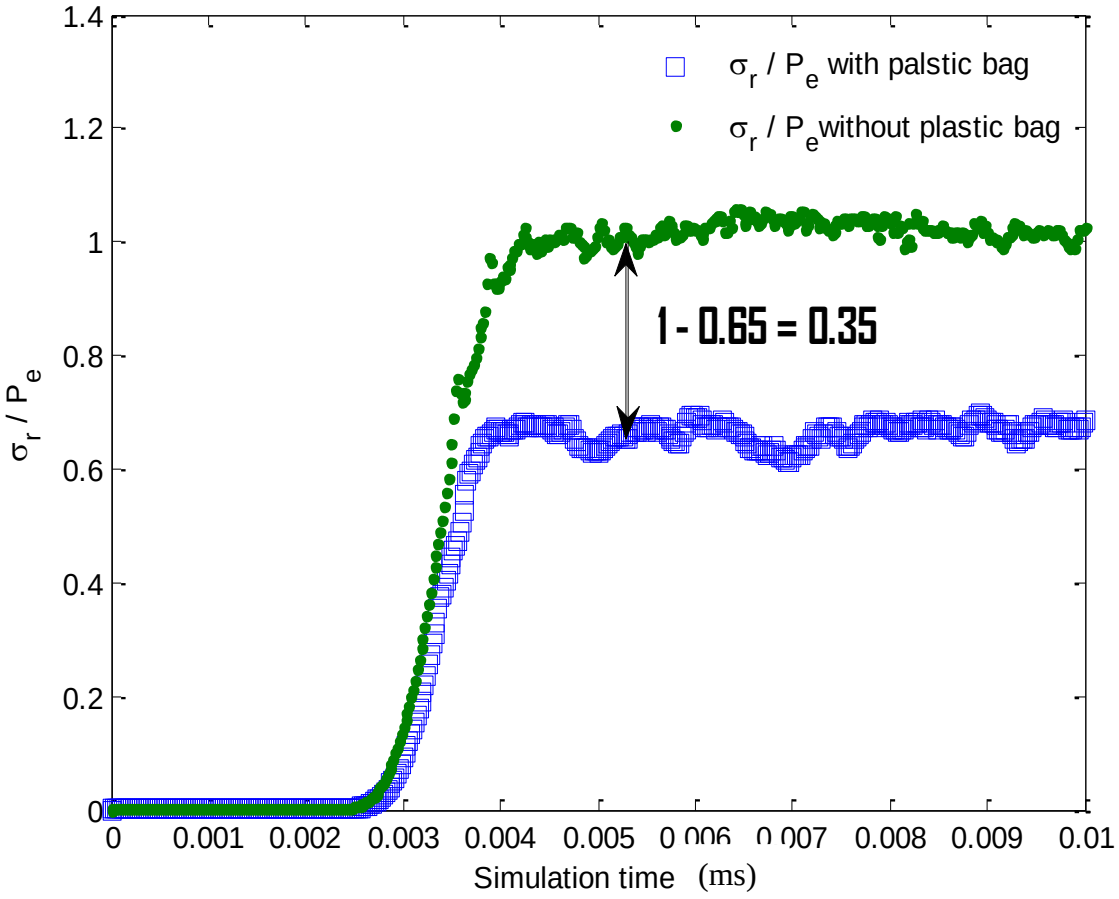

Fig. 4.28. The effect of the plastic bag on radial stress with and without bag.

4.14 Conclusion

The technique of the microorganism disruption using shock waves was investigated mathematically and experimentally. Two mathematical models were developed in this chapter, a static analytical model and a FE model solved using either static or dynamic methods. The analytical model was developed to study the effect of the mechanical properties of cell wall, cytoplasm and water on the tangential, radial and von Mises stress developed on the cell wall. The analytical model is suitable for any type of microorganism that has different material properties such as elasticity, density, and Poisson's ratio.

Von Mises stress was used as a theory of failure and the dynamic load was proved to be concentrated at the bottom of the cell wall. The maximum dynamic σ_v/P_e (0.85)

was found to be over three times greater than the static σ_v/P_e (0.25). The dynamic stress rise was analysed and the reason of this rise was found to be due to the pressure wave reflection when it reached the bottom part of the cell wall. This suggests a location of the cell wall rupture when shock pressure loading is applied; such a result has not previously been reported in the literature.

Another parametric study was conducted using the FE model to evaluate the effect of the cell mechanical properties on the tangential, radial and von Mises dynamic stresses. It was found that σ_v/P_e stress increased when cell wall Poisson's ratio decreased and E/B ratio increased. It was also found that the σ_v/P_e increase when cytoplasm density increases, the E of cytoplasm decreases, and the ν of the cytoplasm increases.

The dynamic FE results show that a minimum pressure of 100 MPa is required to generate 85 MPa von Mises stresses which should be sufficient for rupturing the cell wall of the yeast according to other comparisons with the reported results in the literature. However the experimental results show that σ_v cannot reach 70 MPa when 100 MPa external dynamics pressure is applied. The average yeast log reduction was around 0.25 when external pressure was around 115 MPa.

With respect to the modest yeast disruption observed in the USQ gas gun apparatus, it was found that the simulation model is an excellent tool to provide clear answers of the cause of the modest yeast killing. Reasons of modest microorganism disruption experimentally was due to the plastic bag material, short treatment time, high yeast density in the suspension, and other secondary reasons that were discussed in 4.8.

CHAPTER V

Shear Disruption of Microorganisms

5.0 Introduction

Microstreaming is normally associated with stable cavitation. However additional shear effects will arise from the transient cavitation processes as the viscosity ultimately dissipates a large fraction of the absorbed ultrasonic energy. These shear forces do not necessarily break the cell into fragments but can cause damage to the cell wall. The microorganism thus becomes more fragile and susceptible to subsequent heat treatment. This chapter investigates the effect of the shear stress on the microorganism disruption.

A mathematical model has been developed to evaluate the influence of shear stress due to turbulent flow on microorganisms. A shear stress apparatus was also designed and constructed for this investigation because the relative significance of shock and shear effects in ultrasonic disruption of microorganisms is not clear. The shear apparatus consists of a stationary hollow cylinder (a stator) and rotating cylinder (a rotor) with an annulus of 0.4 mm between these two cylinders. A yeast suspension was injected through the annulus of the shear apparatus; the suspension was subjected to a shear stress due to the speed of the rotor. The mathematical model and experimental results were compared to enhance the understanding of cell wall disruption due to shear stress.

This chapter aims to:

1. provide a fundamental engineering understanding of the relationship between the shear stress generated on the cell wall and the turbulent flow.

2. demonstrate a shear stress apparatus that is capable of generating sufficient shear stress for microorganism disruption in the absence of the significant temperature and pressure effects, and
3. analyze the experimental results with the aid of a mathematical model and other reported results from the literature.

5.1 Review of shear disruption of microorganism

5.1.1 Introduction

As discussed in the section 1.4, microstreaming causes large localized forces to shear the cell wall surfaces resulting in physical damage to the cells (Doula, 1977). Doulah and Hammord (1975) and then Doulah (1977) describe a theory of shear stress as a main cause of microorganism rupturing. Doulah (1977) has also reported that when small gas bubbles oscillate during the compression and rarefaction phases of the sound wave, strong eddies are developed in the area surrounding the bubbles which ultimately spread into the liquid. This effect, which is known as microstreaming, leads to a significant localized shear force that rubs the cell wall surfaces of surrounding organisms and causes cell wall rupture (Doulah, 1977).

According to Walstra (1969) and Doulah (1977), and Hartmann et al. (2006) and Doulah (1977) the use of the Kolmogoroff theory of universal balance is essential for understanding the cell wall damage or rupturing where the flow is turbulent. Others believe that both laminar and turbulent flow can produce the same amount of cell disruption, which indicates that eddies are not an essential feature for disruption (Doulah, 1977). Nevertheless, when the flow is turbulent, eddies play an important role in cell disruption as will be explained in section 5.3.

5.1.2 Mechanical devices

Several mechanical devices that used shear stress for microorganism disruption have been investigated by other researchers, including homogenization in the dairy product industry (Kleinig and Middelberg, 1998), bead mills and microfluidization (Geciova et al., 2002). The apparent cause of the cell disruption in these devices

appears to be a shearing effect. Another relevant field of study, which will be discussed in this section is the development of shear stress due to the flow in blood vessels and animal cell disruption (Born et al., 1992).

Homogenizer

A homogenizer is a device that is commonly used in the dairy industry to break-up fat globules into smaller particles. The fat globules appear to break-up in a homogenization process due to a shearing stress which develops between the milk and the valve and/or the seat of the homogenizer (Mulder and Walstra 1974).

Microorganism disruption can also occur in a high pressure homogenizer. The interaction between the cell and the valve is suspected as one of the reasons for microorganism disruption. However, the real cause and the exact mechanism of cell breakage still remains unknown (Kleinig, 1997).

Another theory attributes the cause of microorganism disruption in the homogenization process to the impact between particles and the side wall of the homogenizer (Walstra, 1969). In addition to these two theories, an additional shear and effect may result from a cavitation process due to the strong pressure gradients which arise in the homogenizer (Anderson et al., 1999; Donsi et al., 2009).

French Press

The *French pressure cell* press is a device that is used to rupture the cell wall. The process is achieved by passing the suspension through a narrow valve subject to high pressure. The French pressure cell for disruption of cells was invented by S. French in the 1950s (Jaschke et al., 2009).

The device can also be used for disintegrating different biological particles including chloroplasts and homogenates of animal tissue (Holger, 2003). The rupturing process occurs by increasing the pressure of the French pressure cell press, and thus the intercellular pressure increases. Once the sample is ejected out the device tube, the external pressure on the cell wall drops to approximately 1 bar. The pressure within

the cell will also drop, but not as rapidly as the external pressure. The pressure difference across the cell wall leads to cell wall rupturing.

The French pressure cell press is able to rupture the cell wall of the cell and maintain cytoplasm and the nucleus intact, which is very important in some biochemical applications. The advantage of using the French pressure cell press is that the cell and microorganism can be treated in the absence of the thermal stress. Because the treatment time is very short, there is not sufficient time for the temperature to increase (Paul et al., 2009). The operating pressure of a particular device described by Kleinig (1997) is approximately 275 MPa for a suspension volume of 35 ml.

Other channel and valve devices

An apparatus that is commonly used in pharmacology applications is called a *microfluidizer processor*. The concept of this method also involves shear stress for cell disruption and is achieved by forcing the suspension at high pressure (approximately 140-200 MPa) through an interaction chamber with a small narrow channel that can generate high shear rates (Geciova et al., 2001).

The *rotor stator processor* is a closed system device used for cell wall rupture. The suspension is induced into the chamber and then pumped through a very fine grid that breaks up the cell wall (Geciova et al., 2001). The microorganism are disrupted due to the shear stress generated in the grids.

The *valve type processor* is another method that operates on placing the sample into a narrow gap located between the valve and its seat under high pressure of 140 MPa to 200 MPa. The fluid will then pass over the valve with higher velocity generating shear stress to rupture the cell wall and leave the intracellular fluid. One of the disadvantages of this method is that it creates a significant amount of heat and therefore the process requires continuous cooling.

Bead mill

The *bead method* of cell rupturing uses beads made of glass combined with a high level of agitation (Zea et al., 2008). It is a simple method that can be achieved by adding beads to the cell suspension in a tube and then the sample is mixed using a traditional laboratory vortex mixer. The advantage of this method is that it is inexpensive and can accommodate many samples at the same time. In this method, the shear stress is considered the main cause of microorganism disruption. Another related configuration that is used involves a high speed rotor placed in a small container containing the cells and beads (Geciova et al., 2001).

Rotational devices

Blood cells can be damaged due to the plasma flow in a rotational viscometer due to shear stress. Leverett et al. (1972) constructed a viscometer using a fixed and a rotational cylinder, the gap between the two cylinders was maintained at 0.1 mm in the first configuration and 0.38 mm in the second configuration. The parametric study by Leverett et al. (1972) included the effect of the solid surface interaction, centrifugal forces, cell–cell interaction, shear layers, time of exposure and blood viscosity.

Leverett et al. (1972) found that there was no significant difference in the hemolysis when the two configurations with 0.1 mm and 0.38 mm gaps were used, which means shear stress can be generated based on the fluid pressure rise and speed of cylinder. It was also found that there was an increase in the fragility of the cell when the blood density increased. The threshold level for blood cell damage was a shear stress and time of exposure of 150 Pa and 100 s respectively. The result shows that for a shear stress of 150 Pa and above generated by the centrifugal pump, extensive cell damage can occur.

Laminar capillary flow

Born et al. (1992) claimed that there was no fundamental information available for the mechanical properties of walls of animal cells that can be used to predict shear damage. Thus, Born et al. (1992) used micromanipulation measurements of animal cell mechanical properties to predict the animal cell damage due to shear stress in a laminar flow field (Born et al., 1992). The Born et al. (1992) results show that the shear stress which caused the damage of the animal cells due to laminar flow ranges from 0.019 Pa to 100 Pa with the exposure time between 10 minutes and 24 hours. The shear stress value and the time of exposure required for cell damage vary with the cell mode of growth, physical environment, and history of the cell culture.

Several studies were conducted to evaluate the sensitivity of the animal cell to shear force, especially in laminar flow since animal cells are generally soft and fragile (Born et al., 1992). West et al. (2008) reported that a 1 to 5 Pa shear stress for 10 minutes is sufficient to cause cellular damage and death using a laminar flow viscometer. The low shear stress values required for damage were due to the fact that animal cells lack a protective cell wall and thus are very susceptible to the shear stress, as reported by Papoutasakis (1991).

Turbulent capillary flow

Others such as Zhang et al. (1993) estimate the extent of animal cell rupturing by turbulent flow. Eddies with a size smaller then the cell sizes are theoretically able to interact with the cell causing a local surface deformation which leads to membrane damage. It is argued that cell wall rupturing is due to the cell wall deformation that leads to an increase in the cell wall tension and cause the surface energy to be above the rupturing limit. Zhang et al. (1993) reported that animal cells were ruptured in the turbulent flow in capillaries at a mean energy dissipation of 2×10^4 kJ/kg.

5.2 Theoretical analysis

5.2.1 Introduction

Due to the lack of reported information about the mechanism and the real cause of the microorganism rupturing in mechanical devices, it was judged essential to investigate the influence of the eddies and the shear stress due to turbulent flow on the cell wall disruption.

Fragile biological structures such as animal cells (Nilsson et al., 1983) can be ruptured using shear stress (Born et al., 1992). For example, animal cells can be damaged using bioreactors or simple flow devices such as laminar cone and plate viscometers. Born et al. (1992) reported that shear stress required for cell wall damage can vary significantly from 0.019 Pa to 100 Pa depending on the treatment time which was varied from 10 minutes to 24 hours. Born et al. (1992) identified the cell disruption of animal cell when the suspension flow was laminar. However, Zhang et al. (1993) used a cone and plate viscometer to evaluate the animal cells disruption by turbulent flow. The finding of Zhang et al. (1993) was that animal cells can be damaged by shear stresses ranging from 0.019 Pa to 577 Pa depending on the treatment time. In this turbulent flow region, Zhang et al. (1993) reported that significant hybridoma and myeloma cell rupturing can be detected when the Kolmogorov micro-scale of turbulence was smaller than the cell diameter.

Ayazi et al. (1994) developed a model of a high speed pressure disruption of the yeast cell. Ayazi et al. (1994) reported that yeast cell wall breakage is determined by the equilibrium between the stress generated from the fluid dynamic condition and the physical strength of the yeast cell. Ayazi et al. (1994) reported that a number of researchers such as Cherry and Papoutsakis (1986), Engler (1985) used the same technique as used by Ayazi et al. (1994) to evaluate the yeast disruption in homogenizers.

When the shear stress increases, the chances of microorganism disruption increase, and thus it is important to couple the relationship between the turbulent flow where eddies are generated with the shear stress and microorganism disruption. A turbulent

flow model was developed as reported in this chapter to predict the amount of shear stress and energy required for microorganism disruption and to assess the relationship between the experimental results and the turbulent theories. The model relating turbulent energy and cell disruption in this chapter largely follows the work of Zhang et al. (1993). Although the Zhang et al. (1993) model was used for animal cells, the approach suggested by Zhang et al. (1993) may still provide an estimate of how much energy is required for rupturing the yeast cell wall. It is noticed that while Zhang et al. (1993) applied the approach to animal cells earlier workers such as Doulah and Hammond (1975) and Doulah (1977) successfully used essentially the same approache to evaluate yeast cell disruption. Doulah and Hammord (1975) used the principle of liquid drop breakage and hydrodynamic flow to estimate the yeast disruption and the energy required to rupture the yeast cell wall using kinetic energy and strain energy. Doulah and Hammord (1975) concluded their work by saying a reasonable agreement between the experimental results and the mathematical model derived on the basis of turbulence in the homogenizer was achieved.

The present study includes assessing the relationship between Reynolds numbers, suspension viscosity, shear stress apparatus geometry and operating conditions (speed and temperature) and their affect on microorganism disruption. The analysis proceeds by considering the flow energy which is dissipated in either laminar or turbulent forms:

1. Laminar energy (E_L) is the energy dissipated into the laminar boundary layers or the laminar sublayers of turbulent flow. In the shear apparatus the sublayer close to the wall will be laminar flow, but this region is typically a very small volume in comparison to the region of turbulence.
2. Turbulent energy (E_t) is the energy dissipated into the suspension due to the turbulent flow within the apparatus which arises due to the flow in the pipe work, circulation pump, or the annulus with or without the rotor moving.

5.2.2 Energy dissipation in laminar and turbulent flow

Born et al. (1992) and Zhang et al. (1993) developed models for estimating the disruption of animal cells due to the laminar and turbulent capillary flow respectively. These models are useful for analysing the situation where the rotor of

the shear apparatus in the present work was stationary while the suspension was circulated through the device. The laminar energy rate (E_L) dissipated in the laminar sublayer can be calculated from equation 5.1 (Born et al., 1992)

$$E_L = \mu\gamma^2 V_L, \qquad 5.1$$

where

μ =viscosity of the suspension

γ = laminar sublayer shear rate (1/s)

V_L = volume of the laminar sublayer.

The laminar shear rate can be calculated using equation 5.2 from Born et al. (1992) which is applicable to fully developed laminar pipe flow and was used in the laminar sublayer. γ is then given by equation 5.2,

$$\gamma = \frac{\Delta P}{(\frac{4L}{D\mu})}\ , \qquad 5.2$$

where

ΔP = pressure drop

L = pipe length

D = pipe diameter

μ = fluid viscosity.

Zhang et al. (1993) reported that equation 5.2 can be used for a laminar sub-layer for the turbulent flow. The wall shear stress can be found using force balance at the pipe wall (equation 5.2). The volume of the laminar sub-layer V_L can be calculated from equation 5.3

$$V_L = \ 0.25 \times \pi[D^2 - (D - 2\delta)^2]L, \qquad 5.3$$

where the thickness of laminar sublayer is

$$\delta = \frac{5\mu}{\rho\sqrt{\frac{\tau_o}{\rho}}}. \qquad 5.4$$

The wall shear stress (τ_o) can be calculated using equation 5.5

$$\tau_o = \frac{\Delta P}{\frac{4L}{D}}. \quad 5.5$$

The energy dissipation rate in the suspension due to *turbulent flow* through the circulation system can be calculated from (Zhang et al., 1993)

$$E_t = 0.25\,\pi\,\Delta P D^2 u_m, \quad 5.6$$

where

u_m = mean velocity

D = pipe diameter = 0.4 mm

The pressure lost (ΔP) is given by (Zhang et al., 1993)

$$\Delta P = 0.5\,f_{an}\,\rho\left(\frac{L}{D}\right)u_{max}^2, \quad 5.7$$

where f_{an} represents the mean friction factor of the annulus which is given by equation 5.8 (Born et al., 1992)

$$f_{an} = \frac{0.296}{(Re\left(\frac{L}{D}\right))^{0.2}}\ . \quad 5.8$$

The pressure drop through the circulation system will be used in evaluating the flow through the system without turning the rotor on.

5.2.3 Energy dissipation in the turbulent Couette flow

The shear stress apparatus consists of a stationary cylinder and a rotational cylinder with a radial gap of 0.4 mm between them. The energy and shear stress required for microorganism disruption will come from the kinetic energy in the turbulence region between the two cylinders. Fig. 5.1 illustrates the velocity profile between the moving plate and the fixed plate. The shear apparatus configuration detail is discussed in section 5.3, but the analysis required for deducing the turbulent energy dissipation rate, which is needed for the microorganism disruption model is introduced here.

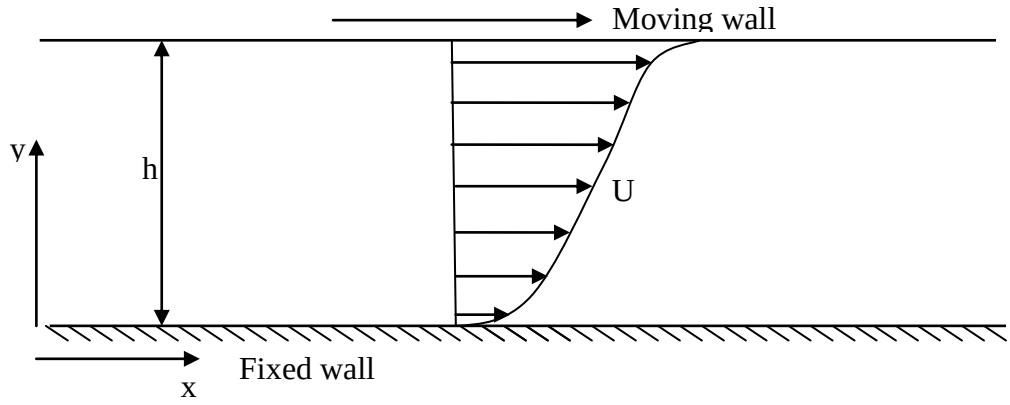

Fig. 5.1 Illustration of the turbulent velocity profile between fixed and moving wall, reproduce from Bradshaw (1971).

Fig 5.2 shows the normalized velocity at different locations between the moving and fixed walls. Bradshaw (1971) introduced a number of important points which are necessary for the analysis of the turbulent Couette flow as follows:

1. The Reynolds shear stress components of ρuv vary with y^3 in the region close to the wall, and this region describes a laminar sublayer, and thus the shear stress in this laminar region can be calculated using (Bradshaw, 1971)

   $$\tau_L = \mu \frac{du}{dy} \qquad 5.9$$

2. In the region close to the wall, the flow in the sub-layer is assumed to be laminar and wall shear stress is dominant. Parameters affecting the shear stress at the wall τ_w are the fluid properties such as density and viscosity providing that the wall is rough.
3. Dimensional analysis indicates that the velocity must be in the form of $u_\tau f(\frac{u_\tau y}{v})$, where the friction velocity u_τ is given by

   $$u_\tau = \sqrt{\frac{\tau_w}{\rho}} \qquad 5.10$$

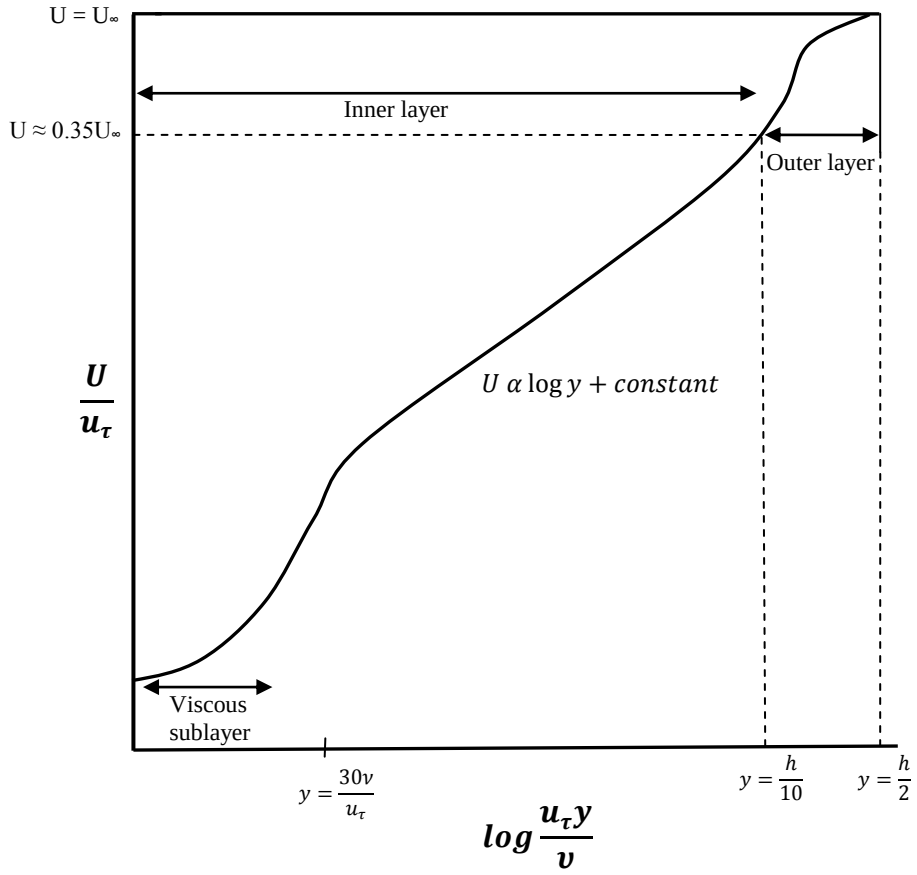

Fig. 5.2 Normalized velocity ($\frac{U}{u_\tau}$) for different position across the annulus ($\frac{u_\tau y}{\nu}$), reproduce from Bradshaw (1971).

The shear stress produced in this region is due to turbulent eddies where the u and v components of the velocity are equal, thus $uv = u_\tau^2$ where,

1. u_τ is the friction velocity but is also measure of the turbulent velocity fluctuation in this case.
2. $\frac{u_\tau y}{\nu}$ is the turbulent Reynolds number. It is empirically reported (Bradshaw, 1971) that turbulent flow occurred when the Reynolds number is greater than 30 (which is outside the viscous laminar sub-layer).

Dimensional analysis shows that mean flow velocity gradient in the region $\frac{u_\tau y}{\nu} > 30$ can be described as follow

$$\frac{\delta U}{\delta y} = \frac{u_\tau}{Ky} \qquad 5.11$$

$$\delta U = \int \frac{u_\tau}{Ky} dy \qquad 5.12$$

Integrating equation 5.11 for turbulent Reynolds number $\left(\frac{u_\tau y}{\nu}\right)$ greater than 30 gives equation 5.13.

$$U = u_\tau(\frac{1}{K}\log(y)) + C \qquad 5.13$$

The time average kinetic energy contained within a sphere of fluid of the same size as the cell, can be estimated from equation 5.14 (Zhang et al., 1993):

$$\overline{E_k} = 1/2\rho_c \int_0^{r_c} \overline{u^2(r_c)} 4\pi {r_c}^2 . dr, \qquad 5.14$$

where

$\rho_c =$ cell density

r_c = cell radius.

Hinze et al. (1994) suggests that for homogenous, isotropic turbulence, the mean square of relative velocity between any two points separated by distance (*r)* can be given as follows

$$\overline{u^2(r)} = c\ (\varepsilon r)^{2/3}, \qquad 5.15$$

where

ε = local energy dissipation rate (W/kg, or m^3/s^3),

c = 2, according to Hinze et al. (1994).

Thus from equation 5.14

$$\overline{E_k} = \frac{12}{11}\pi\rho_c . \varepsilon^{2/3} r^{11/3}. \qquad 5.16$$

The local energy dissipation rate ε can be evaluated through the use of some turbulence length scales that are commonly used to characterize the flow. The large scale l_o represents the distance between two points in the flow where there ceases to be a correlation between the fluctuation velocities (Turns, 2000). The Kolmogorov

microscale l_k is the length scale at which turbulent kinetic energy transfers to internal energy and is related to the energy dissipation rate (ε) and dynamic viscosity (υ) via

$$l_k = (\frac{\upsilon^3}{\varepsilon})^{\frac{1}{4}} \quad 5.17$$

The two length scale (l_o and l_k) are related by

$$l_o/l_k = Re_{l_o}^{3/4} , \quad 5.18$$

where

Re_{l_o} = Reynolds number.

5.2.4 Cell disruption probability model

In this subsection, the turbulent cell disruption model developed by Zhang et al. (1993) will be presented. The model estimates the surface energy (E_s) required for rupturing the cell with a cell wall tension (T_b) and elastic area of compressibility modulus (K) using equation 5.19

$$E_s \geq A_o T_b \left(1 + \frac{T_b}{K}\right) \quad 5.19$$

where the cross section area of the cell wall (A_o) is

$$A_o = \pi r^2 \quad 5.20$$

The yeast cell wall is expected to be ruptured when kinetic energy (E_k) is greater than surface energy E_s

$$\frac{E_k}{E_s} \geq 1 \quad 5.21$$

The critical radius (r_{cr}) at which disruption is likely can be found from the combination of equation 5.16 and 5.19:

$$r_{cr} = [\frac{11T_b\left(1+\frac{T_b}{K}\right)}{3\rho_c\varepsilon^{\frac{2}{3}}}]^{3/5} \quad 5.22$$

The probability of cell rupturing P_ε can be estimated using the energy dissipation rate ε, the elastic area of compressibility modulus K and bursting force T_b as reported by Thomas et al. (1994) and Zhang et al. (1993)

$$P_\varepsilon = \int_{r_c}^{\infty} f(r, \mu_r, \sigma_r)dr, \quad 5.23$$

where $f(r, \mu_r, \sigma_r)$ is the probability density function of the cell radius distribution using a Gaussian theory with a mean bursting radius of μ_r and mean tension of σ_r (Zhang et al., 1993)

$$f(r, \mu_r, \sigma_r) = \frac{1}{\sqrt{2\pi}\sigma_r}\exp\left(-\frac{(r-\mu_r)^2}{2\sigma_r^2}\right). \quad 5.24$$

The anticipated cell rupturing fraction (*P)* can be numerically found by integrating the equation

$$P = \iint_{-\infty}^{\infty} f(T_b, \mu_T, \sigma_T)\, f(K, \mu_K, \sigma_K)\, P_\varepsilon\, dK\, dT_b. \quad 5.25$$

The integration in equation 5.25 can be performed numerically using the mechanical properties given in Table 5.1 and the energy dissipation rate (ε). The $f(T_b, \mu_T, \sigma_T)$ is the tension probability density function with mean μ_T and standard deviation σ_T, and $f(K, \mu_K, \sigma_K)$ is the elastic area of compressibility modulus probability density function with mean μ_K and standard deviation μ_K. The yeast mean elastic area of compressibility modulus (σ_k) was 0.5 N/m and mean bursting cell wall tension (μ_T) was 1.6 N/m and mean cell diameter μ_d was 7.1 μm (Kleinig, 1997; Zhang et al., 1993).

The mechanical properties required for calculating the anticipated cell rupturing fraction namely elastic area of compressibility modulus, surface tension, bursting force, and failure energy have been obtained from experimental results reported by Kleinig (1997) as shown in Table 5.1. The data was obtained by Kleinig (1997) using micromanipulation techniques on two different yeast cells in different growth phases and sizes as illustrated in Table 5.1.

Table 5.1 Mechanical properties of two different yeast cells as evaluated by Kleinig (1997).

S. cervesia properties	Units	Cell
Cell diameter (d)	μm	5.1
Mean elastic area of compressibility modulus (σ_k)	N/m	0.5
Mean bursting cell wall tension (μ_T)	N/m	1.6
Mean bursting radius (μ_r)	μm	3.4

5.2.5 Simulation of cell wall disruption in the turbulent flow

In the present work, it was assumed that the mechanical properties of the yeast will not change during the treatment, consistent with the McQueen et al. (1989) model. Zhang et al. (1993) has also confirmed that the physical properties such as elastic area of compressibility modulus and the size of TB/C3 hybridomas cells that were used in their experiments do not change significantly during treatment - they remain within the acceptable limit of 10%.

To confirm the present implementation of the Zhang et al. (1993) model, and to gain confidence in the application of predicting the percentage of the yeast rupturing using the present shear apparatus, a sample calculation using data presented in Zhang et al. (1993) was performed and is presented in Table 5.2. A TB/C3 hybridomas cell, that is commonly available in the blood of human-beings, was used in the work by Zhang et al. (1993). The mean elastic area of compressibility modulus measured in N/m and the mean bursting cell wall tension measured in N/m was used to predict the cell wall rupturing percentage. The data presented in the first experiments of Zhang et al. (1993) gives a volumetric flow rate of 4.4 mL/s, a Reynolds number of 5093 and ε was 1470 W/kg. The microscale (l_k) was also calculated using equation 5.17.

The kinematic viscosity of the fluid in equation 5.17 was taken as water in Zhang et al. (1993) and in the present work was taken as 0.99×10^{-6} m^2/s. The theoretical ε value was calculated using equation 5.25 as shown in the previous subsection. The analysis shows that the percentage of cell wall rupturing (*P*) of TB/C3 hybridomas using these data is 0.26%. The results of the anticipated cell rupturing fraction (*P*) was compared with results reported by Zhang et al. (1993) which was 0.28% as illustrated in Table 5.2. The analysis shows very good agreement between the two results and gives confidence in the results obtained from this model to predict the yeast disruption using the present shear stress apparatus.

Table 5.2 Calculations to verify the present implementation of Zhang et al. (1993) model.

Items	ε (W/kg)	l_k (μm)	σ_k m.N/m	μ_T m.N/m	μ_d μm	*P* (%)
Zhang et al. (1993) reported results at Q (mL/s) = 4.4 Re = 5093	1470	5.1	0.5	1.6	1.6	0.28%
Present implementation of Zhang et al. (1993) model Q (mL/s) = 4.4 at Re = 5093	1470	5.1	0.5	1.6	1.6	0.26%

5.2.6 Yeast disruption curve

To evaluate the yeast disruption percentage using shear treatment, the mathematical method developed by Zhang et al. (1993) was for animal cell adopted in the present work, noting that the earlier works of Doulah and Hammdon (1975) and Doulah (1977) successfully used a very similar approach to model yeast disruption. The untreated yeast concentration was assumed to be C_i measured in CFU/mL while the yeast concentration after the shear treatment was assumed to be C_o (measured in CFU/mL). According to

Zhang et al. (1993), the fraction of cells remaining per flow pass (*P*) can be treated as constant for each flow pass, and can be calculated using equation 5.26

$$C_o = C_i e^{-PN} \quad 5.26$$

By taking $\log_e$ for both side

$$\log_e\left(\frac{C_o}{C_i}\right) = -PN \quad 5.27$$

Thus, the fraction cell remaining can be calculated using equation 5.28

$$P = -\frac{log_e(\frac{C_o}{C_i})}{N} \quad , \quad 5.28$$

where the mean number of passes through the shear apparatus (N) is

$$N = \frac{Q.t}{V}, \quad 5.29$$

where

Q = volumetric flow rate through the shear annulus

V = volume of the yeast suspension

t = time of treatment.

To obtain the fraction of cells remaining, the C_o/C_i in the suspension was plotted against the treatment time or number of flow passes through the shear region (annulus).

5.3 Shear flow apparatus

5.3.1 Introduction

The mathematical results obtained from the previous section provided useful technical information about the possibility of yeast disruption due to shear stress based on the mechanical properties of the yeast. The next stage was to obtain experimental results to verify the mathematical outcome. The shear apparatus was

designed to provide different rotor speeds, at different treatment times, to evaluate the specific energy required for yeast disruption. The required shear stress was calculated to give another indication on the efficiency of the system in yeast disruption.

Mechanical methods for microorganism disruption such as the high pressure homogenizer typically force the suspension through a small opening and so generate a significant amount of shear stress. However, in the case of homogenizer, the energy dissipated in the suspension is caused by a high pressure difference which may also generate a cavitation effect. Therefore, to isolate the shear effect from shock wave effects, it was necessary to design a device that is able to generate sufficient shear energy and shear stress to disrupt the cell wall in the absence of pressure gradients. Temperature effects must also be avoided so that any disruption can be reliably attributed to the shear effect. In the shear stress apparatus developed in this work, turbulent shear energy is developed in the annulus between the rotational cylinder (a rotor) and the fixed cylinder (the stator) with virtually no pressure gradients. As in section 3.3.1 dealing with the mixing and the residence time distribution of the suspension in the ultrasound cell, is essential to make sure that yeast cells are subjected to shear treatment uniformity. It was demonstrated in section 3.3 that in continuous ultrasound flow processing arrangements where the processing region of interest extends only a few mm beneath the probe tip or when the processing volume is quite small, the characteristic mixing time in such configurations at comparable power levels will be shorter than the batch configuration. It can expected that in the case of a shear motor where the power is 2 kW and the suspension volume is 60 mL, complete mixing will be achieved in a short time due to high shear power and small suspension volume.

5.3.2 Apparatus description

A schematic illustration of the shear apparatus used in the present work is presented in Fig. 5.3. The yeast suspension is delivered into the narrow annulus between the stator and the rotor using a water pump. An electrical motor positioned on top of this apparatus provides a power of up to 2300 W to develop a range of speeds between 3000 RPM to 12000 RPM. The suspension was subjected to high shear stresses when

it passed through the annulus due to the high speed of the rotor. An annular gap of 0.4 mm exists between the outer case and the rotor as shown in Fig 5.3.

Fig. 5.4 presents a photograph of the shear cell unit; the rotor and the stator are shown in Fig 5.3. The speed of the motor was measured using an analogue speed detector at a rate of 20 samples/s using an A/D card and Lab-View software. The shear cell develops high shear stress through the action of the turbulent fluctuations.

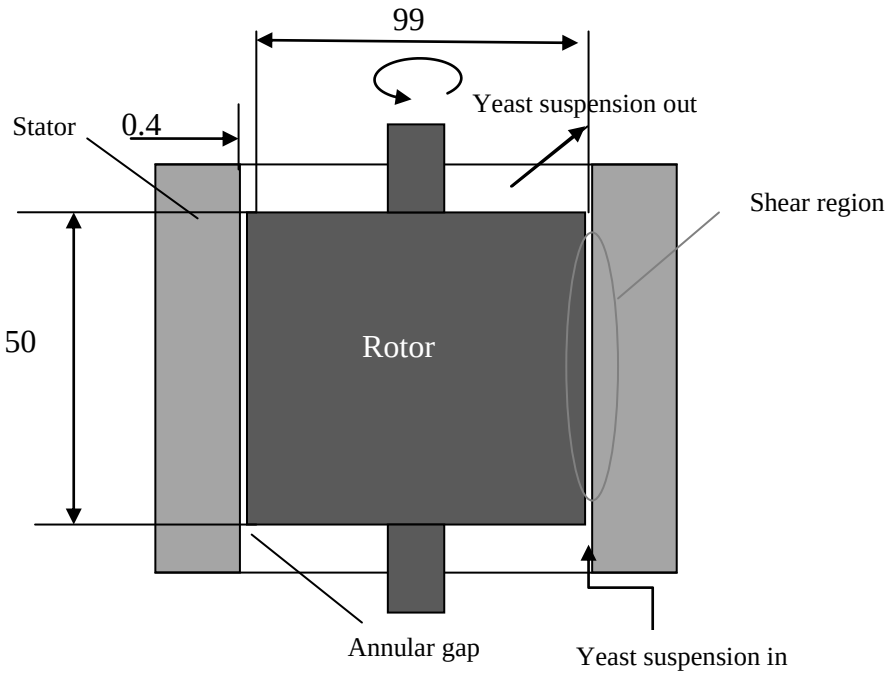

Fig. 5.3 Schematic illustration of a vertical cross-section of the shear flow apparatus, dimensions in millimetres.

5.4 Methodology

5.4.1 Yeast preparation, viable count and contamination

The method of yeast suspension preparation, viable count, and contamination were discussed in chapter 3.

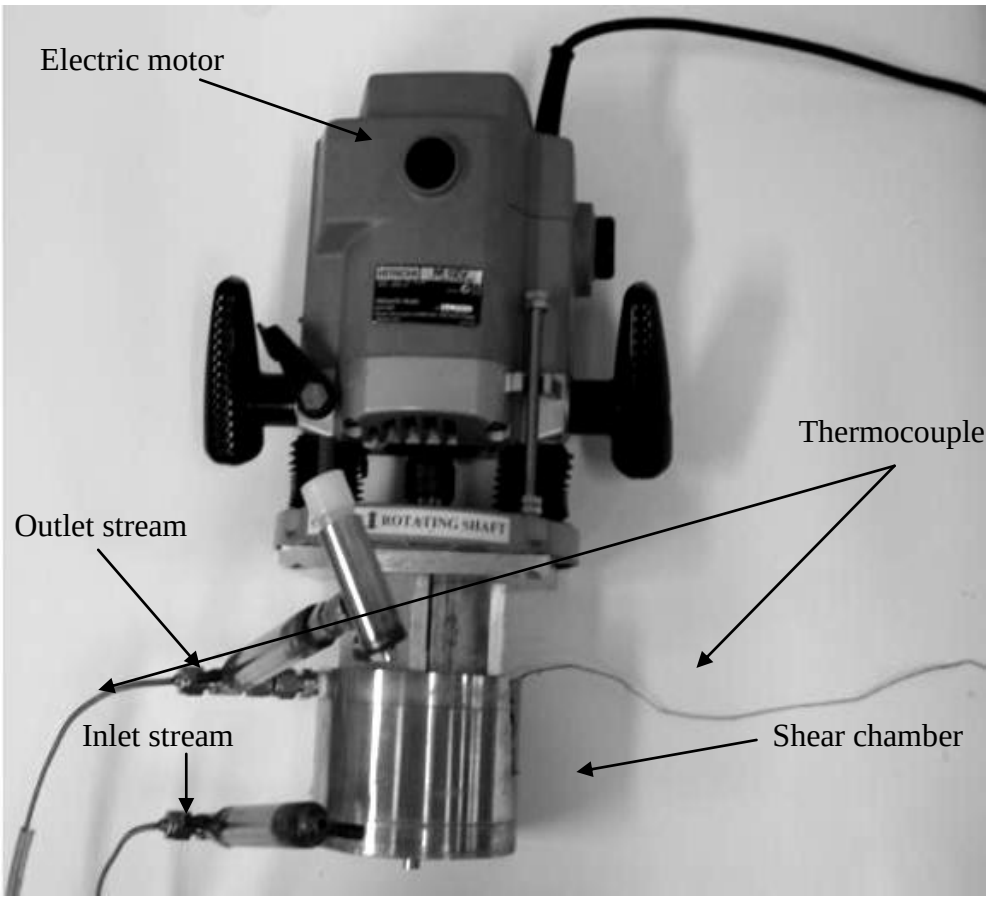

Fig. 5.4 Photograph of shear flow apparatus consists of electric motor, shear chamber, inlet and outlet stream.

5.4.2 Apparatus mechanical performance

5.4.2.1 Power

To evaluate the power dissipated in the suspension, the shear rotor operated at different speed varying from 1000 RPM (low speed) to 12000 RPM (high speed). To obtain information on frictional effects, the motor was turned off at 10000 RPM and the drop in motor speed under the effects of the mechanical and the hydraulic frictional resistances was recorded. A sample of these results showing the speed decreasing from about 11000 RPM to reach zero RPM (in around 10 s) is presented in Fig 5.5.

The motor angular velocity ω was differentiated with respect to time to evaluate the angular acceleration for cases with and without the suspension. The angular acceleration was then used to calculate the torque.

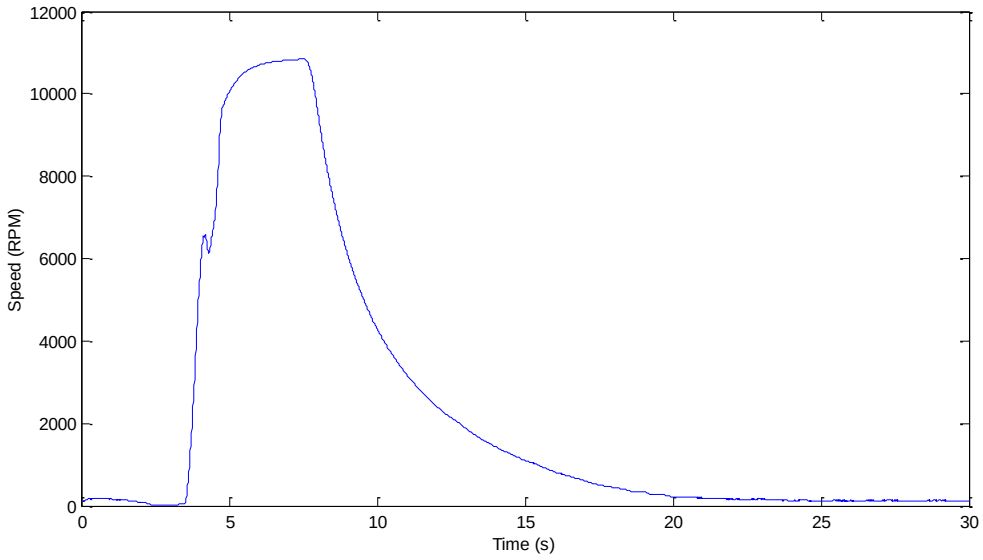

Fig. 5.5 Rotor speed with respect to time when yeast suspension was introduced into the shear apparatus.

The results with and without the suspension was used to calculated the total power dissipated as well as the mechanical friction power. The difference between these two powers is assumed to yield the net power available for the shear disruption in the annular gap, i.e.

Net viscous Power = Total Power – Mechanical Friction Power

For both cases (with and without the suspension), the power dissipated can be calculated using equation 5.30

$$P = T \times \omega, \qquad 5.30$$

where

ω = angular velocity of the rotating cylinder and

T = the motor torque, which can be calculated from equation 5.31

$$T = I \times \alpha, \qquad 5.31$$

where

α = the angular acceleration (obtained from Fig 5.5 in the case of the apparatus with the suspension present).

I = the moment of inertia of the rotating mass which was 3600 kg.mm^2.

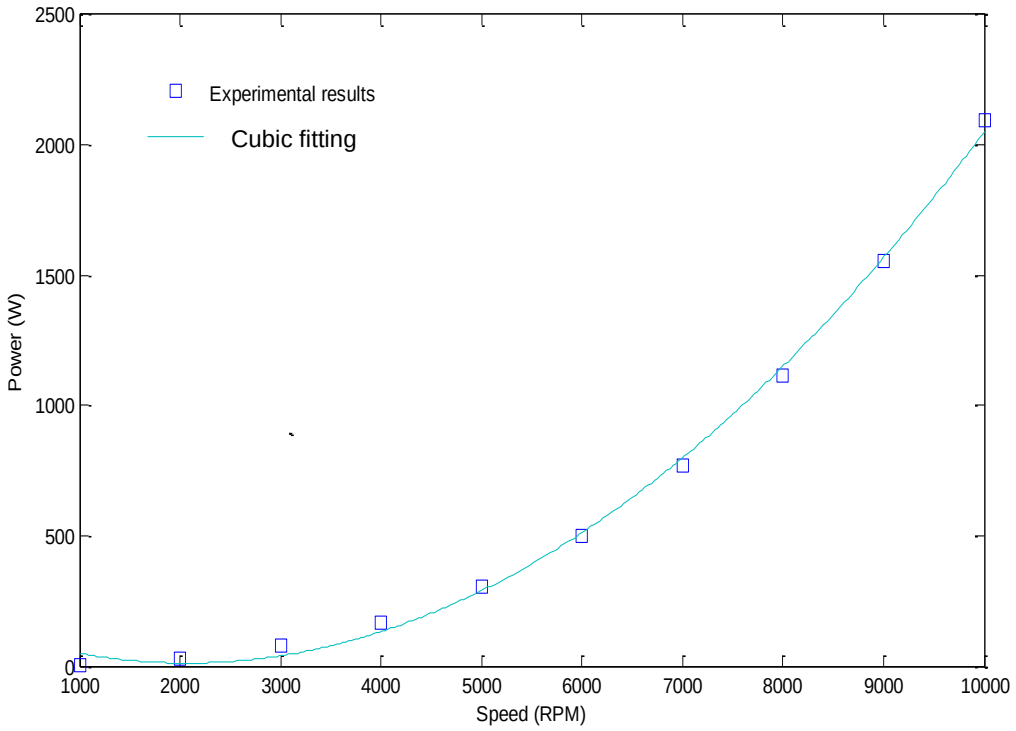

Fig 5.6 The net viscous power generated due to different rotor speeds

Fig. 5.6 shows that when the rotor speed is 10000 RPM, the maximum net viscous power (total power – mechanical friction power) dissipated into the suspension is 2095 W. The mechanical power at this speed was approximately 50 W. The polynomial equation of the curve in Fig. 5.6 is obtained from the experimental results

$$P = -1.74813\times10^{-9} N^3 - 3.55878\times10^{-6} N^2 + 1.088\times10^{-3} N. \quad 5.32$$

where P is the power measured in watts and N is the angular speed measured in RPM. The three angular speeds that were used in this study for yeast treatment were 4000 RPM, 7000 RPM and 10000 RPM. The net power dissipated into the suspension corresponding to the speeds of 4000 RPM, 7000 RPM and 10000 RPM was 168 W, 767 W and 2095 W respectively.

5.4.2.2 Wall shear stress

The energy required to provide sufficient shear stress for yeast disruption is dependent on rotor speed. The wall shear stress generated by the suspension due to rotor speed can be calculated using

$$\tau = \frac{T}{A.r} \quad , \qquad 5.33$$

where

r = radius of the rotor,

A = surface area of the rotor = (πdh),

where

d = rotor diameter = 0.099 m,

h = the height of the rotor = 0.05 m

The surface area of the rotor (not including the base or the top area) was 0.01558 m^2. The wall shear stress can be calculated directly from the net viscous power by substituting equation 5.30 in equation 5.33

$$\tau = \frac{P}{A.r.\omega} \quad . \qquad 5.34$$

The experimental results for the wall shear stress generated in the suspension for different rotor speed is presented in Fig. 5.7.

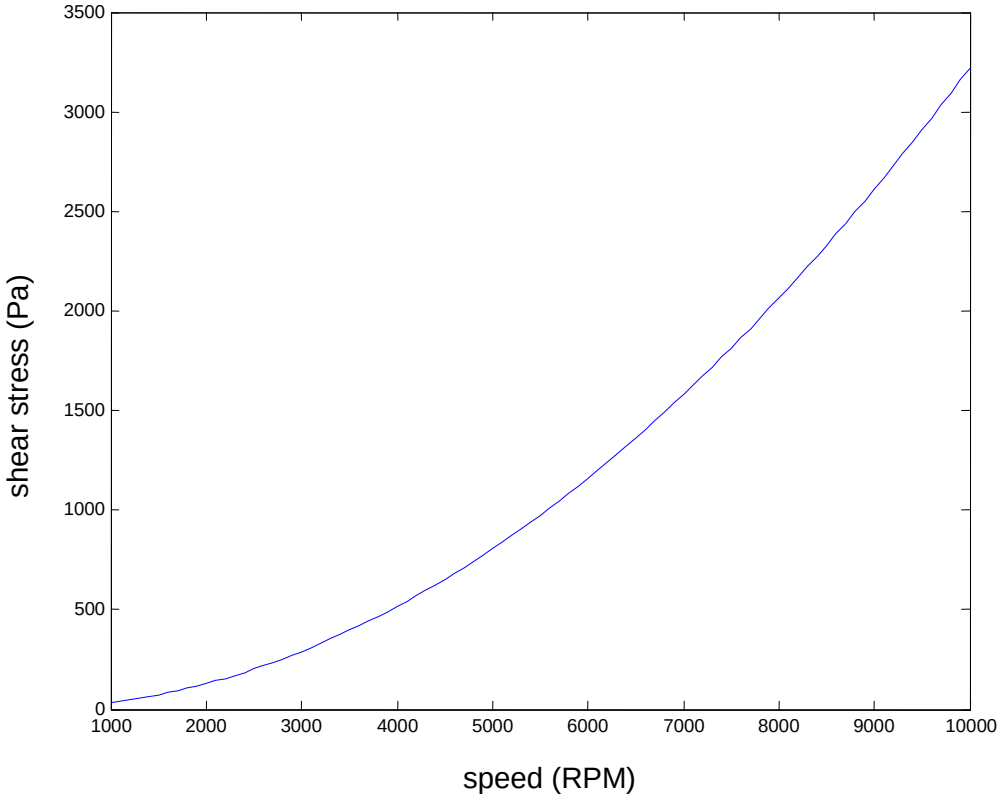

Fig. 5.7 Experimental results for shear stress for different rotor speeds (RPM).

5.4.3 Cooling and circulation arrangements

Initial experiments aimed at understanding the way the shear flow apparatus operated were performed and revealed areas that needed to be addressed in order to conduct further reliable experimental investigations. The first experiment was conducted to evaluate the effect of the shear stress for a suspension in a batch configuration. Results showed the suspension temperature can reach 40 ^{o}C and 55 ^{o}C for different treatment times and different rotor speeds. Such elevated temperatures may lead to thermal disruption the yeast. Under such conditions yeast disruption may arise due to a combination of thermal stress plus mechanical stress. It was necessarily to maintain the temperature of the suspension below 45 ^{o}C, to ensure that the yeast was disrupted because of the shear stress rather than the thermal stress. To avoid this problem and to control the experimental conditions and thereby improve the quality of results, the cooling of the apparatus had to be improved.

A cooling arrangement developed by members of the research team based on an ice bath was used to maximize the removal of heat generated by the shear unit. To improve the temperature uniformity of the ice bath, a stirrer was used to mix the ice and the water. Fig. 5.8 displays the shear cell image within the ice bath. Even with the ice bath fully operational, it was possible to exceed 40 ^{o}C suspension temperatures at the high rotor speed. Final temperature control was achieved by limiting the operation time of the shear unit. The shear unit was only operated until the yeast suspension temperature reached around 40 ^{o}C, at which time the rotor was stopped until the system and yeast suspension cooled.

A water pump was used to circulate the yeast suspension through the shear unit. The water pump was powered by a 12 V DC supply and produced a flow rate of around 1000 mL/min. The water circulation function is to cool the yeast suspension by passing the pipe through the ice bath as shown in Fig. 5.8.

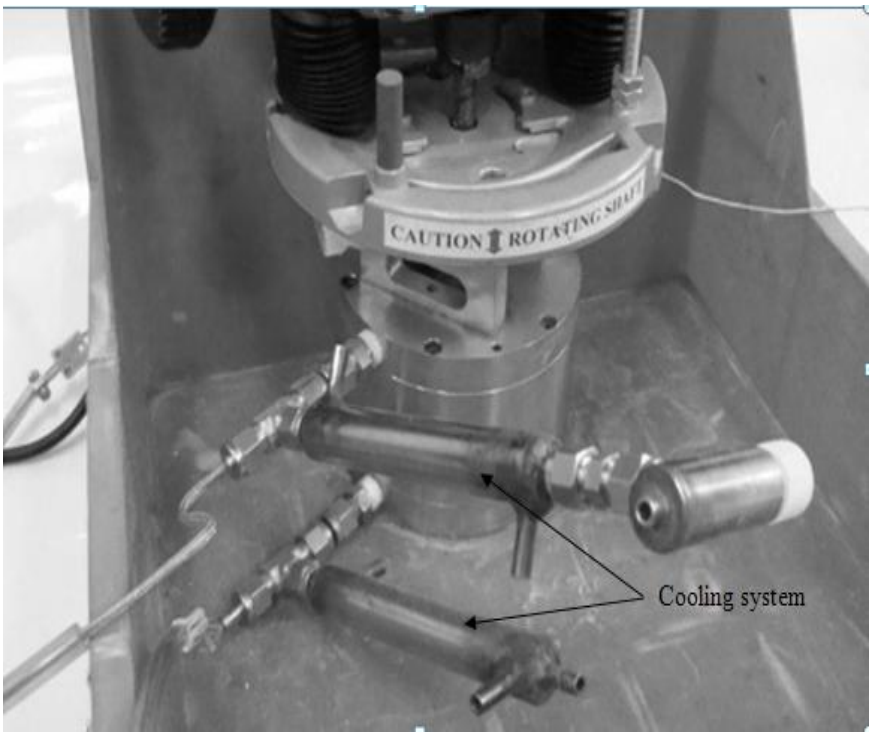

Fig. 5.8 Cooling system arrangement for the shear stress apparatus including heat exchanger and ice bath container.

Additional tests were conducted by the research team to make sure the effect of the temperature on the yeast concentration was eliminated when the shear apparatus was operated. The experimental test showed that there was no viable yeast left in suspension when the temperature of the yeast was held between about 40 ^{o}C and 45 ^{o}C and the treatment time was 5 minutes. Further tests showed that there was less yeast reduction after installing the cooling system and the suspension temperature was maintained below 40 ^{o}C. These results agree with Chen et al. (1999) whose results indicated that yeast cells cannot be thermally damaged when suspension temperature is below 45 ^{o}C. For the shear cell to function as intended, maximum temperature of the yeast must be maintained below 45 ^{o}C. To avoid any thermal stress on upper limit of 40 ^{o}C was adopted for subsequent investigation.

5.4.4 Circulation pump

Prior to running the shear stress apparatus and examining the effect of the shear stress on the disruption of *S. cervesiae*, it was anticipated that the circulation pump could have an influence on the results. Thus a test was conducted to examine the influence of the circulation pump on the yeast disruption. This test was conducted by pumping the yeast suspension of 1×10^{10} CFU/mL through the shear apparatus while the rotor speed was zero. The test was conducted for different suspension flow rate at constant temperature of approximately 25 ^{o}C. A sample of the treated suspension was examined and the CFU/mL was determined as yielding the results in Table 5.3. This simple experiment shows that there is some yeast disruption due to direct mechanical shear from pump impellers and turbulent flow in pump and the rest of flow circuit.

The data presented in Table 5.3 shows that the water volumetric flow rate was 1.72×10^{-6} m^3/s. In the annulus, and in the absence of the rotor movement, the flow will be laminar under these conditions (the Reynolds number was of approximately 100). Thus, the most significant contribution of microorganism rupturing in the absence of the speed of the motor is mainly due to the pressure rise in the pump (2.5 bar) and pressure loss in the circulation pipes. It is also important to note here that there is also a pressure drop thought the pipe circuit due to the laminar and turbulent suspension flow and fitting losses through elbows and other fittings.

Table 5.3 Yeast suspension CFU reduction due to the circulation through the shear apparatus by the water pump. The volumetric flow rate of the suspension was 1.72×10^{-6} m^3/s and pressure difference across the pump was 250 kPa (Speering, 2004).

Test	Time (s)	Original (CFU/mL)	Treated (CFU/mL)	|log reduction ∗∗|
1	0	1×10^{10}	1×10^{10}	0
2	60	1×10^{10}	1×10^{9}	1
3	300	1×10^{10}	1×10^{8}	2

**Log reduction is the log (Treated/Original).

A simple calculation was conducted to evaluate the energy dissipated into the suspension during its laminar flow through the annulus. It was found that that the amount of energy dissipated in the suspension due to the pressure rise when the flow is laminar was very insignificant. The energy dissipation in the suspension (when the suspension flow rate of 1.72×10^{-6} m^3/s) due to the pressure rise in the pump and the pressure loss in the circulation pipes was estimated (using $\Delta P.\dot{v}$) and found to be 0.43 W per one flow pass. The treatment times of experiment ranged between 60 s and 300 s. $\dot{v}$ is the volumetric flow rate which is the volume per unit time.

After confirming that the pump had some impact on the level of yeast disruption in the original configuration, the pumping arrangement was modified to avoid yeast disruption in the circulation pump. This was achieved by fixing the speed of the motor and maintain constant volumetric flow rate to prevent any yeast disruption.

Testing was undertaken to ensure that no yeast disruption occur in the pump by forcing the yeast suspension through the shear apparatus using the modified pump (operated at lower constant speed), and the results show that the yeast disruption was zero. The modified pump was then operated at constant speed over a time period of 300 s. The final yeast viable count after fixing the circulation pump speed shows that the initial count is equal to the final count of 1×10^{10} CFU/mL at constant suspension temperatures of 18 ^oC.

5.4.5 Initial rotor results

Initial shear tests at the lower rotor speeds were conducted using *S. cerevisiae* suspension with a concentration of 1×10^{10} CFU/mL. To evaluate the quality of shear treatment, the effect of motor speed, and the treatment time was investigated for batch and flow configuration while suspension temperature was controlled to be always below 45 ^{o}C. Table 5.4 shows the log reduction of the yeast suspension for different tests with different speeds, different treatment times and suspension temperatures. Tests were conducted in batch and flow configurations as indicated in Table 5.4.

Table 5.4 Result of a treated suspension *S. cerevisiae* for different speed, time and temperature. Total suspension volume was 60 ml at batch configuration and the volumetric flow rate was 1032 ml/minute at flow configuration.

Test No.	Speed (RPM)	Configuration	Treatment time (s)	|log reduction|	Maximum suspension temperature (^{o}C)
Test 1	2000	Batch	120	3	42 - 46
			60	2	41 – 43
Test 2	3000	Batch	120	5	42 - 45
			60	3	42 – 44
Test 3	4000	Batch	120	6	42 – 48
			60	5.5	42 – 45
Test 4	2000	Flow	120	5	39 - 44
			60	4	40 – 41
Test 5	3000	Flow	120	5.5	40 - 45
			60	3.5	40 – 41
Test 6	4000	Flow	120	6	41 – 48
			60	5.5	40 – 42

The test started with an untreated sample of yeast suspension of 1×10^{10} CFU/mL, the sample was then shear treated at a speed of 2000 RPM for 60 s using a batch test arrangement (the yeast suspension was stationary, no circulation). A viability test was used to count the yeast concentration in CFU/mL before and after the treatment. The results of this test (2000 PM) show that the log reduction of the suspension was

approximately 2. The treatment time was then increased to 120 s; and the log reduction increased to 3, which is an indication of treatment improvement.

A second test was conducted by increasing the motor speed from 2000 to 3000 RPM for two different treatment times 60 and 120 s. The log reduction of the treated yeast suspension was found to be 3 and 5, for 60 and 120 s respectively. This result indicates that increasing the speed will also improve the treatment.

A third test was conducted using same treatment times of 60 and 90 s with higher speed of 4000 RPM. The log reduction was improved to be 5.5 and 6 for 60 s and 120 s respectively. These results gave a clear indication that motor speed and treatment time are very important factors in shear treatment, both influencing total energy input. Although the total amount of suspension was 60 mL, the true treated suspension volume was approximately 6 mL (the volume of the annulus). To ensure that all of the entire yeast in the suspension is subjected to shear stress, a suspension flow circulation system was developed to allow recirculation of the yeast suspension between the suspension bottle and shear chamber.

The last three tests presented in Table 5.4 were obtained using a flow configuration. A yeast suspension with a concentration of 1×10^{9} CFU/mL was used for these tests. As can be seen from the results presented in Table 5.4, the general treatment results were improved by approximately 20% when a flow configuration was used. For example, at 3000 RPM and treatment time of 60 s and 120 s, the log reduction was improved from 3.5 and 5.5 respectively (test 5) in comparison to test 2 (both configuration). This is another step toward optimizing the shear stress apparatus. Another test was conducted using a higher speed of 10000 RPM which will be discussed in the following section 5.6.

5.6 Experimental results

5.6.1 Yeast disruption in shear apparatus at 10000 RPM

Experiments were performed by the research team, using the research equipment commissioned by the author of this thesis, at a maximum speed of 10000 RPM for total treatment times ranging between 2 and 20 minutes and for temperatures below

40 ^{o}C. The importance of this test is that this test was undertaken at higher speeds and lower temperatures (< 35 ^{o}C), so the treatment is purely shear stress. The average maximum suspension temperature ranged between 20 ^{o}C and 35 ^{o}C, well below the 40 ^{o}C critical upper limits.

The yeast log reduction results at 10000 RPM ranged between 1 and 2 as illustrated in Table 5.5. Table 5.5 presents the log reduction results at different treatment time and suspension temperature below 35 ^{o}C. As can be seen, a yeast log reduction 1 was achieved when the treatment time was 2 minutes, for which 34 flow passes occurred at a suspension temperature of 32 ^{o}C. In this test (treatment time = 2 minute), the initial yeast suspension count was 8.3×10^{6} CFU/mL, while the treated sample was 8.3×10^{5} CFU/mL, which means the log (or $\log_{10}$) reduction of 1, or natural logarithmic ($\log_{e}$) reduction by a factor of 2.3 (Table 5.5, note the negative sign of $\log_{10}$ and $\log_{e}$ was removed from this Table).

Table 5.5 illustrate the data for treatment times from 2 minutes to 20 minutes, with suspension temperature being controlled between 29 ^{o}C and 35 ^{o}C at 10000 RPM. For example, when treatment time was 20 minutes and the suspension temperature was 29 ^{o}C, the final count of the treated sample was 8.3×10^{4} CFU/mL, or log reduction 2 (or $\log_{e}$ of 4.61).

The energy dissipated into the suspension and the shear stress developed in the suspension due to the rotational speed of 10000 RPM (and the suspension flow rate was 1032 ml/minute), was 2095 W and 3200 Pa as shown in Fig. 5.6 and Fig 5.7 respectively, these values represent the maximum power and maximum shear stress in the present work.

Table 5.5 Reduction results for a suspension of *S. cerevisiae* for 10000 RPM and different treatment times. Volumetric flow rate 1032 mL/minutes and initial yeast concentration 8.3×10^6 CFU/mL. The raw data obtained by Speering (2004) using the research equipment commissioned by the author of this thesis in the initial stage of the candidature.

Test	Time (min)	No. of passes	Suspension Temp (^oC)	Final Count CFU/mL	$\left\lvert\log_{10}(\frac{C_o}{C_i})\right\rvert$	$\left\lvert\log_{e}(\frac{C_o}{C_i})\right\rvert$
1	2	34	32	8.3×10^5	1.00	2.3
2	4	68	35	7.0×10^5	1.07	2.47
3	6	103	34	8.3×10^5	1.00	2.30
4	8	137	34	6.3×10^5	1.12	2.58
5	10	172	35	3.1×10^5	1.43	3.29
6	12	206	33	2.1×10^5	1.60	3.68
7	14	240	33	1.6×10^5	1.71	3.95
8	16	275	34	1.5×10^5	1.74	4.01
9	18	309	30	1.03×10^5	1.91	4.39
10	20	344	29	8.3×10^4	2.00	4.61

5.7 Discussion and analysis

In this section, the results from the shear stress apparatus will be discussed within the context of theoretical and experimental analyses. Initially, the theoretical results of shear stress and dissipated energy into the suspension were calculated for different speeds for the purpose of validation.

For microorganism in a turbulence region, it is suggested that microorganism rupturing can occur due to shear stress or the turbulent energy rate dissipation rate, and sometimes cavitation (Doulah and Hammond, 1975; Doulah et al., 1977). Therefore it is very important to understand the relationship between the shear stress generated in the suspension due to the rotational movement of the cylinder and the energy dissipated in the turbulence region.

5.7.1 Verification of turbulent Couette flow analysis

To verify the mathematical model presented in section 5.2.3, theoretical shear stress and power generated in the suspension will be calculated using equation 5.36 and equation 5.37, and the results were then compared with experimental results obtained from the shear apparatus (equation 5.32 and 5.33). As shown earlier in Fig 5.2, u_τ can be calculated using equation 5.35,

$$u_\tau = \frac{U}{1/K((\log(y) + C))} = \frac{0.35U_\infty}{1/K((\log(h/10) + C))}, \quad 5.35$$

where

U = 0.35 U_∞ (U_∞ = cylinder velocity as shown in Fig. 5.2),

K = 0.41 and

C = 2.01 in the region of turbulence described in equation 5.35.

The y value ranging between $\frac{u_\tau y}{v}$ = 30 and y = 0.1h which is = 1/10 (0.4×10^{-3}) (Bradshaw 1971). The wall shear stress can be calculated using equation 5.36

$$\tau_w = \rho u_\tau^2 , \quad 5.36$$

where ρ = suspension density.

The energy dissipation rate (ε) can be calculated using equation 5.37

$$\varepsilon = \frac{u_\tau^3}{Ky} \quad 5.37$$

Equation 5.37 was used to evaluate the theoretical rate of energy dissipated in the suspension for different rotor speeds. The length scale applies when y = 0.1h and y = 0.9h (Bradshaw 1971). For example, the theoretical energy dissipation rate for a speed of 5000 RPM was calculated using equation 5.35 and 5.37. The friction velocity u_τ was calculated using equation 5.35, where C = 2.01, K = 0.41, U_∞ (for 5000 RPM) = 25.9 m/s for y = 0.1h = $0.1 \times 0.4 \times 10^{-3}$ m.

The results from equation 5.35, 5.36 and 5.37 for 5000 RPM show that τ_w = 670 Pa and ε = 24307 W/kg when y = 0.1 h (detail of calculation is presented in Appendix H). The experimental ε values were calculated using equation 5.38 for the power generated by the rotor at different speeds (Fig 5.19) and the treated mass of the suspension (density of 1130 kg/m^3) in the annulus region. Suspension $mass = \rho_{sup}\pi(0.099 \times 0.0001 \times 0.05) \approx 0.007$ kg

$$\varepsilon = \frac{Power}{Mass}, \qquad 5.38$$

For example, the experimental power generated in the suspension at a speed of 5000 was 300 W as shown in Fig. 5.6, and the mass of the suspension in the annulus at any given time was calculated and was 0.007 kg. The specific power was calculated and found to be 42.85 kW/kg at 5000 RPM. The theoretical shear stress generated in the suspension was calculated using equation 5.36. The experimental shear stress was evaluated using equation 5.34, the results presented in Fig 5.9. For example, the theoretical and experimental shear stress at 3000 RPM and 4000 RPM were calculated and found to be 305 Pa and 495 Pa respectively (see Fig 5.9). The process of validation confirmed that overall there is good agreement between the experimental and theoretical shear stress generated in the annulus of the apparatus, especially in the speed range of 1000-7000 RPM range.

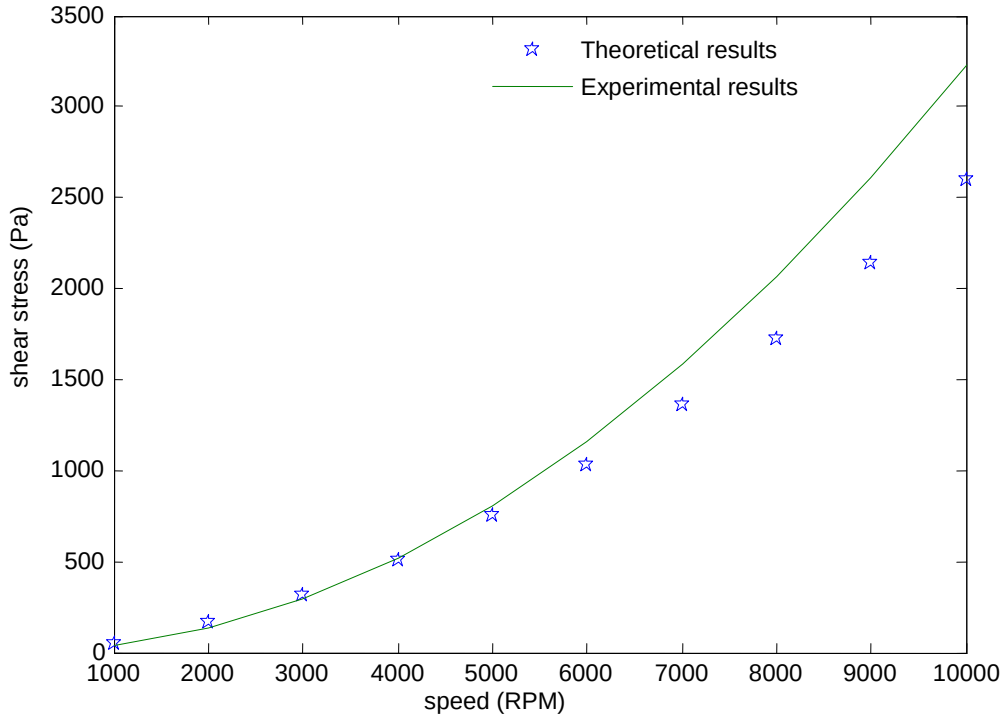

Fig. 5.9 The relationship between the rotor speed and shear stress generated in the suspension (theoretical and experimental).

5.7.2 Energy rate and shear stress for different speeds

The amount of energy required for rupturing the cell wall varies with the type of the cell. As discussed in section 5.1, some animal cells are soft and fragile, and thus they can be ruptured using a low shear value and low energy, whilst other microorganism can be highly resistant to breakage, and yeast is one of them.

The theoretical disruption percentage can be obtained by integrating equation 5.25 for different speeds. A sample of calculations for different speed and different energy dissipation is presented in Table 5.6. The mechanical properties presented in Table 4.1 and 5.1 were used in this calculation.

Zhang et al. (1993) reported that significant cell damage can occur when the Kolmogorov microscale of turbulence is below the cell diameter. As shown in Table 5.6, when l_k has a relatively large of 7.13 μm at 1000 RPM, the reduction percentage was very low, shown as 0 % in Table 5.6. The yeast log reduction percentage was 0.28% when l_k =5.1 μm. This result shows good agreement with Zhang et al. (1993).

Table 5.6 The relationship between the experimental and theoretical energy dissipation into a 60 mL (0.007 kg) suspension and the predicted microorganism disruption for different speeds.

Speed (RPM)	Power (Watt) Theoretical	Power (Watt) Experiment	ε = power/mass (kW/kg) Experiment	l_k μm	P (%) Theory Per pass
*	-		-	5.1	0.28%
1000	4.1	4.5	0.65	7.13	0%
2000	21	25	3.6	4.22	0.38%
3000	70	76	10.86	3.135	0.47%
4000	166	167	33.85	2.514	0.95%
5000	322	320	42.87	1.95	2.32%
7000	860	767	110	0.712	4.2%
10000	2600	2095	300	0.2	6%

* Results of Zhang et al. (1993).

The expected shear stress generated in the annulus when the rotor speed was 7000 RPM (corresponding to a power of 767 W) and 4000 (corresponding to a power of 167 W), was 1350 Pa and 495 Pa respectively. As can be seen in Table 5.6, higher shear stresses generated in the annulus will lead to a higher level of cell wall disruption.

5.7.3 Disruption prediction

The prediction of yeast disruption in the present shear apparatus was calculated and compared with results obtained from Zhang et al. (1993) and others. The theoretical disruption percentage was calculated using the Gaussian approach presented in equation 5.24 (section 5.2.4). The integration of Gaussian equation presented in equation 5.25 was solved using a numerical code developed using Matlab software.

An example of the yeast disruption percentage at 10000 RPM is presented here. As for test 1 shown in Table 5.5, where the suspension volumetric flow rate of yeast was 1023 mL/s, and suspension volume used in this test was 60 mL, and a treatment time was 2 minutes, the expected number of suspension passes through the shear area can be calculated. When N is the number of possess.

$$N = \frac{Q.t}{V} = \frac{1032 \times 2 \times 60}{60} \approx 34\ passes$$

For the same test number 1, natural log reduction ($\log_e$) due to this shear treatment can be calculated from

$$log_e\left(\frac{C_o}{C_i}\right) = log_e\left(\frac{8.3 \times 10^6}{8.3 \times 10^5}\right) = -2.3.$$

Or yeast $\log_{10}$ reduction (Table 5.5)

$$log_{10}\left(\frac{C_o}{C_i}\right) = log_{10}\left(\frac{8.3 \times 10^6}{8.3 \times 10^5}\right) = -1.$$

This procedure was repeated for different N, as illustrated in Table 5.5 for different speeds. Results presented in Table 5.6 are graphically presented in Fig. 5.10, with the number of flow passes represented on the horizontal axes and remaining yeast ratio

$\left(\frac{C_o}{C_i}\right)$ represented on y axes. The present experimental results in Fig 5.10 were fitted by the equation from Thomas et al. (1994)

$$\frac{C_o}{C_i} = e^{30.5N^{-1.32}} \qquad 5.39$$

The two constants of 30.5 and -1.32 were obtained using exponential equation best fit technique. Thomas et al. (1994) uses the same method of evaluating cell damage prediction as Zhang et al. (1993), which is presented in equation 5.19 through to equation 5.25. The curve fit equation to the data presented by Thomas et al. (1994) was given by

$$\frac{C_o}{C_i} = -e^{-0.1N^{0.68}} \qquad 5.40$$

The best fit exponential equation of the present work given in equation 5.40 presented in Fig. 5.10 is consistent with the results presented by Thomas et al. (1994) presented in equation 5.40.

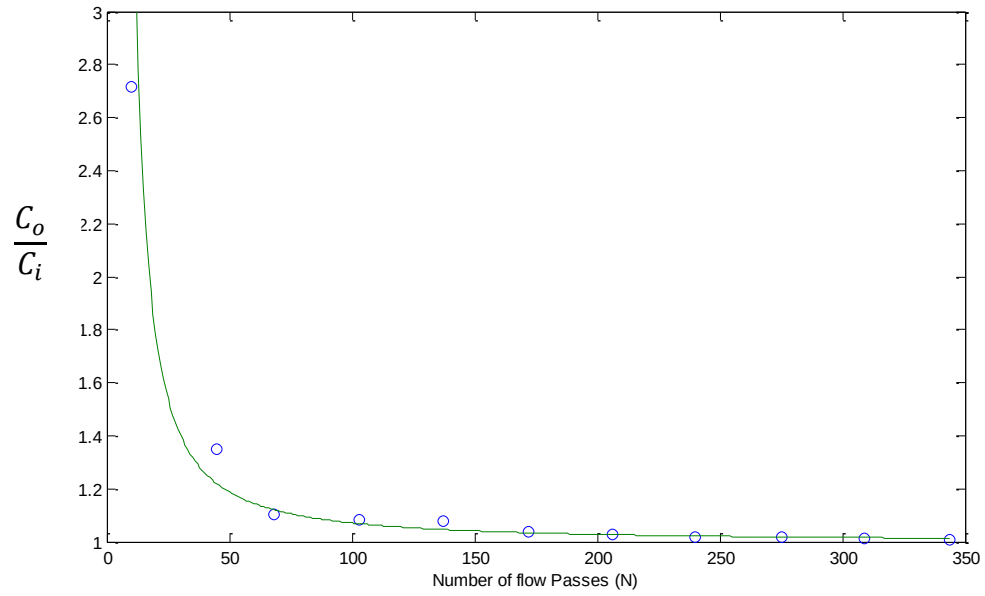

Fig 5.10 Yeast concentration ratio in the suspension against number flow passes in shear apparatus (different rotor speeds).

From Fig. 5.10, the decrease of C_o/C_i is very significant in the first 10 minutes (N between 50 and 200) in comparison to the last 10 minutes of treatment time (for N values between 200 and 350). The remaining yeast ratio (C_o/C_i) in the suspension becomes approximately constant for the last 10 minutes of the shear treatment (N value between 200 and 350). This means the ongoing yeast reduction rate as a function of shear treatment reduces when treatment time exceeds 10 minutes.

Thomas et al. (1994) reported that modest cell damage in such closed systems is due to a large reservoir where cells are exposure to less turbulence in the capillary. The third reason can be attributed to the fact that mechanical properties of the cell wall were assumed to be constant during the treatment, which is not a totally accurate assumption. Some researchers reported that mechanical properties may change during the treatment, thus the theoretical prediction value cannot be very accurate.

A number of researchers such as Ayazi et al. (1994) and Cherry et al. (1986) suggested that the fluid mechanical stress caused by turbulence flow is the main cause of microorganism rupturing in devices that operate in a similar way to the present shear apparatus, such as the homogenizer in dairy product industry and the bead mill. The key parameter for microorganism rupturing in the fully turbulent flow is the ratio of the cell size to the size of the smallest eddies. Ayazi et al. (1994), Zhang et al. (1993), Doulah (1977) and Middelberg et al. (1992) reported that for a particle diameter greater than the size of smallest eddies, the likelihood of cell wall rupture is very high. Therefore, rupture is expected to occur in the present work since the average microscale length was 1.236 μm which is smaller than the size of the yeast used in the present work which is 5.4 μm. McQueen et al. (1987) and Zhang et al. (1993) indicate that cell disruption can only occur if the microscale size is smaller than the size of the cell.

5.8 Conclusion

Many researchers in the field of microorganism disruption using mechanical methods have reported using small scale commercially available devices or laboratory scale devices including homogenizers, bead mill and French press homogenizer. In this work, the author successfully adopted a mathematical method used by Zhang et al. (1993), and Thomas et al. (1994) and good agreement between cell ruptures of both works was achieved. The model was applied to the present shear apparatus by developing the relationship between the specific powers, eddies due to turbulent flow and the shear stress that was required for yeast disruption. The mathematical results show good agreement between the experimental shear stress results and the theoretical results for different rotor speeds. The theoretical energy dissipation rate in the annulus of the shear apparatus was then evaluated for different regions within the annulus.

The shear stress apparatus was designed to generate shear stress and dissipate turbulent energy with virtually no pressure rise. The shear stress apparatus can easily change operating parameters and allow investigation into the effect of various parameters on shear stress and energy dissipation in the microorganism disruption. The shear apparatus was able to perform efficiently and effectively for disrupting *S. cerevisiae* over a spectrum of treatment times, suspension temperature and rotor speeds. This shear apparatus can be modified to operate on different microorganism and different conditions.

When the shear apparatus operates at 10000 RPM, the net energy dissipation and shear stress was 300 kW/kg and 3200 Pa respectively and the power generated by the device was 2095 W. The yeast log reduction was evaluated and compared with the mathematical method, a good agreement between the present work results and the experimental work of Zhang et al. (1993) was achieved. For example, when shear apparatus operated at 10000 RPM, the maximum predicted theoretical yeast disruption was found to be around 6% in comparison with the experimental values which was around 4%. This mathematical method should be applicable for any microbes and not limited to yeast.

The experimental result shows that microorganism disruption will only occur in turbulent flow if the microscale size is smaller than the size of the cell, as achieved in the present work. For example, when the shear apparatus operates at 10000 RPM, the microscale was calculated and found to be 1.2 μm which is smaller than the yeast diameter of 5.4 μm, thus the rupture occurring is expected to be due to shear stress and energy dissipation due to turbulent flow. This result confirms the reported outcome of Tawatchai et al. (2008), Ayazi et al. (1994), Zhang et al. (1993) and Middelberg et al. (1992).

Full treatment can thus likely be achieved in a shorter time by increasing the rotor speed or decreasing the annulus gap. This however is an issue for further investigation.

CHAPTER VI

A Comparison of Ultrasound, Shock and Shear Treatments

6.1 Introduction

The conventional method of microbial disruption in the food processing industry is the thermal method, where the suspension is exposed to a certain temperature history, and this process leads to microorganism inactivation. Alternative mechanical methods of ultrasound, shock wave and shear stress treatments were discussed in chapter 3, 4, and 5 of this thesis. This chapter aims to compare the yeast disruption achieved using the three methods examined in this thesis in terms of energy. The results obtained from the mechanical treatment will also be compared with the conventional method of microorganism inactivation via heat treatment and another method of disruption, the high pressure homogenizer.

6.2 UHT energy analysis

The treatment of microbial cells in suspension using UHT generally results in a complete destruction of the microorganism. However, this treatment will negatively affect the quality of the product as reported in chapter 2, section 2.0.

Sahoo et al. (2002) designed and built a laboratory model helical UHT sterilizer to disrupt *B. Stearothermophilus* with a short residence time, it operates in a temperature range of 90 to 150 ^{o}C. Their UHT treatment involves heating up a mass per time of 0.042 kg/s from 10 ^{o}C to 75 ^{o}C for 15 s, and then further heating it up to 140 ^{o}C for 10 s (Sahoo et al., 2002). In the sterilization process, Shaoo et al. (2002) reported that the suspension temperature was kept between 135 and 145 ^{o}C for 2.64 s. They claimed that using this short time of sterilization of around 2.64 s can achieve a log reduction of 8.

If the heat lost to the walls is ignored, the energy rate ($\dot{Q}$) delivered into the suspension can be calculated using

$$\dot{Q} = \dot{m}\, C\, (T_2 - T_1) \qquad 6.1$$

where

C = Specific heat of the sample (kJ/kgK).

T_1 = Initial temperature (^oC)

T_2 = Final temperature (^oC)

$\dot{m}$ = the mass flow rate (kg/s).

Using equation 6.1 in conjunction with Sahoo et al. (2002) data of a suspension mass flow rate of 0.042 kg/s at 5 bar, density 1000 kg/m^3 and specific heat 4.2 kJ/kg.K, the net heat rate dissipated in the suspension due to the rise of temperature from 93 to 140 ^oC is

$\dot{Q}$ = 0.042 × 4.2 × (140-93) = 8.29 kW.

The specific energy (q) can be calculated, for 31.5 g or 0.042 kg/s using equation 6.2

$$q = \frac{\dot{Q}}{\dot{m}}\ , \qquad 6.2$$

which, for the given above UHT treatment is 197.4 kJ/kg. The specific energy dissipation rate measured in kW/kg can be calculated using equation 6.3

$$\varepsilon = \frac{\dot{Q}}{m}\ , \qquad 6.3$$

where m is the suspension mass = 0.0315 kg. The average specific power is

$$\varepsilon = \frac{8.39\ \text{kW}}{0.0315} = 263.17\ \text{kW/kg}$$

Table 6.1 Sample of calculation of the energy required for microorganism disruption using UHT method.

Quantity	Units	Values Sahoo et al. (2002)
Mass	kg	0.0315
Density	kg/m^3	1000
Treatment time	second	2.64
Specific heat	kJ/kgK	4.2
Specific energy	kJ/kg	197.4
Energy rate (power)	kW	8.29
Specific energy rate (Power)	kW/kg	263.17
Log reduction	-	8

The calculation presented in Table 6.1 will be used as a reference for comparison with mechanical methods for microorganism disruption.

From the results presented in Table 6.1, it can be seen that Sahoo et al. (2002) achieved log reduction 8 at a specific energy of 197.4 kJ/kg and treatment time of 2.64 s. This result revealed that a high cell reduction (greater than 8) would be achieved if 197.4 kJ/kg is used. Summary of the calculated specific energy and specific power results related to UHT treatment is illustrated in Table 6.1.

6.3 Homogenization disruption analysis

A single stage homogenizer was used by Keshavarz et al. (1990) to disrupt commercial yeast using a pressure of 46 MPa, and temperature of 4 ^{o}C. The number of passes in this homogenizer required to achieve 90% cell disruption (which is equivalent to log reduction of 1 was 5. The entry and exit velocity of the suspension were 206 m/s and 200 m/s respectively. For the following analysis, the density is assumed to be the same as water. The mass per pass was calculated using the volume of the chamber between the seat and the valve of the homogenizer chamber multiplied by the density of the water.

When the volume flow rate per pass is 57 L/h (0.0157 L/s), and the pressure drop across the homogenizer is 46 MPa, the work measure in Watt can be calculated using equation

$$\dot{Q} = \Delta P . \dot{v} \qquad 6.4$$

where

ΔP = pressure drop (Pa).

$\dot{v}$ = volumetric flow rate (m^3/s).

Thus

$$\dot{Q} = \frac{46\times10^{6}\times57\times10^{-3}}{3600} = 0.728 \text{ kW}$$

To calculate the specific power dissipation rate and specific energy, the treated mass is calculated using the homogenizer configuration suggested Keshavarz et al. (1990). The average suspension velocity of 206 m/s over the distance of the seat is 0.1 mm (for the KE configuration of Keshavarz et al., 1990), thus the estimated that the treatment time per pass is 5×10^{-6} s. The treatment time for 5 passes (corresponding to 90% cell disruption or a log reduction of 1) is $5 \times 10^{-6} \times 5 = 2.5 \times 10^{-6}$ s. The specific energy of the treated mass (circulated treated volume between the valve and the seat × suspension density) of 0.00039 g is.

$$q = 0.728 \times \frac{2.5\times10^{-6}}{3.9\times10^{-7}} = 4.67 \ \frac{\text{kJ}}{\text{kg}}$$

In homogenizer technology, the region where the shear stress is developed is located between the valve of the chamber and its seat. This is the region where most of the yeast rupture occurred according to Keshavarz et al. (1990). According to Keshavarz et al. (1990), the shear stress can be calculated using equation 6.5

$$\tau_m = \frac{0.16\rho U^2 d^2}{X^2}, \qquad 6.5$$

where

U = exit jet velocity = 200 m/s

d = orifice diameter = 5 mm

X = distance from the seat of the valve to the valve itself.

The shear stress for X = 1.4 mm, exit velocity of 200 m/s and orifice diameter of 5 mm was calculated using equation 6.6, and found to be approximately 81 MPa. This calculated shear stress (81 MPa) will be used for comparison study in the following section. The results presented in Table 6.2 will be used for comparison in the following sections.

Table 6.2 Keshavarz et al. (1990) homogenizer properties for the KE configuration and sample of energy calculation.

Quantity	Units	Value (KE configuration)
Valve distance (X)	mm	1.4
Diameter	mm	5
Radius difference	mm	0.1
Height	mm	12.55
Exit Velocity	m/s	200
Average velocity	m/s	206
Pressure	MPa	46
Specific energy	kJ/kg	4.67
Treatment time	s	2.5×10^{-6}
Specific power	kW/kg	1.868×10^{-6}
Shear stress	MPa	81
Log reduction	-	1

6.4 Comparison of treatment methods

To evaluate the efficiency of each treatment method used in this thesis, the fraction of viable yeast remaining in the suspension or the yeast log reduction values with respect to the amount of energy per unit mass that was used in each method was evaluated and compared. Fig 6.1 shows the relationship between the specific energy (kJ/kg) on the horizontal axes and the yeast log reduction results obtained from chapter 3, 4 and 5 on the vertical axes. Fig 6.1 consists of three subfigures of a, b, and c which present results obtained from the ultrasound treatment, shock treatment and shear treatment respectively. The detail of these results and other data such as time of treatment, temperatures, pressure, shear stress, specific energy measured in kJ/kg and energy dissipation rate measured in kW/kg is also presented in Table 6.2. The methods used to obtain these comparative results are presented in the following sections.

6.4.1 Ultrasound

The ultrasound can create cavitation in the yeast suspension. If the ultrasound power is sufficiently high, the cavitation bubbles will expand until they reach a critical radius at which they collapse. Collapse of the cavitation bubbles releases energy into the suspension which is presumably the reason of microorganism disruption. Whether or not the acoustic energy or the turbulent energy is actually responsible for the disruption is the subject of this dissertation. The relationship between the yeast disruption and the specific energy dissipated into the yeast suspension is focus of the present discussion. The power intensity is the ultrasound power measured in W per unit area

$$P_{int} = \frac{Power}{Probe\ Area} = \frac{117}{\pi 0.0125^2} = 238\ kW/m^2$$

The specific energy is the energy dissipated into the suspension per unit mass, where the mass of suspension was 0.03 kg, and the power measured in Watt was ranged between 74 and 117 W. In the case of ultrasound treatment, the specific energy dissipated into the suspension was calculated and found to be in the range of 250 kJ/kg to 1132 kJ/kg depending on the treatment time. The specific energy was found to be considerably lower than the specific energy used in shear stress apparatus and considerably higher than the shock wave values (discussed in subsequent sections). Results presented in Fig 6.1 (a) show that the approximate maximum yeast log reduction was 4 when specific energy was 1132 kJ/kg as shown in Table 6.3. Ultrasound treatment was carried out on yeast by Ciccolin et al. (1997) at 100 W (203 kW/m^2) for at a suspension temperature of between 50 °C and 60 °C. The effect of using 203 kW/m^2 ultrasound power intensity (on a 60 mL suspension) led to a yeast disruption of log 2, but disruption was less marked at 50 ^{o}C (Ciccolin et al., 1997). Comparing this result with the present results, the yeast log reduction 2 was achieved at a specific energy of around 700 kJ/kg or a power intensity of 238 kW/m^2 (when the suspension volume was 30 mL) as shown in Fig. 6.1(a). The results of the present work were achieved when the yeast suspension temperature was around 30 ^{o}C.

Earnshaw et al. (1995) showed that using ultrasound specific power of 1.65 kW/kg resulted in no yeast disruption as no cavitation was expected to be developed, and therefore the log reduction was zero. In the Earnshaw et al. (1995) experiment, the cross sectional area of the probe diameter was 25 mm, thus ultrasound power intensity was about 101.8 kW/m^2 when 50 W was used. The 101.8 kW/m^2 power intensity is just enough to generate a very small number of bubbles, but these bubbles are not able to produce significant energy when they collapse (as reported by Earnshaw et al., 1995). These cavitation bubbles were reported to be insufficient to even weaken the yeast (Earnshaw et al., 1995). In the present work, the yeast log reduction at approximately 50 W was insignificant. The modest microorganism disruption in the Earnshaw et al. (1995) experimental work as well as the present work when low ultrasound power intensity was used can be attributed to several factors.

One of the reasons for this modest disruption could be due to the power transmission into the suspension, which is directly proportional to the suspension temperature (Ciccolin et al., 1997 and Gogate et al., 2009). If the energy is well propagated and acoustic energy released in the suspension, the possibility of causing microorganism rupturing is expected to be high. In another words, the elevated temperature enhances the transmission of the ultrasound as reported by Ciccolin et al. (1997) and Gogate et al. (2009), and finally enhances the yeast disruption. To enhance the possibility of microorganism disruption using ultrasound, researchers recommended combining ultrasound treatments with heat treatment or pressure treatment as reported by Ordonez et al. (1984). For example, Ordonez et al. (1984) used ultrasound of 20 kHz and 160 W combined with a temperature of up to 62 ^{o}C. This combination was reported to be very effective in comparison to increasing the treatment time and energy consumption, Ordonez et al. (1987).

The ultrasound treatment time of the work done by Cameron et al. (2008) was 10 minutes for 40 mL yeast at 100 W, which is equivalent to a specific energy of 1500 kJ/kg. Cameron et al. (2008) achieved yeast log reduction of 4.3. The reported result of the present work shows that log reduction 4 can be achieved at specific energy of around 1132 kJ/kg. This result show to some extent moderate agreement between the present work and the work done by Cameron et al. (2008). Cameron et al. (2008) has

not reported the detail of yeast log reduction 4, therefore the 4.3 was selected for this comparison.

Ultrasound power intensity is another basis for comparison between treatment methods. In comparison to the present work, Cameron et al. (2008) conducted an experiment to examine the effect of ultrasound power and treatment time on *S. cerevisiae*. A 40 mL yeast suspension was subjected to 100 W ultrasound probe of diameter of 13 mm, giving a power intensity of 744 kW/m^2. In the present work, the power intensity used was calculated and found to be 238 kW/m^2. Both works use same ultrasound power of approximately 100 W, but it seems the possibility of generating cavitation and ultimately microorganism disruption is higher in the Cameron et al. (2008) work due to the higher power intensity. Ultrasound power intensity influences the effectiveness of the treatment and the ultrasound probe diameter is another factor that affects the power intensity, and this leads to an influence on the cell rupturing efficiency when the power is constant. For example, a probe with a diameter of 15 mm can be more effective in cell damage in comparison to the probe with 25 mm diameter using same ultrasound power because the probability of generating cavitation is higher in the 15 mm case due to the higher power intensity.

Gogate et al. (2009) reported that the cavitational effect is more significant closer to the vibrating surface. According to Gogate et al. (2009) the cavitational intensity decreases exponentially with the distance from the probe and cavitation may vanish at a distance of 2 to 5 cm, this figure varies with the supplied energy and the operating frequency. It was also reported that the efficacy of probe type ultrasound systems with larger scales is relatively poor in comparison to other systems such as multiple transducers. This is due to the fact that ultrasonic probe is unable to transmit the acoustic energy throughout a large suspension volume effectively (Gogate et al., 2009).

6.4.1 Shock wave

From the results presented in chapter 4, results have been selected from five experiments results representing the minimum, maximum and three average yeast log reduction values. The external pressure applied on the water tube surface ranged

between 114 MPa and 117 MPa while the corresponding maximum piston velocity ranged between 79 m/s and 81 m/s. The results of shock treatment was selected and presented in Fig 6.1(b). The yeast concentration before treatment was 1.46×10^5 cfu/mL while the treated sample concentration was 1.16×10^5 cfu/mL, this is equivalent of log reduction of 0.13, and this was the minimum disruption result. The maximum yeast log reduction using shock treatment was achieved at 116.6 MPa was found to be 0.57, the yeast concentration before the treatment was 5.3×10^5 cfu/mL, and the yeast concentration after the treatment was 3.0×10^5 cfu/mL. For the present analysis, the energy absorbed by one yeast cell during shock treatment is estimated using work equation

$$\Delta W = P_i \, \Delta V, \qquad 6.6$$

where

ΔV = volume change of the cytoplasm due to external pressure
P_i = internal pressure experienced in the cytoplasm.

The internal pressure (P_i) generated in the cytoplasm due to the external pressure load (P_e) can be calculated from equation 6.7 (equation 4.14 in chapter 4)

$$P_i = \left(\frac{9B(1-\nu)}{3B(1-\nu)(2b^3+a^2) - 2E(a^3-b^3) - 2B\nu(a^3-b^3)}\right)P_e, \qquad 6.7$$

The following yeast cell properties were used to calculate the internal cell pressure

a = cell internal radius = 2.4×10^{-6} m
b = cell external radius = 2.7×10^{-6} m
B = cytoplasm bulk modulus = 2.2 GPa
E = modulus of elasticity of cell wall = 112 MPa
ν = Poisson's ratio = 0.4
P_e = external pressure = 114 - 117 MPa
V = $(4/3)\pi \times (2.6 \times 10^{-6})^3 = 7.3 \times 10^{-17}$ m^3.

The volume change due to the pressure was calculated using equation 6.8, and found to be 3.65 ×10^{-18} m^3.

$$P_i = B(\frac{\Delta V}{V}) \quad 6.8$$

Equation 6.6 was used to calculate the energy absorbed due to the volume changes and the external pressure. For example, for an external pressure of 114, the internal pressure is around P_i is around 112 MPa (see Fig.4.3), the energy per cell was found to be 3.92 × 10^{-10} J. The cell mass is around 8.4 × 10^{-13} kg, so the specific energy (the energy per unit mass) is 4.67 kJ/kg.

The specific energy dissipated into the cell for different pressure loading due to the shock treatment was calculated and presented in Table 6.3 and graphically presented in Fig. 6.1 (b). Fig. 6.1 (b) shows that the specific energy required to achieve a log reduction of approximately 0.25 in yeast using shock wave was approximately 4.68 kJ/kg, which is the lowest specific energy among the three treatments.

Table 6.3 The specific energy (kJ/kg) and log reduction and for different shock tests using different shock tests.

.

Test	Shock pressure (MPa)	Specific energy (kJ/kg)	$\|\log reduction\|$
Control	-	-	0
Test 1	114	4.67	0.13
Test 2	114.5	4.68	0.25
Test 3	115.7	4.73	0.5
Test 4	116.6	4.77	0.57

The specific energy required to have a yeast log reduction of between 0.1 and 0.2 is relatively low, but at the same time, the yeast log reduction values are also low in comparison to ultrasound and shear methods. Shock treatments are more commonly

reported for soft cell rather than relatively hard microorganisms (higher modulus of elasticity and density). For example, the shock treatment method has been used for different applications such as animal cells and medical applications (Tamagawa et al., 1997).

The minimum specific energy required to rupture the cell wall of single yeast was around 4.67 kJ/kg, however the real net energy dissipated into the yeast itself is expected to be smaller than the 4.67 kJ/kg due to some energy loss in the plastic bag, pressure wave propagation through water, and other parameters that were discussed in the second last subsection of chapter 4.

Referring to the static and dynamic analyses of chapter 4, the von Mises stress is assumed to be the main reason of microorganism disruption (von Mises is a failure theory which some researchers think is reasonable to apply to microorganism rupture as discussed in Chapter 4, section 4.2 and 4.3). The von Mises stress required to rupture the cell wall of the yeast was found to be 70 MPa, and this figure was reported by many authors as described in Chapter 4. Calculations indicate that a von Mises stress of 70 MPa can be achieved when the external pressure applied on the cell is around 100 MPa and above, see calculation in section 4.2. In the shock experiments, the external pressure applied on the water tube varied between 114 MPa and 116.6 MPa. However, the magnitude of the loading was attenuated during transmission through the plastic bag as described in detail in section 4.10. An attenuation factor of approximately 0.7 was determined in section 4.10 so the external pressure loading on the cell in the present work is expected to be between 70 MPa and 84 MPa, which is insufficient for substantial disruption.

Treatment time is another important factor that played a vital role in cell disruption using ultrasound and shear treatment; however it was not the case for the shock treatment. In the present work, the treatment time using shock was very small in comparison to ultrasound and shear. In the case of shock wave treatment, the yeast was subjected to around 115 MPa only one time for a fraction of a microsecond second, while the treatment time using ultrasound and shear stress was between 180 s to 900 s and between 360 s and 1200 s respectively (Table 6.4).

It is important to mention here, the pressure rise in the yeast due to the dynamic FE simulation was around three times greater than the static pressure obtained from the analytical calculation in section 4.2 for a given applied external pressure. Therefore the energy absorbed in the actual treatment which is more closely approximated by the dynamic FE simulation is likely to be more than three times greater than the value derived from the quasi static analysis.

6.4.2 Shear stress analysis

Table 6.4 shows that the shear cell generates significant quantities of energy during experimentation. The vast majority of this energy dissipated in the suspension is responsible for yeast disruptions in form of turbulent eddies and shear stress. From Table 6.4, the specific energy required to achieve a log reduction of 4 was found to be 360000 kJ/kg with a treatment time of 20 minutes and 10000 RPM, while the specific energy required to achieve a 2.5 log reduction was around 108000 kJ/kg with a treatment time of 6 minutes in the absence of thermal stress. To compare these results with the homogenization process that was discussed in section 6.3, the specific energy required to disrupt the yeast during homogenization for a yeast log reduction of 1 was found to be 4.67 kJ/kg. However, since the log reduction appears to be approximately linearly proportional with the specific energy of treatment in the case of the shear apparatus, a comparison can be made on the basis of log reduction per specific energy.

In the case of the shear stress apparatus, the yeast log reduction per specific energy (log/kJ/kg) is 1.5×10^{-5} , whereas in the case of the homogenizer (Keshavarz et al. 1990) the yeast log reduction per specific energy is 0.214. This means the disruption efficiency of shear stress apparatus is less than that of the homogenizer of Keshavarz et al. (1990).

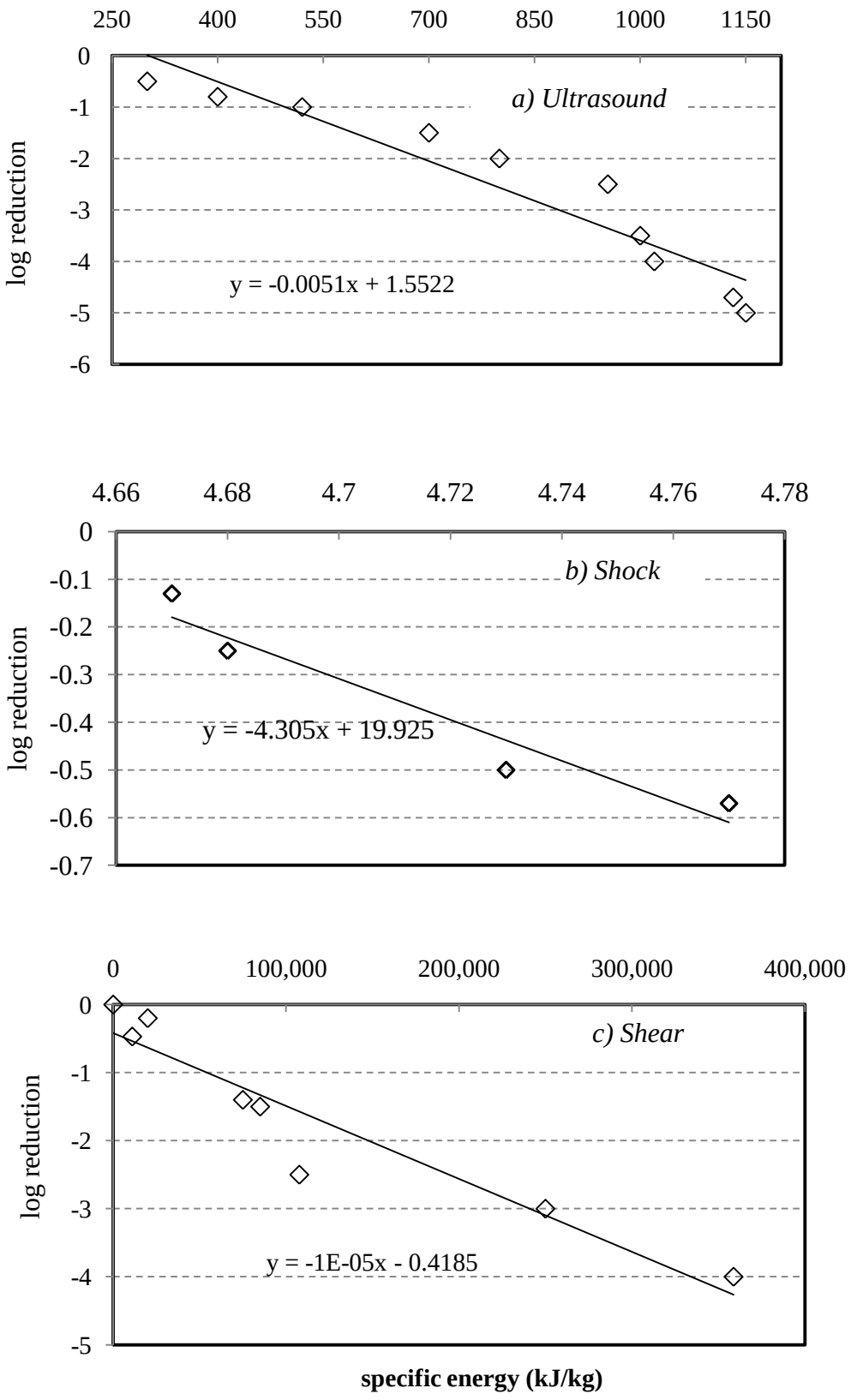

Fig. 6.1 The relationship between specific energy and yeast log reduction using a) Ultrasound treatment, b) Shock treatment, and c) Shear treatment.

6.5 Discussion and conclusion

Ultra heat treatment and high pressure homogenization treatment methods were selected as reference methods for comparison with results obtained from the ultrasound and shock wave, and shear treatments in this study. The main operating parameters that affect the yeast log reduction presented in the second half of Table 6.4 are treatment time, suspension temperature, mass or volume of suspension, operating pressure and rotor speed (in the case of shear apparatus). The results of the experimental work such as specific energy, energy dissipation rate, power, shear stress and log reduction are presented in the first half of Table 6.4 and Fig. 6.1.

The conclusions of this chapter can be summarized as follows:

1. The three methods suggested in this thesis can be successfully used for yeast disruption, and it is expected these can be applied to disrupt other microorganisms which hold similar mechanical properties to yeast. The present shear stress and ultrasound device can generate a large amount of specific energy and thus it is expected to be able to use these for the treatment of hard microorganism.
2. Ultrasound treatment using low power (50 W) with higher temperature 55 ^{o}C can be used to make the yeast more sensitive as reported by Ciccolin et al. (1997), and enhance the cell wall rupturing.
3. Energy wise, it was found that for given log reduction, the shear stress treatment has the highest specific energy in comparison to homogenization, ultrasound and shock treatment.

The log reduction per unit specific energy is defined as the ratio between the yeast log reductions to the required specific energy, which is the slope of the best fit line presented in Fig. 6.1 a, b and c.

Results presented in Fig. 6.1 show that the log reduction per unit specific energy (kJ/kg) was 0.0053, 3.9 and 1.5×10^{-5} using ultrasound, shock wave and shear treatment respectively. The log reduction per unit specific energy for shock treatment was found to be the highest (3.9) among the three followed by ultrasound, while the log reduction per unit specific energy of shear stress treatment was the lowest of 1.5

$\times 10^{-5}$). This result gives a strong indication that within the context of ultrasound processing, the chance of yeast disruption due to shock wave is very high in comparison with the shear stress.

It is important to mention here, that although the experimental shock treatment results show that the maximum log reduction achieved was only around 0.57, this does not mean the shock wave effects are less important to the yeast disruption than the shear stress in ultrasound processing. The modest yeast disruption results (experimentally) were due to many factors related to the experimental setup, the yeast plastic bag, including the number of treatment times and other reasons that were discussed in chapter 4. The simulation and numerical results presented in chapter 4 demonstrated that a 100 MPa external dynamic pressure can lead to a possible yeast disruption. Thus, higher yeast log reduction per specific energy can be achieved using shock treatment, and ultimately a relatively small specific energy is required to achieve yeast disruption when ultrasound treatment is used.

Table 6.4 Specific energy and yeast log reduction results of five different mechanical yeast disruption in different operating conditions.

Treatment	Mass	Power	Specific Power	Shear stress	Specific Energy	Log reduction
	(kg)	(kW)	(kW/kg)	(MPa)	(kJ/kg)	(-)
Ultrasound	0.03	0.117 0.117	3.1 3.1	- -	1132 905	4 2.5
Shear	0.007 0.007	2.095 2.095	300 300	0.002595 0.002595	360000 108000	4 2.5
Shock wave	8.4×10^{-14}	-	-	75	4.77	0.57
UHT	0..315	8.29	263.17	-	197.4	8
Homogenization	0.39×10^{-6}	0.728	1.86×10^{6}	81	4.67	1

Operating parameters

Treatment	Treatment Time	Speed	Time Per Pass	Volume	Temp.	Pressure
	(s)	(RPM)	(s)	(mL)	(^{o}C)	(MPa)
Ultrasound	365 292	-	-	30	30 30	0.1
Shear	1200 360	10000 10000	0.0076 0.0076	60 60	30 30	0.1
Shock wave	-	-	-	7.3×10^{-11}	20	116.6
UHT	2.64	-	-	31.5	93-140	0.5
Homogenization	2.5×10^{-6}	-	5×10^{-6}	3.9×10^{-4}	4	46

Homogenization data from Keshavarz et al. (1990) and UHT data from Sahoo et al. (2002).

CHAPTER VII

Conclusion and Future Work

Ultrasound, ultra high temperature, high pressure homogenization, bead milling and French press are the most common, commercially-available devices that can be used for microorganism disruption. The emphasis of most literature is on commercialization and industrial application of these methods, while the innovation in the area of microbe disruption technology is not evident. The investigation of the ultrasound treatment, and understanding the real cause of microorganism disruption using ultrasound treatment - are shock waves or shear stress are responsible - is the question of this thesis.

The general aim of this thesis was to fill in the gap of knowledge in the area of microorganism disruption due to ultrasound. There are two candidate mechanisms: i) shock wave; and ii) shear effect. It was reported (chapters 1 and 2) that strong shock wave and shearing flow effects are generated by high power ultrasound but the dominant effect on microorganism disruption whether - shock or shear - had not been resolved.

Results in chapter 3 showed that the total heat lost to the surrounding was around 13.5% of the total ultrasound energy. It was also found that one second is sufficient time to achieve a complete suspension mixing. The experimental results of chapter 3 demonstrated that a maximum log reduction of 4 can be achieved at 117 W ultrasound power and a treatment time of 365 s.

This thesis provides a substantial explanation of the effect of the shock treatment on microorganisms disruption, using an analytical model with the aid of a numerical FE technique combined with some experimental results using the shock wave apparatus (chapter 4). The shock treatment results show that, due to the difference in

mechanical properties between the cell wall and cytoplasm, cell wall disruption occurred at the lower part of the cell wall where von Mises stress concentration is developed.

Mathematical methods were developed in chapter 5 using yeast mechanical properties to help analyse the microorganism disruption due to shear stress using a statistical approach. To validate the analysis, a shear stress apparatus was designed and constructed to provide shear stress in the absence of a pressure differential. The experimental and theoretical shear results demonstrated that, yeast disruption occurs due to the high energy dissipation and shear stress in the turbulent region of the suspension in the absence of high pressure and temperature within the annular gap in the shear apparatus. The shear stress experimental apparatus demonstrates that yeast disruption can occur due to shear stress in the absence of high pressure.

Chapter 6 presents a comparative study between ultrasound, shock shear and shear treatment in term of specific energy. The results demonstrated that a yeast log reduction per unit specific energy was approximately 0.0053, 3.9, and 1.5×10^{-5} using ultrasound, shock and shear respectively. This result suggested that shock treatment is the most effective method for microorganism disruption in comparison to shear stress, and it suggested that the major cause of yeast disruption using ultrasound is the shock wave.

The experimental results demonstrates that the specific energy required for yeast disruption using shock wave treatment is far below the specific energy required for shear stress, while the specific energy required for ultrasound treatment was at an intermediate level. In the case of a yeast log reduction of 0.25, it was found that the required ultrasound specific energy was around 70 times greater than the specific energy in the case of shock treatment. In the case of log reduction 4, it was found that the required ultrasound specific energy was around 318 times smaller than the specific energy in the case of shear stress. These data suggested that yeast disruption using ultrasound is due to shock waves rather than shear stress.

The detailed study reported in this thesis provides useful technical information on the real cause of microorganism disruption from ultrasound treatment. Further investigations are recommended in the following areas.

1. The mathematical methods used in ultrasound and shear analysis in chapter 3 and 5 assumed that yeast mechanical properties remain unchanged during treatment. It is recommended to further this study when mechanical properties change during the treatment.
2. The FE simulation using ABAQUS was found to be a very good tool in this research area, so it is suggested that further investigation of non-linear analyses and parametric study using non-dimensional variables should be performed especially in the area of shock treatment.
3. It is also recommended to further investigate the issues in turbulence flow in the annulus of the shear stress apparatus where shear stress and eddies are involved. A further investigation is needed to investigate the localize loading of cell wall due to turbulence in the annulus of the shear apparatus through a static analytical approach in the first instance as some sort of baseline for any future numerical treatment is important.
4. The shock treatment system should be improved so that microorganisms can be subjected to higher pressures (greater than 100 MPa), but for more frequent times.
5. This study used a spherical microorganism, and it is also important to examine the non-spherical types. This study should thus be repeated for other microorganisms shapes such as *E. coli* and other cells such as animal cells.

References

Ahmed, F.I.K. & Russell, C. 1975. Synergism between ultrasonic waves and hydrogen peroxide in the killing of Micro-organism, *Journal of Applied Microbiology*, vol. 39, pp. 31-40.

Akbari Mousavi, S.A.A., Feizi, H., & Madoliat, R. 2007. Investigations on the effects of ultrasonic vibrations in the extrusion process. *J. Materials Proc. Tech.*, vol. 187-188, pp. 657-661.

Alexander, E.S., Zhang, Z., Thomas, C.R., Moxham, K.E. & Middelberg, A.P.J. 2000. The Mechanical properties of *Saccharomyces Cerevisiae*. *Advances in Bioprocess Engineering II*, vol. 97, pp. 9871-9874.

Alliger, H. 1978. New methods in ultrasonic processing, *American Laboratory*, vol. 10, pp. 81- 87.

Alvarez, U.M., Loske, A.M., Castano-Tostado, E. & Prieto, F.E. 2004. Inactivation of Escherichia coli O 157:H7, Salmonella typhimurium and Listeria monocytogenes by underwater shock waves, *Innovative Food Science and Emerging Technologies*, vol. 5, pp. 459-463.

Anderson, A.D., Daubert, C.R., Farkas, B.E. 1999. Rheological characterization of skim milk stabilized with carrageenan at high temperatures, *Proceedings of the 1999 Annual Meeting of the Institute of Food Technologists*, pp. 43.

Armstrong, G.N., Watson, I.A. & Stewart-Tull, D.E. 2006. Inactivation of B. cereus spores on agar, stainless steel or in water with a combination of Nd:YAG laser and UV irradiation. *Innovative Food Science & Emerging Technologies*, 7, 94-99.

Arreola, A.G., Balaban, M.O., Wei, C.I., Peplow, A., Marshall, M., Cornell, J. 1991. Effect of supercritical carbon dioxide on microbial populations in a singles strength orange juice, *J. of Food Quality*, vol. 14, pp 275-284.

Ayazi Shamlou, P., MakTagiansar, H.Y., Ison, A.P., Lilly, M.D. & Thomas, C.R. 1994. Turbulent breakage of filamentous microorganisms in submerged culture in mechanically stirred bioreactors, *Chemical Engineering Science*, vol. 49, pp. 2621-2631.

Balaban, M.O., Arreola, A., Marshall, M., Peplow, A., Wei, C. & Cornell, J. 1991, Inactivation of Pectinesterase in orange juice by Supercritical carbon dioxide, *Journal of Food Science*, vol. 56, pp. 743-749.

Balachandran, S., Kentish, S.E., Mawson, R. & Ashokkumar, M. 2006. Ultrasonic enhancement of the supercritical extraction from ginger, *Ultrasonics Sonochemistry*, 13, 471-479.

Bao X., Lu C. & Frangos J.A. 1999. Temporal gradient in shear but not steady shear stress induces PDGF-A and MCP-1 expression in endothelial cells: role of NO, NF kappa B, and egr-1, *Arterioscler Thromb Vasc Biol*., vol. 19, pp 996-1003.

Beer, F.P., Johnston E.A. & Dewolf J.T. 2005. Mechanics of Materials, 4th edn. McGraw Hill, New York.

Benz, R. & Zimmermann U. 1980. Pulse-length dependence of the electrical breakdown in lipid bilayer membranes, *Biochimica and Biophysica Acta (BBA) - Biomembranes*, vol. 597, pp. 637-42.

Born, C., Zhang, Z., Al Rubaei, M. & Thomas, C.R. 1992. Estimation of disruption of animal cell by laminar shear stress, *Biotechnology Bioengineering*, vol. 40, pp. 1004-1010.

Bradshaw, P. 1971. An Introduction to turbulence and its measurement, Pergamon Press, Oxford, UK, The Commonwealth and International Library of Science and Technology Engineering and Liberal Studies.

Buttsworth, D.R. & Jones, T.V. 1997. Radial conduction effects in transient heat transfer experiments, *Aeronautical Journal*, vol. 101, pp. 209-212.

Cadwell, M.L. & Fogler, H.S. 1971. Ultrasonic gas absorption and acoustic streaming observations, *Chemical Engineering Progress Symposium Series*, vol. 67, pp. 124-127.

Cameron, M., McMaster, L.D. & Britz, T.J. 2008. Electron microscopic analysis of dairy microbes inactivated by ultrasound, *Ultrasonics Sonochemistry*, vol. 15, pp. 960.

Carslaw, H.S. & Jaeger, J.C. 1959. Conduction of heat in solids, 2nd edn, Oxford University Press.

Castro, A.S., Barbosa-Canovas, G.V. & Swanson, B.G. 1993. Microbial inactivation of foods by pulsed electric fields. *J. Food Processing Preservation*, vol. 17, pp.47-73.

Chambers, L.A. & Gaines, N. 1932. Some effects of intense audible sound on living organisms and cells, *Journal of Cellular and Comparative Physiology*, vol. 1, pp. 451-73.

Charras, G. T. & Horton,M. A. 2002. Determination of cellular Strains by combined atomic force microscopy and finite element modeling, *Biophys J.*, vol. 83, pp. 858-879.

Chen, X. 2000. Biofilm removal caused by chemical treatments, *Water Res*., vol. 34, pp. 4229-4233.

Chen, K.C., Nagy, A.C., Bela Gyorffy, John Val, Bela Novak, and John J. Tyson. 1999, Kinetic analysis of a molecular model of the budding Yeast cell cycle. J. of *Molecular Biology of the Cell,* vol. 11 pp. 369-391.

Cheng, L.Y. 1987. Deformation analysis in cell and development biology Part II. *Engineering*, vol. 109, pp. 18-24

Cherry, R.S. & Papoutsakis, E.T. 1986. Hydrodynamic effects on cells in agitated tissue culture reactors, *Bioprocess and Biosystems Engineering*, vol. 1, pp. 29-41.

Ciccolini L., Taillandier, P. Wilhem, A.M., Delmas, H. & Strehaiano, P. 1997. Low frequency thermo-ultrasonication of *Saccharomyces Cerevisiae* suspensions: effect of temperature and of ultrasonic power, *Chemical Engineering Journal*, vol. 65, pp. 145-149.

Cosgrove, D.J. 2000. Expansive growth of plant cell walls, *Plant Physiology and Biochemistry*, vol. 38, pp. 109-124.

Datta N. & Deeth H.C. 2004. Heat treatment, alternatives to other nonthermal technologies, *Encyclopedia of Dairy Sciences*, pp. 1339-1346.

Davies, K.J.A. 1987. Protein damage and degradation by oxygen radicals: I. General aspects, *J. Biology Chemical*, vol. 262, pp. 895-901.

Debs-Louka, E., Louka, N., Abraham, G., Chabot, V. & Allaf, K. 1999. Effect of compressed carbon dioxide on Microbial cell viability, *Applied Environmental Microbiology, vol. 65, pp. 626-31.*

DeMarini D. J., Adams A.E.M., Fares H., De Virgilio C., Valle G., Chuang J. S., Pringle J. R. 1997. A septin-based hierarchy of proteins required for localized deposition of chitin in the Saccharomyces cerevisiae cell wall. J. Cell Biol. vol. 139 pp 75.

Devlieghere, F., Vermeulen, A. & Debevere, J. 2004. Chitosan: antimicrobial activity, interactions with food components and applicability as a coating on fruit and vegetables, *Food Microbiology*, vol. 21, pp. 703-714.

Donsì, F., Ferrari, G. & Maresca, P. 2009. High-Pressure homogenization for food sanitization, *Global Issues in Food Science and Technology*, published by Elsevier pp 309-352.

Doulah, M.S. 1977. Mechanism of disintegration of biological cell in ultrasonic cavitation, *Biotechnology and Bioengineering*, vol. 19, pp 649-660.

Doulah, M.S. & Hammond, T.H. 1975. A hydrodynamic mechanism for the disintegration of *Saccharomyces cerevesiae* in an industrial homogenizer, *Biotechnology and Bioengineering*, vol. 17, pp. 845-58.

Dunn, J.E., LaCosta, R., Pearlman, J.S. & Diego, S. 1987. Methods and apparatus for extending the shelf life of fluid food products, U.S.A Patent, 22 September, vol. 4, pp. 472.

Earnshaw, R.G., Appleyard, J. & Hurst, R.M. 1995. Understanding physical inactivation processes: combined preservation opportunities using heat, ultrasound and pressure, *International Journal of Food Microbiology*, vol. 28, pp. 197-219.

Engler, C.R. 1985. Disruption of microbial cells, *In:* Moo-Young, M. & Coony, C. L. (eds.) *Comperhensive Biotechnology*, Oxford: Pergamon.

Enomoto, A., Nakamura, K., Nagai, K., Hashimoto, T., & Hakoda, M. 1997. Inactivation of food microorganisms by high-pressure carbon dioxide treatment with or without explosive decompression. *Biosci. Biotech. Biochem*, vol. 61, pp. 1133-1137.

Estrada-Girón, Y., Swanson, B.G. & Barbosa-Cánovas, G.V. 2005. Advances in the use of high hydrostatic pressure for processing cereal grains and legumes, *Trends in Food Science & Technology*, vol. 16, pp. 194-203.

Ewis, H.E. & Lu, C.D. 2005. Osmotic shock: A mechanosensitive channel blocker can prevent release of cytoplasmic but not periplasmic proteins. FEMS Microbiology Letters, 253, 295-301.

Feng, W.W. & Yang, W.H. 1973. On the Contact Problem of an Inflated Spherical Nonlinear Membrane. *Journal of Applied Mechanics*, vol. 40, pp. 209-214.

Fleet, G. H. (1991). Cell walls. In Rose A. H. andHarrison, J. S. (Eds). The Yeasts, vol. 4, 2nd edn,Yeast organelles. Academic Press, London, pp. 199– 277.

Flores, H. & Galston A. 1982. Polyamines and Plant Stress: Activation of Putrescine Biosynthesis by Osmotic Shock. *J of Science*. vol. 217, pp 1259-1261.

Fogler, H.S., 1999. Elements of chemical reaction engineering, 3rd edn, Prentice Hall, New York.

Fry, S.C. 1995. Polysaccharide modifying enzymes in the plant cell wall. *Annual Review of Plant Physiology and Plant Molecular Biology*, vol. 46 pp, 497-520.

Garcia, M.L., Burgos, J., Sanz, B. & Ordonez, J.A. 1989. Effect of heat and ultrasonic waves on the survival of two strains of *Bacillus subtilis, J. Appl. Bacteriol*, vol. 67, pp. 619-628.

Garcia-Gonzalez, L., Geeraerd, A. H., Elst, K., Van Ginneken, L., Van Impe, J. F. & Devlieghere, F. 2009. Inactivation of naturally occurring microorganisms in liquid whole egg using high pressure carbon dioxide processing as an alternative to heat pasteurization. *The Journal of Supercritical Fluids*, 51, 74-82.

Geciova, J., Bury, D. & Jelen, P. 2002. Methods for disruption of microbial cells for potential use in the dairy industry-a review, *International Dairy Journal*, vol. 12, pp. 541-53.

Gogate, P. R. & Kabadi, A. M. 2009. A review of applications of cavitation in biochemical engineering/biotechnology. Biochemical Engineering Journal, 44, 60-72.

Gondrexon, N., Renaudin, V., Petrier, C., Clement, M., Boldo, P., Gonthier, Y. & Bernis, A. 1998. Experimental study of the hydrodynamic behaviour of a high frequency ultrasonic reactor, *Ultrasonic Sonochemistry*, vol. 5, pp. 1-6.Guillaume, P Masmoudi M. and Zeglaoui A 2002. From compressible to incompressible materials via an asymptotic expansion *Numerische Mathematik* vol. 91 pp. 649.

Guyot, S., Ferret, E., Boehm, J.B. & Gervais, P. 2006. Yeast cell inactivation related to local heating induced by low-intensity electric fields with long-duration pulses, *International journal of food microbiology*, vol. 113, pp. 180-188.

Hartmann, C. & Delgado A. 2004. Numerical simulation of the mechanics of a yeast cell under high hydrostatic pressure, *Journal of Biomechanics*, vol. 37, pp. 977-987.

Hartmann, C., Delgado A. & Mathmann, K. 2006. Mechanical stresses in cellular structures under high hydrostatic pressure, *Innovative Food Science & Emerging Technologies*, vol. 7, pp. 1-12.

Hinze, J.O. 1994. Fundamentals of the hydrodynamic mechanism of splitting in dispersion processes, *A.I.Ch.E. Journal*, vol. 1, pp. 289-95.

Holger, S. 2003. A device for facilitating the use of the French press, *Analytical Biochemistry*, vol.321, pp. 276-277.

Hong, S.I. & Pyun, Y.R. 1999. Inactivation kinetics of lactobacillus plantarum by high pressure carbon dioxide, *Journal of Food Science*, vol. 64, pp. 728-33.

Hosokawa, T. & Teshima, K. 1997. Cytotoxic effect of high pressure pulses generated by a diaphragm-less shock tube on normal and transformed mammalian cells. Proceeding of the 21st international symposium on shack wave, July 20-285 Australia.

Hughes, D.E. & Nyborg, W.L. 1962. Cell disruption by ultrasound. Science, 138, 108-114.

Jaschke, P., Drake, I. & Beatty, J. 2009. Modification of a French pressure cell to improve microbial cell disruption. Photosynthesis Research, 102, 95-97.

Jacobs, S.E. & Thornley, M.J. 1954. The lethal action of ultrasound waves on bacteria suspended in milk and other liquids, *Journal Applied Bacteriology*, vol. 17, pp. 38-55.

Kargarnovin, M.H., Darijani, H. & Naghdabadi, R. 2007. Evaluation of the optimum pre-stressing pressure and wall thickness determination of thick-walledspherical vessels under internal pressure, Journal of Franklin Institute, vol. 344, pp. 439-451.

Kleinig, A.R. & Middelberg P.J. 1998. On the mechanism of microorganisms cell disruption in high pressure homogenisation, Chemical engineering science, vol. 53, pp. 891-898.

Kleinig, A. R. 1997. Cell disruption mechanics, Thesis in the Faculty of Engineering in the University of Adelaide.

Kerfoot, W.W., Beshai, A.Z. & Carson C. 1992, the effect of isolated high-energy shock wave treatments on subsequent bacterial growth, Urological Research, vol. 20, pp 193-186.

Kinsloe, H., Ackerman, E., & Reid, J.J. 1954. Exposure of microorganisms to measured sound fields, J. Bacteriology, 68, 373-380.

Koda, S., Miyamoto, M., Toma, M., Matsuoka, T. & Maebayashi, M. 2009. Inactivation of Escherichia coli and Streptococcus mutans by ultrasound at 500 kHz,
Ultrasonics Sonochemistry, Vol 16, pp. 655-659.

Lado, B.H. & Yousef, A.E. 2002. Alternative food-preservation technologies: efficacy and mechanisms. Microbes and Infection, 4, 433-440.

Larander, T.J. & Pujara, P. 1980. Compression of spherical cell. Mechanics Today, vol.5, pp 161-176.

Lee, S., Mcauliffe, D. J., Kodama, T. & Doukas, A. G. 2000. In vivo transdermal delivery using a shock tube. *Shock wave*, vol. 10 pp. 307-311.

Lerouge, S., Wertheimer M.R., Marchand R., Tabrizian, M. & Yahia, L'H 2000. Effect of gas composition on spore mortality and etching during low pressure plasma sterilization, *J Biomed Mat Res*, vol. 51, pp.128–3.

Levenspiel, O. 1999. Chemical Reaction Engineering, 3rd edn, John Wiley and Sons, New York.

Leverett, L.B., Hellums, J.D., Alfrey, C.P. & Lynch, E.C. 1972. Red blood cell damage by shear stress, *Biophysical Journal*, vol. 12, pp. 257-73.

Levin, R.L., Ushiyama, M. & Cravalho, E.G. 1979. Water permeability of yeast cells at sub-zero temperatures. *Journal of Membrane Biology*, vol. 46, pp. 91-124.

Lighthill, J. 1978. Acoustic streaming, *Journal of Sound and Vibration*, vol. 61, pp. 391-418.

Lillard, H.S. 1993. Bactericidal effect of chlorine on attached salmonellae with and without sonication. *Journal of Food Protection*, vol. 56, pp. 716–717.

Lin, H.M., Cao, N.J. & Chen, L.F. 1994. Antimicrobial effect of pressurized carbon-dioxide on listeria-monocytogenes. *J Food Sci*, vol. 59, pp. 657–659.

Loske, A.M., Prieto, F.E., Zavala, M.L., Santana, A.D. & Armenta, E. 1998. Repeated application of shock waves as a possible method for food preservation, *Shock Waves*, vol. 9, pp. 49-55.

Ludwig, H. & Schreck, C. 1997. The inactivation of vegetative bacteria by pressure. *In:* Heremans, K. (ed.) *High pressure research in bioscience and biotechnology* Leuven: Leuven University Press.

Maniotis, A.J., Chen, C.S. & Ingber, D.E. 1997. Demonstration of mechanical connections between integrins, cytoskeletal filaments, and nucleoplasm that stabilize nuclear structure, Proc. *Natl. Acad. Sci. U.S.A.*, vol. 94 , pp. 849-854.

Mason, T.J., Lorimer, J.P., Bates, D.M. & Zhao, Y. 1994. Dosimetry in sonochemistry: the use of aqueous terephthalate ion as a fluorescence monitor *Ultrasonic Sonochemistry*, vol. 1, pp 91-95.

Mason, T.J. & Paniwnyk, L. 1996. The uses of ultrasound in food processing, *J Trends Food Sci. Tech*, vol. 6 pp. 293-295.

Mayerhoff, Z.D.V.L., Franco, T.T. & Roberto, I.C. 2008. A study of cell disruption of Candida mogii by glass bead mill for the recovery of xylose reductase, *Separation and Purification Technology*, 63, 706-709.

McQueen, A., Meilhoc, E. & Bailey, J.E. 1987. Flow effects on the viability and lysis of suspended mammalian cells, *Biotechnology Letters*, vol. 9, pp. 831-837.

Melih, T. & Murray, M. 1998. Disruption of *Alcaligenes latus* for recovery of poly (β-hydroxybutyric acid): comparison of high-pressure homogenization, bead milling, and chemically induced lysis, *Ind. Eng. Chem. Res.*, vol. 37, pp. 1807-1814.

Mendelson, N.H., Sarlls, J.E., Wolgemuth, C.W, Goldstein, R.E. 2000. Chiral self propulsion of growing bacteria macrofibers on a solid surface. *Phys Rev Lett*, vol. 84, pp. 1627-1630

Mfoumou, E., Kao-Walter, S. & Hedberg, C. 2006. Remote acoustic monitoring of thin laminates, The 2nd World Congress on Engineering Asset Management (EAM) and The 4th International Conference on Condition Monitoring, Sweden.

Middelberg, A.P.J. 1992. A new model for the disruption of *Escherichia coli* by high pressure homogeneous, model developed and verification, *Institute of chemical engineers*, vol. 70C, pp 205-212.

Miles, C.A., Shore, D., Langley, K.R. 1990. Attenuation of ultrasound in milks and creams, *Ultrasonics*, vol. 28, pp. 394-400.

Missen, R.W., Mims, C.A. & Saville, B. A. 1999. Introduction to chemical reaction engineering and kinetics, New York, John Wiley and Sons.

Monnier, H., Wilhelm, A.M. & Delmas, H. 2000. Effects of ultrasound on micromixing in flow cell, *Chemical Engineering Science*, vol. 55, pp. 4009-4020.

Moore, E.K., Hoare, M. & Dunnill, P. 1990. Disruption of baker's yeast in a high-pressure homogenizer: New evidence on mechanism, *Enzyme and Microbial Technology*, vol. 12, pp. 764-70.

Moreau, M., Orange, N. & Feuilloley, M.G.J. 2008. Non-thermal plasma technologies: new tools for bio-decontamination, *Biotechnology Advances*, Vol. 26, 6, pp. 610-617.

Morgan, T.R., Laudon, V.P., Heston, W.D.W., Zeitz, L. & Fair, W.R. 1988. Free radical production by high energy shock wave; methodologic consideration. *J of UROL*, vol. 141, pp. 965.

Mosqueda-Melgar, J., Raybaudi-Massilia, R.M. & Martín-Belloso, O. 2008. Combination of high intensity pulsed electric fields with natural antimicrobials to inactivate pathogenic microorganisms and extend the shelf-life of melon and water melon juices, *Food Microbiology*, vol. 25, pp. 479-491.

Mulder, H., & Walstra, P. (1974). *The milk fat globule globule: Emulsion science as applied to milk products and comparable foods*. Farnham Royal, England: Commonwealth Agricultural Bureaux.

Nakamura, K., Enomoto, A., Fukushima, H., Nagai, K. & Hakoda, M. 1994. Disruption of microbial cells by flash discharge of high-pressurecarbon dioxide, *Biosci Biotechnol Biochem*, vol. 58, pp. 1297-1301.

Nilsson, K., Scheirer, W., Merten, O.W., Östberg, L., Liehl, E., Katinger, H.W.D. & Mosbach, K. 1983. Entrapment of animal cells for production of monoclonal antibodies and other biomolecules, *Nature*, Vol. 302, pp. 629-630.

Ordenez, J.A., Aguilera, M.A., Garcia, M.L. & Sanz, B. 1987. Effect of combined ultrasonic and heat treatment (thermoultrasonication) on the survival of a strain of staphylococcus aureus. *Journal of Dairy Research*, vol. 54, pp. 61-67.

Ordonez, J.A., Sanz, B., Hermandez, P.E. & Lopez-Lorenzo, P. 1984. A note on the effect of combined ultrasonic and heat treatments on the survival of thermoduric Streptococci, *J. Appl. Bacteriology*, vol. 56, pp. 175-177.

Oshima, Y., Sakamoto, T., Sonoda, K-h., Yoshida, H., Ishibashi, T., Inomata, H. 1997. Effect of electric pulses and antiproliferative drugs on cultured bovine retinal pigment epithelial cells, *Current Eye research*, vol 16, pp. 64-70.

Papoutsakis, E.T. 1991. Fluid-mechanical damage of animal cells in bioreactors, *Trends in Biotechnology*, vol. 9, pp. 427-37.

Pereda, J., Ferragut, V., Quevedo, J.M., Guamis, B. & Trujillo, A.J. 2009. Heat damage evaluation in ultra-high pressure homogenized milk. *Food Hydrocolloids*, 23, 1974-1979.

Perrier-Cornet, J.M., Maréchal, P.A. & Gervais, P. 1995. A new design intended to relate high pressure treatment to yeast cell mass transfer, *Journal of Biotechnology*, vol. 41, pp. 49-58.

Piyasena, P., Mohareb, E. & McKellar, R.C. 2003. Inactivation of microbes using ultrasound: a review, *International journal of food microbiology*, vol. 87, pp. 207-216.

Prakash, S., Huppertz, T., Karvchuk, O. & Deeth, H. 2010. Ultra-high-temperature processing of chocolate flavoured milk. Journal of Food Engineering, 96, 179-184.

Pugin, B. 1987. Qualitative characterization of ultrasound reactors for heterogeneous sonochemistry, *Ultrasonics*, vol. 25, pp. 49-55.

Rachik, M., Barthès-Biesel, D., Carin, M. & Edwards-Levy, F. 2006. Identification of a bioartificial microcapsule wall material parameter with an inverse method and the compression test, *Journal of Colloid and Interface Science*, vol. 301, pp. 217-226.

Radmacher, M. 2002. Measuring the elastic properties of living cells by AFM. *Methods Cell Biol*. 68, 67–84.

Raso J., Condon S. & Sala Trepat F.J. 1994. Mano-thermosonication: a new method of food preservation in Food preservation by combined process, Final report for FLAIR Concerted Action No. 7, Subgroup B.

Roos, D., Van Bruggen, R. & Meischl, C. 2003. Oxidative killing of microbes by neutrophils. *Microbes and Infection*, 5, 1307-1315.

Sahoo, P. K., Ansari, M. I. A. & Datta, A. K. 2002. Computer-aided design and performance evaluation of an indirect type helical tube ultra-high temperature (UHT) milk sterilizer. *Journal of Food Engineering*, 51, 13-19.

Sala, F.J., Burgos J., Condon S., Lopez P. & Raso J. 1995. Effect of Ultrasonic wave on the heat resistance of Bacillus Stearothermophilus spore, *In*: fundamental and applied aspect of bacterial spores, Editors Dring, G.J., Ellars, D.J. & Gould,G.W. , Academic Press, New York, pp. 251-259.

Sale, A.J.H. & Hamilton, W.A. 1967. Effects of high electric fields on microorganisms: I. Killing of bacteria and yeasts, *Biochimica at Biophysica Acta (BBA) - General Subjects*, vol. 148, pp. 781-8.

Sanz, B., Paklacios, P., Leopes, P. 1985. Effect of ultrasound wave on the heat resistants of Bacillus Stearothermophilus spore, *Fed Eur Microbios Soc*. 1985, vol. 18, pp. 251-259.

Scherba, G., Weigel, R.M. & O'Brien, J.R. 1991. Quantitative assessment of the germicidal efficiency of ultrasonic energy, *Applied Environment Microbial*, vol. 57, pp. 2079-2084.

Schlegel, H.G. 1992 Allgemeine Mikrobiologie. 7th ed., Stuttgart, New York: Georg Thieme Verlag.

Schoenbach, K. H., Peterkin, F. E., Alden, R. W., Iii & Beebe, S. J. 1997. The effect of pulsed electric fields on biological cells: experiments and applications. *Plasma Science, IEEE Transactions on*, 25, 284-292.

Schultz, D.L. & Jones T.V. 1973. Heat transfer measurements in short-duration hypersonic facilities, Advisory Group for Aerospace Research and Development, AGARD-AG-165.

Shepherd T. P. 2004. Shock wave disruption of Bacteria, Thesis of final year project, University of Southern Queensland.

Smith, A.E., Zhang, Z. & Thomas, C.R. 2000(a). Wall material properties of yeast cells, part 1 .Cell measurements and compression experiments, *Chemical Engineering Science*, vol. 55, 11, pp. 2043-2053.

Smith, A.E., Moxham, K.E. & Middelberg, A.P.J. 2000(b). Wall material properties of yeast cells. Part II. Analysis. Chemical Engineering Science, 55, 2043-2053.

Smith, A.E., Zhang, Z., Thomas, C.R., Moxham, K.E. & Middelberg, A.P.J. 2000(c). The mechanical properties of *Saccharomyces cerevisiae*. Proceedings of the *National Academy of Sciences*, vol. 97, pp. 9871-9874.

Speering R. 2004. Effect of shear flow on yeast cell and its application to the dairy industry, Thesis of final year project, University of Southern Queensland.

Spilimbergo, S., Elvassore, N. & Bertucco, A. 2002. Microbial inactivation by high-pressure, *The Journal of Supercritical Fluids*, vol. 22, pp. 55-63.

Stenson, J.D., Thomas, C.R. & Hartley, P. 2009. Modelling the mechanical properties of yeast cells. *Chemical Engineering Science*, vol. 64, pp. 1892-1903.

Stenson, J.D., & Hartley, P. 2011. Determining the mechanical properties of yeast cell walls, Biotechnology progress. Vol, pp. 2-23.

Svaldo T., Cacalleri O., Sike K., Rolandi R. & Gliozzi A. 2006. Mechanical properties of a single living cells encapsulated in polyelectrolyte matrixes. J. of Biotechnology, vol. 124, pp 723-731.

Tamagawa, M. & Akamastsu 1997, Mechanism of damage two living cells by plan shock waves in water (mathematical model of two cells), Proceeding of the 21st international Symposium on Shock Wave, July 20 Great Keppel Island Australia.

Tan, T.C. & Lim, E.W.C. 2004. Thermally killed cells of complex microbial culture of biosensor measurement of BOD of wastewater, *Sensors and Actuators B Chemical*, vol. 107, pp.546-551.

Tan, T.C. & Qain, Z. 1999. BOD measurement in the presence of heavy metal ion using a thermally-killed-bacillus subtilise, *Biosensor Water Res*., vol. 33, pp.2923-2928.

Thiebaud, M., Dumay, E., Picart, L., Guiraud, J.P. & Cheftel, J.C. 2003. High-pressure homogenisation of raw bovine milk. Effects on fat globule size distribution and microbial inactivation. *International Dairy Journal*, 13, 427-439.

Thomas, C.R., Al-Rubeai, M. & Zhang, Z. 1994. Prediction of mechanical damage to animal cells in turbulence', *Cytotechnology*, vol. 15, pp. 329-35.

Thomas C.R., Zhang, Z. & Cowen, C. 2000. Micromanipulation measurement of biological materials. *Journal of Biotechnology Letter*, vol. 22, pp. 531-537.

Timoshenko, S.P. & Goodier, J.N. 1982. Theory of elasticity, 3rd edn., McGra-Hill, Auckland.

Touhami, A., Nysten B., & Dufrene Y. F. 2003. Nano-scale mapping of the elasticity of microorganisms cell by atomic force microscopy, *American chemical society, Langmuir*, vol 19, pp. 4539-4543.

Turns R S. 2000. An introduction to combustion (Concept and Application), second edition. ISBN 0771260722, by *McGraw Hill*.

Vanderheiden, G.J., Fairchild, A.C. & Jago, G.R. 1970. Construction of a laboratory press for use with the French pressure cell, *Applied Microbiology*, vol. 19, pp. 875–7.

Vega-Mercado, H., Martin-Belloso, O., Chang, F.J., Barbosa-Cánovas, G. V. & Swanson, B. G. 1996. Inactivation of Escherichia coli and Bacillus subtilis suspended in pea soup using pulsed electric fields, *J Food Process Preserv*. vol. 20, pp. 501-510

Vercet, A., Lopez, P. & Burgos, J. 1997. Inactivation of heat-resistant lipase and protease from pseudomonas fluorescens by manothermosonication, *Journal of Dairy Science*, vol. 80, pp. 29-36.

Vichare, N.P., Gogate, P.R., Dindore, V.Y. & Pandit, A.B. 2001, Mixing time analysis of a sonochemical reactor, *Ultrasonics Sonochemistry*, vol. 58 pp. 23-33.

Walstra, P. 1969. Preliminary note on the mechanism of homogenisation, *Neth. Milk, Dairy Journal*, vol. 23, pp.290-292.

Wang, C.X, Wang, L. & Thomas, C.R. 2004. Modelling the mechanical properties of single suspension-cultured tomato cells, *Annals of Binary*, vol. 93, pp. 443-453.

Ward, G.D., Watson, I.A., Stewart-Tull, D.E.S, Wardlaw, A.C., Wang, R.K. & Nutley, M.A. 2000. Bactericidal action of high-power Nd: YAG laser light on Escherichia coli in saline suspension, *Journal of Applied Microbiology*, vol. 89, pp. 517- 525.

West, J., Becker, M., Tombrink, S. & Manz, A. 2008. Micro Total Analysis Systems: Latest Achievements. Analytical Chemistry, 80, 4403-4419.

Willett J L 2003. Mechanical properties of LDPE/granular starch composite. *Applied Polymer Science* vol. 54 pp. 1685-1695.

Wrigley, D.M. & Liorca, N.G. 1992. Decrease in Salmonella typhimurium in skim milk and egg by heat and ultrasonic wave treatment. *Journal of Food Protection*, vol. 55, pp. 678-680.

Yao, X., Jericho, M., Pink, D. & Beveridge, T. 1999, Thickness and elasticity of gram-negative murein sacculi measured by atomic force microscopy. *J Bacteriol* vol. 181, pp. 6865-6875.

Yu, L.J., Ngadi, M. & Raghavan, G.S.V. 2009. Effect of temperature and pulsed electric field treatment on rennet coagulation properties of milk, *Journal of Food Engineering*, vol. 95 pp. 115-118.

Yusaf, T. & Buttsworth, D.R. 2007. Characterisation of mixing rate due to high power ultrasound, *Ultrasound and Sonochemistry*, vol. 14, 266-274.

Yusaf, T. & Buttsworth, D.R. 2001. Heat transfer measurement in an Ultrasonic flow cell, *Proceeding of the Symposium of the 12th IAHR Cooling Tower and Heat Exchanger* Sydney. November.

Zang, J. 2007. Supercritical carbon dioxide and hydrogen peroxide caused mild change in spore structure associated with high killing rate of Bacillus anthracis', *Journal of Microbiological methods*, vol. 70, pp. 442-451.

Zhang, B., Liu, X. & Gan, Y. 2004. Viability and activity of microorganisms in pressurized and supercritical carbon dioxide. In: Sang-Eon Park, J.-S. C. & Kyu-Wan, L. (eds.) Studies in Surface Science and Catalysis. Elsevier.

Zhang, Z., Alrubeai, M. & Thomas, C.R. 1993. Estimation of Disruption of Animal-Cells by Turbulent Capillary-Flow, *Biotechnology and Bioengineering*, vol. 42, pp. 987-93.

Zhang, Z., Ferenczi, M.A. & Thomas, C.R. 1992, A micromanipulation technique with a theoretical cell model for determining mechanical properties of single mammalian cells, *Chemical Engineering Science*, vol. 47, pp. 1347-54.

Zimmermann, U. 1986. Electrical breakdown, electropermeabilization and electrofusion. *Rev Physiol Biochem Pharmacol*. 105:175-256.

Appendix A
Error Estimate in the FE Simulation

To estimate the error and the convergence order in FE simulation, a difference in calculated pressure between difference global element sizes was used. A 2D model with 4 different mesh sizes was selected to investigate the quality (accuracy) of the numerical solution. The global element size (GES) was selected in the range of 1, 2, 4, 6 and 8. The number of elements is inversely proportional to the GES. The pressure of a specific element was used for the purpose of this study. The difference in pressure was used to determine the convergence order of (p) and the estimated error. The solution scheme order of convergence, p, can be approximately determined using the following relationship

$$p = \left(\frac{f_1 - f_2}{f_2 - f_3}\right) / \ln(\tau), \qquad \text{A1}$$

where τ is the global element size which is 3 in this case and f(s) is the pressure obtained at a particular point (s) at the mesh for different GES values. Evaluating the estimated fractional error, E, using Richardson extrapolation for the first three f(s) gives a scheme order (P) of 3.5. The positive values indicate that the solution is converging. The estimated fractional error is given as

$$E_2 = \varepsilon / (r^p - 1), \quad \textit{where} \quad \varepsilon = (f_1 - f_2) / f_2. \qquad \text{A2}$$

The error estimate is an order approximation to the actual fractional error of the quantity f_2. The approximated errors in calculated the pressure for the first three highest GES were 0.6366%, 0.27% and 0.008%. The consistently decreasing error indicated that the converging in computational scheme is occurred. The error percentage for different GES is presented Fig. A1.

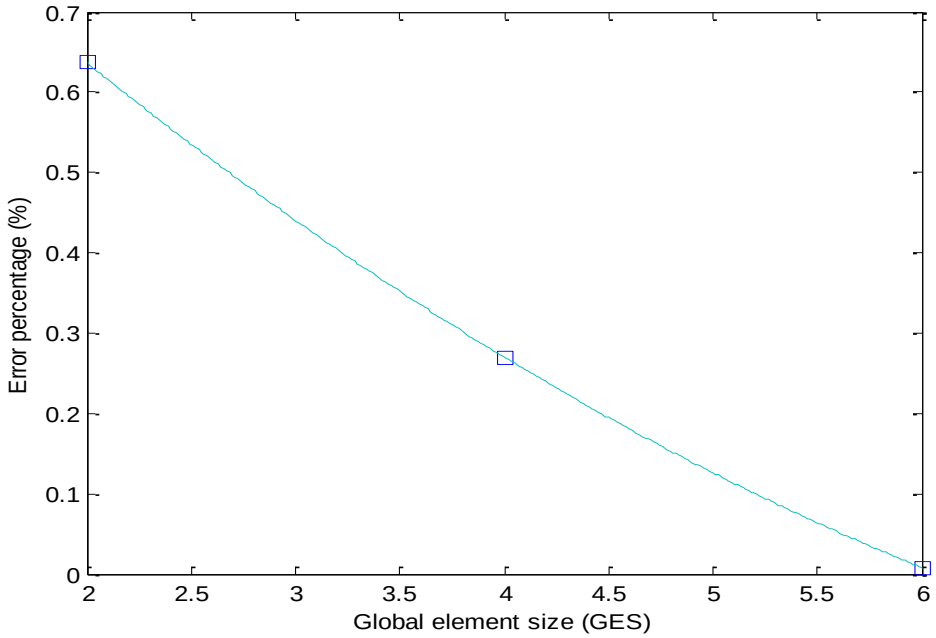

Fig. A1 The relationship between the error percentages against GES

Fig. A1 shows that using global size of 6 in the configuration will reduce the error dramatically. Therefore a global size of around 6 (or close to 6) was used in this simulation.

Appendix B

Pressure wave propagation within water

In the FE simulation presented in chapter 4, water material properties was used in part 1 (water), 2 (cell wall) and 3 (cytoplasm). The aim of this numerical technique is to confirm that the pressure wave will travel smoothly throughout the three parts.

If the model structure presented in Fig. B1 is used; the pressure wave will propagate through the water, strike the cell wall of the cell, and finally penetrate through the cytoplasm. Tabulated uniform pressure values were applied on the top surface of the tube with initial pressure of 1 MPa, Table B1.

Table B1 Sample of tabulated amplitude of external pressure applied to top surface of model with step time of simulation

Time (ms)	Amplitude
0	0
1e-7	1
0.7	1

The time required for a pressure wave to pass the smallest element in the geometry was calculated and compared with the dilatation time presented in the ABAQUS model. To avoid any numerical error related to time step, the dilatation time should always be always less than the time required for the wave to travel from the top of the smallest element to the bottom of the same smallest element in the geometry. To avoid this numerical problem, the size of element was adjusted so simulation time step will stay greater than the dilatation time. The dynamic step time of the model varies with the material properties such as density, modulus of elasticity and Poisson's ratios. Sample of pressure history of a node located in the water was calculated and presented in Fig B1. The pressure wave started from zero and in 1e-7 ms the pressure increased to reach its maximum of 100 MPa. The pressure will then hold for sufficient time so wave can propagate through the water and pass the microbe located at the middle of the water tube.

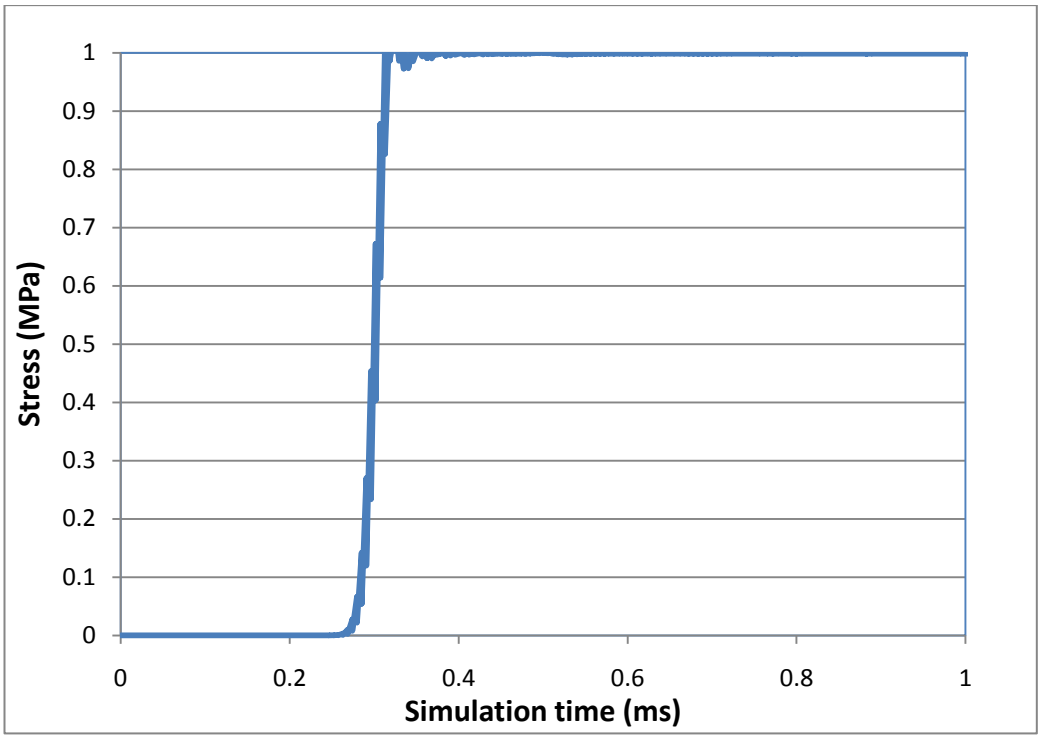

Fig. B Sample of pressure history of node located on the water.

Figure B1 show that the pressure propagation through the water is smooth. This result provide confident that if water is used the pressure is 1 MPa and so far it is fixed.

Appendix C

Dynamics model - accuracy and validation

the purpose of this appendix to provide detail information about the dynamic model for different mesh density. It also aims to run simple model and compare the results of the simulation with relevant analytical calculation. A rectangular geometry model consisting of one material (water) was constructed to evaluate the effect of the mesh density, course and fine, on the output simulated results. Three different geometries with different mesh densities were generated to confirm that the numerical error was insignificant, see Fig. C1. The first mesh consists of 29710 linear triangular CPS3 (as define by ABAQUS) elements. The boundary conditions were set as BC1, BC2 and BC3 as explained in subsection 4.6. The material properties of the cell wall, cytoplasm and water are presented in Table 4.1.

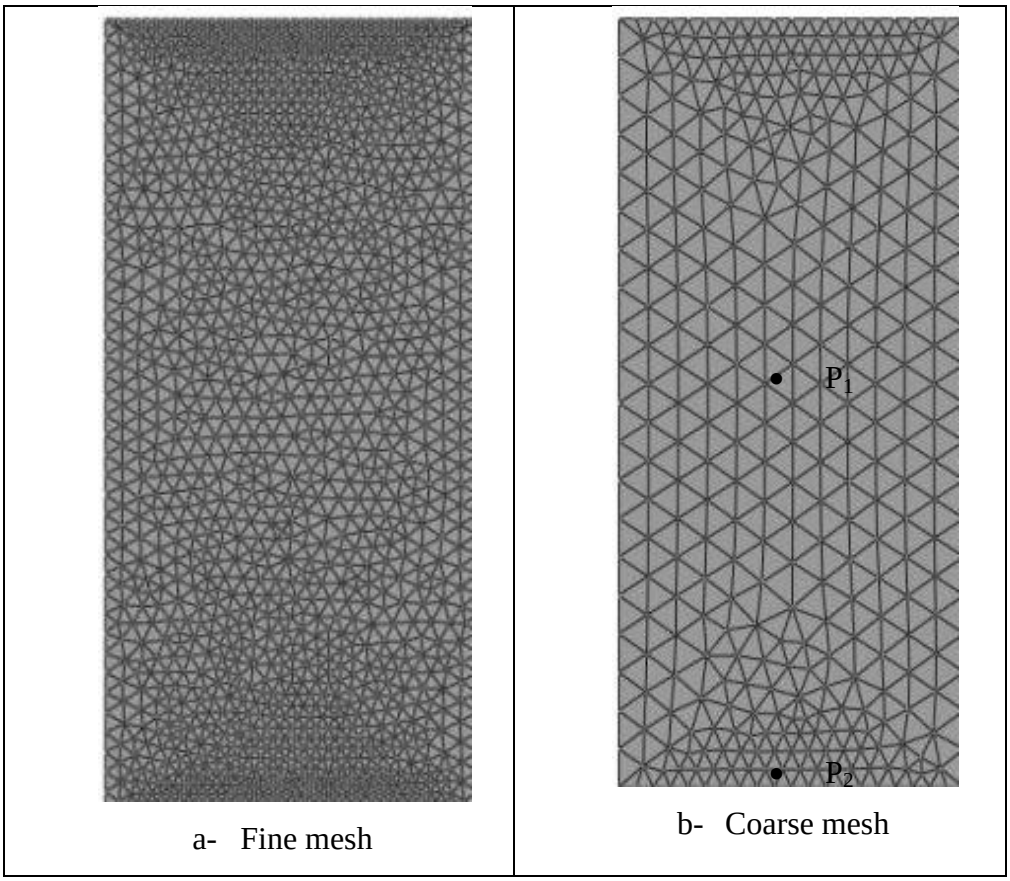

Fig C1 Fine and coarse mesh

Two points located at the middle (P1) and the centre (P2) of the rectangular in Fig. C1 was selected for this verification study. It is theoretically expected that the pressure value at point 1 is half of the pressure value at point 2 as shown in Fig. C1. However the first simulated result of the pressure did not perfectly agree with this expectation, this was due to the mesh density as it was relatively course. Thus mesh density had to be increased by increasing the number of mesh up to 3000000.

The pressure history was calculated and presented in Fig. C2 where 3000000 elements used. In this trial, the pressure history data curve shows that the pressure value at point 1 (Fig. C1 a) is fluctuating from 0, 1 MPa and 2 MPa due to the pressure wave propagation. While the pressure value at point 2 (2 MPa) was 2 MPa since point 2 located at the bottom of the water tube. This result was very expected as described in 4.2. Thus the number of elements was fixed to be 3000000 elements. A third trial was repeated by increasing the number of elements to 4000000 to make sure that increasing the number of mesh will have no influence on the results, the results shows no differences in comparison with 3000000 element mesh.

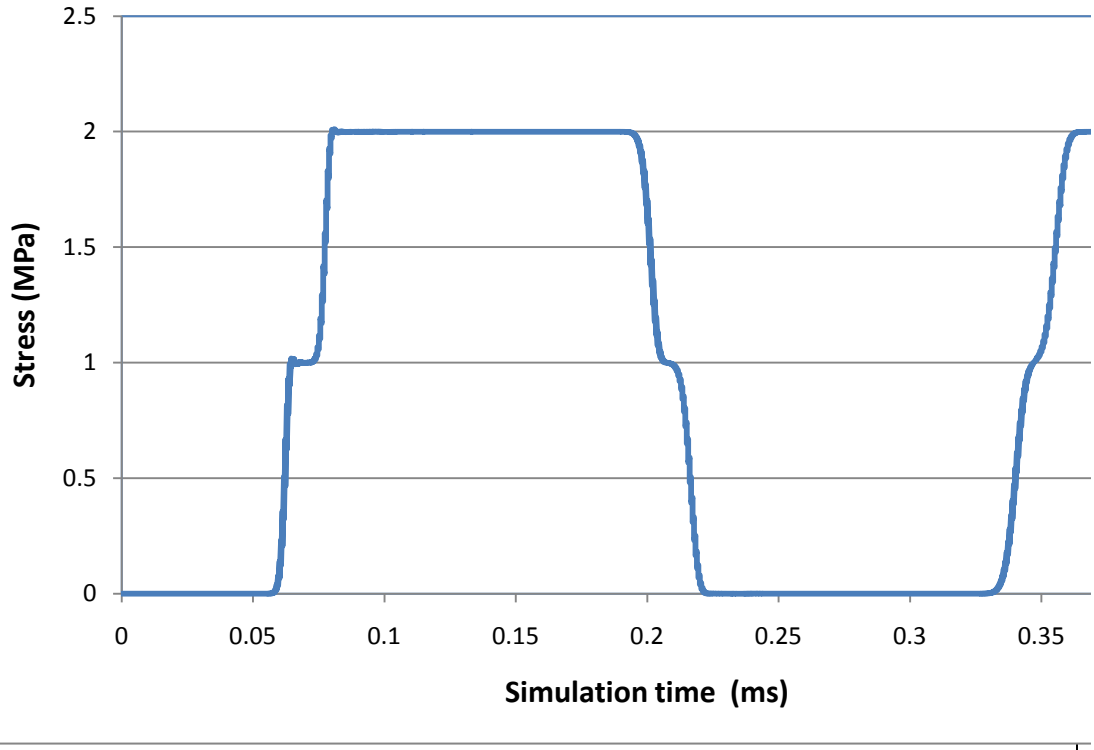

a- Pressure history of point 1 – located at the bottom of the geometry

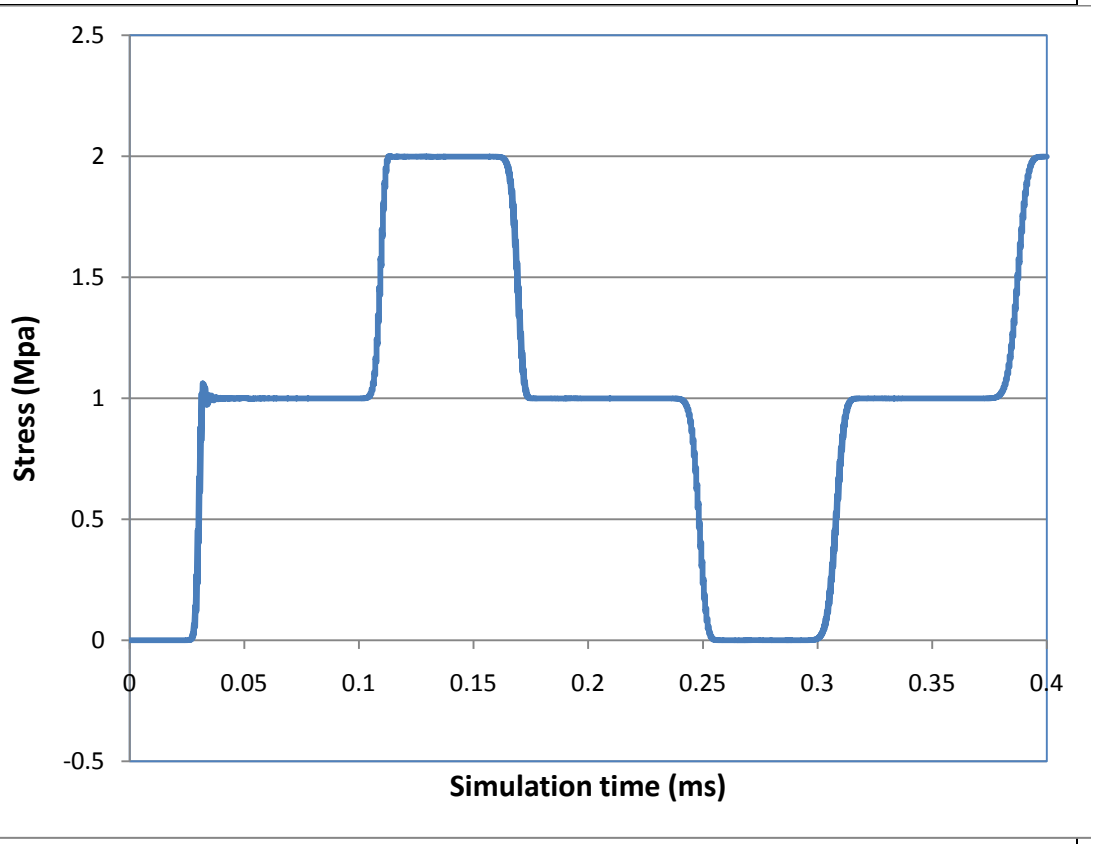

b- Pressure history of point 2 –located at the middle of geometry

Fig. C2 The pressure history of point (1) located at the middle of the geometry and point (2) located at the bottom of the geometry.